I would like to express my deepest gratitude to my supervisor Professor Edwin De Pauw for intellectual, technical and moral support, and for the latitude allowed to experiment and develop personal approaches. His guidance has prepared me well for the challenges that lie ahead.

I am ever so grateful to Professor Bernard Leyh for the time spent reading and discussing my work, and for giving me fruitful input. I could also benefit from constructive and helpful discussions with Professor Dominique Dehareng all along my work.

The members of the De Pauw group, both past and present, are also given thanks for their insights on various issues as well as for their friendship. I would like to express special thanks to Jean-François for his precious help regarding data processing and to Dominique, my "gold mine" and friend, whose constructive discussions and kindness helped me all along my work.

I give all my friends a big thank-you for their encouragement.

Lastly, I wish to express my affectionate thankfulness to my parents and my two little sisters for their love, understanding and constant support.

Abstract

Mass spectrometry has shown its unique potential for studying the structure of proteins. Associated with various specific techniques (H/D exchange, ion mobility, gas-phase spectroscopy, multidimensional mass analysis…), it has demonstrated to be an essential tool allowing primary structures to be analyzed and providing a lot of information about high order conformations. This work assesses the capabilities of these emerging mass spectrometry methods, and especially the gas-phase H/D exchange technique, for the structural analysis of nucleic acids. Gas-phase H/D exchange was first used to study single stranded oligonucleotides. The exchange reactions were performed with CD_3OD in the collision cell of a 9.4 T FT-ICR MS. In these experimental conditions and in integrating the experimental and theoretical results, gas-phase H/D exchange was shown to be controlled by hydrogen accessibility and not by the chemical nature of the heteroatom bearing the exchangeable hydrogen. This allowed the presence of one structure or several conformers that possess different exchange properties to be detected. Moreover, when several structures were observed, increasing the internal energy of the ions at the entrance of the H/D exchange cell gave access to a qualitative estimation of the relative height of the isomerization barriers compared to the H/D exchange ones. Ion mobility experiments confirmed independently the H/D exchange results. Comparing the ion activation experiments for H/D exchange and for ion mobility revealed that the most compact conformer displays the fastest H/D exchange. This observation showed that H/D exchange and ion mobility provide us with complementary information because accessibility and macromolecule compactness are not univocally associated. Two other methods having independent principles of operations were sequentially combined. The fragmentation of a totally deuterated dinucleotide in exchangeable positions demonstrated the coexistence of several fragmentation channels. The latter were classified according to the involvement of non-labile or labile protons in the fragmentation process. Double resonance experiments were also performed and demonstrated the existence of consecutive fragmentation mechanisms. The involvement of labile, and therefore exchangeable protons in the fragmentation mechanism casts doubt on the use of tandem mass spectrometry to localize incorporated deuteriums in oligonucleotides. Finally, an exploratory work on the gas-phase H/D exchange of non-covalent complexes is presented.

Table of Contents

List of Figures

List of Tables

Abbreviations and Acronyms

A	Adenine
AFM	Atomic force microscopy
AMP	Adenosine monophosphate
ATD	Arrival time distribution
BIRD	Blackbody infrared radiative dissociation
C	Cytosine
CD	Circular dichroism
CID	Collision-induced dissociation
CMP	Cytidine monophosphate
dAMP	Deoxyadenosine monophosphate
dCMP	Deoxycytidine monophosphate
dGMP	Deoxyguanosine monophosphate
dTMP	Deoxythymidine monophosphate
DC	Direct current
DNA	Deoxyribonucleic acid
ECD	Electron capture dissociation
EDD	Electron detachment dissociation
EPD	Electron Photodetachment dissociation
ESI	Electrospray ionization
ESI-MS	Electrospray ionization mass spectrometry
ESI-MS/MS	Electrospray ionization tandem mass spectrometry
eV	Electron volt
FAIMS	Field asymmetric waveform ion mobility spectrometry
FT-ICR	Fourier transform ion cyclotron resonance
FTMS, FT-ICR MS	Fourier transform ion cyclotron resonance mass spectrometry
G	Guanine
GMP	Guanosine monophosphate
H/D	Hydrogen/deuterium
ICR	Ion cyclotron resonance
IMR	Ion-molecule reaction
IR	Infrared
ISD	In-source decay
LSQ	Least-squares
m/z	Mass-to-charge ratio

MALDI	Matrix-assisted laser Desorption ionization
MD	Molecular dynamics
MEM	Maximum entropy method
MS	Mass spectrometry
MS/MS	Tandem mass spectrometry
NMR	Nuclear magnetic resonance
Q-Tof	Hybrid quadrupole time-of-flight
RF	Radio frequency
RNA	Ribonucleic acid
RRKM	Rice-Rampsberger-Kassel-Marcus
SORI	Sustained off-resonance irradiation
SORI-CID	Sustained off-resonance irradiation for collision-induced irradiation
SWIFT	Stored-waveform inverse Fourier transform
T	Thymine
Tm	Melting temperature
TMP	Thymidine monophosphate
U	Uracil
UV	Ultra-violet

Chapter 1: Introduction

The function of a biomolecule is tightly coupled to its structure. It is clear that the multiplicity of biomolecular states, as well as transitions among them, are critical determinants of biomolecular functions as diverse as molecular recognition, transport, regulation, and catalysis. Structure determination of biomolecule is therefore one of the key steps in understanding biomolecule action.

The structure of a biomolecule can be investigated at different levels [1-3]. The primary structure of a biomolecule corresponds to the specification of its atomic composition and the chemical bonds connecting these atoms. The primary structure specifies the sequence of the monomeric subunits that compose the biopolymer (nucleotides in nucleic acids and amino acids in proteins). The secondary structure is concerned with the general three-dimensional shape of local segments of the biomolecule. It is formally defined by the location of the hydrogen bonds within the biopolymer. In proteins, the secondary structure is defined by patterns of hydrogen bonds between backbone amide and carboxyl groups. The most common secondary structures are alpha helices and beta sheets. In nucleic acids, the secondary structure results from hydrogen bonding between the nitrogenous bases. The most famous DNA structure is the double stranded right-handed helix (B-DNA), but double stranded DNA can also adopt other structures called the A and Z-forms. Moreover, structures like hairpin, triple helices and G-quadruplexes have been observed. The single-stranded RNA molecules are most notably characterized by secondary structures. The latter are generally divided into helices (contiguous base pairs) and various kinds of loops (unpaired nucleotides surrounded by helices). Finally, the tertiary structure of a biomolecule is its global three-dimensional structure. A lot of interactions stabilize a given conformation: hydrogen bonds, ionic interactions, hydrophobic interactions, disulfide bonds (in protein)… The conformation and these interactions govern a vast majority of biological processes that define the function of the biomolecule. For proteins, a quaternary structure can also be defined and it corresponds to the assembling of multiple folded protein molecules in a multi-subunit complex.

There are a lot of methods that provide information on the different levels of structure.

The primary structure of a biopolymer can be obtained by chemical sequencing (the Edman degradation for protein and the Maxam-Gilbert or the Sanger methods for nucleic acids) [2]. Mass spectrometry is more and more applied as a sequencing tool.

Optical methods are traditionally applied to study molecular structures [1,4,5]. They are, however, indirect and provide structural information at the secondary and tertiary levels only after a careful assignment of relevant spectra or spectral changes. Among these methods, we shall emphasize:

- UV spectroscopy. The absorbance spectra depend on the molecular environment (DNA bases absorb around 260 nm and proteins absorb in the 230 – 300 nm range). For DNA, a major application is the change of absorption intensity when the double helix melts (thermal denaturation).
- Circular dichroism. CD signals are observed in the same spectral region as absorbance bands of a particular chromophore, provided that the chromophore or its molecular environment is asymmetric. CD spectra around 260 nm are much more sensitive than UV to the different DNA helical structures (B, A and Z) that have characteristic and very different CD spectra. For proteins, the CD bands in the far-UV region (170 – 250 nm) are used to characterize the secondary structure and changes therein. In particular the α-helix displays a strong characteristic CD spectrum in this region. The near UV CD spectrum (250 – 300 nm) represents a highly sensitive probe of the native state of a protein.
- Infrared and Raman spectroscopy. They are sensitive to the vibrational structure. Some secondary structures are characterized by specific vibrational absorption frequencies.
- Fluorescence. It is an excellent probe to investigate conformational changes of proteins, but not for nucleic acids since DNA molecules practically do not re-emit absorbed radiation. Fluorescence methods require the binding of strongly fluorescent dye molecules to DNA.

The majority of tertiary biomolecular structures known to date have been solved using X-ray crystallography [1,6,7] (structure in solid phase) and NMR [1,8,9]. X-ray crystallography typically provides data of high spatial resolution but provides no time-dependent information on the biomolecule conformational flexibility. As for NMR, it provides somewhat lower-resolution data in general and is limited to smaller molecules, but it can provide time-dependent dynamical information about the motion of a biomolecule in solution.

More recently, a new microscopic technique has been developed: atomic force microscopy (AFM) [10]. It is one of the most powerful tools for determining the surface topography of native biomolecules at subnanometer resolution. The AFM can also provide insight into the binding properties of biological systems.

Beside their obvious advantages, all these methods, however, have a few limitations. For example, X-ray crystallography requires the conversion of the biomolecule in the form of a crystal. NMR investigates with difficulty biomolecules whose mass is larger than 40 kDa. Moreover, these two methods require large quantities of pure material. In view of the increasing number of identified biomolecules requiring structure elucidation, the systematic use of these techniques would require a considerable time. Other complementary methods have therefore been developed. It is in this framework that mass spectrometry shows its unique potential.

Firstly, mass spectrometry has become a nearly routine tool for biomolecule primary structure analysis. Through the different fragmentation methods, the sequence of the biopolymers can be determined. Moreover, information about ligand binding sites in complexes and interaction sites in three-dimensional structures can be obtained [11].

In the same field of fragmentation experiments of complexes for mapping subcomplexes and studying their topologies, chemical cross-linking and mass spectrometry can be coupled [12-14]. Chemical cross-linking is the process of covalently joining two molecules by the use of cross-linking agents. This method has the aim of fine mapping the contact sites and inferring detailed structural information.

Ion mobility coupled to mass spectrometry is a powerful tool to explore the three-dimensional shape of polyatomic ions [15-17]. Applications include the investigation of conformations of flexible molecules such as biopolymers. The ion structure is obtained by measuring collision cross section in a high pressure drift tube and comparing it to model structure obtained by various theoretical methods. Moreover, since the temperature of the drift tube is generally adjustable, it provides an opportunity to address topics such as unfolding process, kinetics of structural interconversion and thermal motion of floppy molecules.

Gas-phase spectroscopy investigates the conformation of isolated molecules [18]. Line shifts in combination with high-level quantum chemical calculations can help to map conformational landscapes. Gas-phase spectroscopy experiments can be performed through single or double resonance irradiation. According to the method used, the UV and/or the IR wavelengths are fixed or swept and the photofragmentation spectra are recorded.

Hydrogen/deuterium (H/D) exchange coupled to mass spectrometry provides information on molecular structure and dynamics [19-21]. In a typical H/D exchange experiment, a biomolecule is exposed to a deuterated solvent (or gas) for varying periods of time and the extent of H/D exchange is measured by mass spectrometry. By monitoring the level of deuterium incorporation, the method gives information about the solvent accessibility into various parts of the molecule. H/D exchange information is used to identify regions of flexibility, region in which ligands interact and to make inferences about structure and stability.

It is important to notice that for the majority of the structural mass spectrometry studies, comparison with information from theoretical studies (quantum chemical calculations, molecular dynamics) are essential.

All these mass spectrometry methods have been intensively used to study the structure of proteins, but their applications to the structural analysis of nucleic acids are much less common. The aim of the present thesis is to bring a contribution to this emerging field. Our work has consisted in assessing the capability of mass spectrometry methods, and especially the gas-phase H/D exchange technique, for the structural analysis of oligonucleotides. After this first chapter, this thesis is organized as follows:

Chapter 2 provides an overview of mass spectrometry with the main focus on nucleic acid analysis. It describes the Fourier transform ion cyclotron resonance mass spectrometer and gives a brief summary of the gas-phase techniques related to this technique. The couplings of hydrogen/deuterium exchange and ion mobility with mass spectrometry are discussed in details. Finally, the inventory of the structural studies of nucleic acids by gas-phase H/D exchange and ion mobility coupled to mass spectrometry is presented.

Chapter 3 provides an overview of conformational research and geometry optimization in molecular mechanics and dynamics, and in quantum chemistry.

Chapter 4 discusses our results on the gas-phase H/D exchange of single-stranded oligonucleotides; dinucleotides and thymine oligomers. This work suggests hydrogen accessibility as dominant factor. The H/D exchange of DNA is also compared with the one of RNA. This chapter is based on the following paper: *J. Am. Soc. Mass Spectrom.* **2007**, *18*, 1827-1834.

Chapter 5 presents the coupling of H/D exchange with other mass spectrometry methods. As discussed in our paper *J. Am. Soc. Mass Spectrom.* **2008**, *19*, 938-946, compiling data from gas-phase H/D exchange and ion mobility spectrometry suggests the detection of oligonucleotide gas-phase conformers. Moreover, H/D exchange coupled to tandem mass spectrometry suggests identification of fragmentation channels (*J. Am. Soc. Mass Spectrom.* **2009**, Accepted*)*.

Chapter 6 describes an exploratory work on the gas-phase H/D exchange of non-covalent complexes. Perspectives to pursue these investigations are suggested.

Chapter 7 presents a general conclusion.

References

1. Frank-Kamenetskii, M. D. Biophysics of the DNA molecule. *Phys. Rep.* **1997,** *288*, 13-60.

2. Colson, P. Structure et Dynamique Conformationnelle des Acides Nucléiques et Protéines. 2003.

3. Branden, C.; Tooze, J. *Introduction to Protein Structure;* Garland: New York, 1991.

4. Schmid, F. X. Optical spectroscopy to characterize protein conformation and conformational changes. In *Protein Structure: A Pratical Approach*, Creighton, T. E., Ed.; Oxford University Press: Oxford, 1997; pp 261-297.

5. Matagne, A. Spectroscopie et Repliement des protéines. 2004.

6. Berman, H. M.; Gelbin, A.; Westbrook, J. Nucleic acid crystallography: a view from the nucleic acid database. *Prog. Biophys. Mol. Biol.* **1996,** *66*, 255-288.

7. Drenth, J. *Principles of Protein X-Ray Crystallography;* Springer: New York, 2007.

8. Wüthrich, K. *NMR of proteins and nucleic acids;* Wiley: New York, 1986.

9. *Nuclear Magnetic Resonance and Nucleic Acids;* Academic Press, Inc.: San Diego, 1995; Vol. 261.

10. Müller, D. J.; Aebi, U.; Engel, A. Imaging, measuring and manipulating native biomolecular systems with the atomic force microscope. In *From Bones to Atoms (http://www.mih.unibas.ch/Booklet/Booklet96/),* 1996.

11. Gross, M. L. Tandem Mass Spectrometric Strategies for Determining Structure of Biologically Interesting Molecules. *Acc. Chem. Res.* **1994,** *27*, 361-369.

12. Back, J. W.; de Jong, L.; Muijsers, A. O.; de Koster, C. G. Chemical Cross-linking and Mass Spectrometry for Protein Structural Modeling. *J. Mol. Biol.* **2003,** *331*, 303-313.

13. Vasilescu, J.; Figeys, D. Mapping protein-protein interactions by mass spectrometry. *Curr. Opin. Biotechnol.* **2006,** *17*, 394-399.

14. Sinz, A. Chemical cross-linking and mass spectrometry to map three-dimensional protein structures and protein-protein interactions. *Mass Spectrom. Rev.* **2006,** *25*, 663-682.

15. Wyttenbach, T.; Bowers, M. T. Gas-Phase Conformations: The Ion Mobility/Ion Chromatography Method. *Top. Curr. Chem.* **2003,** *225*, 207-232.

16. Borsdorf, H.; Eiceman, G. A. Ion Mobility Spectrometry: Principles and Applications. *Applied Spectroscopy Reviews* **2006,** *41*, 323-375.

17. Bohrer, B. C.; Merenbloom, S. I.; Koeniger, S. L.; Hilderbrand, A. E.; Clemmer, D. E. Biomolecule Analysis by Ion Mobility Spectrometry. *Annu. Rev. Anal. Chem.* **2008,** *1*, 293-327.

18. de Vries, M. S.; Hobza, P. Gas-Phase Spectroscopy of Biomolecur Building Blocks. *Annu. Rev. Phys. Chem.* **2007,** *58*, 585-612.

19. Englander, S. W. Hydrogen Exchange and Mass Spectrometry: A Historical Perspective. *J. Am. Soc. Mass Spectrom.* **2006,** *17*, 1481-1489.

20. Hoofnagle, A. N.; Resing, K. A.; Ahn, N. G. Protein Analysis by Hydrogen Exchange Mass Spectrometry. *Annu. Rev. Biophys. Biomol. Struct.* **2003,** *32*, 1-25.

21. Wales, T. E.; Engen, J. R. Hydrogen exchange mass spectrometry for the analysis of protein dynamics. *Mass Spectrom. Rev.* **2006,** *25*, 158-170.

Chapter 2: Mass Spectrometry

2.1. Electrospray ionization

All the experiments discussed in this thesis rely on electrospray ionization to produce ions in the gas phase. It has become the ionization method of choice for a wide variety of analytes, including large proteins and nucleic acids. During the electrospray ionization process, the analyte is progressively completely desolvated and the ions detected are usually expected to mirror the molecular species present in solution. Electrospray ionization has been developed by Fenn [1] and it corresponds to a complex combination of independent component processes; the electrospray dispersion, the electrostatic dispersion of sample liquid into charged droplets, and ionization, i.e., the production of ions from the charged droplets.

The Electrospray process has been described in detail in several review papers [2-6], only the key features will be presented here.

Electrospray dispersion involves the application of a high electric field between the metal capillary and the counter-electrode (Figure 2.1.1.). This field causes a separation of the positive and negative charges in the solution which leads to the accumulation, at the surface of the liquid at the tip, of ions of the same polarity as the voltage applied to the capillary [1,3,7-9]. This accumulation of charged species destabilizes the liquid at the tip which deforms into what is called the "Taylor cone". This cone continuously produces charged droplets in the gas phase [1,3,7-9]. The rate of the charge separation process is determined by the flow rate, applied voltage, conductivity, and liquid surface tension [1,3,10]. As electrospray produces a continuous current, electrochemical processes must occur at the capillary and at the counter electrode to avoid charge accumulation [1,8,9,11]. These redox processes may correspond to reduction/oxidation reactions involving solvents or analytes, and/or the elimination of cations/anions from solution. However the details of all the electrospray mechanism steps and the different agents involved are often not controlled. In some electrospray source designs, additional control parameters such the possibility of heating part of the capillary or of introducing a flow of nebulizer gas coaxial to the capillary are available in order to facilitate droplet emission and evaporation.

Solvent evaporation from the initially formed droplet occurs due to collisions with a neutral gas (heated or not) which leads to the decrease of the droplet radius at constant charge until reaching the Rayleigh limit. A Coulomb fission of the droplet occurs as the Coulombic repulsion between the charges overcomes the cohesive forces holding the droplet together. The resulting instability disperses the droplet into smaller droplets that continue to evaporate until they too reach the Rayleigh limit and disintegrate. This leads to a very rapid reduction in size and charge of the droplets (Figure 2.1.2.).

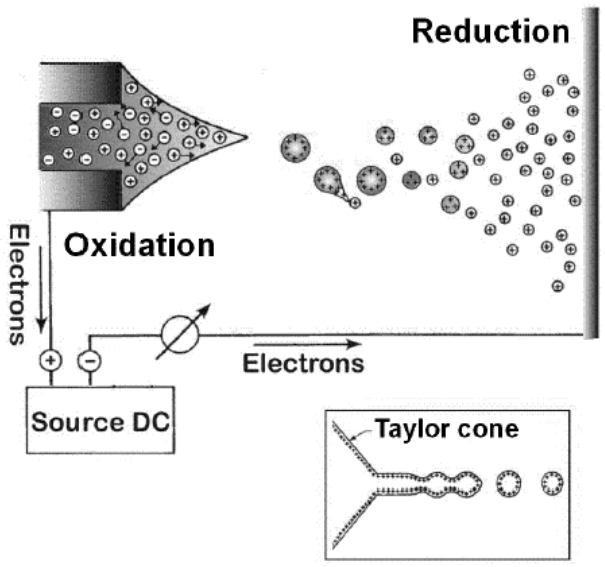

Figure 2.1.1. Production of charged droplets from the analyte solution. (Adapted from reference [4])

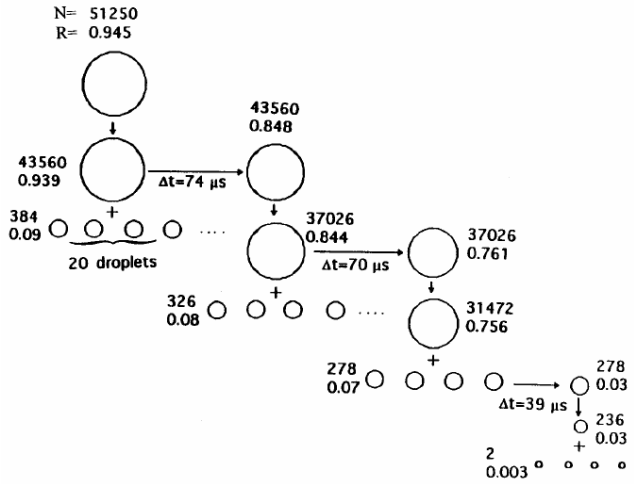

Figure 2.1.2. Droplet evolution scheme due to solvent evaporation at constant charge and Coulomb fissions at the Rayleigh limit. First droplet shown is at the Rayleigh limit. The parent droplet produces 20 offspring droplets which carry off 2% of the mass and 15% of the charge. N corresponds to number of elementary charges and R is the radius in μm. Also given is the time Δt (μs) required to reach the next fission. (Adapted from reference [4])

Two mechanisms are typically considered to explain the production of desolvated ions from charge droplets: the ion desorption model based on the work of Iribarne and Thomson [12-14], and the charge residue model proposed by Dole and co-workers [15]. According to the ion desorption model, at an intermediate stage in the droplet's lifetime (radius larger than the Rayleigh limit), the electric field at the surface of the droplet becomes sufficiently high so that an analyte ion is directly emitted from the charge droplet [3,12,13,16]. It is generally admitted that small ions are produced by this mechanism [16-18]. The charge residue model assumes that the series of droplet fission events results in the formation of a droplet containing a single analyte molecule. This molecule retains its droplet charge to become a free ion as the last of the solvent vaporizes. Large globular proteins are believed to be produced via this mechanism [3,19].

References

1. de la Mora, J. F.; Van Berkel, G. J.; Enke, C. G.; Cole, R. B.; Martinez-Sanchez, M.; Fenn, J. B. Electrochemical processes in electrospray ionization mass spectrometry. *J. Mass Spectrom.* **2000,** *35*, 939-952.

2. Gaskell, S. J. Electrospray : Principles and Practice. *J. Mass Spectrom.* **1997,** *32*, 677-688.

3. Cole, R. B. Some tenets pertaining to electrospray ionization mass spectrometry. *J. Mass Spectrom.* **2000,** *35*, 763-772.

4. Kebarle, P. A brief overview of the present status of the mechanisms involved in electrospray mass spectrometry. *J. Mass Spectrom.* **2000,** *35*, 804-817.

5. Kebarle, P.; Peschke, M. On the Mechanisms by Which the Charged Droplets Produced by Electrospray Lead to Gas Phase Ions. *Anal. Chim. Acta* **2000,** *406*, 11-35.

6. Amad, M. H.; Cech, N. B.; Jackson, G. S.; Enke, C. G. Importance of Gas-Phase Proton Affinities in Determining the Electrospray Ionization Response for Analytes and Solvents. *J. Mass Spectrom.* **2000,** *35*, 784-789.

7. Ikonomou, M. G.; Blades, A. T.; Kebarle, P. Electrospray-Ion Spray: A Comparison of Mechanisms and Performance. *Analytical Chemistry* **1991,** *63*, 1989-1998.

8. Blades, A. T.; Ikonomou, M. G.; Kebarle, P. Mechanism of Electrospray Mass Spectrometry. Electrospray as an Electrolysis Cell. *Analytical Chemistry* **1991,** *63*, 2109-2114.

9. Van Berkel, G. J.; Zhou, F. Characterization of an Electrospray Ion Source as a Controlled-Current Electrolytic Cell. *Analytical Chemistry* **1995,** *67*, 2916-2923.

10. Cech, N. B.; Enke, C. G. Practical implications of some recents studies in electrospray ionization fundamentals. *Mass Spectrom. Rev.* **2001,** *20*, 362-387.

11. Jackson, G. S.; Enke, C. G. Electrical Equivalence of Electrospray Ionization with Conducting and Nonconducting Needles. *Analytical Chemistry* **1999,** *71*, 3777-3784.

12. Iribarne, J. V.; Thomson, B. A. On the evaporation of small ions from charged droplets. *J. Chem. Phys.* **1976,** *64* (6), 2287-2294.

13. Iribarne, J. V.; Thomson, B. A. Field induced ion evaporation from liquid surfaces at atmospheric pressure. *J. Chem. Phys.* **1979,** *71* (11), 4451-4463.

14. Iribarne, J. V.; Dziedzic, P. J.; Thomson, B. A. Atmospheric pressure ion evaporation-mass spectrometry. *International Journal of Mass Spectrometry and Ion Physics* **1983,** *50*, 331-347.

15. Dole, M.; Mack, L. L.; Hines, R. L.; Mobley, R. C.; Ferguson, L. D.; Alice, M. B. Molecular Beams of Macroions. *J. Chem. Phys.* **1968,** *49* (5), 2240-2249.

16. Kebarle, P.; Tang, L. From Ions in Solution to Ions in the Gas Phase. The Mechanism of Electrospray Mass Spectrometry. *Analytical Chemistry* **1993,** *65*, 972A-986A.

17. Camero-Castano, M.; de la Mora, J. F. Kinetics of Small Ion Evaporation From the Charge and Mass Distribution of Multiply Charged Clusters in Electrosprays. *J. Mass Spectrom.* **2000,** *35*, 790-803.

18. Wang, G.; Cole, R. B. Charged Residue Versus Ion Evaporation for Formation of Alkali Metal Halide Clusters in Electrospray Ionization. *Anal. Chim. Acta* **2000,** *406*, 53-65.

19. Camero-Castano, M.; de la Mora, J. F. Mechanisms of Electrospray Ionization of Singly And Multiply Charged Salt Clusters. *Anal. Chim. Acta* **2000,** *406*, 67-91.

2.2. Fourier transform-ion cyclotron resonance (FT-ICR) [1-6]

2.2.1. The FT-ICR mass spectrometry in theory

The first ICR mass spectrometers were reported by Smith [7] and Sommer et al. [8] in 1951 while the coupling of ICR with Fourier transform was introduced in 1974 by Comisarow and Marshall [9,10].

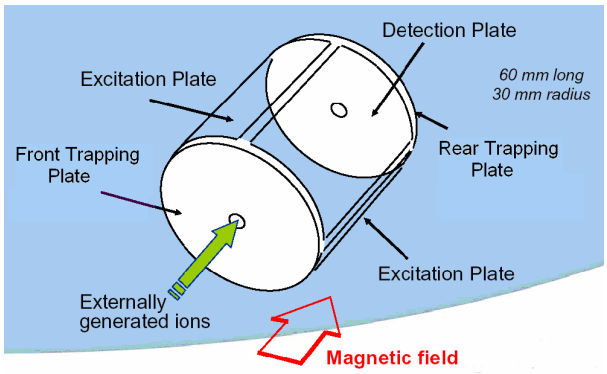

Figure 2.2.1. Scheme of a typical ICR cell. Indicated are the three sets of electrodes. Adapted from [11].

An ion moving in the presence of a spatially uniform magnetic field $\vec{B}$ oriented along the z-axis is subjected to a Lorentz force given by

$$\vec{F} = q \cdot \vec{v} \wedge \vec{B}, \quad \mathrm{F} = q \cdot v_{xy} \cdot B = m \cdot a \tag{1}$$

in which q is the ionic charge, $\vec{v}$ is the ionic velocity and $\vec{B}$ is the static axial magnetic field (z-axis).The magnetic field bends the ions path into a circle of radius r in the xy plane. As $v_{xy} = \sqrt{v_x^2 + v_y^2}$ denotes the ion velocity in the xy plane and because the angular acceleration a is equal to v_{xy}^2/r, Eq(1) becomes

$$\frac{m \cdot v_{xy}^2}{r} = q \cdot v_{xy} \cdot B\,. \tag{2}$$

As the angular velocity (around the z-axis) is defined by

$$\omega = \frac{v_{xy}}{r} \tag{3}$$

Eq(2) can be written

$$m \cdot \omega_c^{\,2} r = q \cdot B \cdot \omega_c \cdot r \tag{4}$$

or simply

$$\omega_c = \frac{q \cdot B}{m}$$ Cyclotron equation (5)

in which ω_c is the ion cyclotron angular velocity. As the angular velocity is related to the frequency by a factor 2π ($\omega_c = 2\pi\ \upsilon_c$), ω_c is commonly named the ion cyclotron frequency. All ions of a given mass to charge ratio, m/q, have the same ICR frequency, independently of their initial velocity and position in the ICR cell.

The ion cyclotron orbital radius is given by

$$r = \frac{m \cdot v_{xy}}{q \cdot B} \quad (6)$$

So far, only the motion in the xy plane has been considered. In the absence of any other field, the resulting trajectory is an endless helicoidal motion around and along the z-axis. To restrict this motion along the z-axis, two trapping plates, perpendicular to the z-axis and set to a repulsive potential, are inserted. Eq(1) becomes

$$\vec{F} = q \cdot \vec{v} \wedge \vec{B} + q \cdot \vec{E}, \quad F = q \cdot v_{xy} \cdot B + q \cdot E \quad (7)$$

where E is the electric field between the two trapping plates.

If it was possible to apply a uniform electric field, parallel to the magnetic field, with plates of infinite length, the ion motion would be helicoidal with periodic oscillations along the z-axis in the electric potential well. A second frequency is then obtained which is named the trapping frequency ω_z and is given by

$$\omega_z = \sqrt{\frac{2q \cdot V_T \cdot \alpha}{m \cdot a^2}} \quad (8)$$

in which a is the distance between the two trapping plates, V_T is the voltage applied to the trapping plates, and α is a geometric scale factor.

As the ideal case of infinite plates does not exist, the electric field can not be parallel to the magnetic field. The electric field has a radial component (xy) in addition to its axial one (z). The three-dimensional axial quadrupolar electrostatic trapping potential is given by

$$\Phi(r,z) = V_T\left[\gamma + \frac{\alpha}{2a^2}(2z^2 - r^2)\right],\ r = \sqrt{x^2 + y^2} \quad (9)$$

in which r is the radial position of the ion in the xy plane, and α and γ are constants that depend on the trap shape. This radial component carries the ions

outside of the cell as the electric field in the center of the cell is minimal along the z-axis but maximal in the xy plane. This force is against the Lorentz one that comes from the magnetic field. The ions are subjected to a force that can be written:

$$F = q \cdot B \cdot \omega \cdot r - \frac{q \cdot V_T \cdot \alpha}{a^2} r \qquad (10)$$

Therefore a third motion is superposed to two previous ones. This motion results in a decrease of the cyclotron frequency and the appearance of a third frequency that is peculiar to the trapped ions. All the frequencies can be found in resolving the following equation:

$$\omega^2 - \frac{q \cdot B \cdot \omega}{m} - \frac{q \cdot V_T \cdot \alpha}{m \cdot a^2} = 0$$

The result is

$$\omega_+ = \frac{\omega_c}{2} + \sqrt{(\frac{\omega_c}{2})^2 - \frac{\omega_z}{2}} \qquad \text{“reduced” cyclotron frequency (11)}$$

$$\omega_- = \frac{\omega_c}{2} - \sqrt{(\frac{\omega_c}{2})^2 - \frac{\omega_z}{2}} \qquad \text{“magnetron” frequency (12)}$$

where ω_c and ω_z have been defined earlier (equations (5) and (8)).

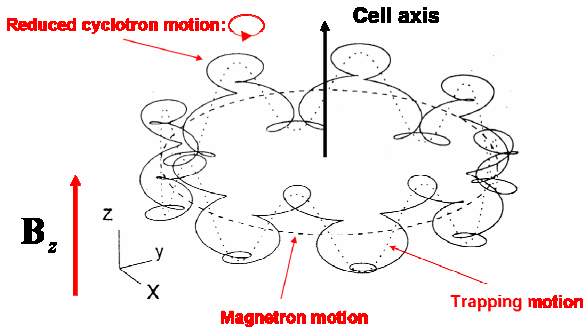

Figure 2.2.2. Ion motion. The dashed line represents magnetron motion only, the dotted line combines magnetron and trapping motion and the solid curve combines magnetron, cyclotron and trapping motion. Adapted from [12].

The produced ion cyclotron frequency can not be directly measured. The ions are produced at different times, with variable kinetic energies which creates a phase (initial orbital position) and a variable orbital radius. It is necessary to turn this incoherent packet of ions with identical m/z into a coherent packet with the same

orbital radius and the same phase. It is performed through an excitation-detection procedure (Figure 2.2.3.).

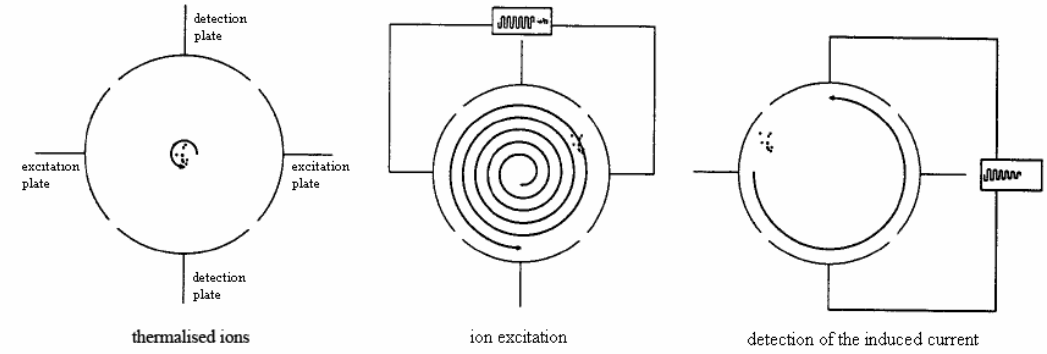

Figure 2.2.3. The different steps leading to ion detection [13].

The excitation step is performed via two excitation plates. They produce a sinusoidal dipolar electric field. When it oscillates at the cyclotron frequency of ions of a particular m/z value, these ions absorb energy and this added energy causes the size of their orbit to increase (the cyclotron motion is resonantly amplified). The reached orbital radius is given by

$$r = \frac{\beta_{dipole} \cdot V_{P-P} \cdot t_{exc}}{2 \cdot d \cdot B} \tag{13}$$

in which β_{dipole} is the dipolar excitation scale factor, $V_{P\text{-}P}$ is the peak-to-peak voltage difference between the two plates, t_{exc} is the excitation time and d is the distance between the two plates. Excitation can be used in three ways: (a) to accelerate ions coherently to a larger, detectable orbital radius, (b) to increase ion kinetic energy above the threshold for ion dissociation and/or ion-molecule reaction, and (c) to accelerate ions to a cyclotron radius larger than the radius of the ion trap, so that ions are removed ("ejected") from the instrument. Different kinds of excitation can be used (Figure 2.2.4.). The mono-frequency excitation is not useful to detect all the ions that are trapped in the cell. To avoid exciting successively each ion frequency, one short excitation pulse that sweeps all the interesting frequencies is generally used. When the electronics allows generating arbitrary functions, another excitation method can be used. It is named SWIFT (stored-waveform inverse Fourier transform). The frequency range is predefined and the excitation wave is calculated by inverse Fourier transformation according to this predefinition.

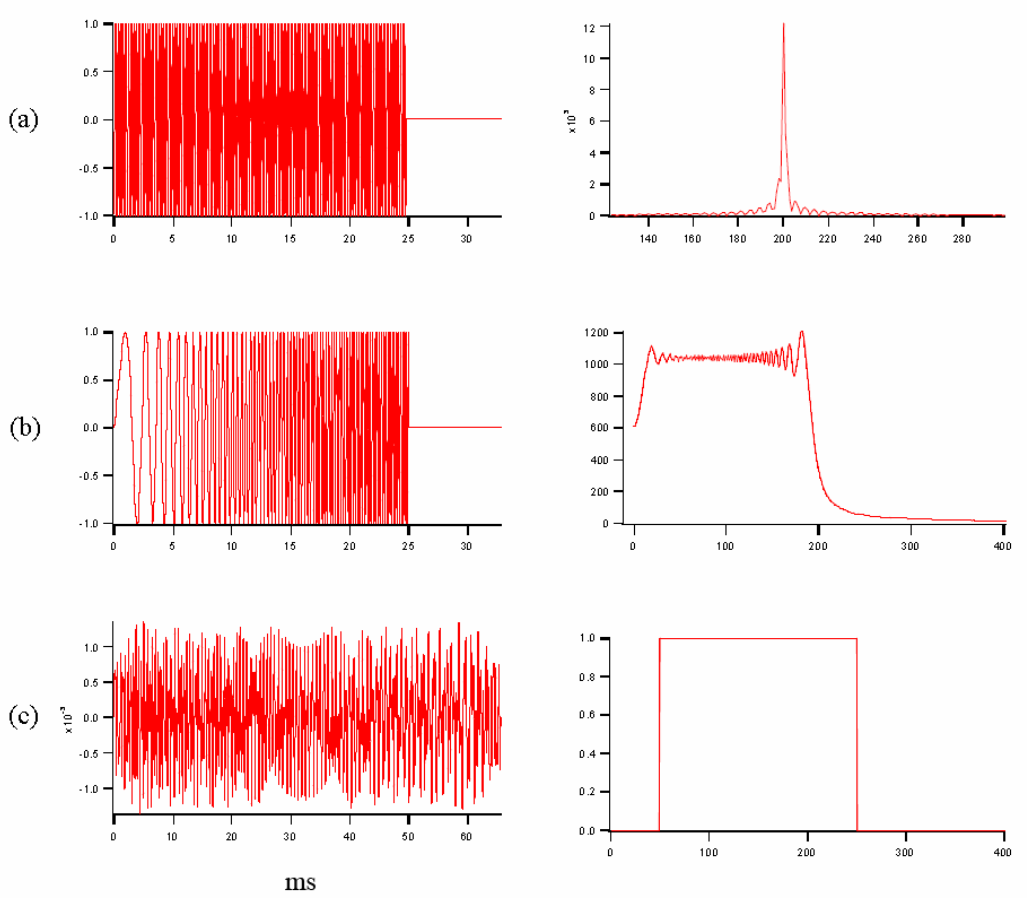

Figure 2.2.4. Different excitation methods: on the left in time scale and on the right their components after Fourier transform. (a) sinusoidal mono-frequency, (b) frequency sweep (chirp) and (c) SWIFT [13].

The time-varying electric field of the rotating ion packets repeatedly passing in front of the detector plates at their individual cyclotron frequency generates an induced image current proportional to the total number of ions. The transient signal is recorded and converted from the time domain to the frequency domain by means of Fourier transform (Figure 2.2.5.). The frequencies are converted to m/z values and the respective amplitudes represent the abundances of the corresponding ions. A two-parameters equation is generally used

$$\frac{m}{z} = \frac{A}{\nu_+} + \frac{B}{\nu_+^2}. \qquad (14)$$

A and B are constants obtained by fitting a particular set of reference ICR mass spectral peak frequencies.

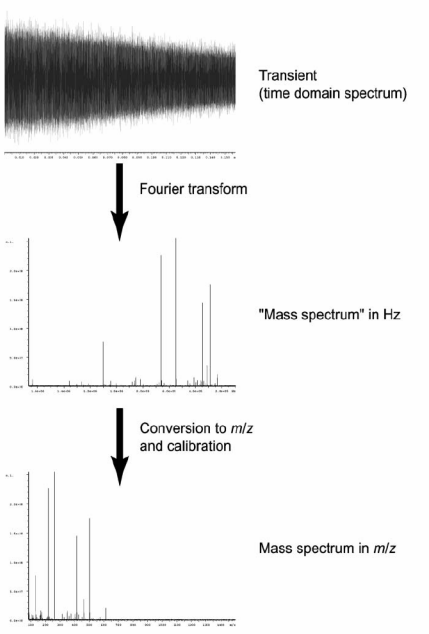

Figure 2.2.5. Illustration of the processing of raw data [6].

Ion-neutral collisions during the recording generate ion displacement from their orbit. As collisions are random, ion packets lose coherence leading to extinction of the induced current in the detection plates. All the models of this phenomenon result in an exponentially dampened sinusoid. This exponential component leads to a limitation of the detection time and a peak broadening. This explains why it is so important to have a pressure as small as possible in the detection cell.

The advantage of a FT-ICR mass spectrometer is the high accuracy with which it is possible to measure a frequency by classical methods of digitalization and Fourier transform. The highest measurable frequency is thus limited by the digitalization frequency and the interval between two frequencies is a function of the number of measured points that depends on the duration of the recorded signal. The high vacuum is crucial for a high resolution. Mass accuracy depends on the resolution and the quality of the calibration. An important parameter of this calibration is the charge space. The presence of ions in the cell changes the electric field for the trapping, the excitation and the detection of the ions. This modification depends on the number and the masses of the ions. These latter parameters are not included in the calibration equation. The internal calibration is preferred to the external one as it partially frees from these problems. The FT-ICR

mass spectrometer is also well-known for its high sensitivity but is criticized for its limited dynamic range which is connected to the charge space effect.

FT-ICR mass spectrometry is some numbers:

- The cyclotron frequency $\nu_c = \frac{\omega_c}{2\pi}$

To give a rough estimate, in a magnetic field of 7 T, the cyclotron frequency is equal to 1.1 MHz for an ion with a m/z ratio of 100, 215 kHz for an ion with a m/z ratio of 500 and 54 kHz for an ion with a m/z ratio of 2000.

- The trapping frequency ν_z

In typical conditions (V_T = 1 V, B = 7 T, a = 6 cm), ν_z is around 1600 Hz for an ion with a m/z ratio equal to 1000.

- The magnetron frequencies are around 1-100 Hz.
- Two parameters are very important to control the ion excitation step; the excitation intensity that is related to the excitation voltage V_{p-p} (around 300 V peak to peak) and the radiation time that is about 60 µs.
- In an instrument with a quite good vacuum (10^{-10} mbar), resolutions higher than 600000 can be obtained for an ion with a m/z ratio equal to 1000. However they result from recordings over narrow frequency ranges. With larger ranges, resolutions of ~ 200000 are usually obtained.
- Accuracies better than 1 ppm can be obtained on a mass range going from 500 m/z to 1500 m/z in internal calibration. In external calibration, with low number of ions in the cell, accuracies of 1-2 ppm are obtained.
- In a magnetic field of 7 T, the lowest m/z ratio that can be detected is equal to 29. The highest one is theoretically equal to 274000. However problems appear before this limit, especially due to the limit of the detection time. The highest experimental m/z ratio is around 27000.

The different ICR trap configurations

The goal that is shared by all the different ICR traps (Figure 2.2.6.) is to manage the requirements of the trapping (to limit the magnetron motion with a radial electric field as low as possible), the excitation and detection processes ("infinite" plates without edge-effect). Values of γ and α (Eq(9)) for the different ICR trap shapes are shown in Table 2.2.I.

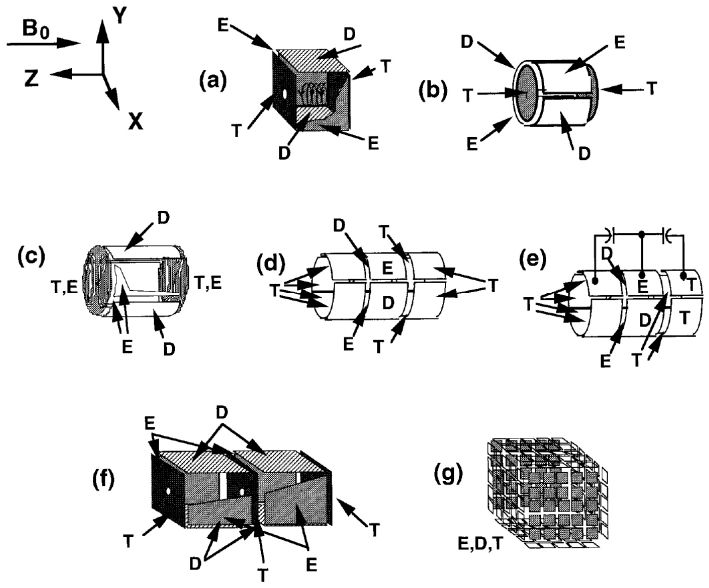

Figure 2.2.6. ICR ion trap configurations from [1]. E = Excitation ; D = Detection ; T = Trapping plate. (a) cubic (Comisarow, 1981; Comisarow, 1980); (b) cylindrical (Comisarow and Marshall, 1976; Elkind et al., 1988; Kofel et al., 1986; Lee et al., 1980); (c) trapping plates segmented to linearize excitation potential ("infinity" trap) (Caravatti and Allemann, 1991); (d) and (e) open-ended, without or with capacitive RF coupling between the three sections (Beu and Laude, 1992; Beu and Laude, 1992; Gabrielse et al., 1989); (f) dual (Littlejohn and Ghaderi, 1986); and (g) "matrix-shimmed" (Guan and Marshall, 1995).

Table 2.2.I. Geometrical characteristics of the ICR cell configurations.

Trap shape	End cap separation	Excitation electrode separation	γ	α	β_{dipole}
Ideal	NA	NA	0.50000	4.00000	1.00000
Cube	a	$d = a$	0.33333	2.77373	0.72167
Cylinder	a	d	0.2787	2.8404	0.80818
Infinity	a	d	0.2787	2.8404	≈ 0.900
Open uncoupled	a	d	0.14527	3.86798	0.86738
Open coupled	a	d	0.14527	3.86798	0.89699
Hyperbolic	a	$d = \sqrt{2}a$	0.44403	4.0905	0.66483
Matrix-shimmed cube	a	d	0.50000	3.9254	≈ 1

2.2.2. Our FT-ICR mass spectrometer

The FT-ICR mass spectrometer used in our laboratory is an apex-Qe FTMS (Bruker Daltonics, Billerica, MA, USA). The magnetic field is generated by a 9.4 T superconducting magnet. This magnet is of the latest technology and employs state-of-the art shielding (actively shielded magnet). It is cooled down by cryogenic liquids (liquid helium and liquid nitrogen).

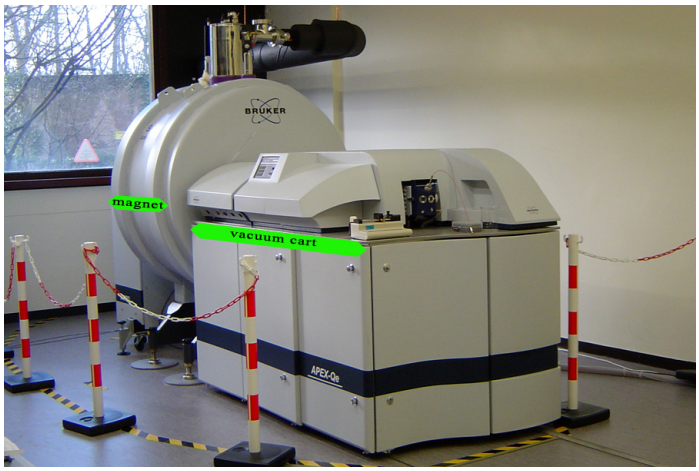

Figure 2.2.7. View of our apex-Qe FTMS from the user side.

Figure 2.2.7. is a view of our FT-ICR mass spectrometer from the user side. It has two major components; the vacuum cart and the superconducting magnet. It is equipped with an electrospray source (on the right hand side on Figure 2.2.7.). The instrument can be divided into four major sections (Figure 2.2.8.); the atmospheric pressure ionization source (Apollo^{TM} API), the Qh interface, the ion transfer optics and the detector. Six differential pumping stages maintained by four turbo-molecular pumps and two mechanical roughing pumps allow the introduction of ions at atmospheric pressure while providing ultra high vacuum of ~ 10^{-10} mbar necessary to operate the analyzer.

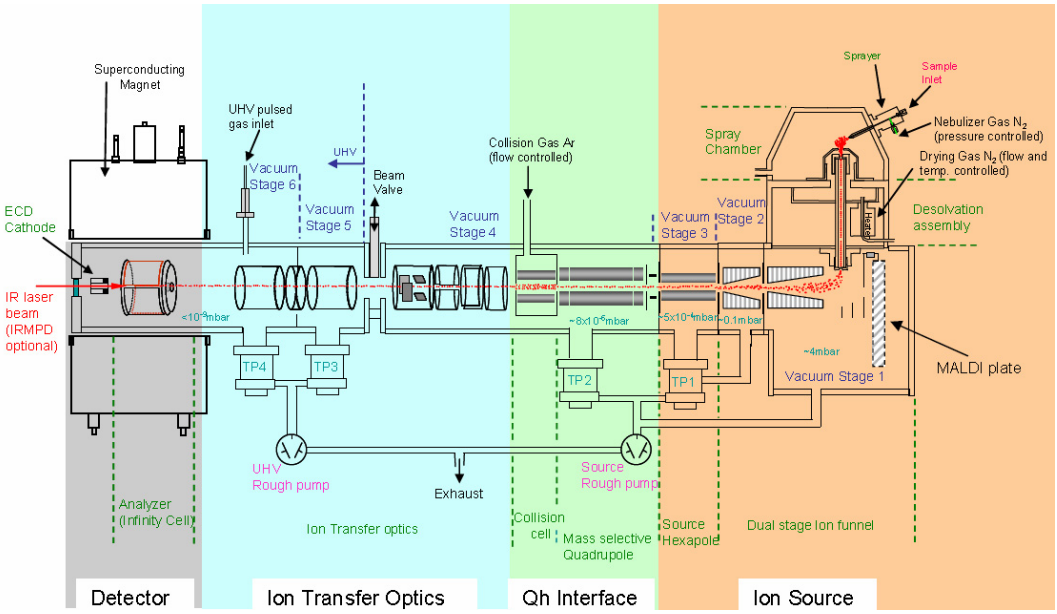

Figure 2.2.8. Schematic overview of the ion optics and pumping system of the apex-Qe FTMS [11].

The atmospheric pressure ionization source (Figure 2.2.9.) [14]

The electric field inside the spray chamber is generated by voltages applied to two electrodes: End-Plate and Capillary (opposite sign to the ion one). To achieve a good desolvation, a balance between the liquid sample flow rate, the drying gas flow and the temperature is required. Generated ions enter the vacuum system through the dielectric Glass Capillary. From the Capillary Exit, the ions pass through the Skimmer and enter into the first RF ion guide. The respective voltages are set to generate a forward dragging electric force (|Cap Exit| > |Skimmer 1| >

|Skimmer 2|). After passing through the first RF ion guide and the second skimmer, ions are accumulated in the second RF ion guide (hexapole 1) by means of an electrical potential applied to the Exit gate electrode. After a cycle period (d1), the voltage on this gate electrode drops and remains open for a predetermined time (d10). Ions emerge from the hexapole until the next cycle of ion accumulation in the ion guide begins.

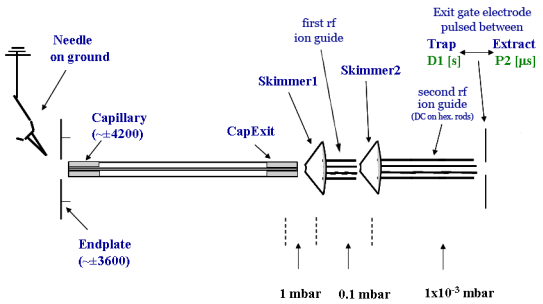

Figure 2.2.9. The electrospray source [15].

The Qh interface [16]

It consists of a quadrupole mass filter (Q1) and a hexapole collision cell (h2).

A quadrupole mass filter consists of four precision rods that are aligned and mounted parallel with respect to one another. It operates with RF and DC potentials applied to these rods which cause particular m/z values to be transmitted or filtered out. These operations are governed by the Mathieu equations [17] which are used to define the Mathieu stability diagram [17]. The quadrupole mass filter operates in RF-only or in RF/DC mode. RF-only mode refers to only RF voltage applied on the rods. It corresponds to the MS mode for observing a complete mass spectrum as a large mass range of ions is passed through the quadrupole in these conditions. The RF/DC mode is used for ion isolation by placing the ion(s) of interest in the upper apex of the stability diagram and forcing all other ions to be outside of the stability diagram.

The collision cell is a hexapole and is called h2. In contrast to Q1, h2 is always operated in RF-only mode. It traps and stores ions before transferring them to the ICR cell. Two plates named “Collision Entrance” and “Collision Exit” are placed on both sides of the hexapole. As h2, they are set to one value when the ions are

entering, and then switched to another value when they are to be extracted towards the ICR cell. Using two voltage settings allows for much easier tuning of the ion transfer and enables one parameter MS/MS operation. Figure 2.2.10. illustrates the voltage profile for the Qh interface when ions are injected into the collision cell and when they are extracted out towards the ICR cell. The pole bias on h2 and the collision entrance and exit plates are set to the trap values so that ions are slowly accelerated into the collision cell and then trapped when they loose energy through low energy collisions with the gas molecules inside (~ 10^{-3} mbar of typically Argon). Once the ions are trapped, the three parameters are pulsed to the extraction value, elevating the ion energy so that the ions can be efficiently transferred into the ICR cell. It is important to notice that for the trapping, the collision entrance plate is set to a value that creates a small potential barrier. This barrier prevents ions with insufficient kinetic energy from entering into the collision cell.

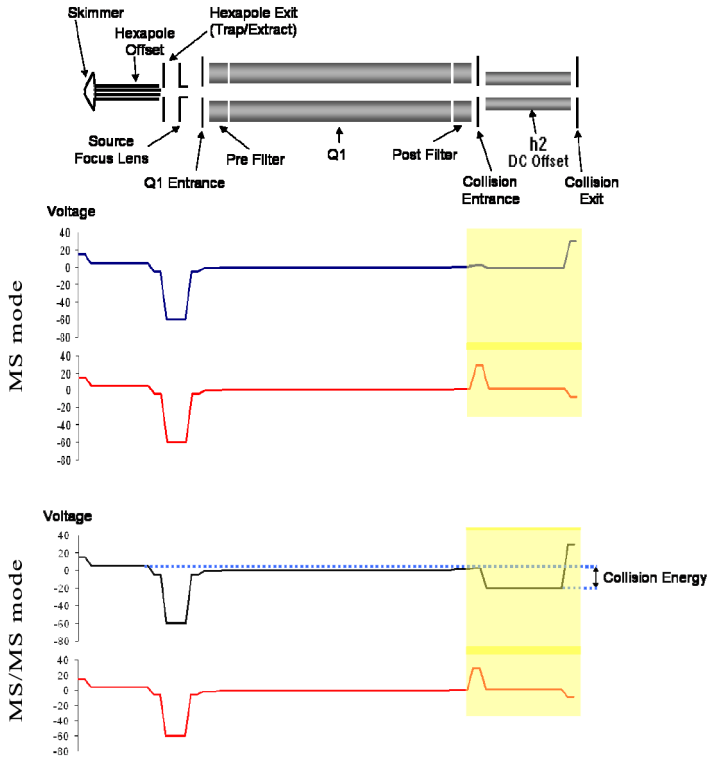

Figure 2.2.10. Voltage profiles for the MS and MS/MS modes [16].

The MS/MS operation (Figure 2.2.10.) is enabled by adjusting the h2 pole bias voltage during trapping. The resulting difference between h1 (source) and h2 pole bias voltages is named the collision energy. It causes the ions to undergo energetic collisions with the gas as they are accelerated into the cell. If the ions gain enough energy, they dissociate and form products.

Here is a picture that summarizes the different times occurring in the source and Qh interface sections:

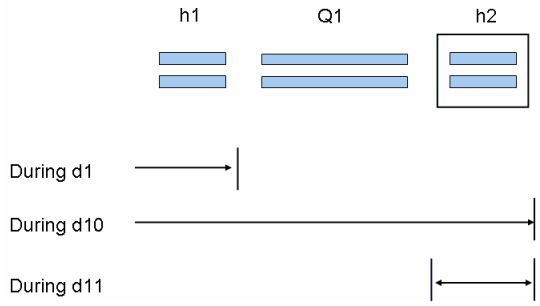

Figure 2.2.11. The different times occurring in the source and Qh interface sections.

d1: accumulation time in the source hexapole h1 (from 0.1 s to ~ 10 s)
d10: accumulation time in the collision hexapole h2 (from 0.01 s to ~ 2 s)
d11: storage time in the collision hexapole h2 (from 0.01 s to 600 s). This time window makes ion/molecule reactions like H/D exchange possible in this hexapole.

The ion transfer optics (Figure 2.2.12.)

After being pulsed out of the collision cell, the ions are accelerated up to ~ 3 kV to focus them through the flow restriction between the differential pumping stages into the ultra high vacuum (UHV). At this stage, ions are steered using two sets of horizontal and vertical beam deflectors (DPL2 – DPL4 and XDFL – YDFL) to correct for the alignment of the instrument. After passing through the gap of the beam valve (separation between the Qh interface and the UHV region), the ions are decelerated and focused through the inhomogeneous fringe field of the superconducting magnet before they reach the ICR cell. DPL2, DPL4, XDFL and YDFL parameters are optimized daily. d2 corresponds to the time during which

the ions are allowed to go from the collision cell to the ICR cell. It depends on the mass to charge ratio of the ions (it must be increased for large m/z ratios – d2 ∈ [0.0011 – 0.0025] s).

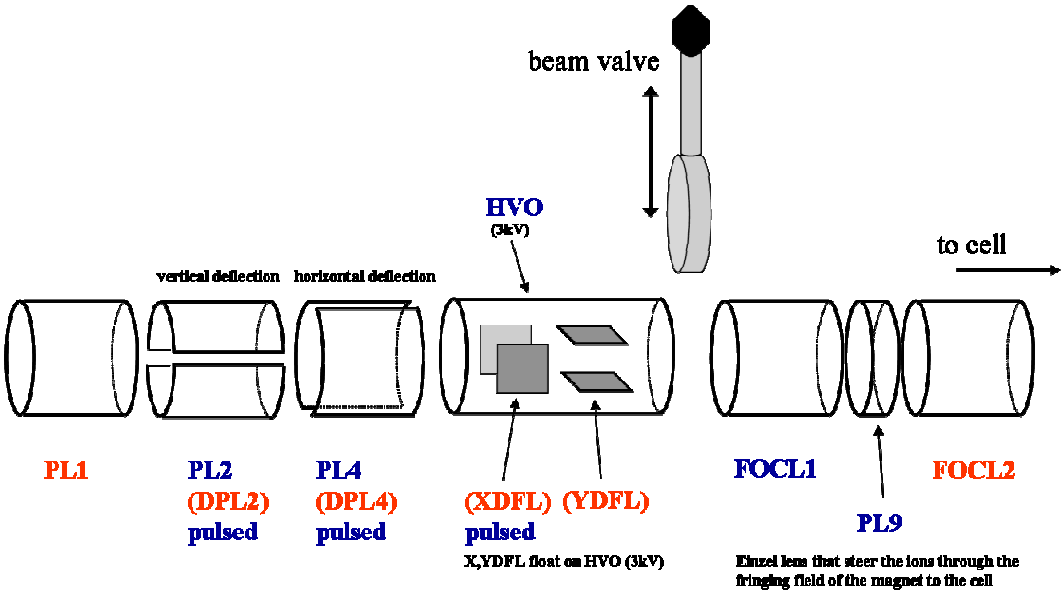

Figure 2.2.12. The ion transfer optics [15].

The analyzer [15,18]

The analyzer, the Infinity Cell™ (Figure 2.2.13.), is a cylindrical ion trap. Ions are confined radially by the high magnetic field (9.4 T) and axially by two trapping plates. Ions are accelerated to higher radii by means of RF excitation across two opposing plates. At the appropriate time, the RF field is turned off and the coherent packet of ions is detected by two other opposing plates.

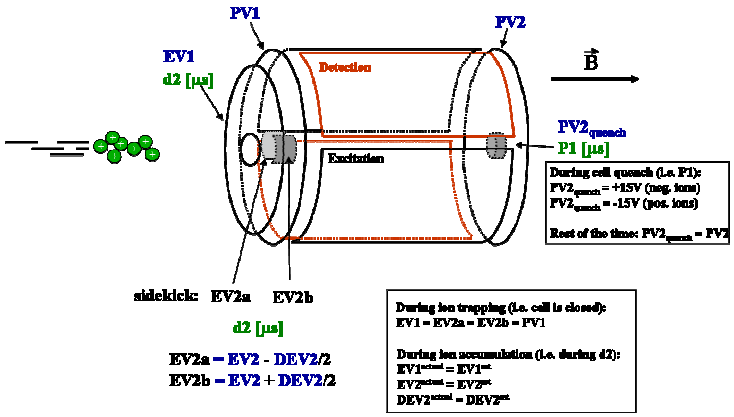

Figure 2.2.13. The detailed Infinity Cell™ of the apex-Qe FTMS [15].

Two trapping methods are available with the apex-Qe: the static and the dynamic trapping (Figure 2.2.14.). For the static trapping, the ions are "injected" in the ICR cell in one time before the detection and they are slightly moved away from the transfer axis when entering the cell. This deflection is due to a potential difference (DEV2) between two small plates EV2a and EV2b located at the entrance of the cell (Figure 2.2.13.). DEV2 determines the width of the ion beam which can be crucial for IRMPD, ECD… experiments.

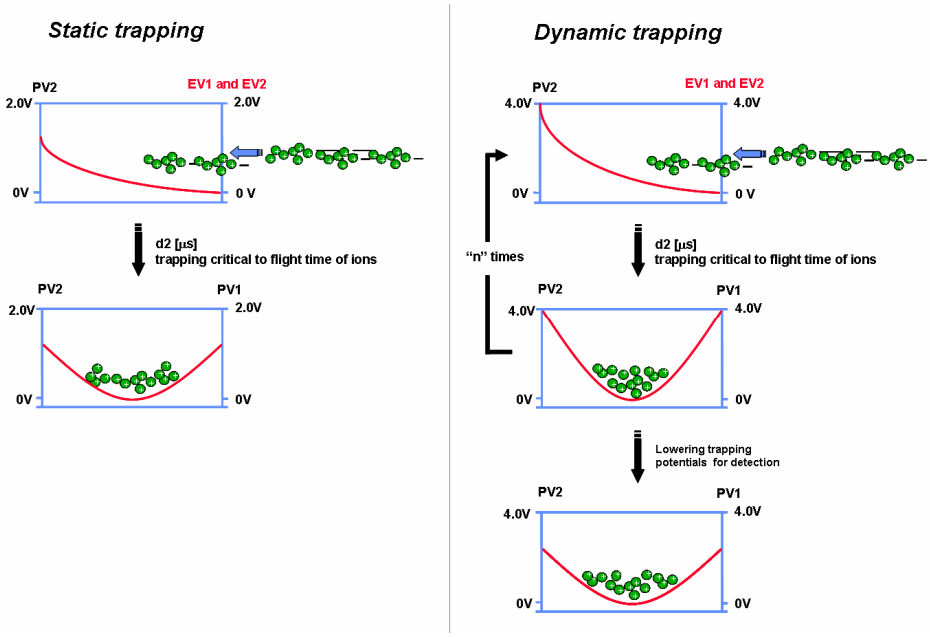

Figure 2.2.14. The two trapping methods: static and dynamic trapping [15].

For the dynamic trapping, the ions are not deflected when entering the ICR cell and they are accumulated in several times before the detection. The steps of source accumulation, accumulation/injection into the collision cell and ejection from the collision cell are repeated “n” times. After “n” repetitions of this loop, the trapping potential which is higher than in the static trapping mode, is lowered in several steps (VSTEP(1)) to a normal value for detection. A “cooling gas” operation can be introduced in the dynamic trapping mode. It is placed in the loop after the ion ejection from the collision cell. This operation corresponds to injecting a pulse of gas, which allows ion cooling during trapping. The gas is pumped out before starting a new loop. The ion accumulation in several times enables to have more ions for detection, resulting in an increase of intensity. However, this approach can decrease the mass accuracy because of the charge space phenomenon.

As previously mentioned, the excitation step corresponds to submitting the ions to an externally amplified RF signal with a frequency matching the cyclotron frequency. This operation excites the ions to a larger cyclotron orbit and provides phase coherence for optimal detection conditions. The frequency range applied during the sweep is automatically determined according to the mass range to analyze. The radiation time (P3) and the attenuation of the frequency amplitude (PL3) are parameters that are accessible to the user. The difference between two successive frequencies that are applied is fixed and equal to 100. The strategy is to fix the radiation time (20 μs) and to optimize the frequency amplitude (around 8 dB). For the optimization, it is important to look not only at the peak intensity but also at the peak shape and at the transient (RF voltage signal before Fourier transform) appearance.

Two detection modes are available with the apex-Qe FTMS: the broadband (bb) and the narrowband (hires) modes. The broadband mode corresponds to a direct detection of the induced signal. The sampling frequency is determined by the software and depends on the lowest m/z ratio that must be detected (the sampling frequency is equal to at least twice that of the lowest m/z ratio in accordance with the Nyquist theorem [19]). For the same file size, the transient will be longer if the lowest m/z ratio is increased. In the narrowband mode, the frequency measurement is more precise but indirect. In a narrow frequency range, the signal is added to another signal that is closed in frequency. It creates a beating with a frequency equal to the frequency difference between the two signals. This

difference, which corresponds to lower frequencies, is analyzed. For a same file size, much larger transients can be recorded. The resolution can be greatly increased. As the m/z ratio range is narrow in the narrowband mode, this latest is not so often used.

2.2.3. Gas-phase techniques related to FT-ICR MS

In order to probe their structure and properties, gas-phase ions can be activated. This chapter presents the different activation techniques that can be used with a FT-ICR mass spectrometer.

Collisional activation and dissociation

Fragmentation coming from energetic collisions between ions and neutral atoms or molecules in the gas phase is very common in mass spectrometry. A wide array of instruments that employ collisional activation has been developed for a variety of objectives. Several elements have to be considered to classify the different CID methodologies:

- the magnitude of energy that can be transferred during a collision
- the distribution of the transferred energy and its variability
- the efficiency of the CID process (defined by its cross section, or its rate constant…)

With the apex-Qe 9.4 T, CID experiments can be performed at different locations in the instrument according to the expected objectives.

- CID in the electrospray source
  The energy of the capillary – skimmer dissociation is a low energy CID around 100 eV (due to voltage difference between capillary exit and skimmer 1, Figure 2.2.9.). All the ions are activated, no ion can be selected.
- CID in the collision hexapole (h2)

The latter corresponds to a slow and low-energy activation. It is a multiple collision process with a timescale of the order of a few hundred microseconds to a few milliseconds, and a collision energy up to 100 eV. As previously explained, ions are accelerated when entering into the collision cell containing usually Ar by adjusting the h2 pole bias value. As a quadrupole mass filter is located before the

collision hexapole, a specific isotopic distribution can be selected for the MS/MS experiment.

- CID in the ICR cell

This corresponds to a very slow activation method. It is characterized by many collisions at a few tens of eV energy and very long timescales. These long timescales are appropriate to achieve very high dissociation efficiency and to access very low dissociation channels. Note that fragment ions do not receive any further internal energy from the resonance excitation, unless they have m/z values that are near the precursor ion one so that further fragmentation is hindered. Target gas molecules are injected into the ICR cell to carry out the collisions and are pumped out before detection. It is important to notice that MS^n tandem experiments can be performed in the ICR cell for the different fragmentation techniques. This is made possible thanks to successive isolations of a peculiar fragment ion by cleanup resonant ejections of other undesired ions.

SORI-CID: Sustained Off-Resonance Irradiation for Collision-Induced Dissociation [20-23]

SORI-CID is a slow and low-energy (< 200 eV) activation method in FT-ICR mass spectrometry. Trapped ions are irradiated at a frequency slightly (~ 500 Hz) above or below the cyclotron frequency. Further to this irradiation, ions undergo series of acceleration/deceleration which result in cycles where their orbital radius in the ICR cell increases and decreases alternatively. Ions reach kinetics energies of a few eV, and in the presence of a target gas, many multiple collisions are required to increase the ion internal energy up to the dissociation threshold. As the ion internal energy increases progressively, the lowest energy pathways for the dissociation of ions are investigated.

IRMPD: InfraRed MultiPhoton Dissociation [23-26]

IRMPD is used to activate and dissociate stable gaseous ions. Molecules can be pumped to high vibrational states and in many cases to their lowest unimolecular reaction thresholds by high-power pulsed infrared lasers through sequential absorption of photons. The mechanism is illustrated in Figure 2.2.15.

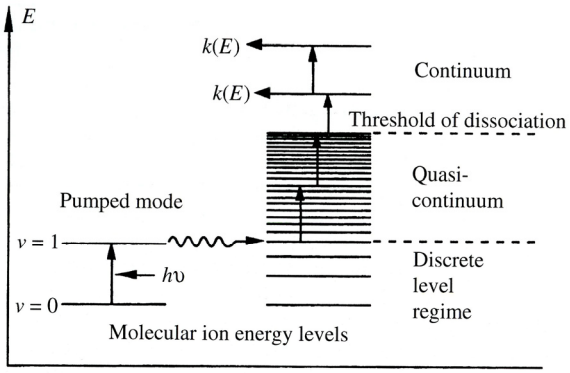

Figure 2.2.15. The infrared multiphoton excitation process [24].

The ions are excited with a CO_2 laser of 10.6 μm wavelength and 25-40 W power. The laser performs irradiation cycles of 200 μs. The user sets the percentage of this cycle where the irradiation is really effective. For example, if the percentage is equal to 50%, ions are irradiated during 100 μs and then trapped without irradiation during 100 μs before a new cycle. The laser beam overlaps the ions stored within the ICR cell and the amount of energy transferred to the ions is a function of the duration of laser irradiation.

Gas-phase spectroscopy techniques

Gas-phase spectroscopy investigates isolated molecules and provides important data for comparison with theory (quantum-chemical calculations). Electronic spectroscopy in molecular beams includes LIF (laser-induced fluorescence), REMPI (resonant-enhanced multiphoton ionization, which allows mass selectivity), and spectral hole burning (double resonance spectroscopy) techniques. The latter measures burnt laser transitions by a decreased signal from a probe laser. Ultraviolet-ultraviolet (UV-UV) double resonance allows the decomposition of a vibronic spectrum into the contributions from different isomers, whereas IR-UV double resonance makes structural assignments possible. According to the used method, the UV and/or the IR wavelengths are fixed or swept and the photofragmentation spectra are recorded. According to the needed wavelength, systems like OPO/OPA or free electron lasers are used. FELIX (Netherlands) and CLIO (France) facilities make such expensive techniques available to the scientific community.

EPD: Electron Photodetachment Dissociation

EPD is a relatively new technique to study absorption properties of gas-phase ions. It relies on the fact that as the size of the ion increases, the excitation energy may relax over an increasing number of degrees of freedom, which prevents an efficient dissociation of the ions following a single photon excitation. Antoine et al. [27] and Gabelica et al. [28] have shown that UV excitation of polypeptides and DNA polyanions induces a resonant electronic excitation of the ions followed by an efficient electron detachment. The electron detachment yield can be used to monitor the excited electronic spectrum of the precursor ions. Moreover, subsequent collisional activation of the produced radical ions gives rise to new fragmentation pathways. This technique combining electron photodetachment and CID is named Electron Photodetachment Dissociation.

BIRD: Black-body Infrared Radiative Dissociation [23,29-32]

BIRD has been developed since the mid-1990s for the study of ion dissociation processes, binding thermochemistry, and structural features of gas-phase ions. It corresponds to a slow heating method in tandem mass spectrometry. It has been demonstrated that ion activation via absorption of blackbody radiation under essentially collision-free conditions can lead to ion dissociation.
For BIRD, ions are trapped for long times (10 – 1000 s) in the ICR cell where they interact with the blackbody radiation field. They absorb and emit photons at rates that depend on the ion structure and the vacuum chamber temperature. Dissociation rates can be varied by changing the temperature. Dissociation of the trapped ions is monitored by sampling the relative abundances of parent and fragment ions as a function of reaction time. The dissociation kinetics exhibit exponential decay of the parent with corresponding appearance of fragments. The dissociation rate can be determined and then used to find the activation parameters of the dissociation reaction, i.e., the activation energy and the preexponential factor.

The apex-Qe 9.4 T is not equipped with a temperature controller for the ICR cell so that BIRD experiments are not feasible on our instrument.

ECD: Electron Capture Dissociation

Electron Capture Dissociation is a relatively new fragmentation method that involves electron-ion interaction. It corresponds to the partial neutralization of multiprotonated proteins with low energy electrons (< 0.2 eV) which causes specific cleavage of the amine bond to form c, z products, in contrast to the amide cleavage b, y products formed by CID, IRMPD… ECD is complementary to traditional tandem mass spectrometry techniques. Disulfide bonds, that are normally stable to vibrational excitation, are preferentially cleaved in ECD. Labile post-translational modifications (phosphorylation [33], O-glycosilation [34], N-glycosilation [35]…) and non-covalent bonds often remain intact after backbone bond dissociation. ECD provides more extensive sequence coverage which has led to the "top-down" approach for protein sequencing, i.e. the fragmentation of intact protein in the gas phase (in contrast with the "bottom up" approach which is based on MS analysis of peptides coming from enzymatic digestion of the intact protein).

The first ECD experiments were reported by R. Zubarev and F.W. Mc Lafferty in 1998-1999 [36,37]. Their proposed mechanism starts with the electron capture by a protonated site of the protein (usually a lysine ε-ammonium group, an arginine guanidinium group, a histidine imidazolium ring, or an N-terminal ammonium group). This capture is a high-energy process that can release an energetic hydrogen atom. This mobile $H^{\cdot}$ atom migrates along the protein towards a carbonyl group yielding an aminoketyl radical intermediate that dissociates by cleavage of the adjacent N-C_α bond. In addition, it is suggested that the aminoketyl radical dissociation occurs before the protein undergoes internal redistribution of vibrational energy. This proposition of non-ergodic dissociation is based on the value of the recombination energy (RE) [38]. The latter is defined as follows:

$$(M + nH^+)^{n+} + e^- \rightarrow (M + (n-1)H^+)^{(n-1)+} + H\bullet + RE \quad (15)$$

$$RE = 13.6[IE(H\bullet)] - PA[(n-1)+] + HA[(n-1)+] \quad (16)$$

where PA and HA are the proton and hydrogen atom affinities. RE is usually between 4 and 7 eV depending on the ionic charge state. Its redistribution over a large number of degrees of freedom would cause only a restricted temperature increase. For example, in a 3 kDa molecule, this increase is estimated to be around 50 – 100 K, which is far less than the typical value of 300 to 600 K for vibrational excitation methods. As follows from equation (16), the recombination

energy does not depend on the molecular mass. The fact that ECD is still efficient for large molecular ions despite the large number of freedom degrees is a strong experimental evidence in favor of the non-ergodic mechanism.

However, the theoretical investigations of F. Tureček [39-41] are not along the same lines. His study shows that dissociation of the N-C_α bonds in aminoketyl radicals and cation radicals occur with unimolecular rate constants > 10^5 s^{-1} at 298 K. This facile N-C_α bond cleavage indicates that it is unnecessary to invoke the hypothesis of non-ergodic behavior for ECD intermediates. In this framework, two mechanisms are proposed (Figure 2.2.16.). The first one considers that the electron is captured by an ammonium group to produce a hypervalent radical. Then, two sub-mechanisms are conceivable for the formation of aminoketyl radical intermediates; H atom transfer competes with N-H bond dissociation followed by recapture of a translationally hot H atom by an adjacent amide carbonyl. Once formed, transient aminoketyl radicals dissociate by cleavage of the C(OH)NH-C_α bond. The second mechanism considers that in the presence of a remote charge, the amide group can exothermically capture an electron in a long-lived electronic state of a valence type. Electron capture by the amide group increases the basicity of the amide carbonyl oxygen (“super-base”) that can exothermically abstract a proton from an amino acid residue and then form an aminoketyl radical that dissociates readily by N-C_α bond cleavage. This mechanism explains why ECD peptide dissociations show low positional selectivity and why electron capture induces efficient N-C_α bond cleavage in systems that lack ammonium and guanidinium groups as hydrogen atom donors.

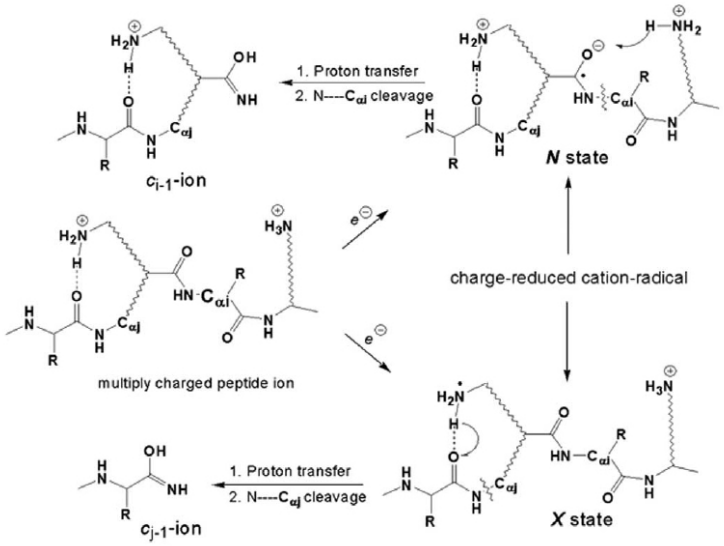

Figure 2.2.16. The two ECD mechanisms proposed by F. Tureček [41].

Other ECD mechanisms have been proposed. O'Connor and coworkers [42] have suggested a dissociation cascade to explain multiple backbone cleavages. The electron capture generates an α-carbon radical that then propagates along the protein backbone. Another suggestion has been advanced. It considers initial capture of the electron in a long-lived high-n Rydberg state followed by conversion to a dissociative electronic state [43,44]. The exact mechanism by which the fragment ions are formed in ECD is, however, still debated.

There are other electron-ion processes that are related to ECD:

- EED (Electronic Excitation Dissociation): it allows product ion detection from singly protonated precursor ions via tandem ionization/dissociation scheme.
- EDD (Electron Detachment Dissociation): it is used for fragmentation of deprotonated ions. It is discussed in more details in a following chapter (see Chapter 6).
- HECD ("Hot" Electron Capture Dissociation): Zubarev and coworkers [45] found that there is a second local maximum for electron capture at around 10 eV. The capture of these ~ 10 eV electrons results in backbone N-C_α cleavage similar to ECD and extensive secondary fragmentation. In particular, secondary fragmentation within leucine and isoleucine side-

chains allows these two isomeric amino acid residues to be distinguished [46].

Figure 2.2.17. illustrates the ECD device of the 9.4 tesla Apex-Qe FT-ICR mass spectrometer. The electrons are emitted by a cylindrical indirectly heated hollow dispenser cathode. It has an outer diameter of 7.6 mm and an inner diameter of 3.5 mm. A heating current of 1.9 A is applied to the heater element located behind the cathode. A lens of 6 mm diameter located in front of the cathode ensures the focalization of the electron beam. The lens voltage has a positive value for ECD experiments (around +1 V) and a negative value for EDD experiments (around -18.8 V). Once produced, the electrons are accelerated using a bias voltage which is around -1 V for ECD experiments and around -18.4 V for EDD experiments. This bias voltage is the DC voltage of the ECD cathode set for the ECD pulse length.

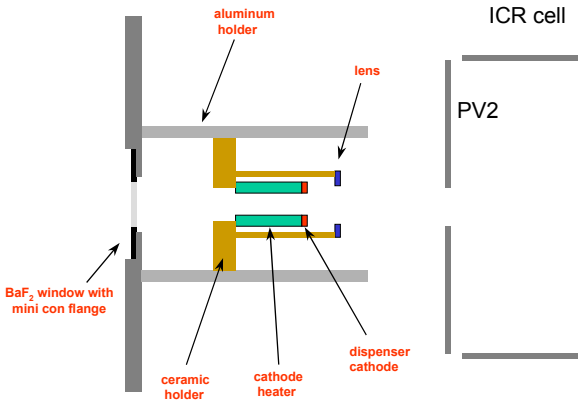

Figure 2.2.17. The hollow dispenser cathode [47].

To obtain information on the intrinsic properties of ionized molecules in a solvent-free environment, ion-molecule reactions (IMR) with neutral reagents can be performed. Gas-phase hydrogen/deuterium exchange is the most famous ion-molecule reaction. It is presented in details in the following section.

References

1. Marshall, A. G.; Hendrickson, C. L.; Jackson, G. S. Fourier transform ion cyclotron resonance mass spectrometry : a primer. *Mass Spectrom. Rev.* **1998,** *17*, 1-35.

2. Guan, S.; Kim, H. S.; Marshall, A. G.; Wahl, M. C.; Wood, T. D.; Xiang, X. Shrink-Wrapping an Ion Cloud for High-Performance Fourier Transform Ion Cyclotron Resonance Mass Spectrometry. *Chemical Reviews* **1994,** *94*, 2161-2182.

3. Marshall, A. G. Fourier Transform Ion Cyclotron Resonance. In *The encyclopedia of Mass Spectrometry: Theory and Ion Chemistry*, Armentrout, P. B., Ed.; Elsevier: Oxford, 2003; pp 131-144.

4. Amster, L. J. Fourier Transform Mass Spectrometry. *J. Mass Spectrom.* **1996,** *31*, 1325-1337.

5. Marshall, A. G.; Grosshans, P. B. Fourier Transform Ion Cyclotron Resonance Mass Spectrometry: The Teenage Years. *Anal. Chem.* **1991,** *63*, 215A-229A.

6. Barrow, M. P.; Burkitt, W. I.; Derrick, P. J. Principles of Fourier transform ion cyclotron resonance mass spectrometry and its application in structural biology. *Analyst* **2005,** *130*, 18-28.

7. Smith, L. G. A new magnetic period mass spectrometer. *Rev. Sci. Instrum.* **1951,** *22*, 115-116.

8. Sommer, H.; Thomas, H. A.; Hipple, J. A. Measurement of e/M by cyclotron resonance. *Physical Review* **1951,** *82*, 697-702.

9. Comisarow, M. B.; Marshall, A. G. Fourier Transform Ion Cyclotron Resonance Spectroscopy. *Chem. Phys. Lett.* **1974,** *25*, 282-283.

10. Comisarow, M. B.; Marshall, A. G. Frequency-sweep Fourier Transform Ion Cyclotron Resonance Spectroscopy. *Chem. Phys. Lett.* **1974,** *26*, 489-490.

11. apex-Qe operator manual, Bruker Daltonics. 2006.

12. Fourier Transform Mass Spectrometry: A Short Course. Part I: Instrumentation and Application Examples, Bruker Daltonics. 2005.

13. Van der Rest, G. Spectrométrie de masse à transformée de Fourier: notions de base et quelques applications, Ecoles de Printemps SFSM - CJSM. 2003.

14. APOLLO™ API Source Users' Manual, Bruker Daltonics. 2000.

15. Fourier Transform Mass Spectrometry: A Short Course. Part II: Operational Facts, Bruker Daltonics. 2005.

16. Q-Interface User and Service Manual, Bruker Daltonics. 2000.

17. Dawson, P. H. *Quadrupole Mass Spectrometry and its Applications;* American Institute of Physics: New York, 1995.

18. Infinity Cell Controler Manual, Bruker Daltonics. 2000.

19. Marshall, A. G.; Verdun, F. R. *Fourier transforms in NMR, optical, and mass spectrometry: A user's handbook;* Elsevier: New York, 1990.

20. Wells, J. M.; McLuckey, S. A. Collisional Activation and Dissociation. In *The Encyclopedia of Mass Spectrometry: Theory and Ion Chemistry*, Armentrout, P. B., Ed.; Elsevier: Oxford, 2003; pp 441-451.

21. Gauthier, J. W.; Trautman, T. R.; Jacobson, D. B. Sustained off-resonance irradiation for collision-activated dissociation involving Fourier transform mass spectrometry. Collision-activated dissociation technique that emulates infrared multiphoton dissociation. *Anal. Chim. Acta* **1991,** *246*, 211-225.

22. Senko, M. W.; Speir, J. P.; McLafferty, F. W. Collisional Activation of Large Multiply Charged Ions Using Fourier Transform Mass Spectrometry. *Anal. Chem.* **1994,** *66*, 2801-2808.

23. McLuckey, S. A.; Goeringer, D. E. Slow Heating Methods in Tandem Mass Spectrometry. *J. Mass Spectrom.* **1997,** *32*, 461-474.

24. Riveros, J. M. Infrared Photodissociation. In *The Encyclopedia of Mass Spectrometry: Theory and Ion Chemistry*, Armentrout, P. B., Ed.; Elsevier: 2003; pp 262-271.

25. Little, D. P.; Speir, J. P.; Senko, M. W.; O'Connor, P. B.; McLafferty, F. W. Infrared Multiphoton Dissociation of Large Multiply Charged Ions for Biomolecule Sequencing. *Anal. Chem.* **1994,** *66*, 2809-2815.

26. Peiris, D. M.; Cheeseman, M. A.; Ramanathan, R.; Eyler, J. R. Infrared Multiple Photon Dissociation Spectra of Gaseous Ions. *J. Phys. Chem.* **1993,** *97*, 7839-7843.

27. Antoine, R.; Joly, L.; Tabarin, T.; Broyer, M.; Dugourd, P.; Lemoine, J. Photo-induced formation of radical anion peptides. Electron photodetachment dissociation experiments. *Rapid Commun. Mass Spectrom.* **2007,** *21* (2), 265-268.

28. Gabelica, V.; Rosu, F.; Tabarin, T.; Kinet, C.; Antoine, R.; Broyer, M.; De Pauw, E.; Dugourd, P. Base-dependent electron photodetachment from negatively charged DNA strands upon 260-nm laser irradiation. *J. Am. Chem. Soc.* **2007,** *129* (15), 4706-4713.

29. Dunbar, R. C. Black-body Infrared Radiative Dissociation (BIRD). In *The Encyclopedia of Mass Spectrometry: Theory and Ion Chemistry*, Armentrout, P. B., Ed.; Elsevier: Oxford, 2003; pp 371-381.

30. Williams, E. R. Tandem FTMS of Large Biomolecules. *Analytical Chemistry News & Features* **1998,** 179A-185A.

31. Schnier, P. D.; Klassen, J. S.; Strittmatter, E. F.; Williams, E. R. Activation Energies for Dissociation of Double Strand Oligonucleotide Anions: Evidence for Watson-Crick Base Pairing in Vacuo. *J. Am. Chem. Soc.* **1998,** *120*, 9605-9613.

32. Dunbar, R. C.; McMahon, T. B. Activation of Unimolecular Reactions by Ambient Blackbody Radiation. *Science* **1998,** *279*, 194-197.

33. Stenballe, A.; Jensen, O. N.; Olsen, J. V.; Haselmann, K. F.; Zubarev, R. A. Electron capture dissociation of singly and multiply phosphorylated peptides. *Rapid Commun. Mass Spectrom.* **2000,** *14*, 1793-1800.

34. Mirgorodskaya, E.; Roepstorff, P.; Zubarev, R. A. Localization of O-glycosilations sites in peptides by electron capture dissociation in a Fourier transform mass spectrometer. *Anal. Chem.* **1999,** *71*, 4431-4436.

35. Hakansson, K.; Cooper, H. J.; Emmet, M. R.; Costello, C. E.; Marshall, A. G.; Nilsson, C. L. Electron capture dissociation and infrared multiphoton dissociation MS/MS of an N-glycosylated tryptic peptide to yield complementary sequence information. *Anal. Chem.* **2001,** *73*, 4530-4536.

36. Zubarev, R. A.; Kelleher, N. L.; McLafferty, F. W. Electron Capture Dissociation of Miltiply Charged Protein Cations. A Nonergodic Process. *J. Am. Chem. Soc.* **1998,** *120*, 3265-3266.

37. Zubarev, R. A.; Kruger, N. A.; Fridriksson, E. K.; Lewis, M. A.; Horn, D. M.; Carpenter, B. K.; McLafferty, F. W. Electron Capture Dissociation of Gaseous Multiply-Charged Proteins Is Favored at Disulfide Bonds and Other Sites of High Hydrogen Atom Affinity. *J. Am. Chem. Soc.* **1999,** *121*, 2857-2862.

38. Zubarev, R. A.; Haselmann, K. F.; Budnik, B.; Kjeldsen, F.; Jensen, F. Towards an understanding of the mechanism of electron-capture dissociation: a historical perspective and modern ideas. *Eur. J. Mass Spectrom.* **2002,** *8*, 337-349.

39. Turecek, F.; Syrstad, E. A. Mechanism and Energetics of Intramolecular Hydrogen Transfer in Amide and Peptide Radicals and Cation-Radicals. *J. Am. Chem. Soc.* **2003,** *125*, 3353-3369.

40. Turecek, F. N-Cα Bond Dissociation Energies and Kinetics in Amide and Peptide Radicals. Is the Dissociation a Non-ergodic Process? *J. Am. Chem. Soc.* **2003,** *125*, 5954-5963.

41. Syrstad, E. A.; Turecek, F. Toward a General Mechanism of Electron Capture Dissociation. *J. Am. Soc. Mass Spectrom.* **2005,** *16*, 208-224.

42. Leymarie, N.; Costello, C. E.; O'Connor, P. B. Electron Capture Dissociation Initiates a Free Radical Reaction Cascade. *J. Am. Chem. Soc.* **2003,** *125*, 8949-8958.

43. Zubarev, R. A.; Horn, D. M.; Fridriksson, E. K.; Kelleher, N. L.; Kruger, N. A.; Lewis, M. A.; Carpenter, B. K.; McLafferty, F. W. Electron Capture Dissociation for Structural Characterization of Multiply Charged Protein Cations. *Anal. Chem.* **2000,** *72*, 563-573.

44. Breuker, K.; Oh, H.; Lin, C.; Carpenter, B. K.; McLafferty, F. W. Nonergodic and conformational control of the electron capture dissociation of protein cations. *PNAS* **2004,** *101*, 14011-14016.

45. Kjeldsen, F.; Haselmann, K. F.; Budnik, B. A.; Jensen, F.; Zubarev, R. A. Dissociative capture of hot (3-13 eV) electrons by polypeptide polycations: an efficient process accompanied by secondary fragmentation. *Chem. Phys. Lett.* **2002,** *356*, 201-206.

46. Kjeldsen, F.; Haselmann, K. F.; Sorensen, E. S.; Zubarev, R. A. Distinguishing of Ile/Leu amino acid residues in the PP3 protein by (hot) electron capture dissociation in Fourier transform ion cyclotron resonance mass spectrometry. *Anal. Chem.* **2003,** *75*, 1267-1274.

47. Dispenser Cathode and Hollow Dispenser Cathode for Electron Capture Dossociation. Operational Manual, Bruker Daltonics. 2003.

2.3. Hydrogen/deuterium exchange coupled to mass spectrometry

Hydrogen/deuterium (H/D) exchange is a chemical reaction in which a covalently bonded hydrogen is replaced by a deuterium atom or vice versa (back-exchange). The method is based on the fact that the parts of the molecule that are accessible to the solvent (in solution) or to the surrounding gas (in gas phase) can exchange. The exchange of hydrogens occurs at specific rates that depend on the molecular structure and the solvent/gas accessibility. Hydrogen/deuterium exchange provides information on molecular structure and dynamics.

2.3.1. Hydrogen/deuterium exchange in solution [1-5]

Hydrogen/deuterium exchange was first introduced by Linderstrøm-Lang and colleagues in the mid-1950s who realized that amide hydrogen exchange rates should reflect the presence of hydrogen bonded structure [6]. In the 1960s, Englander used the advent of liquid scintillation technology to study native protein exchange rates by hydrogen/tritium exchange [7]. In 1979, Rosa and Richards enhanced the special resolution by combining proteolysis with HPLC [8]. Englander et al. improved the protocol by lowering the temperature of the separation step to reduce back-exchange in the early 1980s [9]. In 1993, Zhang and Smith were the first ones to combine H/D exchange with mass spectrometry, using FAB for ionization [10]. Johnson and Walsh first reported the use of electrospray ionization in 1994 [11]. Since the mid-1990s, improvements of the various steps of H/D exchange coupled with mass spectrometry have been reported.

Most of the H/D exchange experiments in solution have been performed to study proteins. The theoretical and experimental parts are described below in the case of proteins. They could be transposed for studying other bio-systems like DNA, RNA, oligosaccharides…

2.3.1.1. Theory

They are three kinds of hydrogen atoms in proteins: (1) hydrogens covalently bonded to carbon that essentially do not exchange, (2) the ones on the side chains that exchange very fast and typically can not be detected, and (3) hydrogens at the backbone amide positions that exchange at rates that can be measured (i.e., ~ 10^{-2} – 10^{-3} s^{-1} at pH = 2.6). As the backbone amide hydrogens are involved in the formation of hydrogen bonds in secondary structural elements (alpha helices, beta sheets), their exchange rates reflect the structure and the structural stability.

The exchange reaction is strongly pH dependent. It is both acid and base catalyzed. The rate constant, k_{ex}, can be expressed as the sum of two terms,

$$k_{ex} = k_H \left[H^+\right] + k_{OH} \left[OH^-\right] \quad (1)$$

where k_H and k_{OH} are the rate constants for acid- and base-catalyzed exchange respectively. At physiological pH, base-catalyzed exchange is the dominant mechanism. The isotopic exchange rate, k_{ex}, for polyamine is given as a function of pH in Figure 2.3.1. The high pH sensitivity of H/D exchange rates requires careful control of pH. Furthermore, this sensitivity is the basis for quenching (dramatic decrease in speed) H/D exchange, thereby making the exchange analysis easier. For backbone amide hydrogens, the average minimum reaction rate occurs at approximately pH 2.6.

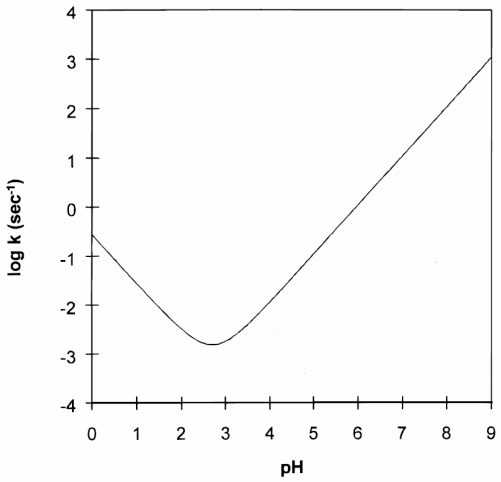

Figure 2.3.1. Rate constant for isotopic exchange of hydrogen located on peptide amide linkages in polyalanine presented as a function of pH [4].

The rate constant for hydrogen/deuterium exchange at each individual amide linkage in a normally folded protein, k_{ex}, can be written as follows

$$k_{ex} = k_f + k_u \tag{2}$$

where k_{ex} is expressed as the sum of the contribution of exchange from folded (k_f) and unfolded (k_u) forms of the protein. This corresponds to a two-process model that is illustrated in Figure 2.3.2.

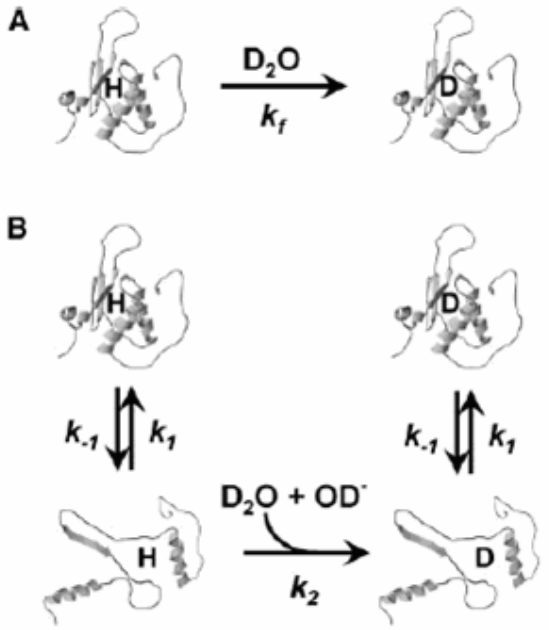

Figure 2.3.2. Models for hydrogen exchange into the folded form (A) and into the unfolded forms (B) [1].

The rate constant of H/D exchange occurring through unfolded forms of proteins depends on the exchange rate constant of the amide hydrogen for the completely unfolded polypeptide (k_2), as well as the unfolding dynamics described by k_1 and k_{-1}. Then k_{ex} is written,

$$k_{ex} = \frac{k_1 \cdot k_2}{k_1 + k_{-1} + k_2}. \tag{3}$$

Most of the literature assumes stable structure ($k_{-1} \ll k_1$) and starts with Eq(4)

$$k_{ex} = \frac{k_1 \cdot k_2}{k_1 + k_2}. \tag{4}$$

For most proteins at neutral pH and in the absence of denaturants, $k_{-1}>>>k_2$ (bimolecular exchange (EX2) kinetics) and the rate constant for isotopic exchange is given by,

$$k_{ex} = \frac{k_1}{k_{-1}} k_2 = K_{unf} \cdot k_2 . \quad (5)$$

Measuring k_{ex} and calculating k_2 (Bai et al. 1993) leads to direct determination of the equilibrium constant and hence ΔG^0 for protein unfolding process, which may be localized to a particular element of secondary structure or regional domain, or may include the entire molecule.

Under some destabilizing conditions (addition of denaturants, extreme pH, high temperature…), $k_2>>>k_{-1}$ (monomolecular exchange (EX1) kinetics), so that the rate of intrinsic amide hydrogen exchange is much faster than the rate of refolding, and the measured isotopic exchange rate constant, k_{ex}, may be used to determine the rate of protein unfolding as $k_{ex} = k_1$. (6)

EX2 kinetics may be seen as involving many rapid and random visits to a state capable of exchange. However, the probability of exchange during a single visit is small. EX1 kinetics is described as a cooperative unfolding event involving several residues, all of which exchange rapidly before refolding occurs. Some proteins may contain regions that undergo EX1 and EX2 kinetics simultaneously. Regions in which H/D exchange occurs by either EX1 or EX2 kinetics can be identified by characteristic isotope patterns in mass spectra. Whereas EX2 exchange leads to a random distribution of deuterium within a peptide, EX1 exchange yields peptides that have regions that contain either no deuterium or are fully deuterated leading to a bimodal isotope pattern in the mass spectra [12].

2.3.1.2. Method

Several methods can be used to introduce deuterium into a protein. The two primary ones are dilution and gel filtration. For dilution, a solution of protein in a protonated buffer is diluted 15-20 times with a deuterated buffer that has a deuterium content of minimum 99%. This raises the deuterium level to more than 95%. As this labeling method dilutes the original sample, more proteins are required or a rapid concentration can be performed with HPLC before the detection. The gel filtration method works by introducing the protein in a protiated buffer into a small spin column that has been equilibrated with the same but deuterated buffer. The protein is eluted out the column into a receiving tube thanks to a brief spin in a centrifuge. The time it takes to elute the protein from a

specific bed volume at a specific centrifuge speed must be known and can be tested with a visible protein.

The actual labeling step, when the protein is in deuterium, can also be done in several ways. There are two kinds of labeling experiments: continuous labeling and pulse labeling (Figure 2.3.3.). In continuous labeling experiments, the protein is exposed to deuterium while the populations of folded and unfolded species are in flux, a flux that results from protein motions induced by some population-altering forces (i.e. addition of denaturant, change in pH or temperature, ligand binding…). After various times, the reaction is quenched by moving an aliquot of sample to quenched buffer. For pulsed-labeling, the protein sits under specific conditions for a period of time, and then a short pulse of deuterium is introduced and the reaction is quenched. The major difference between these two methods is that unlike continuous labeling where a cumulative summary of the populations of the protein is observed, the pulsed-labeling corresponds to an instantaneous snapshot of the protein populations. Continuous labeling is most useful for monitoring slow unfolding transitions as the minor contribution of the unfolded state is integrated over time. Pulse labeling is used to identify protein folding mechanisms and probe kinetic intermediate states in folding reactions.

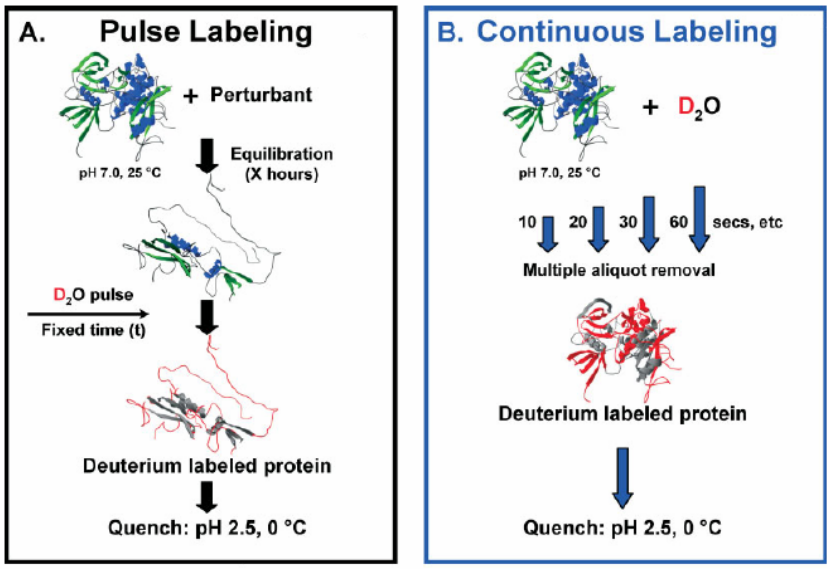

Figure 2.3.3. The two labeling methods: the pulse labeling (A) and the continuous labeling (B) [1].

Rapid mixing systems can be used to investigate events that are as fast as 10 ms such as rapid exchange of surface amide hydrogens or protein folding events. Protein folding can also be studied with a type of pulse labeling where a denaturated protein is allowed to refold. After given refolding times, the protein is submitted to a deuterium-labeling pulse and then quenched. Such analyses can be automated with quench-flow devices.

The kinetics of amide H/D exchange can be measured by several methods. Nuclear magnetic resonance (NMR) spectroscopy and mass spectrometry are the most commonly used ones. The principal advantage of NMR spectroscopy is that it gives residue-specific information for all the residues in the protein simultaneously. A prior assignment of the spectrum for the protein in question is of course needed. The limitations of NMR are its modest sensitivity and its difficulties with proteins having molecular masses higher than 50 kDa. Mass spectrometry has several advantages over NMR: there is no practical size limitation, much less material is needed (concentrations in the sub-micromolar range), and the data are usually faster obtained and interpreted. The same spatial resolution as in NMR can be obtained with the use of MS/MS techniques (see below).

Once the labeling step is done, the next task is to identify which amides have been deuterated. The most used technique to localize the deuteriums is the proteolytic digestion. As this protein digestion and the subsequent analysis of the deuterium levels are done with protiated solvents, undesirable exchanges of deuterium for hydrogen (back-exchange) occur which results in the loss of some of the label. To minimize the back-exchange, sample analysis must be as rapid as possible and be done at 0°C. So the digestion is performed at the quenched pH and at 0°C since lowering both the pH and the temperature results in a ~ 10^5 reduction in the exchange rate. Usually, the obtained peptic digest is separated by HPLC at 0°C before introduction into the mass spectrometer. It can be noticed that different adjustments can be made to compensate for back-exchange. Several adjustment calculations have been described (Zhang and Smith, 1993; Resing, Hoofnagle and Ahn, 1999; Hoofnagle, Resing and Ahn, 2004). The best acid-protease for digestion of the deuterium labeled proteins is pepsin. Although it is a non-specific protease (it generally cleaves at hydrophobic residues), and so the sites of backbone cleavage cannot be predicted from the amino acid sequence, pepsin cuts always at the same place under identical conditions providing reproducibility.

Forest et al. demonstrated the use of other acidic proteases but pepsin was still the most efficient one [13]. The use of multiple enzymes can be very useful as it produces overlapping fragments which increase the spatial resolution. A disadvantage of peptic digestion of large proteins is that it produces undesirable long peptides (>15 residues long) rather than desirable short ones (5 – 10 residues). The obtained resolution is limited by the size and degree of overlap of the peptic peptides. In most case, only a few site-specific hydrogen exchange rates at individual amino acid residues can be determined.

To improve spatial resolution, MS/MS techniques can be used. The major obstacle for this approach is, however, the occurrence of intramolecular migration of amide hydrogen upon activation of the gaseous peptides (or protein; one could think of fragmenting the whole protein without prior proteolytic digestion. This allows the constraints of controlling back-exchange during the digestion and the separation by HPLC to be avoided, but a high performance MS/MS method must be used to obtain a high sequence coverage, a high spatial resolution). This migration is named scrambling. Dr. Jørgensen's team is working for several years on this problematic subject. They have investigated the extent of intramolecular backbone amide hydrogen migration upon different MS/MS techniques using a peptide probe [14] with a unique selective deuterium incorporation. They showed that CID is accompanied by extensive intramolecular hydrogen migration due to an induced mobility of protons/deuterons in the vibrationally excited protonated peptide ions [15]. In contrast, ECD of gas-phase peptide cations was demonstrated to proceed with a very low level of amide hydrogen scrambling [16]. Jørgensen et al. [17] also demonstrated that MALDI ISD (In Source Decay) of selectively labeled peptides yielded fragment ions that retained their solution deuteration pattern. More recently, they have shown that Electron Transfer Dissociation (ETD) in a quadrupole ion trap has retained the site-specific solution-phase deuterium incorporation pattern and has allowed for localization with single residue resolution [18].

Figure 2.3.4., adapted from [1], illustrates the different possibilities for the deuterium localization in mass spectrometry experiments. It can be noticed that this Figure also illustrates global exchange analysis. In this kind of experiments, the quenched samples are directly analyzed with ESI-MS or MALDI-MS. The data provide a global picture of how the protein behaves in the deuterated solvent.

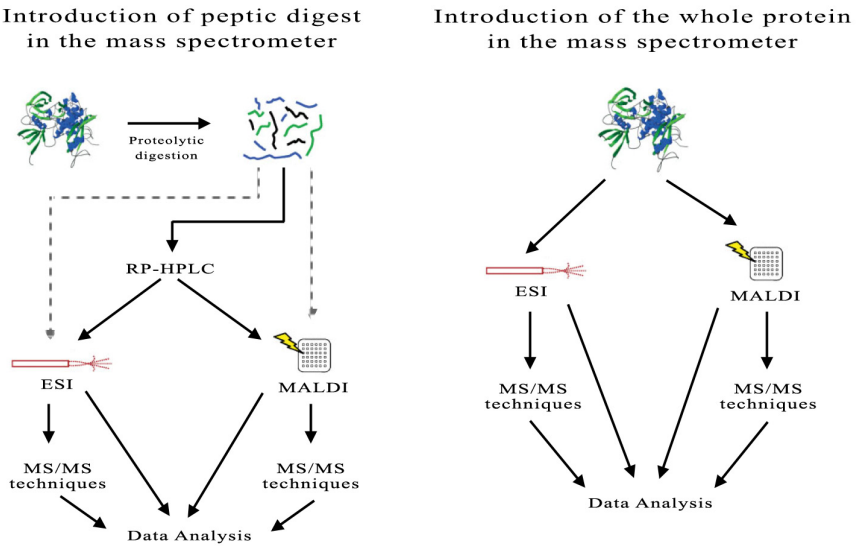

Figure 2.3.4. The different possibilities for hydrogen/deuterium exchange mass spectrometry analyses adapted from [1].

2.3.1.3. Applications

Studies of protein folding/unfolding have traditionally been performed using the more conventional spectroscopy-based techniques: NMR, IR, CD and Fluorescence [19]. H/D exchange can also be used to characterize the folding pathways of proteins, by refolding the protein under exchange or back-exchange conditions. H/D exchange can be used to determine the sequence of various folding events. The parts of the structure that fold rapidly will be protected quickly and so will not (back-) exchange, whereas parts that fold later in the pathway will be exposed for longer periods of time and will show a larger extent of (back-) exchange. It is clear that H/D exchange – MS experiment is even more valuable when combined with conventional methods. An example of such a protein folding study is presented below: the article is currently in preparation.

Folding studies of lysozyme from bacteriophage lambda by Alexandre DiPaolo[1], Dorothée Balbeur[2], E. De Pauw[2], Christina Redfield[3] and André Matagne[1].

[1]Enzymology Laboratory, Centre for Protein Engineering, University of Liège, Belgium
[2]Mass Spectrometry Laboratory, University of Liège, Belgium
[3]Department of Biochemistry, University of Oxford, UK

Refolding of hen lysozyme with its four native disulphide bonds intact has provided a lot of information about the general principles of the protein folding process [20,21]. Nevertheless, the presence of the four native disulphide bonds at the initiation of the refolding process represents a situation that is distinct from that of the folding process *in vivo*. Lysozyme from bacteriophage lambda (λ lysozyme) is an 18 kDa enzyme containing 158 amino acids. Its three-dimensional structure, determined by X-ray methods, shows some of the structural features common to all lysozymes; in particular, it consists of two domains connected by a helix with the catalytic residue, Glu19, located at the interface between the two domains. Interestingly, in contrast to the widely studied C-type lysozymes, λ lysozyme lacks disulfide bridges [22]. It is therefore of interest to study the folding properties of λ lysozyme. As a first step in this study we have assigned the NMR spectrum of λ lysozyme using 15N-labelled protein and standard sequential assignment methodologies. Hydrogen-deuterium exchange (HEX) experiments carried out on native lysozyme, have allowed identification of protected amides in all regions of secondary structure. The folding process followed by quenched-flow hydrogen exchange labelling monitored by ESI-MS and NMR, and by stopped-flow optical methods, has indicated that λ lysozyme refolds according to simple two-state kinetics, and thus differs markedly from the complex process observed for hen lysozyme [23].

As previously said, several optical methods were used. The refolding kinetics of the λ lysozyme was especially followed by stopped-flow intrinsic tryptophan fluorescence at 20°C. Tryptophan fluorescence monitors formation of tertiary structures during refolding. Refolding was initiated by 10-fold dilution of the denaturated protein (in 3 M guanidine chloride) into a HEPES buffer 50 mM, pH = 7 with 0.3 M guanidine chloride. The kinetic curve (Figure 2.3.5.) has been fitted to the sum of two exponentials characterized by rate constants equal to 7.5 s^{-1} and 0.4 s^{-1}.

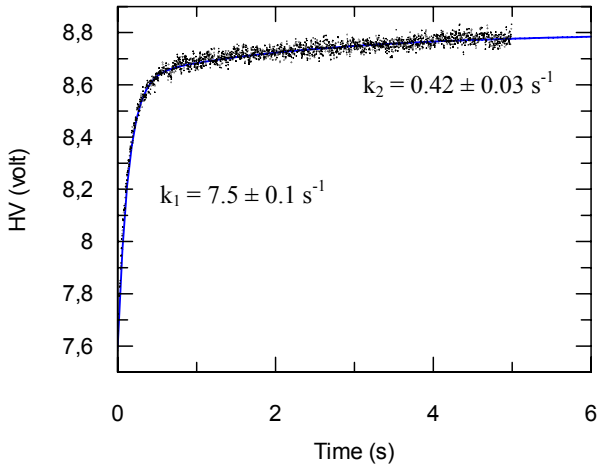

Figure 2.3.5. Intrinsic tryptophan fluorescence: kinetic refolding of λ lysozyme.

The λ lysozyme refolding kinetics was also followed by circular dichroism (CD) in the far UV (222 nm). This technique gives information about the secondary structure content (α-helix) of the protein. The same experimental conditions as for the fluorescence experiments were used. Two phases were also observed. They were characterized by rate constants similar to that of fluorescence (Figure 2.3.6.). The blue square in Figure 2.3.6. corresponds to the circular dichroism signal that the denaturated protein in 0.3 M guanidine chloride should have at the beginning of the refolding experiment (t = 0 s). From Figure 2.3.6., it can be deduced that 80 % of the α-helices are formed during the time-out of the experiment (2.8 ms).

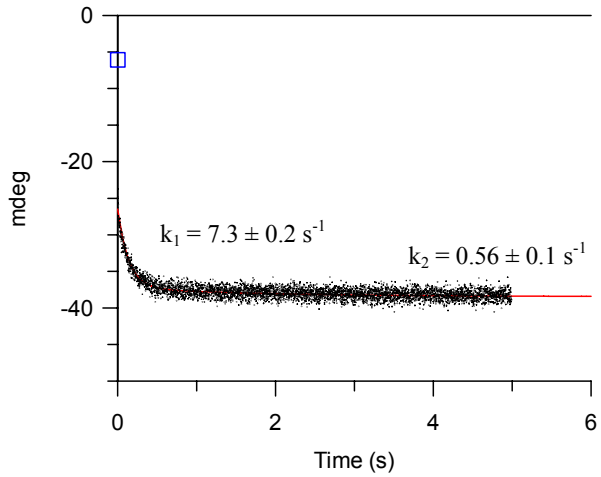

Figure 2.3.6. Circular dichroism: kinetic refolding of λ lysozyme.

The last optical method that was used to follow the refolding kinetics of the λ lysozyme is the fluorescence shift of ANS (8-anilino-1-naphtalen sulfonic acid). ANS is a fluorescent compound that fixes on hydrophobic parts of a protein which changes its fluorescent spectrum. This fluorescent shift allows the condensation of non-polar groups and therefore structural modifications due to refolding to be monitored. During the refolding, precisely during the time-out of the experiment, an increase of the fluorescence intensity was observed compared to ANS alone which could be attributed to the formation of a "molten globule" intermediate. Such an intermediate is characterized by a high content in secondary structures without tertiary structure. Rate constants similar to the previously obtained ones were derived.

Several experiments of H/D exchange at the equilibrium were performed on native λ lysozyme that was dissolved in D_2O. H/D exchange was monitored using HSQC NMR spectrometry. More than 75 amide groups were observed coming principally from α-helices and β-sheets. These protected amides served as probes for the H/D exchange refolding kinetics.

The folding process followed by quenched-flow hydrogen exchange labeling was done at 20°C using a QFM 5 (Bio-Logic, Claix, France) rapid mixing quench flow apparatus. The experimental procedure is illustrated in Figure 2.3.7. λ Lysozyme was initially dissolved in 3 M guanidine deuterochloride in D_2O at pH = 7, leading to complete deuteration and substitution of all exchangeable hydrogens by deuteriums. Refolding was initiated by a 10-fold dilution of this solution into 20 mM sodium acetate, pH = 5-6 in H_2O. At this pH, the half-life of amide exchange is about 16 s, so negligible labeling occurred during this step. After variable refolding times (3.5 – 2000 ms) the solution was diluted again with a volume 5 times that of the initial protein solution of 0.2 M sodium borate, pH = 10. This initiated the labeling. After 8.4 ms, the labeling pulse was stopped by further dilution with a volume again 5 times that of the initial volume of protein solution, of 0.5 M acetic acid in H_2O. The final pH was equal to 4.4 at which the exchange in the native protein is very slow. The protein samples were washed by 10 cycles of concentration/dilution with NH_4Ac 50 mM pH = 4.5 (with formic acid) or deuterated NaAc 10 mM pH = 4.5 (with NaOD and DCl) to a final concentration of 50 μM or 0.5 mM respectively for MS and NMR.

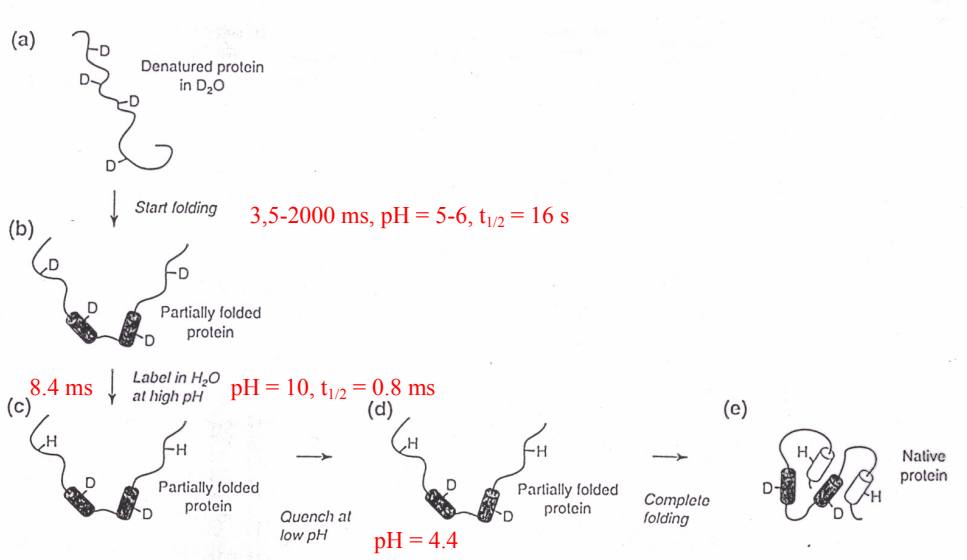

Figure 2.3.7. The procedure of the quenched-flow hydrogen exchange labeling experiments.

Refolding kinetics was monitored by HEX and ESI-MS, and by HEX and NMR. Figure 2.3.8. illustrates the ESI mass spectra of the 9+ charge state of λ lysozyme at different refolding times. Two well defined populations with different masses, i.e., different deuterium contents were detected. They correspond to the unprotected protein (P_0) at 1982 m/z, and the fully protected protein (P_{45}) at 1987 m/z. The absence of any intermediate suggested a cooperative refolding pathway. The refolding kinetics followed by HEX and ESI-MS is showed in Figure 2.3.9. The kinetics of disappearance and appearance of the two species (P_0 and P_{45}) were characterized by only one phase whose kinetic rate constant corresponded to the first phase obtained in fluorescence, CD and ANS fluorescence experiments.

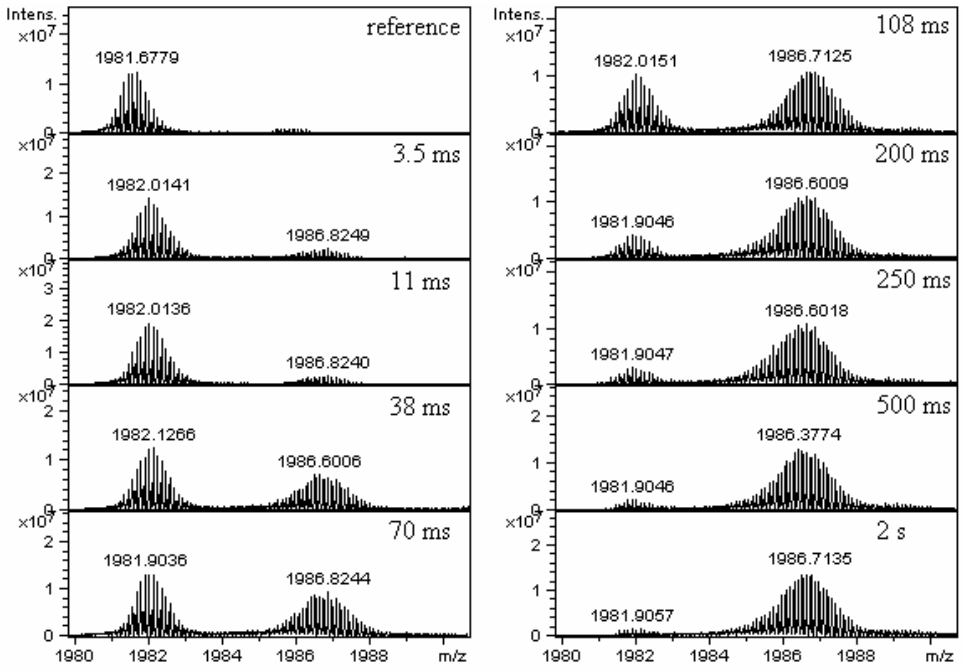

Figure 2.3.8. ESI mass spectra of the 9+ charge state of λ lysozyme at different refolding times.

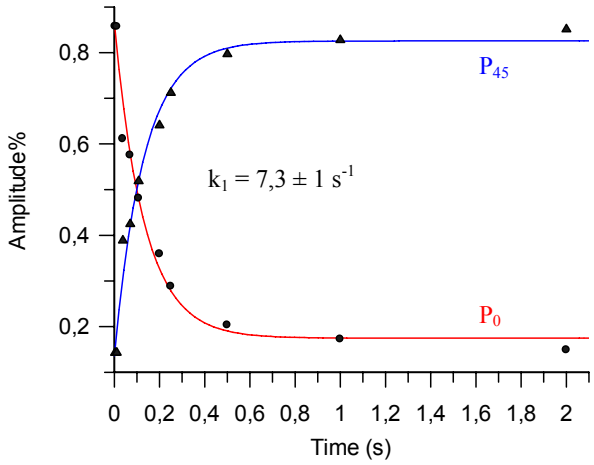

Figure 2.3.9. Refolding kinetics of λ lysozyme followed by HEX-ESI-MS experiments.

HEX was also monitored by NMR which allowed the time-course of protection from exchange at individual amide sites to be followed. The curves showed in Figure 2.3.10. represent the average of a single exponential fit to the time-course for individual amides in most of the α-helices. These single exponential curves were characterized by a kinetic rate constant around 6-7 s^{-1}.

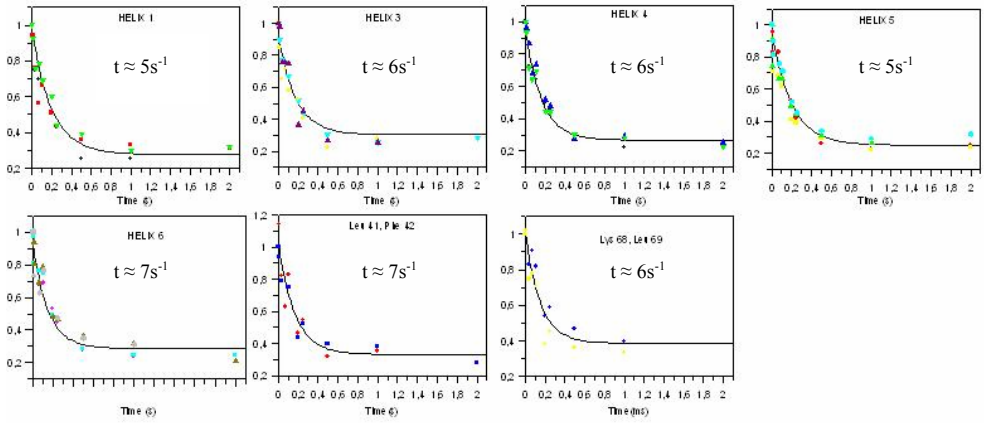

Figure 2.3.10. Time-course of protection of amide groups from H/D exchange monitored by NMR.

In conclusion, HEX experiments on native λ lysozyme showed that protected amides are located in most of the major regions of secondary structure. These protected amides were used as probes to follow the refolding of the protein using quenched-flow HEX monitored by ESI-MS and NMR. The time scale of refolding of the different structural regions was identified. Moreover, the quenched-flow labeling experiments indicated that the time-courses of disappearance of P_0 and appearance of P_{45} are indistinguishable and that λ lysozyme folding is a highly cooperative two states process, with no significant population of partially folded species between the unfolded and native states. Stopped-flow optical experiments, however, revealed the occurrence of a second minor slow phase ($k = 0.4\ s^{-1}$), which was not observed in HEX experiments, and which remains unexplained yet.

Another application of H/D exchange is the characterization of binding interactions [24,25]. These interactions that include protein: small molecule, protein: polypeptide, protein: lipid, protein: nucleic acid, and protein: protein binding, are crucial for protein folding, stability, association and function. The

exchange reaction needs to be carried out with the isolated partners and with the complex. The exchanging regions can then be compared. Interpretation of the data for locating the binding sites of specific ligands on target proteins must be done with caution as binding is know to cause changes in protein dynamics and conformation at sites distant from the actual binding site. Here also combination with conventional methods is useful as much information about the conformational changes is obtained with NMR structural analyses.

There are plenty of examples of H/D exchange – MS experiments being used to study the organization and dynamics of complex molecular assemblies. One of them is the study of the thrombin-thrombomodulin (TM) complex by Mandell et al. [26] with the aim of mapping the TM binding interface. Thrombin is a protease that participates in blood clotting by catalyzing the proteolytic cleavage of two different substrates; fibrinogen and protein C. Thrombomodulin binding to thrombin alters the substrate specificity from fibrinogen to protein C for promoting anti-coagulation. Residues distant from the active site, including the anion binding exosite 1 (ABE1) are postulated to be used by thrombin to recognize specific protein substrates. A model indicated that ABE1 also corresponds to the binding site of thrombomodulin. H/D exchange – MS experiments showed that the most solvent inaccessible amides were within ABE1 and so constitute the interface core. Additional protected amides were found within the ABE1 flanking regions. An allosteric response whereby constraints for protein C binding should be removed was also suspected as both surface and buried amides located along a pathway to the active site showed decreased solvent accessibility.

Two specific methods have also been developed to study protein-ligand interactions. The first one is named PLIMTEX (Protein-Ligand Interaction by Mass Spectrometry, Titration and H/D EXchange) [27]. It is applied to determine conformational change, binding stoichiometry and affinity of protein-ligand interaction. The second one is named SUPREX (Stability of Unpurified Proteins from Rates of H/D EXchange) [28,29]. It measures the change in a protein's thermodynamic stability upon ligand binding. This measured change in stability (i.e., the binding free energy) is then used to calculate the dissociation constant (Kd value) of the protein-ligand complex. This SUPREX method that utilizes MALDI mass spectrometry is also used to study protein alone and so to calculate the protein's folding free energy (i.e., ΔG_f^0) [30].

H/D exchange – MS can also be used to monitor how protein modifications such as phosphorylation (post-translational modification) modulate activity of an enzyme, where modification of a single residue may lead to local and/or long-range changes. For example, Ahn's group [31] demonstrated that upon phosphorylation near the active site cleft, the mitogen-activated protein kinase, ERK2, showed both regions of increased solvent accessibility and regions of decreased solvent accessibility. The residues undergoing the changes were located more than 10 Å from the site of phosphorylation.

It is important to notice that solution H/D exchange – MS experiment localizing the incorporated deuteriums has not yet been reported for nucleic acids. This is probably due to the difficulties of finding quench and digestion conditions with limited back-exchange. The injection of the deuterated whole biomolecule followed by MS/MS methods could be considered, but up to now no high sequence coverage has been obtained for large nucleic acid characterized by non-covalent intramolecular interactions.

2.3.2. Hydrogen/deuterium exchange in the gas phase [32-34]

Gas-phase hydrogen/deuterium exchange reaction is one of the most known ion-molecule reactions. Unlike activation methods (MS/MS) that provide the means to fragment proteins (biopolymers) and identify their amino acid sequences (primary structure information), ion-molecule reactions can provide information on the ion's secondary structure.

The first use of gas-phase H/D exchange reactions was reported by Hunt et al. in 1972 for counting the active hydrogens in organic compounds [35]. Twenty years later, Guarini et al. reported one of the first uses of H/D exchange reactions for larger molecules such as fungichromin, concanamycin B, and other macrocyclic antibiotics [36]. From this time, gas-phase H/D exchange reactions have been used extensively to distinguish between isomeric species, to deduce reaction mechanism and to infer structural features of complex biomolecules.

It is important to notice that for protein, contrary to solution H/D exchange where only the exchange rates of backbone amide hydrogens can be measured, all exchangeable hydrogens (hydrogens that are bound to heteroatoms) can be probed

in the gas phase. This can lead to additional information, but it can also complicate the results analysis for large proteins.

2.3.2.1. Theory

H/D exchange reactions are generally described by a multiple-well potential energy surface [37-39]. This model allows, if it is possible, multiple H/D exchanges between the reagent and the molecule. The potential energy surface is illustrated in Figure 2.3.11. It corresponds to a simplified mechanism that consists of three steps: the initial formation of a loose hydrogen-bonded complex, complete or partial transfer of the proton to the molecule, and finally, dissociation of the complex to yield either the original or the exchanged molecule. To observe the exchange, the energy made available by complex formation must be sufficient to overcome the barrier of the proton transfer. This barrier highly depends on the proton affinity difference between the unprotonated reagent and the molecule. The H/D exchange is more probable when the proton affinities of the reagent and the analyte molecule are similar. Ausloos and Lias [39,40] have suggested for protonated monofunctional compounds that H/D exchange reactions do not occur when the proton affinities differ by more than 20 kcal/mol. Several exceptions to this limit have been observed for polyfunctional molecules such as amino acids and peptides. The feasibility of an exchange reaction between species whose neutrals differ greatly in proton affinities was suspected to be due to a lowering of the barrier to proton transfer with the complex thanks to the formation of multiple hydrogen bonds (Campbell et al., 1994; Gard et al., 1993; Green et al., 1995; Gur et al., 1995).

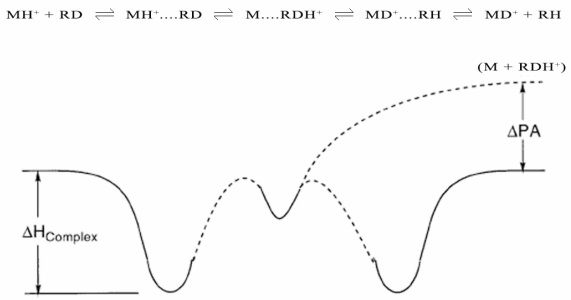

Figure 2.3.11. The simplified mechanism for H/D exchange between a protonated molecule (M) and a deuterating reagent (R). Adapted from [33].

Campbell et al. [41] examined the reactions of glycine oligomers with D_2O, CD_3OD, CD_3COOD, and ND_3. Based on their results and on semi-empirical modeling, they proposed several H/D exchange mechanisms that depend on the nature of the hydrogen involved and on the basicity of the reagent. The rate and extent of H/D exchange were observed to increase with increasing the basicity of the reagent, $D_2O < CD_3OD < CD_3COOD < ND_3$. The five mechanisms that are illustrated in Figure 2.3.12. are: the onium ion, relay, salt bridge, flip-flop, and tautomer mechanisms. They were proposed to explain the H/D exchange reactions of oligomers whose proton affinities differ from the reagent by more than 20 kcal/mol, the H/D exchange of oligomers characterized by a proton affinity difference less than 20 kcal/mol being supposed to principally occur via formation of a strongly hydrogen-bonded species. An onium mechanism is proposed for exchange with basic reagents. A proton is transferred from the N-terminus with simultaneous solvation of the resultant ammonium ion. In the relay mechanism, the deuterating reagent shuttles a proton from the N-terminus to a less basic site (amide oxygen). This mechanism is favorable for reagent such as D_2O, with too low proton affinity for proton transfer from the peptide. In the salt bridge mechanism, the H/D exchange occurs at the C-terminus with basic reagents. The hydroxyl proton is transferred to the exchange gas, creating an ion pair that is stabilized by a nearby charge center. Other exchange of the C-terminus but with less basic reagents will be slower and will probably occur via a multicenter exchange: the flip-flop mechanism. The tautomer mechanism corresponds to a proton transfer from the N-terminus to an amide carbonyl in concert with transfer of the amide proton to the reagent base. This mechanism is favorable for ND_3 as the ammonium ion can be solvated by the tautomerized peptides.

Green and Lebrilla [42] also proposed a relay mechanism since they showed the role of proton-bridged intermediates in the gas-phase H/D exchange of diamines, peptides and proteins. Wyttenbach et al. were also in favor of a relay mechanism to explain the gas-phase H/D exchange of polypeptide ions [43]. Molecular dynamics simulations indicated that water-polypeptide collision complexes had long lifetimes (more than 1 ns) during which the water molecules sampled the peptide surface. Semiempirical and ab initio calculations indicated that for energetic reasons gas-phase H/D exchange has to occur via a relay mechanism involving both a charge site and a nearby basic site. The surface accessibility of the charged sites and the basic sites, and the distances between them were considered to be important factors.

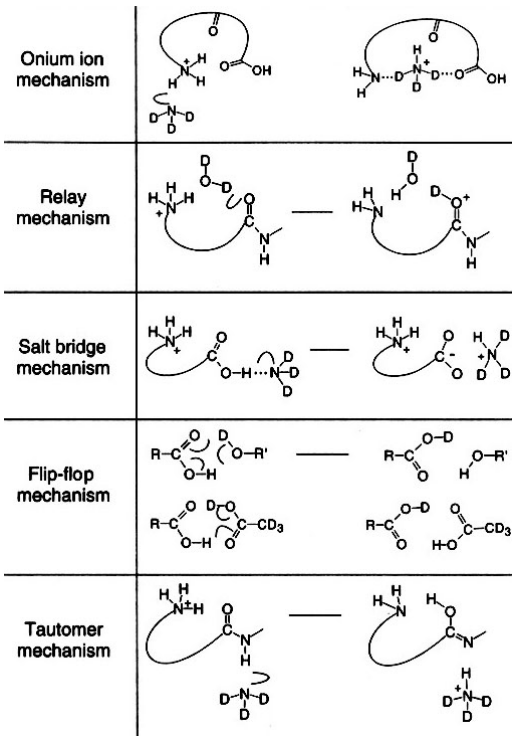

Figure 2.3.12. Summary of the proposed H/D exchange mechanisms for the glycine oligomers with reagent bases. Adapted from [41].

2.3.2.2. Method

The most extensively used exchange reagents are D_2O, CD_3OD and ND_3. Gas-phase H/D exchange reactions can be performed in any mass spectrometer provided the existence of introduction system for the deuterating gas. Gas-phase H/D exchange can be performed for example in an electrospray source. Note that in this case, solution H/D exchange at the droplet surface is also expected. For better control over the reaction conditions, especially for the study of thermalized ions over a wide range of gas temperature, such instruments like flowing drift tube and ion mobility spectrometers must be used. Any instrument that possesses a collision cell or an ion guide can performed H/D exchange with a relatively good control over the reaction conditions. Ion trap instruments allow for a large number of collisions and are well suited to examine H/D exchange over a wide range of exchange rates (10^{-9} – 10^{-13} $cm^3molecule^{-1}s^{-1}$). Thanks to long ion trapping times, radio frequency manipulation of the ion population, nondestructive ion detection,

and high mass resolution, FT-ICR instruments are perhaps the best suited ones. Exchange reactions during one hour at pressures in the range 10^{-9}-10^{-8} mbar can be performed in the ICR cell. This corresponds to 10^6 – 10^7 collisions between the analyte and the deuterating gas. These conditions facilitate studies of the kinetics of very slow exchange processes. It is important to notice that the deuterating gas must be pumped out of the ICR cell before the detection to guarantee high resolution. If the FT-ICR mass spectrometer is equipped with a collision cell, H/D exchange reactions at higher pressure (10^{-3} mbar) can be performed with guaranteed high resolution detection in the ICR cell. Exchange reactions can be performed during up to 600 s. In these conditions, faster H/D exchange occurs and complete exchange can be observed for peptides and small proteins.

2.3.2.3. Applications

In this section, several examples are showed to illustrate the versatility of gas-phase H/D exchange reactions for a wide range of applications.

According to the difference in extent of H/D exchange, gas-phase H/D exchange coupled to mass spectrometry can resolve different gas-phase protein conformations. Freitas et al. [44] used this tool with the aim of evaluating the effectiveness of H/D exchange to study the mechanism by which proteins are affected when they are transferred from solution to the gas phase. Their results demonstrated the capability of H/D exchange FT-ICR MS to resolve different gas-phase protein conformations for subsequent isolation and characterization. They showed that the 5+ and 6+ charge states of ubiquitin displayed broad distributions of conformations with from 0 to 80 % of deuterium incorporation. In contrast, higher charge state, 7-11+ and 13+, showed a single major isotopic distribution, whereas the 12+ charge state was separated into two isotopic distributions of comparable abundance.

A comparison of gas- and solution-phase conformations seems to be very useful to provide insight into the nature of the folding process, particularly as far as the role of the solvent is concerned. Although gas- and solution-phase structures correspondence has not yet been established, hydrophobic effects and hydrogen bonding to the solvent are suspected to explain some difference between gas- and solution-phase. Recently, Wright at al. [45] have studied the conformations of gas-phase ions of ubiquitin, cytochrome c, apomyoglobin and β-lactoglobulin

produced from two different solution conformations with the aim of answering the question: do solution conformations of proteins affect the properties of gas-phase ions formed by ESI? The two different solutions were named the "H" and "H_c" states. The "H" state corresponds to a solution with low pH and 50 % alcohol where proteins adopt denaturated conformations with the loss of tertiary structure. The "H_c" state corresponds to a 90 % alcohol solution where proteins form helical denaturated states with high α-helix content. The "H_c" state is characterized by lower solution H/D exchange levels than those of the "H" state. Both states in solution produce the same charge states in ESI. The ion conformations were studied with cross section measurements and gas-phase H/D exchange. Both the gas-phase collision cross sections and H/D exchange levels of ions of cytochrome c, apomyoglobin and β-lactoglobulin showed no difference for the "H" and "H_c" states. Although the states showed the same cross section, ubiquitin ions produced from the "H_c" state exchanged fewer (13 %) hydrogens that ions produced from the "H" state. This suggested that for ubiquitin, the gas-phase protein ions retained some memory of their solution conformation, but it is not so clear as the cross sections showed that the ions formed from the unfolded "H" and "H_c" states had considerable folded structures.

Recently, Somogyi [46] has described a relatively simple method to obtain information on fragment ion structure. In this method, peptides or proteins are fragmented by SORI-CID and also by SORI/Resonance excitation ion activation. The fragment and the precursor ions then all undergo H/D exchange with D_2O or CD_3OD under the same experimental conditions. The observed relative differences in H/D exchange rates can be correlated to different ion structures: cyclic versus linear, fixed charged versus mobile proton… This SORI(RE)-CID method is useful to probe heterogenous fragment and/or precursor ion populations and to provide information on peptide fragmentation pathways.

2.3.3. From H/D exchange isotope patterns to rate constants

When multiple exchanges are possible, the decay of the parent peak and the growth of the peaks at M + n corresponding to the products containing several deuteriums are observed. The extraction of the H/D exchange rate constants from the molecular ion patterns can be summarized in two steps: (1) determination of the deuterium contents from the molecular ion patterns, and (2) extraction of the exchange rate constants from the time evolution of the deuterium level.

2.3.3.1. Determination of the deuterium contents from the molecular ion patterns

Except if the monoisotopic peak of the full H and full C_{12} molecule is isolated before the H/D exchange reaction (which is possible for example in gas-phase H/D exchange experiments), the H/D exchange patterns of the molecular ion have contributions from the natural abundance of isotopes (C_{13}, etc.) and from an excess of deuteriums. Several methods have been proposed to determine the deuterium levels from the molecular ion patterns.

In the most used approach, the deuterium content is determined from the centroid of the molecular ion isotopic peaks. The deuterium incorporation percentage is given by the following equation (adapted from Zhang and Smith [10]):

$$\%\,\text{deuterium incorporation} = \frac{\left\langle m/z \right\rangle_{obs} - \left\langle m/z \right\rangle_{0}}{\left\langle m/z \right\rangle_{100\%} - \left\langle m/z \right\rangle_{0}} \cdot 100\% \qquad (7)$$

where $\langle m/z \rangle_{obs}$, $\langle m/z \rangle_{0}$ and $\langle m/z \rangle_{100\%}$ are respectively the isotope-averaged centroids after a particular exchange time, prior to H/D exchange, and after full deuteration of all exchangeable hydrogens. Note that for H/D exchange experiments in solution, this equation takes into account the deuterium gain/loss during digestion and HPLC fractionation since it includes the analysis of the non-deuterated and fully deuterated forms of the molecule.

The other proposed methods work with all the isotopic exchange distribution and try to eliminate the “natural” isotopic distribution due to less abundant isotopes of C, S, O, N… in order to determine the number of incorporated deuteriums.

For example, before the data fitting, all the data can be normalized and isotopic corrections to peak intensities can be made based on the theoretical amount of C_{13}

in each peak. For doing that, one procedure is to substract the isotopic natural abundance distribution from the lowest-mass peak that corresponds to abundance of the species with the least number of deuteriums and then iterate to higher numbers of deuteriums [10]. This subtraction method is mathematically equivalent to the Gauss-Jordan elimination used to find the solutions of simultaneous linear equations or to calculate the inverse of a square positive-definite matrix. With this method, if the experimental data are noisy or the number of variables is large, the result obtained is not very reliable.

Another procedure is named the least-squares (LSQ) fitting for the linear coefficients (i.e., the deuterium distribution) [47]. The mass spectrum of a deuterated molecule is expressed as linear combinations of mass-shifted natural isotopic abundance. The deuterium distribution is obtained as the solution of a set of linear equations, which generally requires the inversion of a matrix. Note that if the matrix is not well conditioned, the inverse becomes unstable and the results are not reliable.

Our H/D exchange mass spectra were analyzed by a least-squares method. Because, currently, no software is commercially available for deconvoluting H/D exchange mass spectra, an in-house software was developed. This software utilizes the known isotopic distribution (percentage of each peak) of the non-deuterated ion. Moreover, it is considered that the ion with a fixed number, X, of exchanged hydrogens has the same isotopic distribution but shifted by X/z unit. The software determines, at each reaction time, the composition of each deuterated species that best fits the experimental isotopic distribution. For solving the simultaneous linear equations, the in-house software uses the approach of the pseudo-inverse matrices. The function “void LASVD_IP” from the Lapack library is used to obtain the pseudo inverse of the matrix of the coefficients for the linear system of equations to be solved. This pseudo inverse in turns gives the solution by multiplication with the vector containing the relative intensities of the measured signal. Because no constraint with respect to sign is included in the software, a deconvoluted mass spectrum with negative-magnitude abundances can be obtained for large exchange distributions with low signal signal-to-noise ratios. A collaboration with the Center for Statistics from the Hasselt University for designing a deconvolution software is under way. A first adjustment has just been developed. It corresponds to a least-squares method with a constraint for respecting the positive sign. The used reasoning is similar to the in-house software

one except that the theoretical isotopic distribution of the non-deuterated ion is used instead of the experimental one. The algorithm set fmincon ("Optimization" toolbox from MatLab) is used to solve the simultaneous linear equations.

The last proposed approach is the maximum entropy method (MEM) [47]. The main advantage of MEM is that the inversed matrix need not be generated directly, which avoids the instability problem. On the contrary to the LSQ method, MEM produces all positive deuterated species abundances. The abundance distribution of molecules with monoisotopic masses $m_{min} < m < m_{max}$ can be described as the probability that a given molecule has monoisotopic mass m. The abundance distribution can therefore be recast as a probability distribution. Entropy is a measure of the amount of uncertainty in a probability distribution. The maximum entropy method finds the highest-entropy solution subject to the error range of the original experimental data.

Direct solution of linear equations and the least-squares method give very good results if the experimental mass spectral signal-to-noise ratio is high and the number of monoisotopic masses (i.e. deuterated species) to be determined is small. On the other hand, the MEM method is most useful for mass spectra with large number of peaks, but it can require much more computation time than the least-squares method.

2.3.3.2. Extraction of the H/D exchange rate constants from the time evolution of the deuterium level

Several approaches have been proposed to analyze the kinetics of the H/D exchange reactions. They are briefly described in the following paragraphs.

- The system is treated as series of successive reactions [48]

As previously explained, the data consist of the deuterium distribution, i.e., the relative intensities of the deuterated species D_0, D_1… D_n, where D_n represents a protonated/deuterated species with n deuteriums, measured at different reaction times. A series of n + 1 coupled differential equations (from (8) to (12) for a system with four exchangeable hydrogen atoms associated with the exchange reactions (13) – (16)) are solved iteratively in a fitting procedure. This yields the

rate constants k_n and n + 1 curves that describe the time behavior of the different deuterated species.

$$-\frac{d[D_0]}{dt} = k_1[D_0][CH_3OD] - k_{-1}[D_1][CH_3OH] \quad (8)$$

$$\frac{d[D_1]}{dt} = k_1[D_0][CH_3OD] - k_{-1}[D_1][CH_3OH] - k_2[D_1][CH_3OD] - k_{-2}[D_2][CH_3OH] \quad (9)$$

$$\frac{d[D_2]}{dt} = k_2[D_1][CH_3OD] - k_{-2}[D_2][CH_3OH] - k_3[D_2][CH_3OD] - k_{-3}[D_3][CH_3OH] \quad (10)$$

$$\frac{d[D_3]}{dt} = k_3[D_2][CH_3OD] - k_{-3}[D_3][CH_3OH] - k_4[D_3][CH_3OD] - k_{-4}[D_4][CH_3OH] \quad (11)$$

$$\frac{d[D_4]}{dt} = k_4[D_3][CH_3OD] - k_{-4}[D_4][CH_3OH] \quad (12)$$

$$D_0 + CH_3OD \underset{k_{-1}}{\overset{k_1}{\rightleftharpoons}} D_1 + CH_3OH \quad (13)$$

$$D_1 + CH_3OD \underset{k_{-2}}{\overset{k_2}{\rightleftharpoons}} D_2 + CH_3OH \quad (14)$$

$$D_2 + CH_3OD \underset{k_{-3}}{\overset{k_3}{\rightleftharpoons}} D_3 + CH_3OH \quad (15)$$

$$D_3 + CH_3OD \underset{k_{-4}}{\overset{k_4}{\rightleftharpoons}} D_4 + CH_3OH \quad (16)$$

The values k_1, k_2… k_n represent the rate constants for the respective exchange of one, two… n hydrogens. In reality, these rate constants are combinations of rate constants made up of n exchange sites. This treatment can be modified to obtain the rate constants for the individual sites. This approach is presented in the next point. Note that although reactions (13) – (16) are written as reversible reactions, in reality equilibriums are not necessarily obtained during the experiment.

Moreover, the reverse reactions (back-exchange) can not be considered according to the used experimental method. For example, when the reactions are performed in a continuous flow of exchange gas, the amount of produced protonated gas can be considered as negligible.

- Determination of the rate constants for the individual sites [49]

In this approach, the system is treated as a series of independent reactions, each following a simple first order rate law:

$$S_j(H) + CH_3OD \underset{k_{-j}}{\overset{k_j}{\rightleftharpoons}} S_j(D) + CH_3OH \qquad (17)$$

where S_j represents the j^{th} exchange site. In this case, the observed populations of the D_n species are related to the populations of the individual sites. For example, in a system of three independent sites, a, b and c, the D_2 species actually represents the sum of three species, D_{ab} , D_{ac} and D_{bc}. The rate constants that are determined iteratively represent the rate of exchange of individual sites.

The two previous approaches have the disadvantage that they are computationally time-consuming. For more than about fifteen exchanges, they become impractical. The next treatment is perhaps less precise, but it is more simple to carry out.

- Logarithm of the number of hydrogens remaining versus time

In this data handling procedure, the number of exchangeable hydrogens in the ion has to be known, and the logarithm of the number of hydrogens remaining has to be plotted according to the reaction time. If one or more straight sections are observed, then the rate constants and the number of exchanged hydrogens associated with them can be obtained from the slope and the intercept respectively. This approach can be applied to any number of exchangeable hydrogens but a large number of time points are required.

References

1. Wales, T. E.; Engen, J. R. Hydrogen exchange mass spectrometry for the analysis of protein dynamics. *Mass Spectrom. Rev.* **2006,** *25*, 158-170.

2. Busenlehner, L. S.; Armstrong, R. N. Insights into enzyme structure and dynamics elucidated by amide H/D exchange mass spectrometry. *Arch. Biochem. Biophys.* **2005,** *433*, 34-46.

3. Hoofnagle, A. N.; Resing, K. A.; Ahn, N. G. Protein Analysis by Hydrogen Exchange Mass Spectrometry. *Annu. Rev. Biophys. Biomol. Struct.* **2003,** *32*, 1-25.

4. Smith, D. L.; Deng, Y.; Zhang, Z. Probing the Non-covalent Structure of Proteins by Amide Hydrogen Exchange and Mass Spectrometry. *J. Mass Spectrom.* **1997,** *32*, 135-146.

5. Krishna, M. M. G.; Hoang, L.; Lin, Y.; Englander, S. W. Hydrogen exchange methods to study protein folding. *Methods* **2004,** *34*, 51-64.

6. Hvidt, A.; Nielsen, S. O. Hydrogen exchange in proteins. *Adv. Protein Chem.* **1966,** *21*, 287-386.

7. Englander, S. W. A hydrogen exchange method using tritium and sephadex: its application to ribonuclease. *Biochemistry* **1963,** *2*, 798-807.

8. Rosa, J. J.; Richards, F. M. An experimental procedure for increasing the structural resolution of chemical hydrogen-exchange measurements on proteins: application to ribonuclease S peptide. *J. Mol. Biol.* **1979,** *133*, 399-416.

9. Englander, J. J.; Rogero, J. R.; Englander, S. W. Protein hydrogen exchange studied by the fragment separation method. *Anal. Biochem.* **1985,** *147*, 234-244.

10. Zhang, Z.; Smith, D. L. Determination of amide hydrogen exchange by mass spectrometry: A new tool for protein structure elucidation. *Protein Science* **1993,** *2*, 522-531.

11. Johnson, R. S.; Walsh, K. A. Mass-Spectrometric Measurement of Protein Amide Hydrogen-Exchange Rates of Apo-Myoglobin and Holo-Myoglobin. *Protein Science* **1994,** *3* (12), 2411-2418.

12. Miranker, A.; Robinson, C. V.; Radford, S. E.; Aplin, R. T.; Dobson, C. M. Detection of transient protein-folding populations by mass spectrometry. *Science* **1993,** *262*, 896-900.

13. Cravello, L.; Lascoux, D.; Forest, E. Use of different proteases working in acidic conditions to improve sequence coverage and resolution in hydrogen/deuterium exchange of large proteins. *Rapid Commun. Mass Spectrom.* **2003,** *17*, 2387-2393.

14. Rand, K. D.; Jorgensen, T. J. D. Development of a Peptide Probe for the Occurrence of Hydrogen ($^1H/^2H$) Scrambling upon Gas-Phase Fragmentation. *Anal. Chem.* **2007,** *79*, 8686-8693.

15. Jorgensen, T. J. D.; Gardsvoll, H.; Ploug, M.; Roepstorff, P. Intramolecular Migration of Amide Hydrogens in Protonated Peptides upon Collisional Activation. *J. Am. Chem. Soc.* **2005,** *127*, 2785-2793.

16. Rand, K. D.; Adams, C. M.; Zubarev, R. A.; Jorgensen, T. J. D. Electron Capture Dissociation Proceeds with a Low Degree of Intramolecular Migration of Peptide Amide Hydrogens. *J. Am. Chem. Soc.* **2008,** *130*, 1341-1349.

17. Bache, N.; Rand, K. D.; Roepstorff, P.; Jorgensen, T. J. D. Gas-Phase Fragmentation of Peptides by MALDI in-Source Decay with Limited Amide Hydrogen ($^1H/^2H$) Scrambling. *Anal. Chem.* **2008,** *80*, 6431-6435.

18. Zehl, M.; Rand, K. D.; Jensen, O. N.; Jorgensen, T. J. D. Electron Transfer Dissociation Facilitates the Measurement of Deuterium Incorporation into Selectively Labeled Peptides with Single Residue Resolution. *J. Am. Chem. Soc.* **2008,** *130*, 17453-17459.

19. van Mierlo, C. P. M.; Steensma, E. Protein folding and stability investigated by fluorescence, circular dichroism (CD), and nuclear magnetic resonance (NMR) spectroscopy: the flavodoxin story. *J. Biotechnol.* **2000,** *79* (3), 281-298.

20. Dobson, C. M.; Evans, P. A.; Radford, S. E. Understanding how proteins fold: the lysozyme story so far. *Trends Biochem. Sci.* **1994,** *19*, 31-37.

21. Matagne, A.; Dobson, C. M. The folding process of hen lysozyme: a perspective from the "new view". *Cell. Mol. Life Sci.* **1998,** *54*, 363-371.

22. Evrard, C.; Fastrez, J.; Declercq, J. P. Crystal structure of the lysozyme from bacteriophage Lambda and its relationship with V and C-type lysozymes. *J. Mol. Biol.* **1998,** *276*, 151-164.

23. Matagne, A.; Jamin, M.; Robinson, C. V.; Radford, S. E.; Dobson, C. M. Thermal unfolding of an intermediate is associated with non-Arrhenius kinetics in the folding of hen lysozyme. *J. Mol. Biol.* **2000,** *297*, 193-210.

24. Man, P.; Montagner, C.; Vernier, G.; Dublet, B.; Chenal, A.; Forest, E.; Forge, V. Defining the interacting regions between apomyoglobin and lipid

membrane by hydrogen/deuterium exchange coupled to mass spectrometry. *J. Mol. Biol.* **2007,** *368* (2), 464-472.

25. Seyfried, N. T.; Atwood, J. A.; Yongye, A.; Almond, A.; Day, A. J.; Orlando, R.; Woods, R. J. Fourier transform mass spectrometry to monitor hyaluronan-protein interactions: use of hydrogen/deuterium amide exchange. *Rapid Commun. Mass Spectrom.* **2007,** *21* (2), 121-131.

26. Mandell, J. G.; Baerga-Ortiz, A.; Akashi, S.; Takio, K.; Komives, E. A. Solvent accessibility of the thrombin-thrombomodulin interface. *J. Mol. Biol.* **2001,** *306*, 575-589.

27. Zhu, M. M.; Rempel, D. L.; Du, Z.; Gross, M. L. Quantification of Protein-Ligand Interactions by Mass Spectrometry, Titration, and H/D Exchange: PLIMSTEX. *J. Am. Chem. Soc.* **2003,** *125*, 5252-5253.

28. Ghaemmaghami, S.; Fitzgerald, M. C. A Quantitative, High-throughput Screen for Protein Stability. *Proc. Natl. Acad. Sci. U. S. A.* **2000,** *97*, 8296-8301.

29. Ma, L.; Fitzgerald, M. C. A New H/D Exchange- and Mass Spectrometry-Based Method for Thermodynamic Analysis of Protein-DNA Interactions. *Chemistry & Biology* **2003,** *10*, 1205-1213.

30. Powell, K. D.; Wang, M. Z.; Silinski, P.; Ma, L.; Wales, T. E.; Dai, S. Y.; Warner, A. H.; Yang, X.; Fitzgerald, M. C. The accuracy and precision of a new H/D exchange- and mass spectrometry-based technique for measuring the thermodynamic stability of proteins. *Anal. Chim. Acta* **2003,** *496*, 225-232.

31. Hoofnagle, A. N.; Resing, K. A.; Goldsmith, E. J.; Ahn, N. G. Changes in protein conformational mobility upon activation of extracellular regulated protein kinase-2 as detected by hydrogen exchange. *Proc. Natl. Acad. Sci. U. S. A.* **2001,** *98*, 956-961.

32. Beauchamp, J. L. H/D exchange Reactions of Biological Molecules in the Gas Phase. In *The encyclopedia of Mass Spectrometry: Theory and Ion Chemistry*, Armentrout, P. B., Ed.; Elsevier: Oxford, 2003; pp 843-866.

33. Green, M. K.; Lebrilla, C. B. Ion-molecule reactions as probes of gas-phase structures of peptides and proteins. *Mass Spectrom. Rev.* **1997,** *16*, 53-71.

34. Brodbelt, J. S. Analytical Application of ion-molecule reactions. *Mass Spectrom. Rev.* **1997,** *16*, 91-110.

35. Hunt, D. F.; McEwen, C. N.; Upham, R. A. Determination of active hydrogen in organic compounds by chemical ionization mass spectrometry. *Anal. Chem.* **1972,** *44*, 1292-1294.

36. Guarini, A.; Guglielmetti, G.; Andriollo, N.; Vincenti, M. Labile hydrogen counting in biomolecules using deuterated reagents in desorption chemical ionization and fast atom bombardment mass spectrometry. *Anal. Chem.* **1992,** *64*, 204-210.

37. Olmstead, W. N.; Brauman, J. I. Gas-Phase Nucleophilic Displacement-Reactions. *J. Am. Chem. Soc.* **1977,** *99*, 4219-4228.

38. Asubiojo, O. I.; Brauman, J. I. Gas-Phase Nucleophilic Displacement-Reactions of Negative-Ions With Carbonyl-Compounds. *J. Am. Chem. Soc.* **1979,** *101*, 3715-3724.

39. Lias, S. G. Thermoneutral Isotope Exchange-Reactions in Proton-Bound Complexes of Water With Organic-Molecules-Correlations With Energetics of Formation of the Corresponding Association Ions. *J. Phys. Chem.* **1984,** *88*, 4401-4407.

40. Ausloos, P.; Lias, S. G. Thermoneutral Isotope Exchange-Reactions of Cations In The Gas-Phase. *J. Am. Chem. Soc.* **1981,** *103*, 3641-3647.

41. Campbell, S.; Rodgers, M. T.; Marzluff, E. M.; Beauchamp, J. L. Deuterium Exchange Reactions as a Probe of Biomolecule Structure. Fundamental Studies of Gas Phase H/D Exchange Reactions of Protonated Glycine Oligomers with D_2O, CD_3OD, CD_3CO_2D, and ND_3. *J. Am. Chem. Soc.* **1995,** *117*, 12840-12854.

42. Green, M. K.; Lebrilla, C. B. The role of proton-bridged intermediates in promoting hydrogen-deuterium exchange in gas-phase protonated diamines, peptides and proteins. *Int. J. Mass Spectrom. Ion Processes* **1998,** *175*, 15-26.

43. Wyttenbach, T.; Bowers M.T. Gas Phase Conformations of biological Molecules: The Hydrogen/Deuterium Exchange Mechanism. *J. Am. Soc. Mass Spectrom.* **1999,** *10*, 9-14.

44. Freitas, M. A.; Hendrickson, C. L.; Emmet, M. R.; Marshall, A. G. Gas-phase bovine ubiquitin cation conformations resolved by gas-phase hydrogen/deuterium exchange rate and extent. *Int. J. Mass Spectrom.* **1999,** *185/186/187*, 565-575.

45. Wright, P. J.; Zhang, J.; Douglas, D. J. Conformations of Gas-Phase Ions of Ubiquitin, Cytochrome c, Apomyoglobin, and β-Lactoglobulin Produced from Two Different Solution Conformations. *J. Am. Soc. Mass Spectrom.* **2008,** *19*, 1906-1913.

46. Somogyi, A. Probing Peptide Fragment Ion Structures by Combining Sustained Off-Resonance Collision-Induced Dissociation and Gas-Phase H/D

Exchange (SORI-HDX) in Fourier Transform Ion-Cyclotron Resonance (FT-ICR) Instruments. *J. Am. Soc. Mass Spectrom.* **2008,** *19*, 1771-1775.

47. Zhang, Z.; Guan, S.; Marshall, A. G. Enhancement of the Effective Resolution of Mass Spectra of High-Mass Biomolecules by Maximum Entropy-Based Deconvolution to Eliminate the Isotopic Natural Abundance Distribution. *J. Am. Soc. Mass Spectrom.* **1997,** *8*, 659-670.

48. Gard, E.; Green, M. K.; Bregar, J.; Lebrilla, C. B. Gas-Phase Hydrogen/Deuterium Exchange as a Molecular Probe for the Interaction of Methanol and Protonated Peptides. *J. Am. Soc. Mass Spectrom.* **1994,** *5*, 623-631.

49. Green, M. K.; Penn, S. G.; Lebrilla, C. B. The Complexation of Protonated Peptides with Saccharides in the Gas Phase Decreases the Rates of Hydrogen/Deuterium Exchange Reactions. *J. Am. Soc. Mass Spectrom.* **1995,** *6*, 1247-1251.

2.4. Ion mobility coupled to mass spectrometry [1-6]

The ion mobility of a gas-phase ion is the quantity that describes how fast the ion moves through a drift cell filled with pressure of buffer gas under the influence of a weak electric field. Small, compact ions with small collision cross sections drift more quickly than large, extended ions with large collision cross sections. Ion mobility spectrometry is a gas-phase electrophoretic technique that allows analytes to be distinguished on the bases of their mass, charge and collision cross section (i.e., size and shape). The Figure 2.4.1. illustrates schematically an ion mobility experiment.

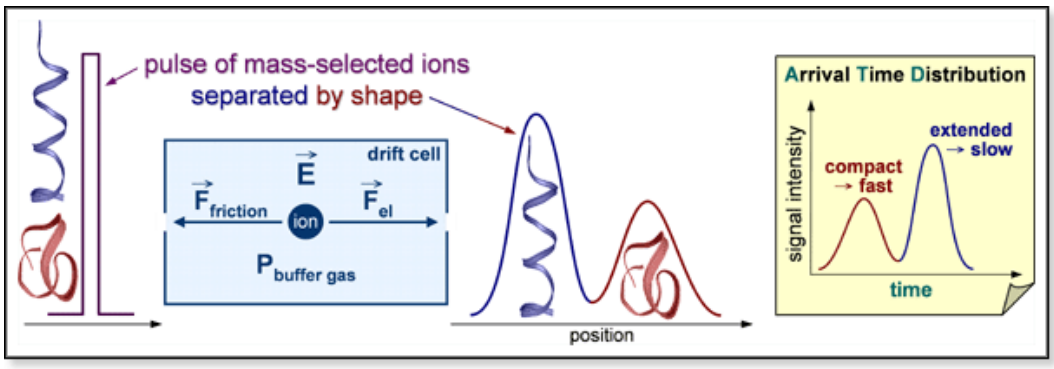

Figure 2.4.1. Schematic illustration of an ion mobility experiment.

The first investigations of mobility of gaseous ions in electric fields at ambient pressure started in the late 1890s and the mobility theory was developed before 1910. The first commercial ion mobility spectrometers were introduced only in 1970. From this time, the technique has been widely used to detect chemical warfare agents, explosives and narcotics, and to study the structure of small molecules. In the early 1990s, the use of ion mobility to obtain structural information started to emerge, and thanks to the coupling of ion mobility spectrometry with ESI and MALDI ion sources, the study of the conformations and structures of a wide range of biomolecules in the gas phase became allowed.

2.4.1. Theory

In 1896, Thomson and Rutherford discovered that gaseous ions drift under the influence of an electric field with an average velocity that is proportional to the field. $\vec{J}$, the ion flux vector is written

$$\vec{J} = n \cdot \overrightarrow{v_d} = n \cdot K \cdot \vec{E} \quad (1)$$

where n is the ion number density, $\overrightarrow{v_d}$ is the ion velocity vector, $\vec{E}$ is the electric field vector, and K is called the ion mobility.

In 1902, Langevin discovered that the mobility of positive ions is inversely proportional to the pressure. It implies that a relationship exists between the mobility and the gas number density, n_0. The ion mobility is typically converted to a "reduced" mobility K_0.

$$K_0 = \frac{n_0 \cdot K}{N_0} = K \cdot \frac{P \cdot T_0}{P_0 \cdot T} \quad (2)$$

The Loschmidt's constant, $N_0 = 2.686763 \times 10^{25}$ m^{-3}, is the number density of an ideal gas at $T_0 = 273.15$ K and $P_0 = 101325$ Pa.

By combining the equations (1) and (2), and knowing that

$$\left|\vec{E}\right| = \frac{V}{L} \quad (3)$$

where V is the applied voltage across the cell and L is the drift length, an expression is obtained in terms of P and V for the amount of time the ions spend in the drift cell (t_d):

$$t_d = \frac{L}{v_d} = \frac{L}{K \cdot E} = \frac{L^2 \cdot T_0}{K_0 \cdot P_0 \cdot T} \frac{P}{V}. \quad (4)$$

The ion intensity as a function of time can be measured, generating a plot called an arrival time distribution (ATD). The arrival time corresponds to the amount of time between the formation of the initial ion pulse and the ion arrival at the detector. This amount of time is equal to $t_d + t_0$ where t_0 is the time the ions spend outside the drift cell. Plotting $t_d + t_0$ versus P/V for a given temperature gives a straight line with a intercept equal to t_0 and the slope of the line that is proportional to $(K_0)^{-1}$.

Using kinetic theory, the reduced mobility K_0 can be related to the collision cross section:

$$K_0 = \frac{3 \cdot e}{16 \cdot N_0} \left(\frac{2\pi}{\mu k T} \right)^{1/2} \frac{1}{\Omega}. \quad (5)$$

e is the charge of the ion, μ is the reduced mass of the buffer gas-ion pair, T is the effective temperature [7] and Ω is the momentum-transfer collision integral. By measuring K_0, a value is obtained for Ω and is assumed to be equal to the experimental cross section. Ω is generally difficult to calculate theoretically, unless it is calculated for a rigid sphere. In this case it is equal to the projection cross section σ. Differences between Ω and σ up to 20% are obtained for exotic geometries with large concave surfaces, otherwise the projection cross section is a good approximation for the collision integral. For similar shapes, the differences between Ω and σ are similar and can be corrected empirically.

To deduce structural information about the ions, the measured mobility (experimental cross section) must be compared to mobilities (cross sections) estimated for theoretical candidate structures. Because experimental cross sections are the results of an ion-buffer gas scattering process, it is not obvious to understand how the Cartesian coordinates of an assumed geometry can be converted into a collision cross section. As previously said, simple projection cross sections are after careful calibration, good approximations to the collision integrals. Different methods have been developed to determine theoretical collision cross sections. The projection approximation is widely used for small ions (10-200 atoms). For medium ions (200-1000 atoms), the trajectory calculation method is well suited. It corresponds to a trajectory calculation on a realistic ion-buffer gas interaction potential centered at the position of each atom. The agreement between the measured and calculated mobilities has been greatly improved over that obtained with the hard-sphere projection approximation [8,9]. For large molecules (> 1000 atoms), other trajectory calculation using hard spheres centered at the position of each atom is employed. It is called the exact hard sphere scattering (EHSS) method [10]. The trajectory calculation works well for any ion size, but the calculations are very time consuming. The projection approximation fails for large system as the details of the scattering process are not taken into account. As for the EHSS method, it fails for small systems because the ion-buffer gas interaction becomes important compared to the geometry of the ion and careful calibration of the atomic radii is essential.

2.4.2. Method

The drift tube resolving power is defined by the experimental parameters L, E, P and T. Revercomb and Mason showed that the theoretical resolving power can be approximated from

$$R = \frac{t_d}{\Delta t} \approx \left(\frac{L \cdot E \cdot n \cdot q}{16 \cdot k_B \cdot T \cdot \ln 2} \right)^{1/2} \quad (6)$$

where Δt corresponds to the full width at half-maximum of the peak. This relation shows that the resolving power can be increased by increasing the drift field or length, or decreasing the temperature. Although not shown in the equation, the buffer gas pressure plays a key role. At high fields, the gas must remain stable, so a pressure for which no electrical discharge occurs is required. Another practical issue for obtaining high resolution is to isolate the ion source region from the drift region. The resolving power of the drift tube is function of the density of the ion packet that is injected. This constraint leads to two general instrumental designs: a high-pressure, high-resolution configuration in which ions are produced at atmospheric-pressure and guided into the drift region, and a low-pressure, low-resolution configuration in which ions are produced in an external source, extracted into a vacuum, and then injected into the drift tube. The advantages of high-resolution system are clear as it can resolve components of similar mobilities, but low-pressure instruments are also very attractive as they can be coupled with the MS ion sources, trapping devices and analyzers.

The early ion mobility instruments described in 1970 consist of: (1) a sample inlet; (2) a radioactive ^{63}Ni isotope ion source; (3) an ion-molecule reaction region; (4) an ion shutter grid for initiating experiments; (5) a uniform field drift region; (6) an exit gate grid; and (7) an electrode for measuring ion current. It is illustrated in Figure 2.4.2. Note that many aspects of this design are similar to configurations used in modern instruments.

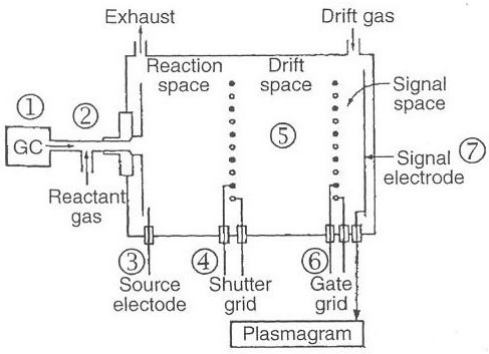

Figure 2.4.2. A schematic diagram of an early ion mobility spectrometer [2].

With such instruments, the delay time for opening the gate grid must be scanned with respect to the introduction pulse. In the 1970s and 1980s, incorporation of multichannel analyzers made it possible to remove the second gate grid and record the complete ion mobility distribution for each initiation pulse. From 1990s, several groups have coupled mass spectrometers to drift tubes. One of these couplings corresponds to the incorporation of a magnetic sector or a quadrupole mass filter above the drift tube with the aim of dispersing different isomers in the drift tube while passing a single m/z value through the mass spectrometer. Another important coupling design corresponds to drift tubes with time-of-flight (Tof) mass spectrometers. Unlike combination of drift tube with scanning mass spectrometers where the mobility distributions are recorded for only a narrow m/z range, the m/z and mobility information for all species that are present can be recorded with Tof MS. Because flight times in the evacuated flight tube of the mass analyzer can be recorded on μs timescales, whereas, mobility distributions are measured on millisecond timescales, it is possible to record data such that time-of-flight information is nested within individual drift time windows. More recently, trap has been inserted at the front of the drift tube/Tof instruments. This allows to accumulate continuous ion beams in order to generate concentrated ion packets for the pulsed experiment. It makes it also possible to synthesize ions in the trap by ion-molecule reactions or by collisional activation with the buffer gas.

Recently, a number of separation devices that utilize nonuniform fields to separate ions based on differences in mobilities have emerged. The separating power of such systems is usually higher than the one of uniform fields thanks to the longer distance covered by the ions. However, to determine the ion mobility K from the

arrival time distribution, the ion velocity v_d and the electric field E must be known at each moment, which is possible only with uniform drift tube. The current limitation of the nonuniform systems is that it is not readily possible to obtain absolute collision cross sections. The two commercial nonuniform systems are FAIMS (Field Asymmetric waveform Ion Mobility Spectrometry) [11,12] and Synapt^{TM} High Definition MS [13]. In FAIMS, the ions pass between two cylindrical electrode surfaces across which an asymmetric RF potential waveform is applied. The ions are alternatively exposed to strong and weak electric fields. Different mobilities of the ions during the high field versus low field portion of the waveform result in a drift of the ions towards one of the electrodes. This drift can be compensated for by using a DC potential. Varying the "compensation" voltage allows the ions to be separately transmitted through the FAIMS device into the mass spectrometer. The Synapt^{TM} High Definition MS system corresponds to a hybrid quadrupole/traveling wave ion mobility separator/orthogonal acceleration time-of-flight instrument [13]. A schematic diagram is shown in Figure 2.4.3.

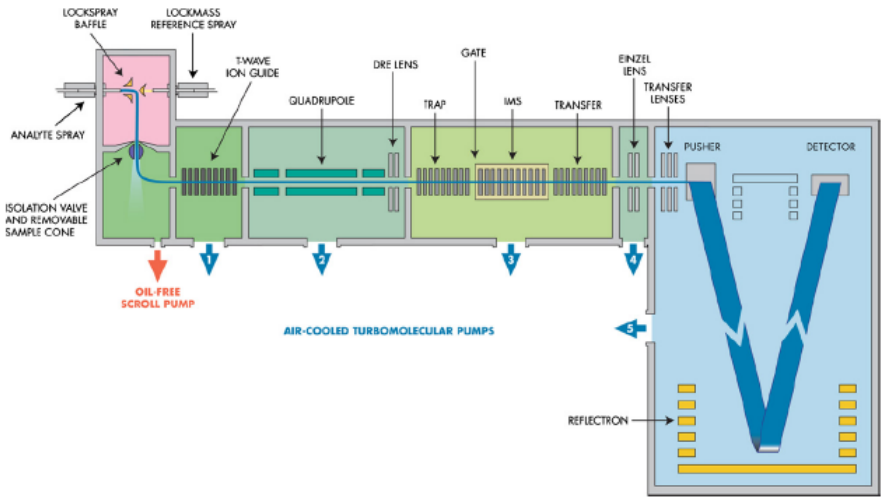

Figure 2.4.3. A schematic diagram of the Synapt^{TM} HDMS system [13].

The ion mobility section consists of three traveling wave stacked ring ion guides (Figure 2.4.3.). The trap ion guide accumulates ions during the previous mobility separation and then an ion packet is released into the ion mobility guide for separation. The transfer ion guide, the last one, is used to transfer the mobility separated ions to the oa-Tof. An ion guide comprises a series of planar electrodes

that are perpendicular to the ion transmission axis. Opposite phases of an RF voltage are applied to adjacent electrodes, which provides a radially confining effective potential barrier. Superimposed on the RF voltage, a transient DC voltage is applied to a pair of adjacent electrodes in a repeating sequence along the length of the device. This propels ions through the gas. As illustrated in Figure 2.4.4., a continuous sequence of traveling waves is generated by the subsequent application of the series of potential hills to the next pair of electrodes. Recording the temporal arrival profile of ions is achieved by synchronization of the oa-Tof acquisition with the gated release of ions from the trap into the ion mobility guide.

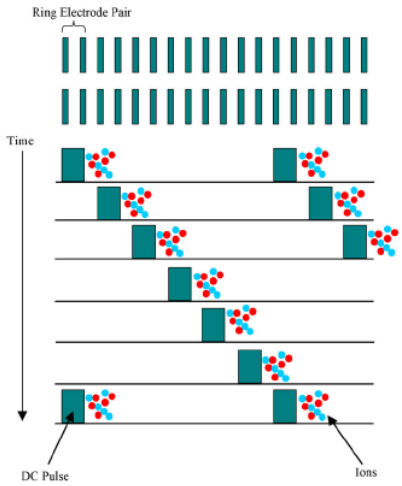

Figure 2.4.4. Illustration of the operation of a traveling wave ion guide for ion propulsion in the presence of background gas [13].

2.4.3. Applications

The recorded arrival time profile can be used in several ways; the ion mobility can be used to calculate the collision cross section and the drift times can determine reaction rate constants.

If one or more conformers are present in the sample, and if their interconversion is slow compared to the drift time, these conformers can be resolved. Measuring their mobilities allows to calculate their collision cross sections and to compare to theoretical ones obtained from candidate structures. For example, Baumketner et al. [14] performed ion mobility experiments on the Aβ42 (amyloid β-protein

composed of 42 amino acid residues) 3- charge state electrosprayed from solution. They observed a bimodal arrival time distribution. As illustrated in Figure 2.4.5., this distribution was quantitatively fitted using cross sections from dehydrated forms of three families of calculated solution structures (noted (#1, #2 and #3 in Figure 2.4.5.e) and one calculated solvent-free family of structures (noted sf in Figure 2.4.5.e).

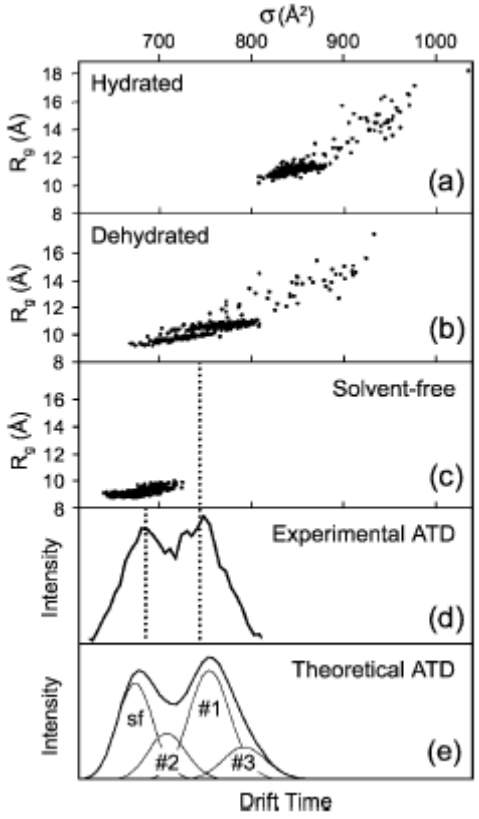

Figure 2.4.5. Scatter plot of radius of gyration (R_g) versus cross section of hydrated (a), dehydrated (b), and solvent free (c) theoretical Aβ42 structures. (d) Experimental arrival time distribution of Aβ42 charge state 3-. (e) Theoretical arrival time distributions of solvent-free (sf) and dehydrated Aβ42 structures (#1, #2 and #3) [14].

When two or more conformers are present in the sample and some fractions of them either interconvert or do not interconvert but fragment during the time in the drift cell, the arrival time distribution can be used to find rate constants for interconversion or fragmentation processes. As the amount of time that the ions

spend in the drift tube can be controlled by changing the pressure and the voltage, and as the relative concentrations of the different ion species can be obtained from the mass spectrum (only for fragmentation processes), the rate constants can be calculated from measuring concentration as function of time. Bowers' group also proposes another way for determining rate constants from the shape of the arrival time distribution peaks. If an ion maintains its conformation during the drift time, its arrival time peak will be symmetric. But if it dissociates or isomerizes to a different conformation, the shape of its peak will change. The new shape will depend on the rates at which the fragmentation or isomerization reactions occur. By modeling the peak shape, rate constants can be obtained.

Note that ion mobility is also used for top-down sequencing of proteins as it provides an additional dimension of separation aiding the interpretation of the complex, multiply-charged datasets.

References

1. Viehland, L. A. Transport Properties. In *The encyclopedia of Mass Spectrometry: Theory and Ion Chemistry*, Armentrout, P. B., Ed.; Elsevier: Oxford, 2003; pp 491-498.

2. Hilderbrand, A. E.; Clemmer, D. E.; Valentine, S. J. Drift Tubes: Instrumentation and Applications to Biomolecules. In *The encyclopedia of Mass Spectrometry: Theory and Ion Chemistry*, Armentrout, P. B., Ed.; Elsevier: Oxford, 2003; pp 506-520.

3. Bohrer, B. C.; Merenbloom, S. I.; Koeniger, S. L.; Hilderbrand, A. E.; Clemmer, D. E. Biomolecule Analysis by Ion Mobility Spectrometry. *Annu. Rev. Anal. Chem.* **2008,** *1*, 293-327.

4. Borsdorf, H.; Eiceman, G. A. Ion Mobility Spectrometry: Principles and Applications. *Applied Spectroscopy Reviews* **2006,** *41*, 323-375.

5. Wyttenbach, T.; Bowers, M. T. Gas-Phase Conformations: The Ion Mobility/Ion Chromatography Method. *Top. Curr. Chem.* **2003,** *225*, 207-232.

6. Creaser, C. S.; Griffiths, J. R.; Bramwell, C. J.; Noreen, S.; Hill, C. A.; Thomas, C. L. P. Ion mobility spectrometry: a review. Part 1. Structural analysis by mobility measurement. *Analyst* **2004,** *129*, 984-994.

7. Illenseer, C.; Löhmannsröben, H. Investigation of ion-molecule collisions with laser-based ion mobility spectrometry. *Phys. Chem. Chem. Phys.* **2001,** *3*, 2388-2393.

Eq(5) relies on the so-called one-temperature model, which means that the apparatus, the ions and the bath gas have the same effective temperature, T_{eff}, which is related to T by:

$$T_{eff} = T + \frac{M \cdot v_d^{\,2}}{3k_B}$$

where M is the mass of the bath gas and v_d the drift velocity. Under their experimental conditions, the authors found that the second term on the right side was always below 0.1 K, so that T is equal to T_{eff}.

8. Mesleh, M. F.; Hunter, J. M.; Shvartsburg, A. A.; Schatz, G. C.; Jarrold, M. F. Structural Information from Ion Mobility Measurements: Effects of the Long-Range Potential. *J. Phys. Chem.* **1996,** *100*, 16082-16086.

9. Shvartsburg, A. A.; Schatz, G. C.; Jarrold, M. F. Mobilities of carbon cluster ions: Critical importance of the molecular attractive potential. *J. Chem. Phys.* **1998,** *108*, 2416-2423.

10. Shvartsburg, A. A.; Jarrold, M. F. An exact hard-spheres scattering model for the mobilities of polyatomic ions. *Chem. Phys. Lett.* **1996,** *261*, 86-91.

11. Shvartsburg, A. A.; Tang, K.; Smith, R. D. Optimization of the design and operation of FAIMS analyzers. *J. Am. Soc. Mass Spectrom.* **2005,** *16*, 2-12.

12. Kolakowski, B. M.; Mester, Z. Review of applications of high-field asymmetric waveform ion mobility spectrometry (FAIMS) and differential mobility spectrometry (DMS). *Analyst* **2007,** *132* (9), 842-864.

13. Pringle S.D.; Giles K.; Wildgoose J.L.; Williams J.P.; Slade S.E.; Thalassinos K.; Bateman R.H.; Bowers M.T.; Scrivens J.H. An investigation of the mobility separation of some peptide and protein ions using a new hybrid quadrupole/travelling wave IMS/oa-ToF instrument. *Int. J. Mass Spectrom.* **2007,** *261*, 1-12.

14. Baumketner, A.; Bernstein, S. L.; Wyttenbach, T.; Bitan, G.; Teplow, D. B.; Bowers, M. T.; Shea, J. Amyloid β-protein monomer structure: A computational and experimental study. *Protein Science* **2006,** *15*, 420-428.

2.5. Nucleic acids in mass spectrometry

Nucleic acids and their components play an important role in a variety of fundamental biological processes. It is well known that deoxyribonucleic acid (DNA) is the carrier of genetic information in all cells and many viruses, and ribonucleic acids (RNA) are the initial products of all genes. DNA and RNA are both heteropolymers of heterocyclic bases that are linked via a ribose moiety to a phosphodiester link. They differ from each other by the sugar glycone that corresponds to a D-ribose in RNA and deoxy-D-ribose in DNA, and by the nucleobase uracil in RNA that replaces thymine in DNA (Figure 2.5.1.). Moreover, while DNA is usually paired in a double strand, RNA is singly stranded.

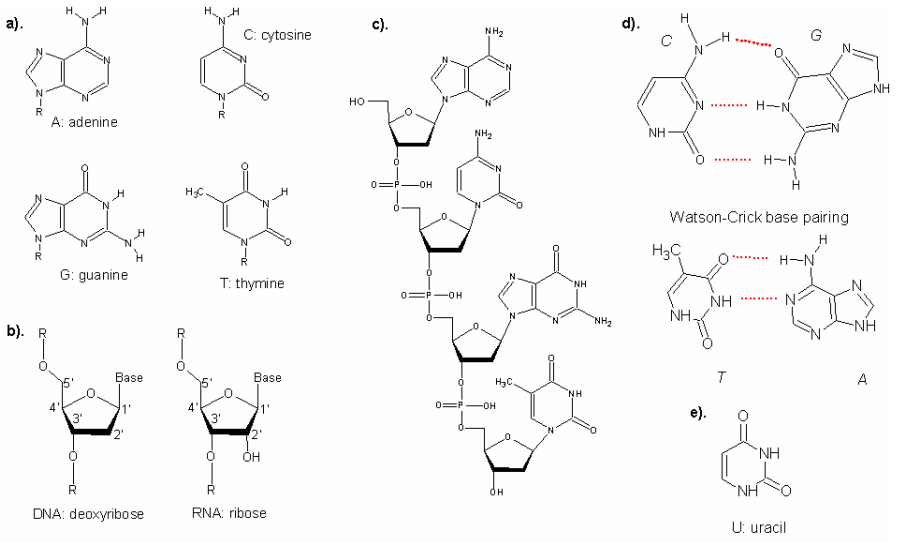

Figure 2.5.1. a). The four DNA bases. **b).** Atom numbering on the deoxyribose and ribose sugar. **c).** DNA primary structure ACGT. **d).** Watson-Crick base pairing. **e).** The uracil RNA base.

DNA and RNA may adopt a variety of structures depending on their sequences and environment conditions: double-stranded helices, hairpins, bulges, quadruplexes… The DNA and RNA structures and conformations have important biological roles as they can determine, for example via noncovalent interactions, a vast majority of biological process (recognition, regulation…). In this thesis, gas-

phase hydrogen/deuterium exchange and ion mobility are coupled with mass spectrometry to study the gas-phase structures of nucleic acids.

2.5.1. Method

This section describes how to prepare a nucleic acid sample for its injection in a mass spectrometer equipped with an electrospray source. Some peculiar protocol steps for nucleic acids are discussed.

All nucleic acids we work with are synthetic oligonucleotides (quality OliGold^{TM}) provided by Eurogentec (Seraing, Belgium). Their lyophilized sequences are dissolved to 400 µM in bi-distilled water. To check that the sample is in good condition (undamaged, not too much salted…), it is injected in the mass spectrometer.

If too much sodium or potassium adducts are observed and if it perturbs the analysis, the sample needs to be desalted. Different techniques such as a centrifugal filter device or a micro-column based on steric exclusion can be used. As explained later, a NH_4Ac solution is often used as the conditioning and washing solutions.

It is important to notice that solvents containing more than 1 mg/kg of Na and K are systematically avoided for the sample preparation. During the electrospray process, the solvent droplets evaporate and positive ions condense around the negatively charged nucleic acids (in negative ion mode). A distribution of species [D(R)NA + n Na/K] is observed. Moreover, glassware is also avoided as it can be contaminated with NaCl and KCl that are not removed by autoclaves. Polystyrene tubes are preferred even if some low quality ones may contain traces of polyethylene glycol solubilized by methanol which gives peaks separated by 44 Da in the mass spectra. Because Na and K must be avoided, a substitute salt is needed to maintain an ionic strength; ammonium acetate is chosen. An ammonium ion that condenses around a phosphate transfers a proton to it and leaves as ammonia and the acetate anion abstracts a proton to leave as a neutral acetic acid. In an electrospray source, NH_4Ac can be used at concentrations up to 150 mM which corresponds to the physiological ionic strength. Note that ammonium acetate has no buffering capacities: if necessary, acetic acid or ammonium hydroxide can be used to tune the pH.

After the desolvation and the possible desalting, the exact concentration of the oligonucleotide is determined by UV absorption spectrophotometry at 260 nm.

Stock aliquots of 20-50 µL are made and stored at – 20°C.

Some peculiar precautions must be taken for manipulating RNA. In order to avoid the degradation of the sample, a RNAse free equipment is required; spray for cleaning work surfaces and micropipettes, filter tips, microtubes, water and ammonium acetate solutions. Stock aliquots of RNA are stored at – 80°C.

To study nucleic acid complexes (duplexes, ligand-DNA complexes…) or nucleic acids having particular structures (hairpin, G-quadruplexes…), oligonucleotides undergo a pairing operation (annealing) before the complex formation and the injection in the mass spectra. It consists in heating the sample during a few minutes (from 2 to 5 minutes) and allowing it to cool down to room temperature. This operation provides the correct pairing of complementary sequences and avoids the coexistence of several species in solution. The annealing must be renewed before each manipulation.

The nucleic acid concentration in the injection solution varies from 1 to 50 µM with the most frequent concentration being 10 µM. Some methanol is added to the sample before the injection. This decreases the surface tension of the solution compared to pure water making droplet evaporation more favorable. The electrospray signal is therefore increased. Usually the injection solution contains 15 – 20% of methanol. As reported by Mel'nikov et al., up to 50% of methanol does not perturb DNA conformations [1]. Note that oligonucleotide solutions are not stored with methanol added; it is added directly before the injection.

Most ESI-MS investigations of nucleic acids have been carried out using negative ion mode. This seems to be logical from the knowledge that the phosphodiester backbone is fully deprotonated under most experimental conditions because it has a pKa < 1. Several papers showed that working in negative ion mode gives reliable apparent binding constants for DNA duplexes [2,3], DNA-quadruplexes [4], and RNA structures [5,6]. Rosu et al. demonstrated that positive ion mode gives a systematic underestimation of the binding constants of drug-DNA complexes [7]. It is advisable for the mass spectrometry analysis to start from any negative ion parameters and to be prepared to lower all voltages (End-Plate and

Capillary in our FT-ICR MS) and temperature in the source especially for the study of complexes.

2.5.2. Gas-phase H/D exchange of nucleic acids

Deoxyribose monophosphate nucleotides are the fundamental building blocks of oligonucleotides that build the complicated secondary structure of DNA via inter- and intramolecular hydrogen bonds. Gas-phase H/D studies of nucleic acids started with these structural units in 1998.

In these first studies, Robinson et al. investigated the H/D exchange kinetics of deoxyribose monophosphates with D_2O [8]. They measured the gas-phase exchange rates of the 3'- and 5'-monophosphates of the four nucleosides: deoxyadenosine monophosphate (dAMP), deoxycytidine monophosphate (dCMP), deoxyguanosine monophosphate (dGMP), and the deoxythymidine monophosphate (dTMP), as well as 3'- and 5'-cyclic forms of dAMP, dGMP and dTMP (Figure 2.5.2.). The H/D exchange reactions were performed in the ICR cell of a FT-ICR mass spectrometer. D_2O was leaked into the system at a pressure of 1.33×10^{-7} mbar and the exchange was followed by a 20 s pump down to obtain a pressure of 1.33×10^{-8} mbar for the detection. The exchange kinetics was fit with a set of five coupled differential equations and exchange reactions were considered as first-order processes. The initial isotopic abundance was taken into account and a variable rate of back-exchange which turned out to be negligible was incorporated into the model. The geometries and transition states of complexes between the 3'-/5'-nucleotides and water were modeled using semiempirical and ab initio calculations.

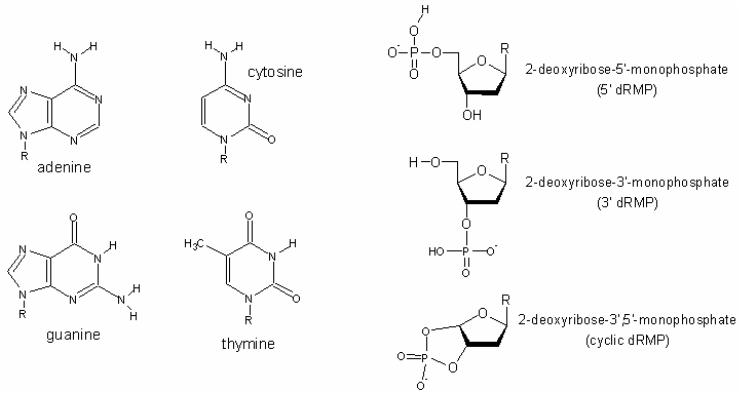

Figure 2.5.2. Primary structures of the 3'- and 5'-monophosphates and 3'- and 5'-cyclic monophosphates of the four nucleosides (adapted from [8]).

The gas-phase acidity at the exchange sites was suspected to be an important factor. The calculated gas-phase acidities of the DNA bases are presented in Table 2.5.I. It is assumed that the H/D exchange reaction is more favored when the gas-phase acidities of the reagent and the molecule are close in value. As the gas-phase acidity of D_2O is equal to 390.7 kcal/mol and based on the data in Table 2.5.I., the predicted (initial) exchange trend would be dCMP > dAMP > dTMP > dGMP (note that exchange for gas-phase acidity differences larger than 20 kcal/mol can be attributed to complex formation between the ion and the reagent).

Table 2.5.I. Calculated gas-phase acidities of the nucleic acid bases and model compounds. All values are reported as kcal/mol (adapted from [8]).

Adenine	Amino proton (1)	349.0
	Amino proton (2)	350.0
Cytosine	Amino proton (1)	345.6
	Amino proton (2)	351.5
Guanine	Amino proton (1)	333.4
	Amino proton (2)	335.8
	Imino proton	337.3
Thymine	Imino proton	344.1
Ethylisopropyl-phosphate	Hydroxyl proton	336.8

The comparison of the relative exchange rates of all the exchangeable hydrogens of the 3'-nucleotides (Table 2.5.II.) gave the overall trend 3'-dGMP > 3'-dAMP ≈ 3'-dCMP ≈ 3'-dTMP. This trend does not follow the calculated gas-phase acidity trend. To find an explanation, the access of the 3'-phosphate group to the exchangeable protons was probed. As deduced from the structure of a 3'-nucleotide (Figure 2.5.2.), the phosphate group is on one side and the base on the other side of the sugar ring. Moreover, the exchangeable protons of the DNA base are on the top of the ring structure except for guanine where the hydrogen atoms of the 2'-amino group can reside near the phosphate group. This proximity explained the faster exchange rates of 3'-dGMP. The possible exchange of the phosphate and the sugar hydroxyl groups was also accounted for by the structures adopted by the nucleotides. Molecular modeling showed that the charged 3'- or 5'-phosphate groups can bond to the hydroxyl hydrogen of the sugar. This stabilizing interaction slows the exchange rates of the hydroxyl and phosphate protons but as a D_2O molecule can link to these two moieties, their H/D exchange can however happen.

Table 2.5.II. Relative rates of exchange for exchangeable protons in each nucleotide base[a]. The rates reflect the number of exchanges per second (adapted from [8]).

proton	3'-dAMP	3'-dCMP	3'-dGMP	3'-dTMP	5'-dAMP	5'-dCMP	5'-dGMP	5'-dTMP
1	0.784	0.817	1.000	0.772	0.204	0.641	0.019	0.188
2	0.211	0.218	0.455	0.209	0.009	0.376	0	0.068
3	0.094	0	0.218	0	0	0.045	0	0.021
4	0	0	0.082		0	0	0	
5			0				0	

[a] All rate constants are reported relative to 3'-dGMP + D_2O.

The comparison of the relative exchange rates of each exchangeable proton of the 5'-nucleotides (Table 2.5.II.) gave the overall trend 5'-dCMP > 5'-dAMP > 5'-dTMP >> 5'-dGMP. Unlike the 3'-nucleotide exchange rates, the 5'-nucleotide exchange rate trend corresponds to the calculated gas-phase acidity trend. However, the gas-phase acidity is not the only important factor, the different conformations adopted by the nucleotides seem to play a role. Geometry optimizations of the 5'-dGMP suggested that the 5'-phosphate and a hydrogen of

the G amino group could form an hydrogen bond when the glycosidic bond adopts a –syn orientation. This hydrogen bond that stabilizes the charge of the phosphate group restricts the motion of the molecule and prevents the H/D exchange.

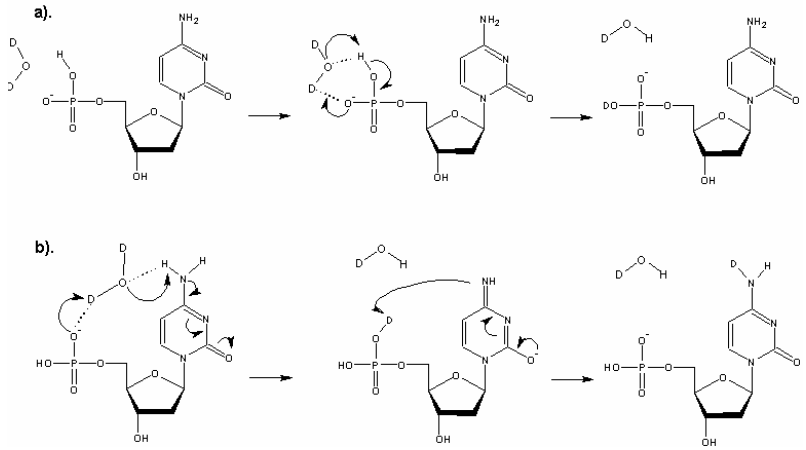

Figure 2.5.3. Proposed mechanism for negative ion H/D exchange of mononucleotides. One pathway (a) involves the charged phosphate group only; the other pathway (b) involves cooperative interaction between the base and the charged phosphate group (adapted from [8]).

Two mechanisms were proposed for the nucleotide exchange (Figure 2.5.3.). The first one only involves exchange of the phosphate group hydrogen. Because the exchange rates of the 5'-nucleotides follow the gas-phase acidity trends of the bases, the second mechanism involves the base groups of the nucleotides. It shows a cooperative exchange between the charged phosphate group and the base. The requirement of a flexible charged phosphate group was checked through the H/D exchange of three cyclic nucleotides since negligible exchange was observed for these cyclic nucleotides. This lack of H/D exchange also suggested that a direct tautomeric process between a deuterium oxide molecule and the bases is unfavorable.

Robinson et al. suggested that the H/D exchange rates may be sensitive to internal motions and deformations in the structure.

Soon after, Freitas et al. performed H/D exchange experiments with D_2O and D_2S of nucleoside 5'-monophosphate anions (GMP, dGMP, AMP, dAMP, CMP, dCMP, UMP, and dTMP) and sugar phosphate controls (ribose 5'-monophosphate (R5P) and 2-deoxyribose 5-monophosphate (dR5P)) [9]. The H/D exchange reactions occurred in the ICR cell of a FT-ICR MS, too. The monoisotopic $[M\text{-}H^+]^-$ ions were isolated by combination of frequency sweep and SWIFT excitation events before H/D exchange. D_2O or D_2S were leaked into the system at a pressure of 6.67×10^{-8} mbar and the typical base pressure for detection varied from 0.67×10^{-9} to 1.33×10^{-9} mbar. A system of N+1 (where N is the number of observed exchanged hydrogens) differential equations was used to model the exchange kinetics. A back-exchange term was also included. The rate constants were determined by fitting the experimental data. Ab initio calculations were performed on model compounds in order to calculate the gas-phase acidity of each exchangeable hydrogen. These ab initio results predicted that the most favored sites of exchange should follow the order; $RO_3PO\text{-}H$ > $R_2N\text{-}H$ > (R_2O-H on ribose) > $RN\text{-}H_2$ > (R_2O-H on 2'-deoxyribose). These data supported the fact that the phosphate site is the most acidic one which undergoes the initial exchange. As the gas-phase acidity of D_2S is equal to 351.3 kcal/mol, the gas-phase acidity difference between the exchange reagent and the nucleotide is smaller than for D_2O. As expected, D_2S significantly enhanced the rates and often the extents of the H/D exchange reactions of the nucleotides. Interestingly, the deoxyadenosine-5'-monophosphate (4 exchangeable hydrogens) and the adenosine-5'-monophosphate (5 exchangeable hydrogens) exchanged only two hydrogens whereas two and three exchanges were respectively expected (the phosphate proton and the hydroxyl hydrogens on the sugar).

Freitas and Marshall found an explanation in 2001 by studying the gas-phase H/D exchange of the adenosine-5'-monophosphate, cyclic-adenosine-5'-monophosphate, adenosine-5'-carboxylic acid, ribitol-5-5-phosphate, and 2-deoxy-ribitol-5-phosphate with D_2S [10]. Two mechanisms were discussed; the stepwise and the relay mechanism already proposed by Robinson (Figure 2.5.3.). In the stepwise exchange, two rates determine the overall rate of exchange; the initial rate of exchange with the phosphate group and the rate at which the phosphate exchanges internally. For the relay mechanism, the rate depends only on the exchange between the neutral reagent and the nucleotide anion. The adenosine-5'-carboxylic acid exchanged only a single hydrogen. Because of the lack of an exchangeable proton on the carboxylic functional group, it can not

exchange via a stepwise mechanism. But, this compound can easily form an ion-molecule complex where the exchange can occur. This supported the relay mechanism. The single exchanged hydrogen atom was supposed to be the one on the 3'-hydroxyl group because it is adjacent to the carbonyl group. In a similar way for AMP, the two exchanged protons were supposed to be the phosphate and the 3'-hydroxyl ones. The relay mechanism explained why AMP and dAMP exchanged exactly the same number of protons (2 protons). In addition to the conformation considerations, the thermodynamics also supports the relay mechanism. The modelisation of the H/D exchange mechanism between the ribitol-5-phosphate and the two exchange reagents D_2S and D_2O was performed. The theoretical results predicted that the identity of the exchange reagent influences strongly the thermochemical stability of the reaction intermediates, and should therefore have a strong influence on the reaction kinetics. This is, however, not the case for the stepwise process. As experimentally, the exchange reagent has a strong influence, the relay mechanism is the most plausible one.

In 2003, Crestoni et al. performed gas-phase H/D exchange reactions of adenosine-5'-mono-, di-, and triphosphate ions with CD_3OD, CD_3CO_2D and ND_3 [11]. In the ICR cell of a FT-ICR MS, the ions were exposed to a deuterating reagent pressure of 10^{-8} – 10^{-7} mbar. These experiments demonstrated the relevant role of a conformationaly flexible (poly)phosphate chain in making remote labile hydrogen atoms accessible to H/D exchange in adenosine nucleotides.

Up to then, none of the H/D exchange reactions of the 5'-monophosphate nucleotides were observed to go to completion. In 2007, Chipuk and Brodbelt examined the gas-phase H/D exchange of both anionic 3'- and 5'-mononucleotides in a quadrupole ion trap [12]. D_2O was used as the deuterating agent and introduced into the trap up to a pressure of ~ 4.67 x 10^{-4} mbar. H/D exchange data were fit by solving sets of coupled ordinary differential equations. Before the fitting, all the data were normalized and isotopic corrections to peak intensities were made based on the theoretical contributions of ^{13}C in each peak. Ab initio determinations of the gas-phase acidities of the various deprotonation sites in the mononucleotides were performed. In addition, dynamic simulations were carried out to investigate the different gas-phase conformations and to probe the impact of conformation variations on the distance between the deprotonated charge site and the remaining exchangeable hydrogens.

Contrary to the previously reported studies where the gas-phase acidities were calculated for isolated nucleobases, this study determined the gas-phase acidities of the complete monophosphate nucleotides. It showed that the phosphate group was the most likely site of deprotonation for the 5'-monophosphate nucleotides. For the 3'-monophosphate nucleotides, the calculated gas-phase acidities of the 3'-phosphate group and the 5'-hydroxyl group were found to be very similar due to the formation of a hydrogen bond between these two groups when the negative charge was placed at either of the two sites. From the examination of the rate constants (Table 2.5.III.) and exchange extents, all the deprotonated 2'-deoxymononucleotides were observed to exchange at least two hydrogen atoms after 10 s of reaction. In all cases, the exchange of the first two protons occurred more quickly for the 3'-phosphate than for the 5'-phosphate nucleotides. For the 2'-deoxycytidine and 2'-deoxythymidine monophosphate isomers, complete exchange was observed for the 5'-phosphate isomers with only two incorporated deuteriums for the 3'-phosphate isomers. Because the phosphate in the 5'-position is located on the same side of the ribose ring as the nucleobase, whereas the 3'-phosphate is on the opposite side, the 5'-position is more favorable than the 3' for exchange of the nucleobase protons via the relay mechanism. Moreover, the 5'-phosphate nucleotides have an additional degree of freedom because there are four flexible bonds between the deprotonation site and the sugar instead of three bonds for the 3'-phosphate nucleotides. For the cytosine and thymidine compounds, the 5'-phosphate moiety participates in several different exchange reactions while the 3'-phosphate moiety is principally stabilized by the interaction with the 5'-ribose hydroxyl group.

Table 2.5.III. Relative apparent rate constants for H/D exchange of deprotonated mononucleotides reacting with D_2O[a] (adapted from [12]).

Mononucleotide	k values[a]				
(number of exchangeable hydrogens)	k1	k2	k3	k4	k5
5'-dAMP (4)	57.2	25.7	0.0	0.0	
5'-dCMP (4)	14.9	5.6	0.9	0.4	
5'-dGMP (5)	1.3	1.0	0.6	0.2	0.01
5'-dTMP (3)	5.6	3.3	1.2		
3'-dAMP (4)	98.2	31.1	0.0	0.0	
3'-dCMP (4)	23.5	8.2	0.0	0.0	
3'-dGMP (5)	100.0	53.6	15.0	7.0	0.02
3'-dTMP (3)	15.8	7.4	0.0		

[a]All rate constants are reported relative to 3'-dGMP + D_2O and expressed as relative rate × 100.

The 3'-dGMP isomer exchanged must faster than the 5'-dGMP isomer, but both exchanged four of their five exchangeable hydrogens after 10 s of reaction. From the modeling calculations, the guanine was shown to be the only nucleobase in favor of a –syn orientation (Figure 2.5.4.). For the 5'-dGMP isomer, the conformation is suitable for a relay mechanism, but the stabilization of the labile protons by hydrogen bonding seems to slow the reaction rate. For the 3'-dGMP isomer, the intramolecular interactions between the phosphate, nucleobase and ribose hydroxyl group seem to be not as strong as those in the 5'-isomer since faster exchange was observed for 3'-dGMP.

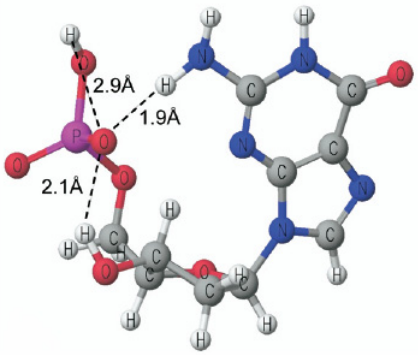

Figure 2.5.4. Molecular dynamics conformation of 5'-dGMP (adapted from [12]).

Neither 5'-dAMP nor 3'-dAMP exchanged more than two hydrogens. Unlike the guanine nucleobase which has its primary amine at the 2 position, the primary amine of the adenine is at the 6 position. In the –syn orientation, the amine group is far away from the deprotonated site. The adenine is in favor of an –anti orientation where the larger size of the purine ring compared with the pyrimidine one places the labile protons too distant from the deprotonated site for a relay mechanism. Only the hydrogens of the phosphate and ribose hydroxyl groups that interact in both 5'- and 3'-isomers exchange.

The molecular modeling calculations confirmed that the phosphate was the most likely deprotonation site and the calculated distances between the phosphate and various labile hydrogens correlated strongly with the experimental H/D exchange results.

The observed variations in the exchange behaviors of the mononucleotides isomers confirm that the H/D exchange reactions depend on both the identity of the nucleobase and the position of the phosphate moiety.

Larger oligonucleotides have also been studied. The results of these experiments are briefly presented below. If it is necessary for the discussion of our results, they will be described in more details later (Chapter 6).

In 1999, Griffey et al. investigated the gas-phase H/D exchange of two 5mer phosphorothioate oligodeoxynucleotides, d(GTCAG) and d(TCGAT), using a 9.4 T electrospray FT-ICR mass spectrometer [13]. D_2O was introduced in the ICR cell at a pressure of 1.33×10^{-7} mbar. They observed differences in the H/D exchange rates as a function of charge state. They proposed that remote charged sites can catalyze the H/D exchange reactions, and also that an additional charge may be sequestered (internal bonding) and not available to increase the exchange. The locations and environments of the charged residues were proposed to be critical for H/D exchange. The observation of bimodal exchange profiles suggested that each ion can adopt more than one gas-phase conformation, and that these structures can exchange at different rates.

In 2001, Griffey et al. reported that the H/D exchange rates for DNA duplex anions were > 10-fold slower than the rates for the respective single strands [14].

Gabelica et al. investigated the gas-phase H/D exchange of DNA G-quadruplexes [15]. The experiments were performed using a FT-ICR mass spectrometer. CD_3OD was leaked into the ICR cell up to a pressure of $8.0 \pm 1 \times 10^{-9}$ mbar. They observed that the quadruplex [$(TGGGGT)_4.3NH_4^+$] exchanged very fast, in both positive and negative ion mode, compared to DNA duplexes, other quadruplexes and to the corresponding single-stranded TGGGGT. This was unexpected for such a compact and rigid structure.

Håkansson et al. performed gas-phase H/D exchange experiments with D_2S in the external collision cell of a hybrid quadrupole-FT-ICR mass spectrometer [16]. Note that in this group, the percentage of H/D exchange is calculated based on the average m/z of the entire oligonucleotide isotopic distribution. Their results for the DNA homohexamers showed exchange rates in the sequence $dC_6 \approx dA_6 > dG_6 > dT_6$ that correlated with the gas-phase acidities except for guanine. The H/D exchange of RNA homohexamers was faster than for DNA which suggested that another relay mechanism may involve the 2'-hydroxyl group. Presumably due to the intermolecular hydrogen bonds between nucleobases, duplexes exchanged slower than their corresponding single strands.

Recently, Håkansson et al. used gas-phase H/D exchange to characterize nucleic acid higher order structures [17]. They investigated nucleic acid hairpin structures in varying hairpin stabilities by changing their loop size, stem length, and stem composition (ratio of G/C and A/T(U) base pairs in the stem). The observed gas-phase H/D exchange rates of these hairpins were consistent with their relative solution-phase stabilities; less stable nucleic acid hairpins exchanged faster than more sable ones.

To summarize this short review, the gas-phase H/D exchange of nucleic acids and especially of monophosphate nucleotides has been shown to depend on:

- The reagent used for exchange. The extent and rates of exchange depend on its concentration and gas-phase acidity. Compared to D_2O, D_2S was observed to significantly enhance the rates of H/D exchange.
- The nucleobase. The gas-phase acidity of the exchangeable hydrogens and also the orientation of the nucleobase with respect to the sugar and the phosphate group were shown to influence the H/D exchange reactions.
- The phosphate group position (3' or 5') and flexibility.
- Internal motions and deformations in the structure.

A mechanism that involves the phosphate group and the nucleobase was retained for the oligonucleotide H/D exchange. This mechanism, that is named the relay mechanism, corresponds to a cooperative exchange between the charged phosphate and the base. It requires the formation of a hydrogen-bonded complex between a hydrogen donor site of the nucleotide, the deuterating reagent and a deuterium acceptor site (the phosphate group) of the nucleotide, the deuterating reagent bridging the two sites of the nucleotide.

2.5.3. Ion mobility spectrometry of nucleic acids

Ion mobility coupled with mass spectrometry is another powerful technique for investigating the gas-phase structure of biomolecules. In ion mobility experiments, the drift speed of ions through a buffer gas under the influence of a uniform or oscillating electric field is measured. This drift time is directly linked to the mobility of the ions which yields information about their structures because compact ions, which have relatively small collision cross sections, move faster than extended ones, which have large collision cross sections. The gas-phase conformations of many nucleic acids have been investigated by ion mobility. Relevant experimental works are summarized below.

Clemmer et al. reported the first study of the conformations of a deprotonated DNA oligomers in the gas phase: a 10-mer oligothymidine [18]. Deprotonated ions were formed by electrospraying a 10-mer oligothymidine solution in 49.9:49.9:0.2 H_2O:ACN:NH_3. These ions were injected into a drift tube containing ~ 4.00 mbar of helium. Drift times were converted into experimental collision cross sections and compared with the calculated ones. These latter were obtained for an array of conformers generated by molecular modeling techniques. The average projection when the coordinates are rotated through all possible orientations was calculated to estimate theoretical cross sections. A single mobility peak was observed for each charge state. A sharp structural transition was observed when four or more protons were removed; lower charge states favoring compact conformers and higher ones favoring more open conformations. The calculations showed that the gas-phase conformation depends strongly on the number and location of the charge sites. Their results suggested that for the -4 to -6 states, the charges were distributed rather evenly along the 10-mer. Clemmer et al. proposed that an unfolding transition occurs when coulomb repulsion exceeds the hydrogen bonding and van der Waals interactions between residues. For dT_{10},

this transition occurred when ~ 50% of the phosphodiester linkages were charged. The binding of sodium atoms led to more compact structures for the high charge states.

Gidden and Bowers used ion mobility experiments and molecular modeling calculations to investigate the gas-phase conformations of the 16 deprotonated DNA dinucleotides [19]. The ions were formed by MALDI and injected into a drift cell filled with ~ 4.00 mbar of He. The temperature of the drift cell could be varied from 80 to 500 K by flowing warmed or cooled nitrogen through passages surrounding the cell. The experimental cross sections obtained from the arrival time distributions (ATDs) were compared with the theoretical ones. Molecular dynamics calculations were used to generate model conformations of the 16 dinucleotide ions. 100 low energy model structures were obtained for each dinucleotide by a series of simulated annealing and energy minimization cycles. The angle-averaged collision cross section of each structure was calculated with a developed temperature-dependent projection model. At high temperatures ($\geq$ 300 K), only one peak was observed in the ATDs, but when the temperature was lowered to 80 K, multiple peaks appeared. The dinucleotides were grouped into four categories based on the number and relative intensities of peaks present in the 80 K ATDs. These groups are showed in Figure 2.5.5. dAT, dCT, dGT, dTT and dTG were part of the first group (a). The second group (b) was composed of dAA, dCA, dTA, dAG and dGC. dGA and dGG were the only oligonucleotides of the third group (c). The fourth group (d) had three peaks in the 80 K ATDs and dAC, dCC, dGC and dTC were members of this group. The presence of multiple peaks in ATDs indicated that the dinucleotides have multiple conformations that do not rapidly interconvert on the experimental time scale (500 ± 200 μs) at 80 K.

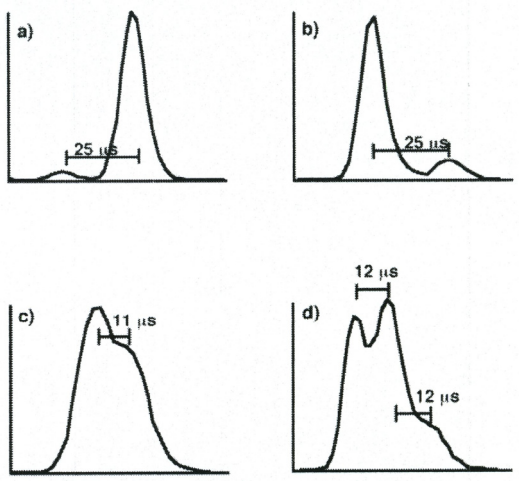

Figure 2.5.5. 80 K ATDs for (a) dAT, (b) dTA, (c) dGA, and (d) dGC. All 16 dinucleotides had 80 K ATDs that ressembled one of the four showed here (adapted form [19]).

The theoretical modeling allowed to determine three distinct families of conformers; stacked, H-bonded and open (Figure 2.5.6.). The family, where the two nucleobases were stacked, had the smallest cross section and was predicted to be lowest in energy. In the H-bonded family, the two bases were approximately in the same plane and hydrogen-bonded to each other. These structures were similar in energy to the stacked ones but had 10-12 $Å^2$ larger cross sections. In the latest family, the open one, the two bases were separated from each other. This corresponded to the largest cross sections that were predicted to be slightly higher in energy than the stacked forms.

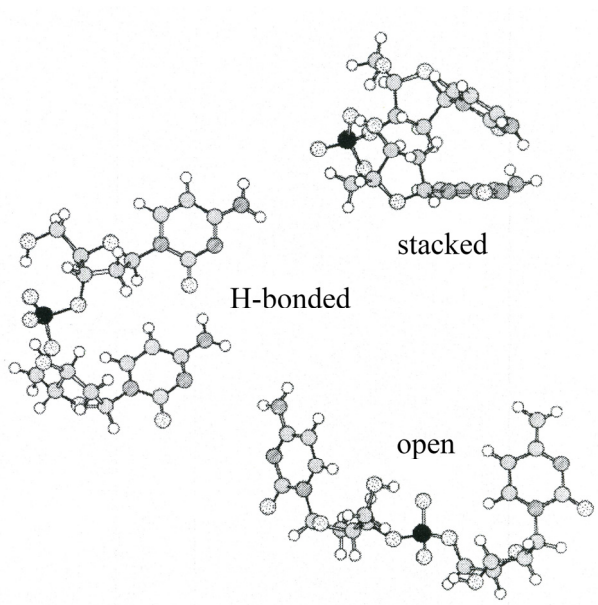

Figure 2.5.6. Representatives of the three families of conformations. Carbon atoms are gray, oxygens are spotted, nitrogens are striped, hydrogens are white, and the phosphorous atom is black (adapted form [19]).

The different 80 K ATD peaks were identified for all the dinucleotides based on comparison of cross-sectional differences observed from experiment and theory. These identifications are summarized in Table 2.5.IV.

Table 2.5.IV. Categories into which the dinucleotides could be grouped based on the conformations observed in their 80 K ATDs. [a]Dominant peak in the ATD. [b]the stacked peak is slightly dominant for dGA while the H-bonded peak is dominant for dGG (adapted form [19]).

Observed conformers	dinucleotides
Stacked / open[a]	dAT, dCT, dGT, dTT, dTG
Stacked[a] / open	dAA, dCA, dTA, dAG, dGG
Stacked[b] / H-bonded[b]	dGA, dGG
Stacked / H-bonded[a] / open	dAC, dCC, dGC, dTC

The 3' base appeared to play a major role in directing the conformational preferences of the dinucleotides. Dinucleotides with a 3'T favored open conformations, those with a 3'A preferred stacked conformation and those with a 3'C preferentially adopted H-bonded structures. The conformation adopted by the dinucleotides with a 3'G tended to be more dependent on the 5' base; dAG and dCG preferred stacked conformations, dGG preferred the H-bonded conformation, and dTG preferred the open conformation. An explanation of these preferences has not been yet found. The G base is known to form a –syn conformation when it is in the 3'-position which leads to a hydrogen bond to the phosphate group [20,21]. This additional H-bond in the open conformers of dinucleotides with a 3'G was suspected to be part of the reason why dTG favored the open conformation, why dAG opened up, why dGA did not. The theoretical modeling of ATDs as a function of temperature allowed to measure the heights of the isomerization barriers which range from 0.8 to 12.9 kcal/mol.

Gidden and Bowers also studied the gas-phase conformations of three deprotonated trinucleotides ($dGTT^-$, $dTGT^-$, $dTGG^-$) in order to investigate the possibility of zwitterion formation [22]. $dTGT^-$ was theoretically modeled assuming a zwitterionic and a non-zwitterionic structure while $dGTT^-$ and $dTGG^-$ were considered as non-zwitterions. The ion mobility experiments and the molecular dynamics calculations indicated that $dTGT^-$ is not a stable zwitterion in the gas phase; the theoretical structures predicted for the zwitterionic form did not correlate with the ion mobility data. However, when $dTGT^-$ was modeled as a singly deprotonated species (independently of which phosphate group was deprotonated), theoretical and experimental results agreed with each other; two conformers were predicted and observed (a folded conformation in which G stacked with one of the T bases and the other T folded towards this stacked pair and an open conformation in which the other T extended away from the T/G stacked pair). $dGTT^-$ and $dTGG^-$ provided further evidence that $dTGT^-$ is not a zwitterion since similar folded and open conformers and cross sections were determined.

In 2004, Gidden et al. investigated the gas-phase conformations of DNA duplexes by ion mobility and molecular modeling[23,24]. They tested the influence of metal ions on Watson-Crick base pairing, and observed that it was enhanced in dinucleotides which were cationized by d_{10} metals [24]. The onset of helicity was probed as a function of strand length [23]. For poly $d(CG)_n$, the 4-mer and 6-mer

duplexes were found to have globular conformations. The helical structures appeared at the 8-mer length, the globular form being still observed and remaining the more favored conformer. For the 10-mer, 14-mer and 18-mer, only helical structures were observed. The helical structures were also observed to be base dependent, with A-T pairs preferentially broken over C-G pairs, and sequence dependent because A-T pairs on the ends of the duplexes were more easily disrupted than if they were in the middle of the duplex [24]. Note that in almost all cases, the structures observed in the ion mobility experiments were not the lowest energy structures predicted by molecular dynamics calculations.

Bowers et al. studied experimentally the sequential addition of water molecules to the four deprotonated 5'-mononucleotides by equilibrium measurements using an ESI-MS equipped with a drift cell containing ~ 1.33 mbar of H_2O. In addition molecular modeling and density functional theory calculations were performed [25]. Theory indicated that the first water molecule bound to the charge-carrying phosphate group. Moreover, this first water molecule bound more strongly than the second to fourth water molecule. The latter were found to have about the same binding energy regardless of the nucleotide. Furthermore, theory predicted that these second to fourth water molecules bound equally to a number of functional groups, as well to the phosphate group as to the deoxyribose hydroxyl group and to various functional groups on the nucleobases. On the contrary to amino acids and peptides that undergo significant structural changes upon addition of only a few water molecules, a remarkable conservation of conformation with hydration was observed for mononucleotides.

In 2006, Baker et al. determined that G-quadruplexes in telomeric repeats were present in a solvent-free environment [26]. They investigated different lengths of the telomeric repeat $d(T_2AG_3)n$ (n = 1, 2, 4 and 6) and dTG_4T with mass spectrometry, ion mobility and molecular dynamics calculations. Experimental cross sections were obtained using ion mobility methods and quantitatively matched to model cross sections for specific strand orientations (parallel/antiparallel) and structures.

Soon after, Gabelica et al. demonstrated that G-quadruplex intramolecular folds were stabilized by NH_4^+ cations and several ligands [27]. Their solvent-free experimental observations and theoretical calculations revealed structures that are highly relevant to the solution-phase structures.

References

1. Mel'nikov, S. M.; Khan, M. O.; Lindmann, B.; Jönsson, B. Phase Behavior of Single DNA in Mixed Solvents. *J. Am. Chem. Soc.* **1999,** *121*, 1130-1136.

2. Wan, K. X.; Shibue, T.; Gross, M. L. Non-covalent complexes between DNA-binding drugs and double-stranded oligodeoxynucleotides: A study by ESI ion-trap mass spectrometry. *J. Am. Chem. Soc.* **2000,** *122* (2), 300-307.

3. Rosu, F.; Gabelica, V.; Houssier, C.; De Pauw, E. Determination of affinity, stoichiometry and sequence selectivity of minor groove binder complexes with double-stranded oligodeoxynucleotides by electrospray ionization mass spectrometry. *Nucleic Acids Res.* **2002,** *30* (16), e82.

4. Rosu, F.; De Pauw, E.; Guittat, L.; Alberti, P.; Lacroix, L.; Mailliet, P.; Riou, J. F.; Mergny, J. L. Selective interaction of ethidium derivatives with quadruplexes: An equilibrium dialysis and electrospray ionization mass spectrometry analysis. *Biochemistry* **2003,** *42* (35), 10361-10371.

5. Sannes-Lowery, K. A.; Griffey, R. H.; Hofstadler, S. A. Measuring dissociation constants of RNA and aminoglycoside antibiotics by electrospray ionization mass spectrometry. *Anal. Biochem.* **2000,** *280* (2), 264-271.

6. Sannes-Lowery, K. A.; Drader, J. J.; Griffey, R. H.; Hofstadler, S. A. Fourier transform ion cyclotron resonance mass spectrometry as a high throughput affinity screen to identify RNA binding ligands. *Trac-Trends in Analytical Chemistry* **2000,** *19* (8), 481-491.

7. Rosu, F.; Pirotte, S.; De Pauw, E.; Gabelica, V. Positive and negative ion mode ESI-MS and MS/MS for studying drug-DNA complexes. *Int. J. Mass Spectrom.* **2006,** *253*, 156-171.

8. Robinson, J. M.; Greig, M. J.; Griffey, R. H.; Venkantraman, M.; Laude, D. A. Hydrogen/Deuterium Exchange of Nucleotides in the Gas Phase. *Anal. Chem.* **1998,** *70*, 3566-3571.

9. Freitas, M. A.; Shi, S. D. H.; Hendrickson, C. L.; Marshall, A. G. Gas-Phase RNA and DNA Ions. 1. H/D Exchange of the $[M-H]^-$ Anions of Nucleoside 5'-Monophosphates (GMP, dGMP, AMP, dAMP, CMP, dCMP, UMP, dTMP), Ribose 5-Monophosphate, and 2-Deoxyribose 5-Monophosphate with D_2O and D_2S. *J. Am. Chem. Soc.* **1998,** *120*, 10187-10193.

10. Freitas, M. A.; Marshall, A. G. Gas-Phase RNA and DNA Ions. 2. Conformational Dependence of the Gas-Phase H/D Exchange of

Nucleotide-5'-Monophosphates. *J. Am. Soc. Mass Spectrom.* **2001,** *12*, 780-785.

11. Crestoni, M. E.; Fornarini, S. Gas-Phase Hydrogen/Deuterium Exchange of Adenine Nucleotides. *J. Mass Spectrom.* **2003,** *38*, 854-861.

12. Chipuk, J. E.; Brodbelt, J. S. Gas-Phase Hydrogen/Deuterium Exchange of 5'- and 3'-Mononucleotides in a Quadrupole ion Trap: Exploring the Role of Conformation and System Energy. *J. Am. Soc. Mass Spectrom.* **2007,** *18*, 724-736.

13. Griffey, R. H.; Greig, M. J.; Robinson, J. M.; Laude, D. A. Gas-phase Hydrogen-Deuterium Exchange in Phosphorothioate d(GTCAG) and d(TCGAT). *Rapid Commun. Mass Spectrom.* **1999,** *13*, 113-117.

14. Hofstadler, S. A.; Griffey, R. H. Analysis of noncovalent complexes of DNA and RNA by mass spectrometry. *Chem. Rev.* **2001,** *101*, 377-390.

15. Gabelica, V.; Rosu, F.; Witt, M.; Baykut, G.; De Pauw, E. Fast gas-phase hydrogen/deuterium exchange observed for a DNA G-quadruplex. *Rapid Commun. Mass Spectrom.* **2005,** *19*, 201-208.

16. Mo, J.; Hakansson, K. Oligonucleotide Gas-Phase Hydrogen/Deuterium Exchange with D_2S in the Collision Cell of a Quadrupole-Fourier Transform Ion Cyclotron Resonance Mass Spectrometer. *Anal. Chem.* **2007,** *79*, 7893-7898.

17. Mo, J.; Todd, G. C.; Hakansson, K. Characterization of Nucleic Acid Higher Order Structure by Gas-Phase H/D Exchange in a Quadrupole-FT-ICR Mass Spectrometer. *Biopolymers* **2009,** *91*, 256-264.

18. Hoaglund, C. S.; Liu, Y.; Ellington, A. D.; Pagel, M.; Clemmer, D. E. Gas-Phase DNA: Oligothymidine Ion Conformers. *J. Am. Chem. Soc.* **1997,** *119*, 9051-9052.

19. Gidden, J.; Bowers, M. T. Gas-phase conformational and energetic properties of deprotonated dinucleotides. *Eur. Phys. J. D* **2002,** *20*, 409-419.

20. Nir, E.; Imhof, P.; Kleinermanns, K.; de Vries, M. S. REMPI Spectroscopy of Laser Desorbed Guanosines. *J. Am. Chem. Soc.* **2000,** *122*, 8091-8092.

21. Rodgers, M. T.; Campbell, S.; Marzluff, E. M.; Beauchamp, J. L. Low-Energy Collision-Induced Dissociation of Deprotonated Dinucleotides: Determination of the Energetically Favored Dissociation Pathways and the Relative Acidities of Nucleic Acid Bases. *Int. J. Mass Spectrom. and Ion Processes* **1994,** *137*, 121-149.

22. Gidden, J.; Bowers, M. T. Gas-Phase Conformations of Deprotonated Trinucleotides ($dGTT^-$, $dTGT^-$, and $dTTG^-$): The Question of Zwitterion Formation. *J. Am. Soc. Mass Spectrom.* **2003,** *14*, 161-170.

23. Gidden, J.; Ferzoco, A.; Baker, E. S.; Bowers, M. T. Duplex Formation and the Onset of Helicity in Poly $d(CG)_n$ Oligonucleotides in a Solvent-Free Environment. *J. Am. Chem. Soc.* **2004,** *126*, 15132-15140.

24. Gidden, J.; Baker, E. S.; Ferzoco, A.; Bowers, M. T. Structural motifs of DNA complexes in the gas phase. *Int. J. Mass Spectrom.* **2005,** *240*, 183-193.

25. Liu, D.; Wyttenbach, T.; Bowers, M. T. Hydration of Mononucleotides. *J. Am. Chem. Soc.* **2006,** *128*, 15155-15163.

26. Baker, E. S.; Bernstein, S. L.; Gabelica, V.; De Pauw, E.; Bowers, M. T. G-quadruplexes in telomeric repeats are conserved in a solvent-free environment. *Int. J. Mass Spectrom.* **2006,** *253*, 225-237.

27. Gabelica, V.; Baker, E. S.; Teulade-Fichou, M.-P.; De Pauw, E.; Bowers, M. T. Stabilization and Structure of Telomeric and c-myc Region Intramolecular G-Quadruplexes: The Role of Central Cations and Small Planar Ligands. *J. Am. Chem. Soc.* **2007,** *129*, 895-904.

Chapter 3: Conformational research and geometry optimization [1-4]

The nuclear arrangement of a molecule is defined by a set of coordinates. These coordinates can be the Cartesian ones but the internal ones are usually preferred. The internal coordinates are the bond lengths, the valence angles and the dihedral angles. If NA is the number of nuclei that compose the molecule and if the relative coordinates are used (which means that the coordinates of the mass center and the rotation coordinates (Euler angles) of the whole molecule are not taken into account), 3NA-6 nuclear coordinates globally noted C_R are considered.

The potential energy of the nuclei, $U(C_R)$, depends on the nuclear coordinates C_R and therefore on the geometry. This function of 3NA-6 coordinates is defined as a hypersurface of potential energy. As it usually varies continuously, its partial derivatives $\frac{\delta U}{\delta C_{Ri}}$, i = 1,…,3NA-6 can be calculated. They make up the gradient of the potential energy:

$$\vec{\nabla} U = \vec{G} \qquad (1)$$

A critical point is a point of the surface where all the gradient components are equal to zero. These points are also named the stationary points. They correspond to geometries where the forces that act on the nuclei vanish. These points correspond to either stable or unstable equilibriums. They can be classified according to the second derivative of the potential energy which is makes up the Hessian matrix. It is a hermitian matrix. A minimum, i.e. a stable equilibrium point, is characterized by a Hessian matrix whose all eigenvalues are positive with the possibility that the lowest value could be close to zero if the surface is very flat. A critical point of n^{th} order ($n \neq 0$) is characterized by a Hessian matrix that has n negative eigenvalues. In particular, if n = 1, the critical point is called a transition state. In general terms, for a minimum point, the energy increases for all displacements with respect to the point where $\vec{G} = 0$. For a critical point of n^{th} order, the energy increases for all displacements from the point where $\vec{G} = 0$ except in n orthogonal directions along which all motions involve an energy decrease.

The geometry optimization process aims at finding the critical points for which $\vec{G} = 0$. A constraint regarding the number of negative eigenvalues can be imposed to look for minima or transition states. The gradient, calculated in an analytical way, is inserted in an automatic process. As the gradient is a vector that is oriented along the direction of the highest increase of the function, the direction corresponding to the opposite of the gradient - $\vec{G}$ must be followed in order to reach the stationary point. Different methods exist according to the descent direction that can only be opposite to the gradient (the steepest descent method) or can take the previous directions (conjugate gradients methods) into account. To localize a critical point that differs from a minimum, the structure of the Hessian matrix must be taken into account. The potential energy of the nuclei $U(C_R)$ is then developed at least up to the second order. The used method is named the Newton-Raphson method. Various versions of this method exist and are named the "level-shifted Newton-Raphson" method and the pseudo Newton-Raphson methods.

3.1. Molecular mechanics and dynamics

Molecular mechanics is a field that takes the nucleus interactions in a molecule into account in a parametric way using simple analytical expressions to describe the forces that act on the nuclei.

The forces that act on the nuclei are linked to the potential energy $U(C_R)$ by the following expression,

$$\vec{F} = -\vec{\nabla}U \qquad (2)$$

The potential energy of the nuclei $U(C_R)$ is determined in an empirical way by adjustment to results obtained from quantum chemistry and/or experiments. Generally, the U function is defined and used for one family of related molecules.

A molecular structure is defined by three characteristics:

1. Its conformation which is given by the position of each nucleus
2. The nature of the constitutive atoms (their masses, their atomic numbers, their van der Waals radii, the bonds in which they are involved…)
3. The force field that characterizes the response of the molecule to deformation of its structure

The force field defines the energy cost coming from all modification of the optimal structure. A large number of force fields exist. They can be classified according to different generations:

1. The first generation uses harmonic terms and no crossed term is taken into account (AMBER, CHRAMM)
2. Higher order terms and non-diagonal components of the matrix of the force constants are considered in the second generation of force fields (MM2,MM3)
3. In the third generation, some terms that take into account chemical effects like electronegativity, hyperconjugation… are added (MM4,MMFF94)
4. Recently, a fourth generation has appeared which is more universal. For example, the DREIDING force field uses force constants and geometrical parameters which are more flexible because they are associated with atom types and simple hybridization considerations [5].

Apart from the last generation, each force field is programmed for a kind of macromolecule. For example, the AMBER and CHARMM force fields are dedicated to peptides and nucleic acids, the MM2, MM3 and MM4 force fields are optimized for hydrocarbon molecules…

The potential energy of the nuclei can be minimized in molecular mechanics to find stable conformers. Numerically, a point where the gradient is exactly equal to zero can not be found. A threshold of convergence is defined.

Another important application of molecular mechanics is molecular dynamics. This method allows to consider one conformation not like an energy minimum, but like an average set of structures according to the temperature at constant pressure and volume. Molecular dynamics simulations are based on the solution of the Newton equations;

$$m_i \frac{d^2 \vec{r_i}}{dt^2} = -\vec{\nabla}_i U(\vec{r_1}, \vec{r_2}, ..., \vec{r_N}) \quad (3)$$

If the expression of U and the initial conditions of the system are known, the state of the system can be determined at any time. The initial conformation comes from a geometric optimization in molecular mechanics and the initial velocities are chosen at random according to the temperature from the Maxwell-Boltzman law $\exp(-\frac{E_{k,i}}{k_B \cdot T})$ where $E_{k,i}$ is the kinetic energy of the i^{th} atom and k_B is the

Boltzman constant. The molecular dynamics results can lead to qualitative values of thermodynamic parameters.

3.2. Geometry optimization in quantum chemistry

The Schrödinger equation is the fundamental equation of quantum mechanics. Solutions of the time-independent Schrödinger equation are called stationary-state wave functions. These wave functions give a complete description of the selected system. The time-independent Schrödinger equation is written,

$$\mathbf{H}\Psi(C_R, c_r) = E\Psi(C_R, c_r) \quad (4)$$

where **H** is the Hamiltonian operator associated with the total energy E of the system, and C_R and c_r are respectively the nuclear and electronic coordinates.

The Hamiltonian operator is written,

$$\mathbf{H} = \mathbf{T_N} + \mathbf{T_e} + \mathbf{V_{eN}} + \mathbf{V_{ee}} + \mathbf{V_{NN}} = \mathbf{T_N} + \mathbf{H^e} + \mathbf{V_{NN}} \quad (5)$$

where $\mathbf{T_N}$ and $\mathbf{T_e}$ are respectively the nuclear and electronic operators of the kinetic energy, $\mathbf{V_{eN}}$, $\mathbf{V_{ee}}$ and $\mathbf{V_{NN}}$ are the operators that correspond to the energy of electrostatic interactions between the electrons and nuclei ($\mathbf{V_{eN}}$), between the electrons ($\mathbf{V_{ee}}$), and between the nuclei ($\mathbf{V_{NN}}$).

Within the framework of the Born-Oppenheimer approximation where the motions of electrons and nuclei are adiabatically decoupled, the wave function can be written like a product;

$$\Psi(C_R, c_r) = \mathrm{X}_N(C_R)\Psi^e(c_r; C_R) \quad (6)$$

The Schrödinger equation can then be solved as follows:

$$\mathbf{H}^e\Psi^e(c_r; C_R) = E^e(C_R)\Psi^e(c_r; C_R) \quad (7)$$

$$(\mathbf{T_N} + E^e(C_R) + \mathrm{V_{NN}}(C_R))\mathrm{X}_N(C_R) = E\mathrm{X}_N(C_R) \quad (8)$$

If $E^e(C_R) + \mathrm{V_{NN}}(C_R)$ is replaced by $U(C_R)$ in equation (8), it can be written

$$(\mathbf{T_N} + U(C_R))\mathrm{X}_N(C_R) = E\mathrm{X}_N(C_R) \quad (9)$$

where $U(C_R)$ corresponds to the potential energy of the nuclei discussed in the previous subsections.

As previously explained, a geometry optimization consists in finding the critical points for which the gradient is equal to zero. With this aim in view, $U(C_R)$ and therefore $E^e(C_R)$ have to be calculated. Several methods exist to find and minimize the electronic energy $E^e(C_R)$. Among these methods, some are said to be ab initio. This means that the correct Hamiltonian operator is used and that no experimental data except the fundamental physical constants are integrated in the

method. The Hartree-Fock-SCF-MO method is an ab initio one. Other methods, non-ab initio, better describe the electronic correlation; the Møller-Plesset method which is based on a perturbative approach (MP2, MP4) and the Density functional Theory which rests on the use of the electronic density (LDA, B3LYP).

The wave functions are usually developed on basis functions. Several kinds of basis functions exist. Among these ones, the split-valence basis sets are very well-known. For example, the basis set 6-31G is usually used. It corresponds to:

- Linear combinations of six primitive Gaussian functions with fixed coefficients to describe the 1s core orbitals
- Two sets of Gaussian functions to describe the valence orbitals:
    - One fixed linear combination of three primitive Gaussian functions for the inner components of the valence orbitals.
    - One Gaussian function for the outer component of the valence orbitals.

Several basis functions can be implemented with the aim of bringing some flexibility to the total wave function. When they have some characteristics of the p,d or f atomic orbitals, they are called the polarization functions and are referenced with an asterisk (6-31G*). For molecular system with a negative charge, s and p diffuse functions are added to minimize the repulsion energy between the electrons. They are referenced with a plus sign (6-31+G).

References

1. Remacle, F. Chimie Physique Moleculaire. 2002.

2. Dehareng, D. Aide à l'utilisation de la chimie quantique. 2005.

3. Dehareng, D. Mécanique et dynamique moléculaires. 2008.

4. Jensen, F. *Introduction to computational chemistry;* Wiley: New York, 1999.

5. Mayo, S. L.; Olafson, B. D.; Goddard III, W. A. DREIDING: A Generic Force Field for Molecular Simulations. *J. Phys. Chem.* **1990,** *94*, 8897-8909.

Chapter 4: Gas-phase H/D exchange of single stranded oligonucleotides

As already discussed in chapter 2, hydrogen/deuterium (H/D) exchange combined with mass spectrometry is an efficient tool for studying the gas-phase structure of biomolecules. Structural isomers can be distinguished and structural and thermochemical features can be deduced through the determination of the number of exchanged hydrogen and the analysis of the H/D exchange kinetics.

The present chapter focuses on the gas-phase H/D exchange of single stranded oligonucleotides (DNA and RNA). These gas-phase H/D exchange experiments have been performed in the hexapole collision cell of our 9.4 T FT-ICR mass spectrometer with CD_3OD as the deuterating agent. The aim of these experiments is to understand the mechanisms of the reactions that happen during H/D exchange, and to identify the major parameters governing the extent and rates of exchange. For that purpose, H/D exchange experiments have been investigated not in the ICR cell (as usually proposed) but in the collision cell (second hexapole). This allows a higher exchange gas pressure to be reached (10^{-3} mbar instead of 10^{-8} - 10^{-7} mbar) ensuring that the H/D exchange reaction is not the limiting step. Molecular mechanics and dynamics computations have also been performed to substantiate the analysis of the experimental data.

4.1. Conformationally driven gas-phase H/D exchange of dinucleotide negative ions

This study has been published in the Journal of The American Society for Mass Spectrometry (*J. Am. Soc. Mass Spectrom.* **2007**, *18*, 1827-1834). To improve the reading quality, it is presented in author post-print format.

Conformationally Driven Gas-Phase H/D Exchange of Dinucleotide Negative Ions

Balbeur Dorothée[1], Dehareng Dominique[2], De Pauw Edwin[1]

[1] Laboratory of Mass Spectrometry, University of Liège, Liège, Belgium
[2] Center for protein Engineering, University of Liège, Liège, Belgium

Gas-phase hydrogen/deuterium exchange of six deprotonated dinucleotides with CD_3OD was performed in the second hexapole of a Fourier transform ion-cyclotron resonance (FTICR) mass spectrometer. To complete these experiments, dynamic simulations were carried out to investigate the different conformations adopted by the dinucleotides. In the experimental conditions and in integrating the experimental and theoretical results, H/D exchange was shown to be controlled by hydrogen accessibility and not by the chemical nature of the heteroatom bearing the exchangeable hydrogen. A model including simultaneous H/D exchanges at the experimental time scale was used to reproduce the dinucleotide H/D exchange kinetic plots. The relay mechanism was not relevant for dinucleotides. This allowed the H/D exchange rates to be directly linked to conformations.

Introduction

The conformations of biomolecules depend on intramolecular non-covalent interactions. These interactions determine, at a molecular level, a vast majority of biological processes (molecular recognition, regulation, transport,…) that define the function of the biomolecule. Hydrogen/Deuterium (H/D) exchange combined with mass spectrometry is an efficient tool for studying the gas-phase structure of biomolecules [1-16]. The rate of gas-phase H/D exchange has been shown to be a function of the reagent used for exchange, the concentration of this reagent, the charge states of the biomolecule, the gas-phase basicity/acidity of exchangeable sites and of the internal structure of the biomolecular ions [1-16]. So the

determination of the exchanged hydrogen number and of the H/D exchange kinetics allows structural isomers of the biomolecule to be distinguished and structural and thermochemical features to be deduced. H/D exchange reactions have been performed using a Fourier transform ion-cyclotron resonance (FTICR) mass spectrometer [1-11] or a quadrupole ion trap [10-16]. Though these two instruments show several differences, they allow the ions to be trapped for variable periods of time in the presence of the deuterating reagent held at a constant pressure.

Deoxyribose monophosphate nucleotides are the structural units of DNA. The gas-phase H/D exchange of these units have been carried out in positive [7,8] or in negative ion mode [3-5,8] with an FTICR-MS and more recently in negative ion mode with a quadrupole ion trap [16]. These different studies have shown that the extents and rates of exchange depend on the nucleobase (identity, orientation and gas-phase acidity of the exchangeable hydrogen) and on the position (3' or 5') and flexibility of the terminal phosphate group. They have also concluded that the most probable mechanism of exchange is the relay mechanism. This mechanism requires the formation of a hydrogen-bonded complex between a hydrogen donor site of the nucleotide, the deuterating reagent and a deuterium acceptor site (the phosphate group) of the nucleotide, the deuterating reagent bridging the two sites of the nucleotide.

The present work focuses on the examination of the gas-phase H/D exchange behavior of six deprotonated dinucleotides. The gas-phase conformations of dinucleotides have already been investigated by molecular modeling calculations and ion mobility experiments [17]. The dinucleotides adopt distinctive conformations that interconvert at the experimental time scale of an FTICR-MS. To determine the life time of the distinctive structures, experimental conditions (the type and pressure of the exchange gas) were chosen such that the H/D exchange reaction was not the limiting step. The data presented here underline the importance of hydrogen accessibility to explain the rates of hydrogen exchange. The accessibility of the exchangeable hydrogen is controlled not only by the distinctive structures adopted by the dinucleotide but also by the protection extent of the hydrogen in these structures, which is linked to the mean time spent in the various isomeric structures. The relay mechanism is not relevant for dinucleotides as the distances between the hydrogen donor and deuterium acceptor sites are not compatible.

Experimental

Sample Preparation

The six dinucleotides (dTT, dAT, dAA, dTG, dAG and dGG) were obtained from Eurogentec (Seraing, Belgium). CD_3OD was purchased from Euriso-Top (Gif sur Yvette, France). All of these compounds were used without further purification. Stock solutions of the dinucleotides (400×10^{-6} M) were prepared in water. Working solutions (1.1765×10^{-5} M) were obtained by dilution in water. The injection solutions were prepared by adding the appropriate amount of MeOH to obtain a $MeOH/H_2O$ ratio of 15/85 (v/v) and a dinucleotide concentration of 10^{-5} M.

Mass Spectrometry

Experiments were performed with a 9.4 Tesla Apex-Qe FTICR mass spectrometer (Bruker Daltonics, Billerica, MA). The dinucleotide solutions were infused via an external Apollo electrospray ion source at a flow rate of 120 µL/h with the assistance of N_2 nebulizing gas. The off axis sprayer was grounded, the end-plate was set to 3 kV and the inlet capillary was set to 3.5 kV for the generation of dinucleotide anions. N_2 heated drying gas (250 °C) was applied to assist desolvation of ESI droplets. Ions were accumulated in the first hexapole for 1.5 s and transferred non-mass selectively through the quadrupole into the second hexapole for 10 ms. They were trapped for variable periods of time in this second hexapole (h2) to carry out H/D exchange reactions and were then transferred through high-voltage ion optics and captured by static trapping in an ICR cell. All mass spectra were acquired with XMASS (version 7.0.8, Bruker Daltonics) in broadband mode from m/z 350 to 900 with 512 k data points and summed over 5 scans. A mass list, in which m/z values and peak heights are recorded, was created by DataAnalysis (version 3.4, Bruker Daltonics).

H/D exchange

All of the H/D exchange reactions were conducted in the gas-phase in the collision cell (second hexapole h2) of the 9.4 Tesla Apex-Qe FTICR mass spectrometer. CD_3OD was used as the deuterating agent. Due to its vapor pressure at ~ 20° C, it was introduced into the second hexapole through the nozzle valve usually used for the collision gas (Ar). Using this system, only CD_3OD was

introduced into h2 with a measured pressure in the surrounding vacuum chamber of 3.75×10^{-6} Torr which corresponds to a pressure in the collision cell of ~ 7.5×10^{-4} Torr. The extent of exchange was observed by monitoring the relative abundance of the precursor ion and of the deuterated species while the CD_3OD pressure was held at ~ 7.5×10^{-4} Torr. Ions were accumulated in the collision cell for 10 ms and were then trapped for H/D exchange reactions from 10 ms to 600 s (the ions entered the hexapole in one group and no other ions entered during the exchange time). The six dinucleotides were analyzed individually on the same day under identical conditions. The experiments were repeated on other days for the same reaction times under conditions as similar as possible to assess reproducibility.

To analyze H/D exchange spectra, an in-house software was used. This software utilizes the known isotopic distribution (percentage of each peak) of the non-deuterated ion. Moreover, it is considered that the ion with a fixed number, X, of exchanged hydrogens has the same isotopic distribution but shifted by X/z unit. The software determines, at each reaction time, the composition of each deuterated species that fits best to the experimental isotopic distribution. The plotting of these compositions to obtain the kinetic plots was done with SigmaPlot (version 9; Systat Software, Inc., San Jose, CA). Several methods for quantitation of peak magnitudes exist and are based on peak height or peak area [18]. In this work, isotopic distributions were described from relative peak heights as advised by A. G. Marshall [19]. Peak area measurements can be problematic because of the presence of wiggles, known as “Gibbs Oscillations”, in FTICR mass spectra. These oscillations result from truncation of the time-domain ICR signal at time, t, before it has decayed to zero.

Molecular Modeling

Dynamic simulations were carried out with HyperChem (version 7; Hypercube, Inc., Gainesville, FL) to investigate the different conformations adopted by the dinucleotides. BIO+ (CHARMM) was used as the force field. Before dynamic simulations, the charges of different atoms were recalculated; atoms of the phosphate group, the first carbon and hydrogen atoms near the phosphate group and the hydrogen atoms of 3’ and 5’ OH extremities. These charge recalculations were performed by single point calculation with ZINDO/1 (semi-empirical SCF method). The net atomic charges were recalculated in order to take into account

the negative charge on the phosphate group. For each deprotonated dinucleotide, two molecular dynamics simulations of 10000 ps at ~ 300 K were done. In these simulations, snapshots were saved every 0.05 ps and distances between key atoms were monitored. The two dynamic simulations differed by the molecule conditioning. For the first simulation, the deprotonated dinucleotide was heated for 100 ps at 900 K and then cooled during 152 ps from 900 K to 300 K. For the second simulation, the ion was geometrically optimized, heated during 150 ps from 0 K to 300 K and then kept for 50 ps at 300 K.

It has been shown via REMPI spectroscopy [20] and in modeling calculations [6,21-23] that guanine favors a syn orientation in the gas-phase. Syn and anti are terms that are associated with the orientation of the nucleobase with respect to the sugar. In the anti orientation, the six-membered pyrimidine ring in purines and O_2 in pyrimidines are pointing away from the sugar and in the syn orientation, it is over or toward the sugar [24]. To analyze the behavior of deprotonated dTG, dAG and dGG in the previous molecular dynamics calculations, ab initio geometry optimizations with syn and anti conformations of G in the 3' position were performed with Gaussian03 [25]. To compare the minimized energy obtained for the two conformations syn and anti, different levels of theory and different basis sets were used; RHF/6-31G-*aug*, B3LYP/6-31G-*aug*, RHF/6-31*G-*aug*, *aug* meaning that the basis set is augmented with diffuse functions on the oxygens and nitrogens and polarization functions on phosphorus. The added basis functions were each represented by one gaussian function. They corresponded, on the one hand, to s and p diffuse functions for oxygen and nitrogen atoms (with an exponent equal to 0.0845 and 0.0639 for oxygen and nitrogen atoms respectively) and on the other hand to d polarization functions for the phosphorus atom (with an exponent equal to 0.55). Five starting points were used for each conformation.

Kinetic simulations

To analyze the H/D exchange kinetics, the software Matlab (version 7.3.0; The MathWorks, Inc., Natick, MA) was used. This software allows personal sets of coupled differential equations and personal sets of rate constants to be introduced. The construction of kinetic plots was done to reproduce H/D exchange experimental plots.

Results and Discussion

H/D Exchange

The typical progression of the hydrogen/deuterium exchange reactions of the deprotonated dinucleotides with CD_3OD in the second hexapole of the FTICR-MS is illustrated in the case of dTG^- in Figure 4.1.1. As the reaction time increased from 0.01 s to 600 s, the increase of exchanged hydrogen number (D(X) corresponds to X exchanged hydrogen atoms) was observed with a corresponding decrease of the abundance of the precursor ion, D(0). As described previously, an in-house software was used to analyze the H/D exchange mass spectra. Kinetic plots were obtained from the calculated composition of each deuterated species at each reaction time. The kinetic plots of dTT^- , dAA^- and dTG^- are presented in Figure 4.1.2. From the kinetic plots, some features were underlined (the major species at given exchange times, the partial exchange, the simultaneous increase of the D(1) and D(2) species, the fast increase of species with a large number of exchanged hydrogens). They are summarized for all of the six deprotonated dinucleotides in Table 4.1.I. These features could not be explained by only the hydrogen gas-phase acidities of 5' and 3'-phophate mononucleotides [16]. So to explain the features, the three-dimensional gas-phase structure of the six deprotonated dinucleotides was investigated by molecular dynamics calculations.

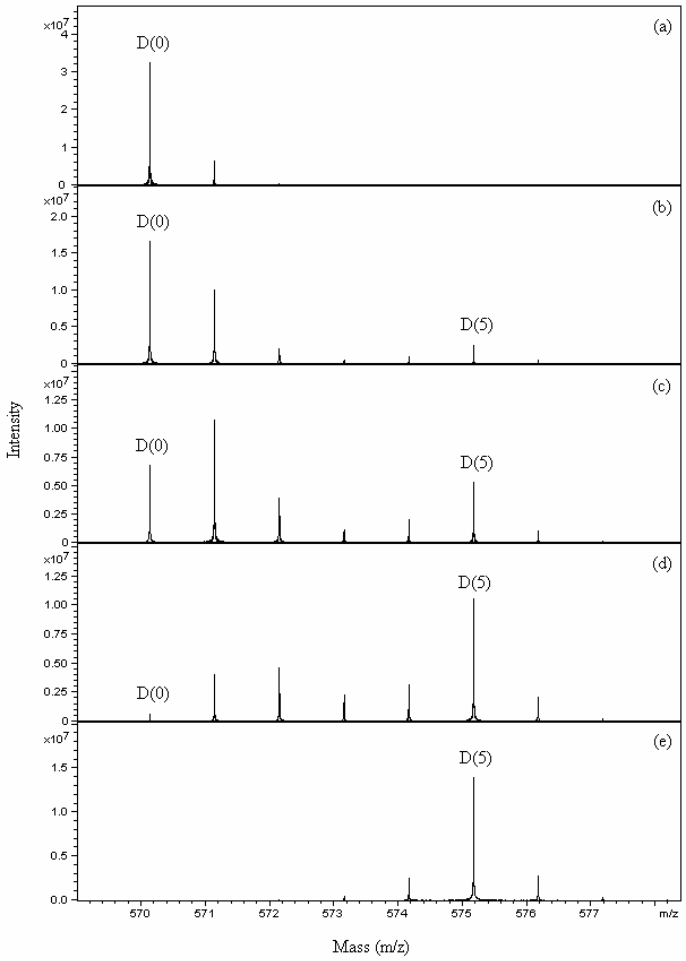

Figure 4.1.1. Representative mass spectra for the reaction of deprotonated dTG with CD_3OD in the second hexapole of an FTICR-MS. H/D exchange reaction times are (a) 0 s, (b) 30 s, (c) 60 s, (d) 150 s and (e) 600 s.

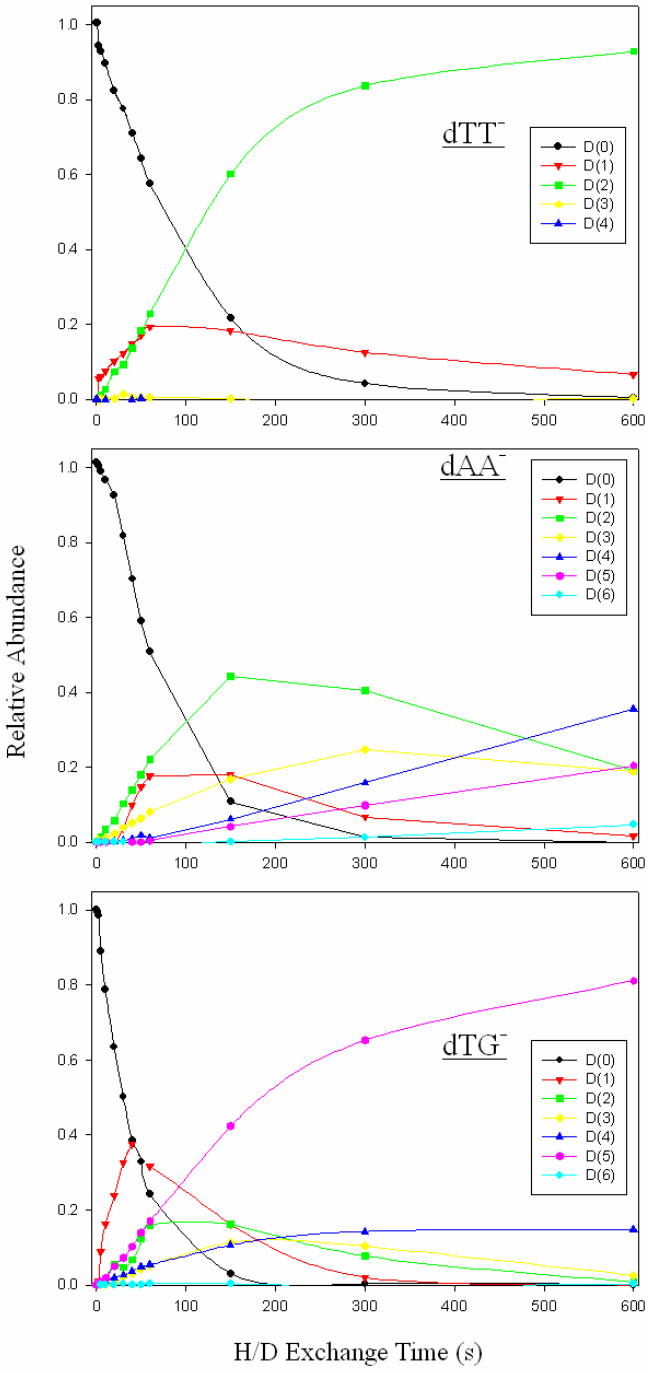

Figure 4.1.2. Kinetic plots of the H/D exchange reaction of deprotonated dTT, dAA and dTG.

Table 4.1.I. Summary of underlined features for all of the six deprotonated dinucleotides.

The deprotonated dinucleotide	The number of exchangeable hydrogens	The number of exchanged hydrogens after 600 s of reaction	features	
			Major species at given reaction times	Kinetic progression
dTT^-	4	2	**D(2)** was always the major species	A non-ordinary kinetic behavior was observed. D(2) appeared at the same time as D(1). The H/D exchange kinetics seemed to be non-consecutive
dAT^-	5	2	**D(2)** was always the major species	
dAA^-	6	6	**D(2)** was the major species until 475 s of reaction	
dTG^-	6	5	**D(1)** was the major species from 0 to 90 s and **D(5)** became the major species after 90 s of reaction	A fast increase of species with a large number of exchanged hydrogens was observed
dAG^-	7	7	**D(1)** was the major species from 0 to 150 s of reaction, **D(5)** was the major species from 150 s to 360 s	
dGG^-	8	8	**D(1)**, **D(2)** and **D(3)** were the major species at first reaction times. **D(8)** became the major species after 200 s of reaction	

Molecular Modeling

During molecular dynamics calculations, distances between exchangeable hydrogens and heteroatoms with which they could interact were monitored. Distinctive structures adopted by the dinucleotide were grouped according to these distances. For each structure or group of structures (in which structures interconverted rapidly), protection percentages were established for each exchangeable hydrogen. These protection percentages were defined as the time percentages (with regard to the “life” time of the structure) during which

exchangeable hydrogens interacted with heteroatoms. The hydrogens were considered to be interacting when the distance between them and the heteroatom was between 1.5 and 4.5 Å. The previously mentioned concept of protection follows from the electrostatic approach. It illustrates the fact that when a hydrogen is involved in an interaction, it is blocked in a particular geometry for a given time during which it is made energetically non-exchangeable. For some hydrogen atoms, the protection extent was also estimated by the time percentage during which these atoms were protected in a cavity. This corresponds to a group of atoms that, surrounding a hydrogen, make it sterically inaccessible for H/D exchange. The distinctive structures and the protection extents are summarized for all of the six deprotonated dinucleotides in Table 4.1.II. A closed structure, unlike an open structure, corresponds to a structure where the two nucleobases are one above the other; a hydrogen of one nucleobase being able to interact with a heteroatom of the other nucleobase. In dTG^- and dAG^-, the base G was always in the syn orientation. Because of this syn orientation, one hydrogen from the NH_2 group of the base G interacted with an oxygen of the phosphate group [6,20-23]. For dTG^-, the interacting hydrogen was the same during the molecular dynamics calculations. For dAG^-, the interacting hydrogen changed once during the molecular modeling. This could explain the stopped H/D exchange to D(5) for dTG^- and the complete exchange for dAG^-. As dAG^- was observed as a group of rapidly interconverted structures, these conformations were analyzed in more detail. In each of these structures, two hydrogens (not necessary the same ones) were more protected. This could explain that D(5) was the major species from 150 s to 360 s of exchange. Taking into account data in Table 4.1.II. and according to the previous analysis, the vast majority of the observed features (Table 4.1.I.) were justified. To confirm the major influence of the hydrogen accessibility on H/D exchange and to explain the observed non-consecutive reaction kinetics, kinetic plots were simulated from the protection extents.

Table 4.1.II. Summary of the distinctive structures and of the protection extents for all of the six deprotonated dinucleotides.

The deprotonated dinucleotide	The distinctive structures	The life time in percentage of the structure	The protection extent of each labile hydrogen	
			5'	3'
dTT^-	The open structure	10.9 %	OH: 0 % NH: 0 %	OH: 0 % NH: 0 %
	The closed structure	**90.1 %**	OH: 0 % NH: 85 %	OH: 0 % NH: 87 %
dAT^-	The open structure	14.9 %	OH: 0 % NH2: 0 % - 0 %	OH: 0 % NH: 0 %
	The closed structure	**85.1 %**	OH: 0 % NH2: 76 % - 78 %	OH: 0 % NH: 75 %
dAA^-	The open structure	2.3 %	OH: 0 % NH2: 0 % - 0 %	OH: 0 % NH2: 0 % - 0 %
	The group of closed structures	**97.7 %**	OH: ~ 30 % NH2: 53 % - 52 %	OH: 0 % NH2: 69 % - 68 %
dTG^-	The closed structure A	50 %	OH: 0 % NH: 0 %	OH: 0 % NH: 0 % NH2: 100 % - 0 %
	The closed structure B	50 %	OH: 54 % NH: 65 %	OH: 0 % NH: 64 % NH2: 100 % - 62 %
dAG^-	The group of closed structures	100 %	OH: ~ 25 % NH2: 69 % - 70 %	OH: 0 % NH: 50 % NH2: 65 % - 35 %
dGG^-	The closed structure with 3' G in syn orientation	50 %	OH: 0 % NH: 75 % NH2: 94 % - 94 %	OH: 0 % NH: 0 % NH2: 10 % - 90 %
	The closed structure with 3' G in anti orientation	50 %	OH: 100 % NH: 75 % NH2: 49 % - 45 %	OH: 0 % NH: 96 % NH2: 92 % - ~ 25 %

In dGG^-, the 3' base was in the syn orientation (one hydrogen from the NH_2 group interacts with an oxygen of the phosphate group) for one molecular dynamics calculation and in the anti orientation (the previously mentioned interaction is not present) for the second molecular modeling (Figure 4.1.3.). To compare this different behavior with respect to dTG^- and dAG^-, ab initio

geometry optimizations for the syn and anti conformations of the 3' nucleobase G were performed with Gaussian03 for these three deprotonated dinucleotides. The obtained energies at different levels of theory and with different basis sets are presented in Table 4.1.III. For each conformation, all starting points resulted in identical local minimum. For dTG^- and dAG^-, the more stable orientation of the 3' nucleobase G is the syn orientation. For dGG^-, the syn and anti orientations seem to have the same energy and so the same probability.

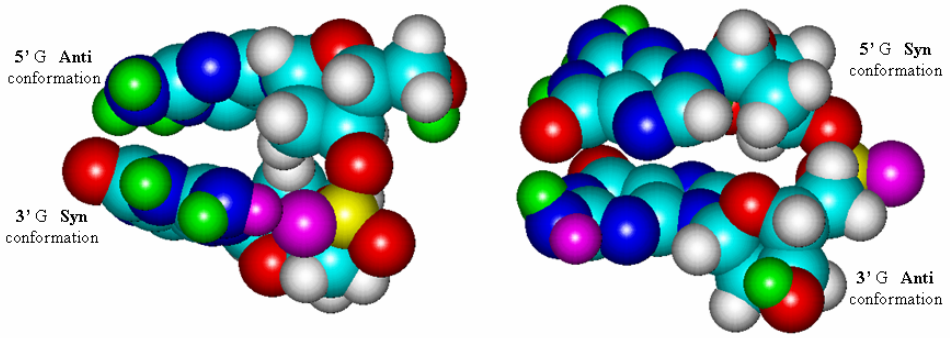

Figure 4.1.3. The distinctive structures of dGG^-. On the left structure, the 3' nucleobase is in the syn orientation. One hydrogen from the NH_2 group of this nucleobase interacts with an oxygen of the phosphate group (the interacting atoms are painted in purple). On the right structure, the 3' nucleobase is in the anti orientation and the previously mentioned interaction is not present. The exchangeable hydrogens are painted in green.

Table 4.1.III. The energy difference between the anti and syn orientations (kcal/mole). The syn orientation is lower in energy.

The deprotonated dinucleotide	RHF/6-31G-*aug*	B3LYP/6-31G-*aug*	RHF/6-31*G-*aug*
dTG^-	5.2256	6.4934	4.7621
dAG^-	7.5325	11.3691	8.1387
dGG^-	0.8655	0.3710	0.2215

Kinetic Simulations

As mentioned above, the H/D exchange itself was not the limiting step. The D(1) and D(2) species appeared at the same rate and species with a large number of exchanged hydrogens appeared rapidly. To explain these observations, a new kinetic mechanism was proposed. It is illustrated for three exchangeable hydrogens with the diagram in Figure 4.1.4. This kinetic mechanism indicates that if the number of collisions between deuterated methanol and dinucleotide ions was sufficient and if two hydrogens on the same deprotonated dinucleotide were accessible at the same time, these two hydrogens could be exchanged simultaneously at the experimental time scale. This mechanism was used to reproduce the H/D exchange experimental plots. To build these simulated kinetic plots, each exchangeable hydrogen was given an exchange rate constant according to its protection extent. Moreover, the model was based on the assumption that the rate constant of the simultaneous exchange reaction of two hydrogens corresponded to the rate constant of the slowest. The rate constants that were used for the simulation of dAA^- kinetic plot are given in tables 4.1.IV. and V. The simulated plots of dTT^- and dAA^- are presented in Figure 4.1.5. For dTG^-, the experimental plot was approached in adding the kinetic contributions of the two structures. This kinetic mechanism was also applied to previously published mononucleotide H/D exchange [16]. A very good agreement with the kinetic plots was obtained. As previously mentioned, the relay mechanism requires the formation of a hydrogen-bonded complex between a hydrogen donor site of the nucleotide, the deuterating agent and a deuterium acceptor site (the phosphate group) of the nucleotide, involving the restriction of the distance between the hydrogen donor and acceptor sites. The formation of such a three partners complex is entropically unfavorable. Moreover, for dinucleotides, this relay mechanism is not appropriate as the distances between the hydrogen donor and deuterium acceptor sites are not compatible. A “direct” H/D exchange between the deuterating agent and the site bearing the exchangeable hydrogen is more relevant for dinucleotides. This “direct” exchange could be combined with the relay mechanism to explain the mononucleotides H/D exchange. In suitable experimental conditions, the simultaneous exchange should be taken into account for mononucleotides exchange. It is possible that this could be applied to the relay mechanism if this one is sufficiently fast in comparison to the experimental time scale. For all of the kinetic simulations, the value of the simultaneous exchange probability was either equal to or in the range of up to twice the value of the

consecutive exchange probability. The fact that these two probabilities can differ is not excluded and must depend on the H/D exchange experimental conditions. To support the simultaneous exchange of two accessible hydrogens, the number of collisions between a dinucleotide ion and a CD_3OD gas was estimated. At the experimental pressure and according to [26], the mean free path should be such that the dinucleotide ions undergo at least 10^4 collisions per second.

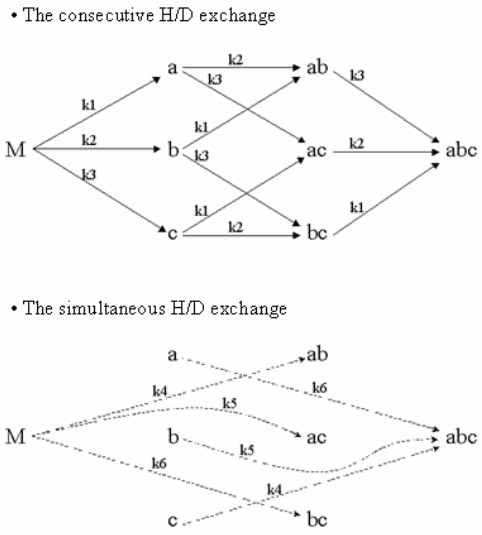

Figure 4.1.4. Illustration of the proposed kinetic mechanism that consists of consecutive and simultaneous H/D exchange reactions. M is the non-deuterated ion, a, b and c correspond to the three exchangeable hydrogens and k1, k2 and k3 are their rate constants.

Table 4.1.IV. The protection extent and the corresponding rate constant of each exchangeable hydrogen of dAA^- (the used set of coupled differential equations corresponds to the five most exchangeable hydrogens).

	The labile hydrogens	The protection extents	The rate constants $(s^{-1})^a$	
5'	OH	30%	0.0012	b
	NH_2	53%	0.00075	c
		52%	0.00075	d
3'	OH	0%	0.002	a
	NH_2	69%	0.00045	e
		68%	0.00045	

[a]As CD_3OD is in excess, its concentration can be considered as constant and the reaction as having an apparent first-order kinetics.

Table 4.1.V. The set of rate constants $(s^{-1})^a$ used to simulate the kinetic plot of dAA^-.

	The consecutive H/D exchange	The simultaneous H/D exchange
M	a = 0.002	ab = 0.0012
		ac = 0.00075
	b = 0.0012	ad = 0.00075
		ae = 0.00045
	c = 0.00075	bc = 0.00075
		bd = 0.00075
	d = 0.00075	be = 0.00045
		cd = 0.00075
	e = 0.00045	ce = 0.00045
		de = 0.00045

[a]As CD_3OD is in excess, its concentration can be considered as constant and the reaction as having an apparent first-order kinetics.

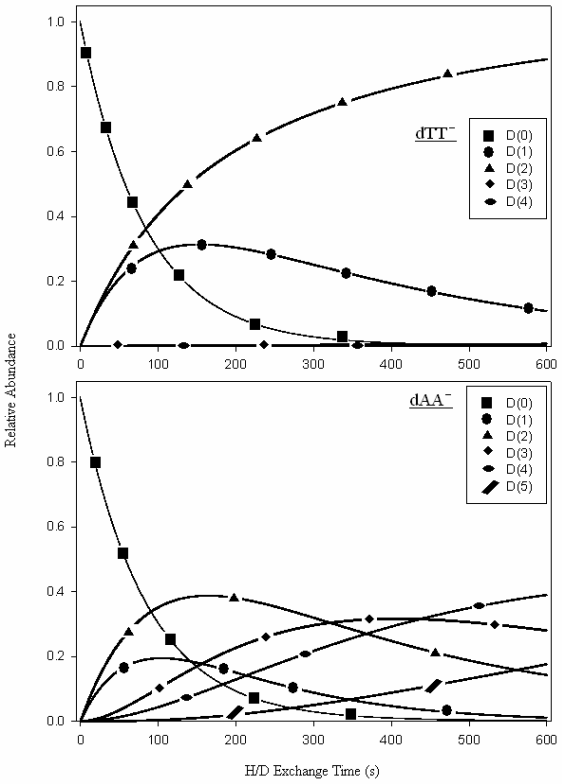

Figure 4.1.5. Kinetic simulated plots of dTT^- and dAA^- using MatLab. For dTT^-, the simultaneous exchange probability is twice the consecutive exchange probability. For dAA^-, these two probabilities are the same (for dAA^-, the used set of coupled differential equations corresponds to the five most exchangeable hydrogens).

Conclusions

Studies have been performed on six dinucleotides with CD_3OD as the deuterating agent in the second hexapole of an FTICR-MS to assess the ability of the H/D exchange to characterize coexisting conformers. In the experimental conditions, the H/D exchange has been shown to be controlled by hydrogen accessibility. This hydrogen accessibility is in direct relationship with the biomolecular conformation and can be a function not only of interactions with heteroatoms but also of protection in a cavity. With hydrogen accessibility as the dominant factor, the H/D exchange study of biomolecular structures can be done without taking into account the chemical nature of the heteroatom bearing the hydrogen. This

argument will be correct while the H/D exchange reaction is faster than the structure interconversion. Within this framework, a model including simultaneous H/D exchanges at the experimental time scale is proposed. This model allows dinucleotide H/D exchange kinetic plots and also mononucleotide H/D exchange kinetic plots to be reproduced. These conclusions are important for the study of the gas-phase conformations of larger biomolecules including non-covalent complexes. With hydrogen accessibility as the main factor for the exchange rates, structural modifications during ligand binding can be studied by direct counting of proton in groups associated with different structures.

Acknowledgments

We would like to acknowledge Jean-François Greisch for the adjustment of the in-house software and Dominique Toye for the programming of Matlab. This work was supported by the FRS-FNRS (Fond de la Recherche Scientifique-FNRS, Belgium). DD was supported by the BelSPo Program IAP P6/19.

4.2. Gas-phase H/D exchange of thymine oligomers

This section discusses the gas-phase H/D exchange of single stranded thymine oligomers composed of from 2 to 6, and of 10, 15, 20 and 30 nucleobases. The influence of the oligonucleotide size at constant charge and of the charge at constant size has been probed. As previously described (see the experimental part in the 4.1. section), the gas-phase H/D exchange reactions were performed with CD_3OD in the second hexapole of a FT-ICR mass spectrometer.

4.2.1. From 2 to 6 thymine nucleobases

The thymine oligomers studied in this section are dT_2^-, dT_3^-, dT_4^-, dT_5^-, dT_5^{2-}, dT_6^- and dT_6^{2-}. Through the use of our in-house software for the analysis of the H/D exchange mass spectra, the relative abundances of the deuterated species were obtained according to the reaction time. The evolution of the deuterated species abundances as a function of the reaction time is illustrated for all of the oligomers in Figure 4.2.1. From these 3D bar charts, some features can be underlined. They are summarized in Table 4.2.I. To complete the H/D exchange experiments, several dynamic simulations were carried out. The same procedure as for the dinucleotides was followed (see the molecular modeling part in the 4.1. section). For these simulations, the negative charge was located on a central phosphate group for the mono-deprotonated oligonucleotides and the two negative charges were located one at each terminal phosphodiester group for the bi-deprotonated oligomers [27].

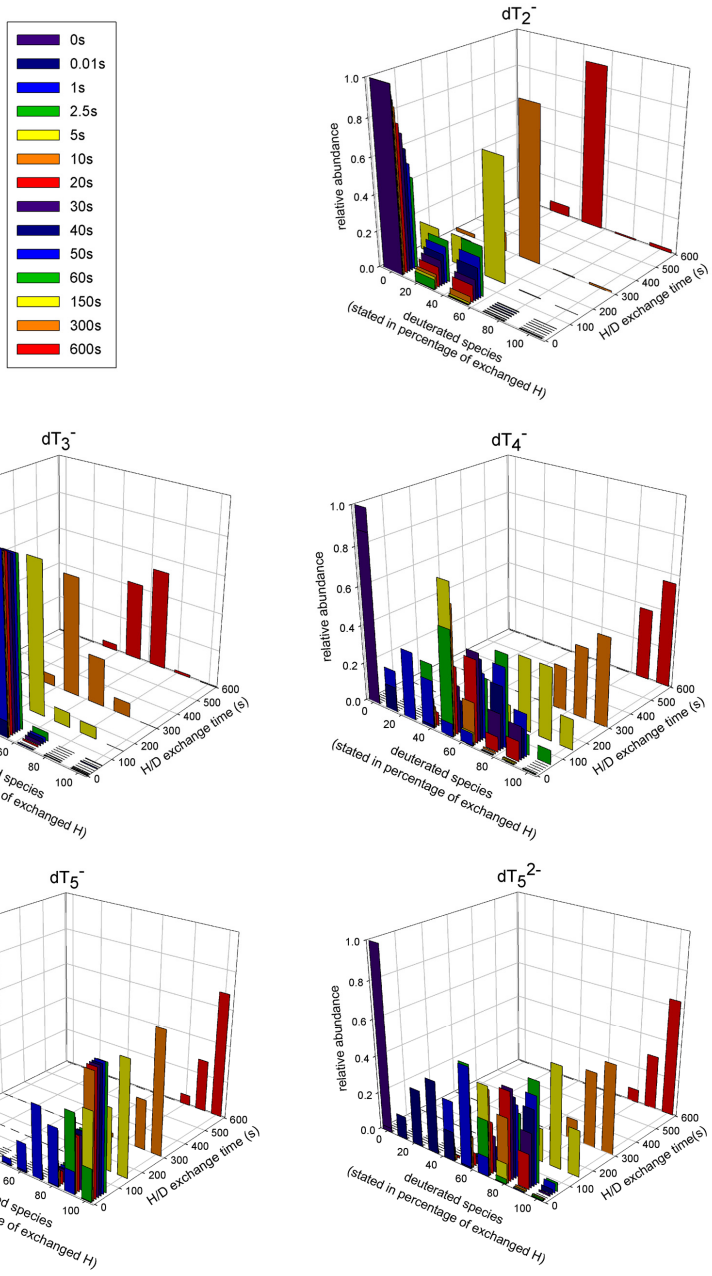
0s
0.01s
1s
2.5s
5s
10s
20s
30s
40s
50s
60s
150s
300s
600s
dT2-
dT3-
dT4-
dT5-
dT5 2-
relative abundance
deuterated species
(stated in percentage of exchanged H)
H/D exchange time (s)
H/D exchange time(s)

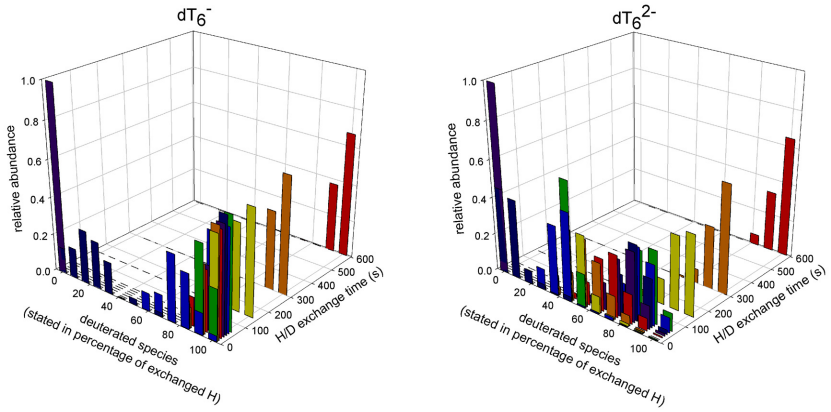

Figure 4.2.1. Evolution of the deuterated species abundances as a function of the reaction time.

Table 4.2.I. Summary of underlined features for all of the thymine oligomers composed of from 2 to 6 nucleobases.

The thymine oligomer	The number of exchangeable hydrogens	The number of exchanged hydrogens after 600 s of reaction	features
			Major species at given reaction times
dT_2^-	4	2	**D(2)** was always the major species. Its abundance was equal to 80% after 200 s of H/D exchange reaction
dT_3^-	6	4	**D(4)** became the major species after 500 s of reaction. The abundance of **D(1)** is equal to 80% after 0.75 s of H/D exchange reaction
dT_4^-	8	8	**D(8)** became the major species after 250 s of reaction. The abundance of **D(4)** is around 80% after 5 s of H/D exchange reaction
dT_5^-	10	10	**D(10)** became the major species after 5 s of reaction
dT_5^{2-}	9	9	**D(9)** became the major species after 250 s of reaction
dT_6^-	12	12	**D(12)** became the major species after 4 s of reaction
dT_6^{2-}	11	11	**D(11)** became the major species after 150 s of reaction

From all of these observations, different items can be discussed:

- For dT_3^-, dT_4^-, dT_5^- and dT_6^-, a quite detailed analysis of molecular dynamics calculations was made with the aim of correlating the observed behavior to the existence of several conformations. Through the dynamic simulations of 10000 ps, the distances between the exchangeable hydrogens and the heteroatoms with which they could interact were measured every 500 ps. Hydrogen protection in a cavity was also taken into account.

For dT_3^-, 3 hydrogens are observed to be particularly available, and on the opposite, 2 hydrogens are supposed to be specifically inaccessible for exchange as they interact 90% of the time with heteroatoms. Moreover, on average, 4 hydrogens (not always the same, different conformations) are observed to be accessible at the same time. The high abundance of D(3) and the exchange of 4 out of 6 hydrogens are therefore conformationally confirmed.

For dT_4^-, at every measure points, 4 hydrogens are accessible on average. Among these hydrogens, only two ones are available all the time. The observation of a high abundance of D(4) after 5 s of H/D exchange reaction could be explained by the fact that, on average, 4 hydrogens are accessible even if they are not always the same four ones. No hydrogen is continuously in interaction, the exchange of all the hydrogens can therefore be observed.

For dT_5^-, the full H/D exchange is rapidly observed (after 5 s of reaction). Not much time is available for observing deuterated intermediate species. The analysis of molecular dynamics calculations only informs that dT_5^- seems to be quite flexible (no blocked interaction) and that no hydrogen is continuously in interaction. The fast and full exchange seems to be reasonable. The same behavior is observed for dT_6^-.

For the analysis of the dynamic simulations, the fact that a hydrogen could be exchanged or not was considered with respect to its accessibility and not regarding the chemical nature of the heteroatom that bears it. The obtained results were in agreement with the ones for the dinucleotides: hydrogen accessibility is the dominant factor.

- At constant charge, the larger the number of nucleobases, the faster the full exchange was observed.

- The comparison between dT_5^- and dT_5^{2-}, and dT_6^- and dT_6^{2-} showed that at constant size, the 2- charge state exchanged slower. This observation could not be explained based on conformational differences. The analysis of the dynamic simulations being not detailed enough, no obvious difference between the charge states 1- and 2- was observed indeed. We shall come back to the interpretation of this behavior after having presented the corresponding data for longer oligonucleotides.

4.2.1. dT_{10}, dT_{15}, dT_{20} and dT_{30}

The thymine oligomers studied in this section are dT_{10}^{3-}, dT_{15}^{3-}, dT_{15}^{4-}, dT_{20}^{3-}, dT_{20}^{4-}, dT_{20}^{5-}, dT_{30}^{4-}, dT_{30}^{5-} and dT_{30}^{6-}. The evolution of the deuterated species abundances as a function of the reaction time was obtained for all of the oligomers through the use of our in-house software. From these evolutions, the needed reaction time for observing the full H/D exchange was underlined. It is summarized for all the oligomers in Table 4.2.II. Note that quite broad distributions of the deuterated species were observed which could reflect the existence of several conformations.

Table 4.2.II. Summary of the needed reaction time for observing the full H/D exchange for the thymine oligomers composed of 10, 15, 20 and 30 nucleobases.

The thymine oligomer	The charge state	the needed reaction time for the observation of the full H/D exchange
dT_{10}	3-	The 18 hydrogens are exchanged after **20 s** of reaction
dT15	3-	The 28 hydrogens are exchanged after **20 s** of reaction
	4-	The 27 hydrogens are exchanged after **20 s** of reaction
dT_{20}	3-	The 38 hydrogens are exchanged after **30 s** of reaction
	4-	The 37 hydrogens are exchanged after **20 s** of reaction
	5-	The 36 hydrogens are exchanged after **10 s** of reaction
dT_{30}	4-	The 57 hydrogens are exchanged after **150 s** of reaction
	5-	The 56 hydrogens are exchanged after **60 s** of reaction
	6-	The 55 hydrogens are exchanged after **20 s** of reaction

Two major items can be displayed:

- At constant size of the oligomers, the higher the number of negative charges, the faster the full H/D exchange was observed.

- At constant charge, the higher was the number of thymine nucleobases, the later the full H/D exchange was observed.

These two behaviors are opposite to those observed for the thymine oligomers composed of 2 to 6 nucleobases.

To explain this puzzling behavior, we have first to note that, for the shorter oligonucleotides, the number of charges is small (< 3), whereas it is larger (3 – 6) in the longer oligonucleotides. The addition of supplementary charges at constant size of the oligonucleotide can therefore be discussed by distinguishing two situations:

- The number of negative charges is < 3

  In order to minimize the Coulombic repulsion, the two negative charges of a bi-deprotonated single strand are suspected to be located at the two terminal phosphate groups. For a mono-deprotonated oligonucleotide, there is, in principle, no constraint for the charge location. In comparison with the bi-deprotonated species that is characterized by one possible charge location, the single charge of the mono-deprotonated species can be located equally on each phosphate group which corresponds to a large number of possible conformations. On the opposite, a bi-deprotonated single strand should present a low number of structures in which the presence of the second charge should decrease the flexibility of the oligonucleotide in promoting additional interactions. This could explain why the 2- charge state exchanged slower than the 1- for dT_5 and dT_6.

- The number of negative charges is > 3

  For minimizing the Coulombic repulsion, the negative charges are suspected to be distributed more or less evenly along the single strand which is therefore supposed to adopt more elongated conformations. The addition of a supplementary charge should, in this case, induce an increase of the H/D exchange rates.

The addition of supplementary bases at constant charge for the oligonucleotides composed of more than 10 bases and carrying at least 3 negative charges will decrease the charge repulsion. This will in turn allow the formation of higher order structures where the hydrogens are less accessible. For smaller single strands, the increase of the exchange rates is not yet explained. These oligonucleotides are suspected to correspond to special cases, where only a detailed structural study could help to find an answer.

4.3. DNA versus RNA

dC_6^{2-} versus C_6^{2-} and dG_6^{2-} versus G_6^{2-} were studied. dC_6^{2-} exchanged faster than C_6^{2-} and dG_6^{2-} exchanged as fast as G_6^{2-}. Moreover, C_6^{2-} displayed a bimodal H/D exchange (see point 6.2. in Chapter 6). Some molecular dynamics simulations of these oligonucleotides were performed. From these simulations, it can be argued that in RNA some hydroxyl groups at the 2' position of sugars are inside the structure and so not directly accessible for H/D exchange (in interaction or in a cavity). The accessibility of these hydrogens must be therefore studied like the one of other exchangeable hydrogens. Unlike Håkansson et al. [28] who suggested that another relay mechanism may involve the 2'-hydroxyl group to explain the faster H/D exchange of RNA (dA_6 versus A_6 and dT_6 versus U_6), we suggest that there is no general rule that differentiates between DNA and RNA. The possible different H/D exchange behavior between DNA and RNA (as for dC_6 and C_6) may not be due for example to a different mechanism, but may be a function of each oligonucleotide structure(s).

References

1. Gard, E.; Green, M. K.; Bregar, J.; Lebrilla, C. B. Gas-Phase Hydrogen/Deuterium Exchange as a Molecular Probe for the Interaction of Methanol and Protonated Peptides. *J. Am. Soc. Mass Spectrom.* **1994,** *5*, 623-631.

2. Campbell, S. C.; Rodgers, M. T.; Marzluff, E. M.; Beauchamp, J. L. Deuterium Exchange Reactions as a Probe of Biomolecule Structure. Fundamental Studies of Gas Phase H/D Exchange Reactions of Protonated Glycine Oligomers with D_2O, CD_3OD, CD_3CO_2D, and ND_3. *J. Am. Chem. Soc.* **1995,** *117*, 12840-12854.

3. Freitas, M. A.; Shi, S. D. H.; Hendrickson, C. L.; Marshall, A. G. Gas-Phase RNA and DNA Ions. 1. H/D Exchange of the $[M-H]^-$ Anions of Nucleoside 5'-Monophosphates (GMP, dGMP, AMP, dAMP, CMP, dCMP, UMP, dTMP), Ribose 5-Monophosphate, and 2-Deoxyribose 5-Monophosphate with D_2O and D_2S. *J. Am. Chem. Soc.* **1998,** *120*, 10187-10193.

4. Robinson, J. M.; Greig, M. J.; Griffey, R. H.; Venkantraman, M.; Laude, D. A. Hydrogen/Deuterium Exchange of Nucleotides in the Gas Phase. *Anal. Chem.* **1998,** *70*, 3566-3571.

5. Freitas, M. A.; Marshall, A. G. Gas-Phase RNA and DNA Ions. 2. Conformational Dependence of the Gas-Phase H/D Exchange of Nucleotide-5'-Monophosphates. *J. Am. Soc. Mass Spectrom.* **2001,** *12*, 780-785.

6. Wyttenbach, T.; Bowers, M. T. The Hydrogen/Deuterium Exchange Mechanism. *J. Am. Soc. Mass Spectrom.* **1999,** *10*, 9-14.

7. Gree-Church, K. B.; Limbach, P. A.; Freitas, M. A.; Marshall, A. G. Gas-Phase Hydrogen/Deuterium Exchange of Positively Charged Mononucleotides by Use of Fourier-Transform Ion Cyclotron resonance Mass Spectrometry. *J. Am. Soc. Mass Spectrom.* **2001,** *12*, 268-277.

8. Crestoni, M. E.; Fornarini, S. Gas-Phase Hydrogen/Deuterium Exchange of Adenine Nucleotides. *J. Mass Spectrom.* **2003,** *38*, 854-861.

9. Wang, F.; Freitas, M. A.; Marshall, A. G.; Skyes, B. D. Gas-Phase memory of Solution-Phase Protein Conformation: H/D Exchange and Fourier Transform Ion Cyclotron Resonance Mass Spectrometry of the N-terminal Domain of Cardiac Troponin C. *Int. J. Mass Spectrom.* **1999,** *192*, 319-325.

10. Herrmann, K.; Wysocki, V.; Vorpagel, E. R. Computational Investigation and Hydrogen/Deuterium Exchange of the Fixed Charge Derivative Tris(2,4,6-Trimethoxyphenyl) Phosphonium: Implication of tha Aspartic Acid Cleavage mechanism. *J. Am. Soc. Mass Spectrom.* **2005,** *16*, 1067-1080.

11. Herrmann, K. A.; Kuppannan, K.; Wysocki, V. H. Fragmentation of Doubly-Protonated Peptide Ion Populations labeled by H/D Exchange with CD_3OD. *Int. J. Mass Spectrom.* **2006,** *249-250*, 93-105.

12. Reid, G. E.; Simpson, R. J.; O'Hair, R. A. J. Probing the Fragmentation Reactions of Protonated Glycine Oligomers Via Multistage Mass Spectrometry and Gas-Phase Ion-Molecule Hydrogen/Deuterium Exchange. *Int. J. Mass Spectrom.* **1999,** *191*, 209-230.

13. Felix, T.; Reyzer, M.; Brodbelt, J. Hydrogen/Deuterium Exchange of Nucleoside Analogs in a Quadrupole ion Trap Mass Spectrometer. *Int. J. Mass Spectrom.* **1999,** *191*, 161-170.

14. Reyzer, M. L.; Brodbelt, J. S. Gas-Phase H/D Exchange Reactions of Polyamine Complexes: $(M+H)^+$, (M+alkali metal$^+$), and $(M+2H)^{2+}$. *J. Am. Soc. Mass Spectrom.* **2000,** *11*, 711-721.

15. Zhang, J.; Brodbelt, J. S. Gas-Phase Hydrogen/Deuterium Exchange and Conformations of Deprotonated Flavonoids and Gas-Phase acidities of Flavonoids. *J. Am. Chem. Soc.* **2004,** *126*, 5906-5919.

16. Chipuk, J. E.; Brodbelt, J. S. Gas-Phase Hydrogen/Deuterium Exchange of 5'- and 3'-Mononucleotides in a Quadrupole ion Trap: Exploring the Role of Conformation and System Energy. *J. Am. Soc. Mass Spectrom.* **2007,** *18*, 724-736.

17. Gidden, J.; Bowers, M. T. Gas-Phase Conformational and Energetic Properties of Deprotonated Dinucleotides. *Eur. Phys. J. D* **2002,** *20*, 409-419.

18. Goodner, K. L.; Milgram, K. E.; Williams, K. R.; Watson, C. H.; Eyler, J. R. Quantification of Ion Abundances in Fourier Transform Ion cyclotron Resonance Mass Spectrometry. *J. Am. Soc. Mass Spectrom.* **1998,** *9*, 1204-1212.

19. Marshall, A. G.; Comisarow, M. B.; Parisod, G. Relaxation and Spectral Line Shape in Fourrier Transform Ion Resonance Specroscopy. *J. Chem. Phys.* **1979,** *71*, 4434-4444.

20. Nir, E.; Imhof, P.; Kleinermanns, K.; de Vries, M. S. REMPI Spectroscopy of Laser Desorbed Guanosines. *J. Am. Chem. Soc.* **2000,** *122*, 8091-8092.

21. Rodgers, M. T.; Campbell, S.; Marzluff, E. M.; Beauchamp, J. L. Low-Energy Collision-Induced Dissociation of Deprotonated Dinucleotides: Determination of the Energetically Favored Dissociation Pathways and the Relative Acidities of Nucleic Acid Bases. *Int. J. Mass Spectrom. and Ion Processes* **1994,** *137*, 121-149.

22. Gidden, J.; Bowers, M. T. Gas-Phase Conformation of Deprotonated and Protonated Mononucleotides Determined by Ion Mobility and Theoretical Modeling. *J. Phys. Chem.* **2003,** *107*, 12829-12837.

23. Liu, D.; Wyttenbach, T.; Bowers, M. T. Hydratation of Mononucleotides. *J. Am. Chem. Soc.* **2006,** *128*, 15155-15163.

24. Saenger, W. Principles of Nucleic Acid Structure. Cantor, C. R., Ed.; Springer-Verlag: New York, 1984; pp 14-23.

25. Gaussian 03, Revision C.02,
M. J. Frisch, G. W. Trucks, H. B. Schlegel, G. E. Scuseria, M. A. Robb, J. R. Cheeseman, J. A. Montgomery, Jr., T. Vreven, K. N. Kudin, J. C. Burant, J. M. Millam, S. S. Iyengar, J. Tomasi, V. Barone, B. Mennucci, M. Cossi, G. Scalmani, N. Rega, G. A. Petersson, H. Nakatsuji, M. Hada, M. Ehara, K. Toyota, R. Fukuda, J. Hasegawa, M. Ishida, T. Nakajima, Y. Honda, O. Kitao, H. Nakai, M. Klene, X. Li, J. E. Knox, H. P. Hratchian, J. B. Cross, C. Adamo, J. Jaramillo, R. Gomperts, R. E. Stratmann, O. Yazyev, A. J. Austin, R. Cammi, C. Pomelli, J. W. Ochterski, P. Y. Ayala, K. Morokuma, G. A. Voth, P. Salvador, J. J. Dannenberg, V. G. Zakrzewski, S. Dapprich, A. D. Daniels, M. C. Strain, O. Farkas, D. K. Malick, A. D. Rabuck, K. Raghavachari, J. B. Foresman, J. V. Ortiz, Q. Cui, A. G. Baboul, S. Clifford, J. Cioslowski, B. B. Stefanov, G. Liu, A. Liashenko, P. Piskorz, I. Komaromi, R. L. Martin, D. J. Fox, T. Keith, M. A. Al-Laham, C. Y. Peng, A. Nanayakkara, M. Challacombe, P. M. W. Gill, B. Johnson, W. Chen, M. W. Wong, C. Gonzalez, and J. A. Pople, Gaussian, Inc., Wallingford CT 2004.

26. McDonnell, L. A.; Giannakopulos, A. E.; Derrick, P. J.; Tsybin, Y. O.; Hakansson, P. A Theoretical Investigation of The Kinetic Energy of Ions Trapped in a Radio-Frenquency Hexapole Ion Trap. *Eur. J. Mass Spectrom.* **2002,** *8*, 181-189.

27. Favre, A.; Gonnet, F.; Tabet, J. C. Location of the negative charge(s) on the backbone of single-stranded deoxyribonucleic acid in the gas phase. *European Journal of Mass Spectrometry* **2000,** *6* (5), 389-396.

28. Mo, J.; Hakansson, K. Oligonucleotide Gas-Phase Hydrogen/Deuterium Exchange with D_2S in the Collision Cell of a Quadrupole-Fourier

Transform Ion Cyclotron Resonance Mass Spectrometer. *Anal. Chem.* **2007,** *79*, 7893-7898.

Chapter 5: H/D exchange coupled to other techniques

Hydrogen/deuterium exchange has become a valuable tool for obtaining conformational information about biomolecule in solution or in the gas-phase. In this chapter, we combine H/D exchange with other mass spectrometry methods. This combination can be sequential, i.e. the two techniques are applied one after the other on the same instrument, or parallel, i.e. analyzing the data from two distinct experiments. By compiling data from methods having independent principles of operation, we expect to highlight new aspects and obtain complementary information.

5.1. Ion activation before or during gas-phase H/D exchange

In this section, different ways of activating the ions before or during their gas-phase H/D exchange in the second hexapole (collision cell) of a 9.4 tesla Apex-Qe FT-ICR mass spectrometer are presented. The different activation methods correspond to:

- The ion acceleration at the entrance of the H/D exchange cell
- The H/D exchange under different temperature conditions
- The IR activation during H/D exchange

5.1.1. Ion acceleration at the entrance of the H/D exchange cell

Some experiments where the ions were accelerated when entering the H/D exchange cell (the second hexapole) were performed. For that purpose, the Col-Cell Trap parameter, which is the voltage applied on the “collision entrance” lens (Figure 2.2.10.) of the second hexapole and which usually was equal to 5 V, was increased up to 7.5, 10, 15 and 20 V. With such an acceleration, ion collisonal activation with CD_3OD takes place only during a short period of time at the entrance of the H/D exchange cell after which the ions oscillate in this cell from 10 ms to 300 s for H/D exchange with no further activation. The activation and H/D exchange steps are therefore by and large time- and space-separated.

Several oligonucleotides were studied: dT_2^-, dAT^-, dTG^-, dC_6^{2-} and C_6^{2-}. The major features that were underlined for the H/D exchange reactions of these samples without ion activation are summarized in Table 5.1.I.

Table 5.1.I. Summary of underlined features for all of the oligonucleotides studied by H/D exchange without ion activation.

The studied oligonucleotide	The number of exchangeable hydrogens	The number of exchanged hydrogens after 300 s of reaction	The major features
dTT^-	4	2	**D(2)** was always the major species
dAT^-	5	2	**D(2)** was always the major species
dTG^-	6	5	**D(1)** was the major species from 0 to 90 s and **D(5)** became the major species after 90 s of reaction. A bimodal H/D exchange profile is observed
dC_6^{2-}	17	17	Complete exchange observed after 30 s of reaction
C_6^{2-}	23	23	A bimodal H/D exchange profile is observed

First of all, it is important to point out that no fragmentation was observed in the used voltage range. The mass spectra obtained with and without ion acceleration were compared for several H/D exchange times. No difference was observed for dT_2^-, dAT^-, dTG^- and dC_6^{2-}. But for C_6^{2-}, the bimodal profile was modified. The results are illustrated with ion acceleration at 20 V for dTG^- and C_6^{2-} in Figure 5.1.1. a and b.

For C_6^{2-}, the ratio of the two populations is altered with ion activation; the abundance of the first population, which is associated with the less deuterated species, decreases, and the abundance of the second contribution, which is associated with the most deuterated species, increases. Moreover, the positions and widths of these two contributions are not affected by the acceleration step. However, the positions shift when the reaction time increases (Figure 5.1.1. c). Acceleration and reaction time do not therefore play the same role. Even after 300s of H/D exchange reaction, ion acceleration keeps on influencing the ion distribution. Although the two contributions can no longer be distinguished, ion acceleration keeps on shifting the distribution more and more towards complete deuteration of the sample.

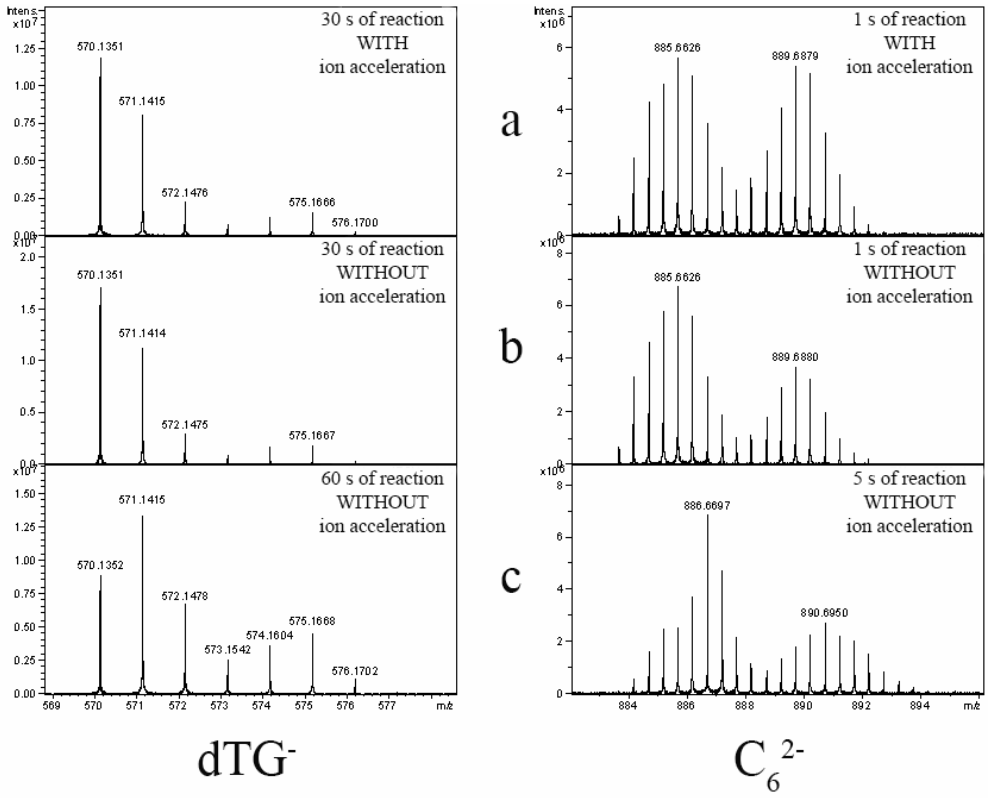

Figure 5.1.1. Comparison of dTG^- and C_6^{2-} H/D exchange mass spectra recorded with and without ion acceleration.

dTG^- and C_6^{2-} both display a bimodal H/D exchange. However, only the C_6^{2-} bimodal profile is influenced by the ion activation step. From our previous study of the gas-phase H/D exchange of dinucleotides (point 4.1. in Chapter 4) and especially from the dynamic simulations, dTG^- is known to present two distinctive structures that interconvert within the duration of a dynamic simulation (10 ns). From these observations, C_6^{2-} is suspected to present two conformers (or groups of conformers displaying close exchange rates) that, on the opposite to dTG^-, do not interconvert within the experimental time scale. Moreover, the ion acceleration step is suspected to allow the isomerization between these two conformers. Collisional activation during the acceleration step could indeed increase the interconversion rate constant and lead to a new concentration ratio between both conformers. This new ratio would be eventually frozen when the ions are cooled down after the activation step by multiple collisions with CD_3OD that lead preferentially to deactivation. This idea of deactivating collisions

experienced by the trapped ions is corroborated by the absence of any activation signature for dTG^-. The fast interconversion between these two conformers even in the absence of activation leads to the same equilibrium between the two species as the one before H/D exchange.

A modification of the C_6^{2-} bimodal profile (always along the same lines) was observed at each value of the collision entrance voltage. For each acceleration voltage, the decrease rate of the first population which is equal to the increase rate of the second contribution was calculated with respect to the bimodal profile obtained without ion activation (Col-Cell Trap voltage = 5 V). This rate was obtained by subtraction of the relative intensities of the H/D exchange isotopic peaks that were observed at the acceleration voltage and at 5 V. The increase rate for the different acceleration voltages and at several H/D exchange reaction times is illustrated in Figure 5.1.2.

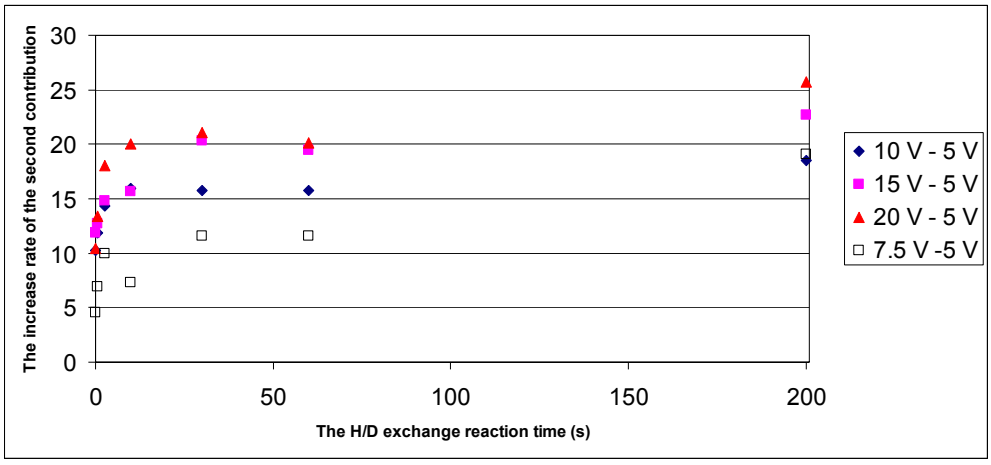

Figure 5.1.2. The increase rate for the different acceleration voltages and at several H/D exchange reaction times.

The distinction between the two contributions is not obvious at the short and long H/D exchange reaction times. At short exchange times, the H/D exchange of the second conformation (with the fastest exchange rate constants) contributes to the first exchange distribution. At long exchange times, it is the opposite; the H/D exchange of the first conformation (with the slowest exchange rate constants) contributes to the second exchange distribution. The calculated rate of increase can therefore only be discussed when the two contributions can be easily

distinguished (from 30 s to 200 s of H/D exchange). From this rate, the ion distribution modification is observed to increase when the acceleration voltage ranges from 7.5 to 15 V, but levels off from 15 to 20 V. This could indicate that an equilibrium distribution results from the activation step.

All the assumptions made in this section are discussed in a following point (5.2.). Thanks to the use of a method independent of the H/D exchange one, ion mobility coupled to mass spectrometry, these hypotheses will be confirmed.

5.1.2. Gas-phase H/D exchange under different temperature conditions

With the aim of probing the influence of the temperature on H/D exchange, gas-phase H/D exchange experiments of dT_2^-, dAT^- and C_6^{2-} were performed at different temperatures. For that purpose, a Salamender ceramic infrared heating element (Mor Electric Heating Assoc., Inc., MI, USA) was inserted into the collision cell "block", above the hexapole. A thermocouple located just below the hexapole and connected to an electronic regulator (CAL3200 autotune temperature controller, CAL Conrols, Libertyville, IL, USA) allowed a given temperature to be obtained and kept constant.

50 and 75°C were tested and compared to room temperature (25°C) experiments. The obtained mass spectra after 150s of H/D exchange reactions are illustrated for dAT^- in Figure 5.1.3. As expected, an increase of the H/D exchange rates is observed, particularly at 75°C, but the H/D exchange still remains limited to a partial H/D exchange.

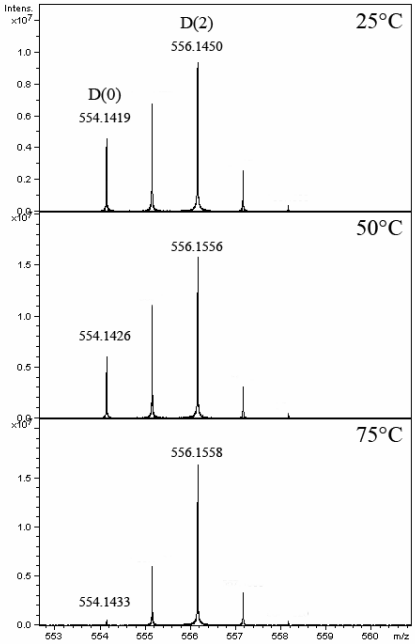

Figure 5.1.3. The H/D exchange mass spectra of dAT^- after 150 s of reaction at 25, 50 and 75°C.

For C_6^{2-}, the analysis is quite difficult. As illustrated on Figure 5.1.4., the H/D exchange rate constants and the isomerization rate constant are both influenced by the temperature (the ratio and the positions of the two populations are altered). Moreover, the temperature is not the only variable parameter: the pressure inside the H/D exchange cell also changes. In order to assess the influence of the temperature alone, the pressure should be kept constant. For that purpose, a pressure gauge should be inserted inside the H/D exchange cell since presently the pressure is measured in the ion transfer optics and not in the collision hexapole.

Through the control of the temperature and the gas pressure in the H/D exchange cell, several experiments can be considered. Thermal denaturation of duplexes and hairpins could be monitored by H/D exchange based on the fact that hydrogen bonding involved in base pairing protects nucleobase hydrogens from exchange as will be discussed in detail in Chapter 6 (section 6.1.).

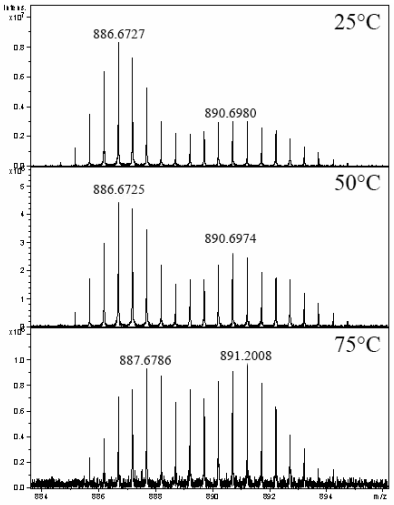

Figure 5.1.4. The H/D exchange mass spectra of C_6^{2-} after 60 s of reaction at 25, 50 and 75°C.

Note that another activation method of the ions during the H/D exchange was considered: the IR activation. The 9.4 telsa Apex-Qe FT-ICR mass spectrometer is equipped with an infrared laser (Figure 2.2.8., Chapter 2). It is a 25 W laser (Synrad, Mukilteo, WA, USA) with a wavelength of 10.6 μm. If the instrument is perfectly lined up, the IR laser beam passes through the ICR cell, the ion transfer optics, the hexapole collision cell and even through the source. However, such a perfect alignment is very difficult to obtain and sometimes half a day is required to reach it. In view of this constraint, these experiments were not performed.

5.2. Detection of Oligonucleotide Gas-Phase Conformers: H/D Exchange and Ion Mobility as Complementary Techniques

This study has been published in the Journal of The American Society for Mass Spectrometry (*J. Am. Soc. Mass Spectrom.* **2008**, *19*, 938-946). To improve the reading quality, it is presented in author post-print format.

Detection of Oligonucleotide Gas-Phase Conformers: H/D Exchange and Ion Mobility as Complementary Techniques

Dorothée Balbeur[1], Joëlle Widart[1], Bernard Leyh[2], Laetitia Cravello[3] and Edwin De Pauw[1]

[1] Laboratory of Mass Spectrometry, University of Liège, Belgium
[2] Molecular Dynamics Laboratory, University of Liège, Belgium
[3] Waters Corporation, Atlas Park, Simonsway, Manchester M22 5PP, UK

Gas-phase hydrogen/deuterium exchange of small oligonucleotides (dTG, dC_6 and C_6) with CD_3OD was performed in the second hexapole of a Fourier transform ion-cyclotron resonance (FTICR) mass spectrometer. Ion activation experiments were conducted by accelerating the ions at the entrance of the H/D exchange cell under conditions promoting exclusively collisional isomerization. These experiments allowed us to assess the presence of several conformers, and to probe the height of the isomerization barrier separating these conformers. Ion mobility experiments were also performed. Their results were consistent with the H/D exchange data. A model accounting for the competing isomerization and H/D exchange reactions is proposed. Comparing the ion acceleration experiments for H/D exchange and for ion mobility reveals that the most compact conformer displays the fastest H/D exchange. This observation shows that H/D exchange and ion mobility provide us with complementary information because hydrogen accessibility and macromolecule compactness are not univocally associated.

Introduction

The knowledge and the understanding of biomolecule conformations are important challenges in chemistry. The conformations of biomolecules depend on intramolecular noncovalent interactions. These interactions govern a vast majority

of biological processes (self-assembly, molecular recognition, regulation, transport, etc.) that define the function of the biomolecules.

Hydrogen/deuterium (H/D) exchange combined with mass spectrometry has become an efficient tool for obtaining conformational information about isolated biomolecules in the gas-phase [1-18]. The rate of gas-phase H/D exchange has been shown to be a function of the reagent used for exchange (nature and concentration), the charge state of the biomolecule, the gas-phase basicity/acidity of exchangeable sites, and the internal structure of the biomolecular ions [1-18]. Probing the number of exchanged hydrogens and the H/D exchange kinetics makes it possible to distinguish ion populations and to elucidate their structural and thermochemical features. Gas-phase H/D exchange has been applied extensively for structural studies of proteins and peptides [1-6] and is now also most commonly used for structural characterizations of oligonucleotides [7-18]. Mononucleotides studies have shown that the extent and rate of exchange depend on the nucleobase (nature, space orientation, and gas-phase acidity of the exchangeable hydrogen), and on the position (3' or 5') and flexibility of the terminal phosphate group [7-11]. Moreover, these studies have been in favor of the relay mechanism [7-11]. The latter was shown not to be relevant for dinucleotides [14]. Furthermore, gas-phase H/D exchange of dinucleotides has been shown to be controlled by hydrogen accessibility rather than by the chemical nature of the heteroatom bearing the exchangeable hydrogen. Studies of larger oligonucleotides have also been published. Gas-phase H/D exchange reactions were performed on DNA duplexes and on the corresponding single strands. They showed that H/D exchange was slower for the duplex than for the single strands [15,16]. In a previous study, a quadruplex was shown to undergo very fast H/D exchange compared to its constituent monomer, an unexpected situation for such a compact and rigid structure [17]. Gas-phase H/D exchange of 5-mer phosphorothioate oligonucleotides was also examined; bimodal exchange profiles were observed, suggesting that each ion could adopt more than one gas-phase conformation [18].

The present work focuses on the bimodal H/D exchange of oligonucleotides. A simple interpretation of such a behavior is that one conformer contains exchangeable hydrogens that mostly belong to two groups with very different H/D exchange rate constants, the latter being similar within each group. The situation

can, however, be more complex. Two or more conformers may be present. If the exchangeable hydrogens of each conformer belong to either of two groups with well-differentiated H/D exchange rates and if these two groups behave similarly in all conformers, then a bimodal exchange pattern will show up. The probability that two groups of exchangeable hydrogens have close rate constants for all conformers decreases when the number of conformers increases. As a result the observation of more than two modes in the H/D exchange mass spectrum becomes more probable when there are more than two conformers. Moreover, when several conformers are present, two situations can be met. Either the different conformers interconvert on the spectrometer time-scale and at the experimental temperature or they do not. Usual H/D exchange measurements cannot discriminate these two situations. In order to assign the observed bimodal H/D exchange to the presence of one or several structures, and in order to decide whether these distinct conformers interconvert or not, ion activation experiment must be performed. For these experiments, the ions are activated before H/D exchange under selective conditions promoting exclusively collisional isomerization.

Another powerful technique for investigating the gas-phase structure of biomolecules is ion mobility coupled with mass spectrometry. The ion mobility of a gas-phase ion is a measure for the drift speed of this ion through a buffer gas under the influence of a uniform or oscillating electric field. Measuring the drift time directly linked to the mobility of an ion yields information about its structure because compact ions, which have necessarily relatively small collision cross sections, move faster than extended ones which have large collision cross sections. The gas-phase conformations of many oligonucleotides have been investigated by ion mobility: deprotonated mononucleotides [19,20], dinucleotides [21] and trinucleotides [22], deprotonated oligothymidines [23], DNA complexes [24], G-quadruplex [25,26], etc.

Both hydrogen/deuterium exchange and ion mobility spectrometry provide us with information about the structures and relative stabilities of gas-phase conformers. Studies combining these two techniques have illustrated the difficulty to compare results from H/D exchange with ion mobility results because these two methods probe different physical properties of an ion [5,6]. In the present work, ion mobility measurements are used to investigate oligonucleotide structures independently of the H/D exchange experiments. As for H/D exchange,

experiments involving collisional activation of the ions prior to the mobility drift were performed.

The dTG DNA dinucleotide, the dC_6 DNA hexanucleotide and the C_6 RNA hexanucleotide have been selected for this study. Other small oligonucleotides have also been screened. However, among all of them, only dTG and C_6 displayed a bimodal H/D exchange. This is the reason why we submitted them to a detailed investigation. dC_6, displaying a mono-modal H/D exchange, was chosen as a counter-example. No detailed structural study by molecular modeling was carried out in this work for the selected oligonucleotides.

Experimental

Sample Preparation

The DNA dinucleotide (dTG), the DNA hexanucleotide (dC_6) and the RNA hexanucleotide (C_6) were obtained from Eurogentec (Seraing, Belgium). CD_3OD was purchased from Euriso-Top (Gif sur Yvette, France). All these compounds were used without further purification. Stock solutions of the oligonucleotides (with precisely known concentration around 400×10^{-6} M) were prepared in water. Working solutions (1.1765×10^{-5} M) were obtained by dilution in water. The injection solutions were prepared by adding the appropriate amount of MeOH to obtain a MeOH/H_2O ratio of 15/85 (v/v) and an oligonucleotide concentration of 1.0000×10^{-5} M. For the injection solutions of the RNA hexanucleotide, NH_4Ac was added in order to reduce sodium adducts. The NH_4Ac concentration was equal to 50 mM.

Gas-Phase H/D Exchange coupled with Mass Spectrometry

All H/D exchange experiments were performed with a 9.4 tesla Apex-Qe FTICR mass spectrometer (Bruker Daltonics, Billerica, MA) in negative ion mode as previously described [14]. Briefly, the oligonucleotide solutions were infused via an external Apollo electrospray ion source at a flow rate of 120 µL/h with the assistance of N_2 nebulizing gas. The off axis sprayer was grounded, the end-plate was set to 3 kV and the inlet capillary was set to 3.5 kV for the generation of oligonucleotide anions. A N_2 heated drying gas (250 °C) flow assisted desolvation

of ESI droplets. The H/D exchange data were generated from mono-deprotonated dinucleotide ions and doubly deprotonated hexanucleotide ions. These ions were stored in the hexapole collision cell for 10 ms and then trapped in the presence of CD_3OD from 10 ms to 300 s (the ions entered the hexapole in one bunch and no other ion entered during the exchange time). The CD_3OD pressure inside the collision cell was estimated to be ~ 1×10^{-3} mbar from the measured pressure in the surrounding vacuum chamber, equal to 5×10^{-6} mbar [14].

For the ion activation experiments, the ions were accelerated when entering the collision cell. For that purpose, the Col-Cell Trap parameter, which is directly related to the voltage applied on the entrance lens of the hexapole and which usually was equal to 5 V, was increased up to 7.5, 10, 15 and 20 V. No fragmentation was observed in this range. It is also essential to notice that ion activation takes place only during a short period of time at the entrance of the hexapole collision cell after which they oscillate in this hexapole from 10 ms to 300 s for H/D exchange with no further activation. Multiple collisions with CD_3OD lead then preferentially to desactivation. We shall elaborate on this point in the discussion. The activation and H/D exchange steps are thus by and large time- and space-separated.

Ion Mobility coupled with Mass Spectrometry

Ion mobility measurements were made on the Synapt™ High Definition MS™ system (Waters® Corporation, Milford, USA) [27]. This hybrid quadrupole orthogonal acceleration Time-of-Flight (oa-ToF) mass spectrometer combines high resolution tandem mass spectrometry with high efficiency ion mobility (IMS) based on gas-phase separations. It was operated in negative ion mode and samples were infused via a ZSpray™ source at a flow rate of 300 µL/h. The electrosprayed ions were transferred non-mass selectively through the quadrupole into the IMS enabling Triwave™ device. The Triwave™ consists of three traveling wave ion guides (T-Wave™). The first, the Trap T-Wave, traps and accumulates ions. These stored ions are then gated into the IMS T-Wave in which the ion mobility separation occurs. The Transfer T-Wave is then used to transport the separated ions into the orthogonal acceleration time-of-flight (oa-ToF) mass spectrometer for mass analysis. The pressure in the Trap and Transfer T-Wave regions was about 2.25×10^{-2} mbar of Argon and the pressure in the IMS T-Wave was 0.56 mbar of Nitrogen. The RF amplitude used on the IMS T-Wave was

380 V peak-to-peak, IMS traveling wave velocities of 300 m/s were used, and the wave pulse heights were ramped from 8 to 12 V during the course of a single mobility separation. Recording the temporal arrival profile of ions (the so-called mobilogram) was achieved by synchronizing the oa-ToF acquisition with the gated release of ions from the Trap to the IMS T-Wave. The following sequence has been repeatedly applied to reach an acceptable signal/noise ratio: gated pulse followed by 200 TOF mass spectra with a pusher period of 64 µs. This leads to an overall mobility recording time of 200 × 64 µs = 12.8 ms.

For several experiments, the dC_6 and C_6 ions were accelerated in the source by increasing the cone voltage from 20 V in the other experiments to 50 V and then to 70 V. No fragmentation was observed in this voltage regime.

Decomposition of ion mobility data was performed using Igor Pro 4.07 (WaveMetrics, Inc., Lake Oswego, USA). The data have been fitted to a double Gaussian distribution:

$$I(n) = \frac{A_1}{\sigma_1\sqrt{2\pi}} e^{-\frac{(n-n_1)^2}{2\sigma_1^2}} + \frac{A_2}{\sigma_2\sqrt{2\pi}} e^{-\frac{(n-n_2)^2}{2\sigma_2^2}}$$

where A_i is the area under each partial contribution characterized by its center n_i and its standard deviation σ_i.

It is essential to notice that the ion acceleration experiments for H/D exchange and ion mobility may be compared. The experimental conditions have been selected such that the internal energy transferred upon collisions does not reach the onset of the fragmentation channels: only the low-energy isomerization channel is open in both experiments, even though they cover different time-scales.

Results

H/D Exchange

As the H/D exchange reaction time increased from 0.01 to 300 s, an increase of the number of exchanged hydrogens [D(X) corresponds to X exchanged hydrogen atoms] was observed with a corresponding decrease of the abundance of the precursor ion, D(0). The H/D exchange mass spectra after the reaction times of 0.01, 2.5, 40, 120 and 300 s are presented in Figure 5.2.1. for the three

investigated oligonucleotides. A bimodal distribution is observed for dTG^- and C_6^{2-}. It should be noted that no noticeable difference appeared in gas-phase H/D exchange of C_6^{2-} with or without NH_4Ac in the injection solution. After 300s of H/D exchange, dTG^- exchanged mainly five of its six exchangeable hydrogens, and some totally deuterated ions were observed for dC_6^{2-} (17 deuteriums) and C_6^{2-} (23 deuteriums). It should be noticed that these latter situations still differ from the full H/D exchange of the sample which would correspond to all ions being totally deuterated.

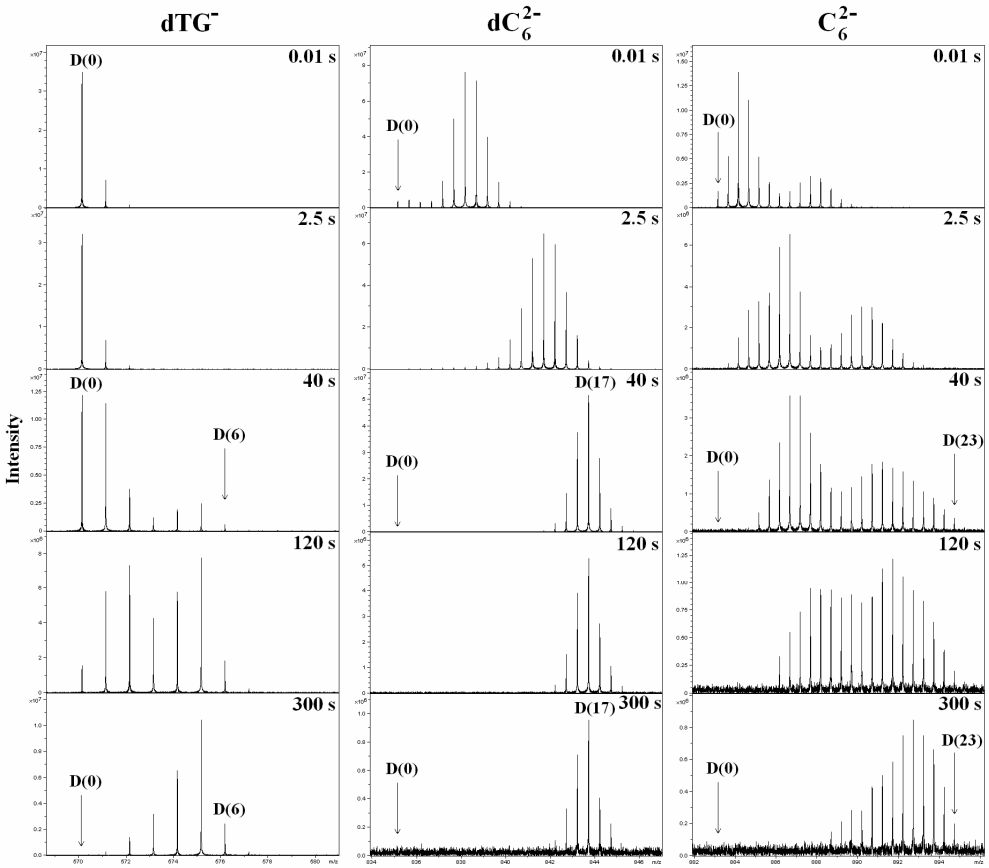

Figure 5.2.1. H/D exchange mass spectra at the reaction times of 0.01, 2.5, 40, 120 and 300 s for the three studied oligonucleotides.

The rates of H/D exchange reactions of ions that were accelerated upon entering the collision cell were also monitored. For a given H/D exchange time, the mass spectra obtained with and without ion acceleration were compared. No difference was observed for dTG^- and dC_6^{2-}. But for C_6^{2-}, the bimodal profile was modified. The results are illustrated with ion acceleration at 20 V in Figure 5.2.2.a & b. With ion acceleration, the ratio of the two populations is altered; the abundance of the first population, which is associated with the less deuterated species, decreases and the abundance of the second contribution, which is associated with the most deuterated species, increases. At a given reaction time, the Maximum-minimum-Maximum (M-m-M) positions, that characterize the positions and widths of the two contributions, are not affected by the acceleration step. However these positions shift when the reaction time increases (Figure 5.2.2.b & c). In other words, acceleration and reaction time do not play the same role: a mass spectrum obtained with ion acceleration after a given reaction time, will never be the same as a mass spectrum obtained without ion acceleration after a longer reaction time (Figure 5.2.2.a & c). Even after an exchange reaction time of 300 s, ion acceleration keeps on influencing the ion distribution. Although the two contributions can no longer be distinguished, ion acceleration keeps on shifting the distribution more and more towards complete deuteration of the sample.

As mentioned in the Experimental section, several values of the Col-Cell Trap parameter were tested for the H/D exchange activation experiments. A modification of the C_6^{2-} bimodal profile (decrease of the abundance of the first contribution and increase of the abundance of the second one) was observed at each value. This ion distribution modification increased when the Col-Cell Trap parameter ranged from 7.5 to 15 V, but levelled off from 15 to 20 V.

For the analysis and the discussion of the previous results, reference will be made to results that were obtained during our previous study of the gas-phase H/D exchange of dinucleotides [14]. In that work, dynamic simulations were carried out to complement the H/D exchange experiments, and to investigate the different conformations adopted by the dinucleotides. dTG^- presents two distinctive structures that interconvert within the duration of a dynamic simulation (1 ns). The experimental kinetic plot of the dTG^- H/D exchange was approximated by adding the kinetic contributions of the two structures.

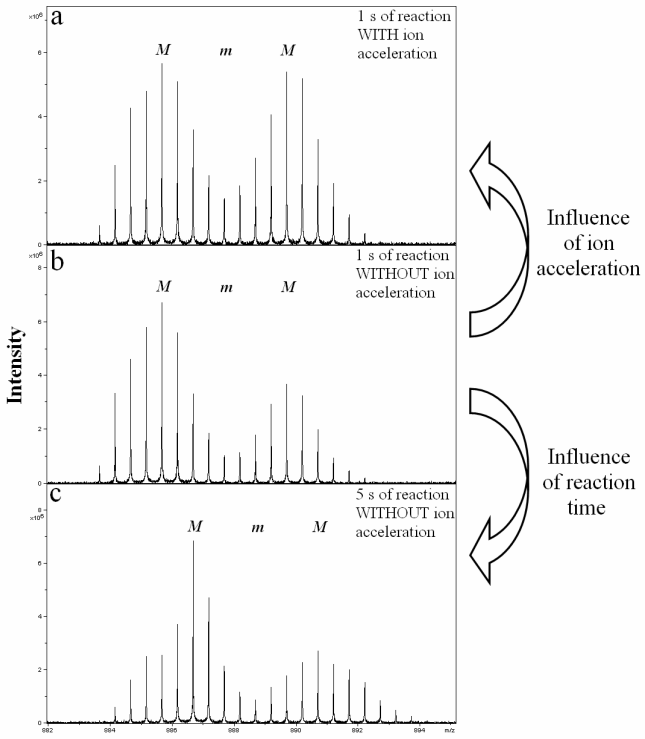

Figure 5.2.2. Comparison of C_6^{2-} H/D exchange mass spectra recorded with and without ion acceleration; **a** 1 s of reaction with ion acceleration at 20 V, **b** 1 s of reaction without ion acceleration, and **c** 5 s of reaction without ion acceleration.

Ion Mobility

The recorded arrival time profiles (extracted mass mobilograms, stated in scans [27]) are shown in Figure 5.2.3.a-c for dTG^-, dC_6^{2-} and C_6^{2-}. dTG^- and dC_6^{2-} give rise to a single mobility peak. C_6^{2-} shows a very wide drift time and its extracted mass mobilogram presents a composite mobility peak. A few experiments with ion acceleration in the source were carried out. No influence was observed for dC_6^{2-}, while the double mobility peak of C_6^{2-} was affected as illustrated in Figure 5.2.4.. The increase of the cone voltage induced an increase of the short drift time contribution without affecting the drift times themselves (Figure 5.2.4. and Table 5.2.I.). The mobilogram at 70 V is the same as the one at 50 V (Table 5.2.I.).

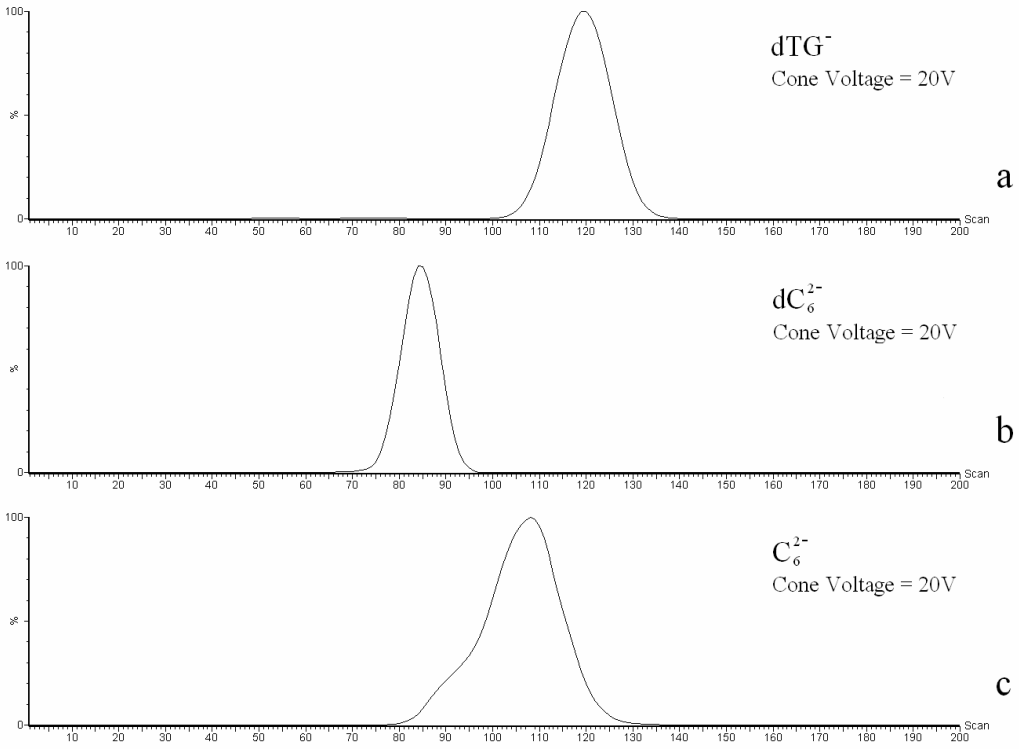

Figure 5.2.3. Mass mobilograms of the three studied oligonucleotides. (a) dTG^-; (b) dC_6^{2-}; (c) C_6^{2-}.

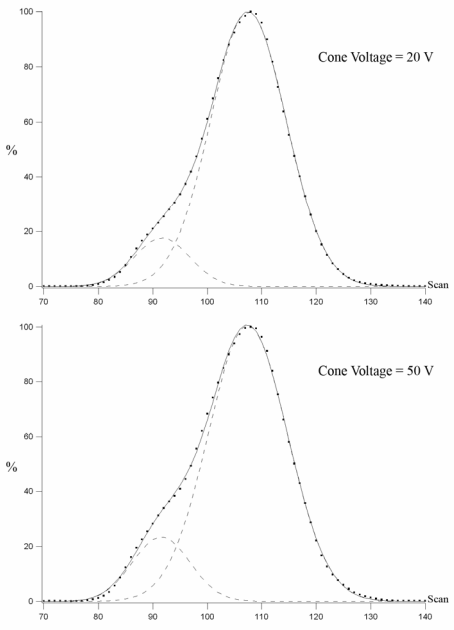

Figure 5.2.4. Comparison of C_6^{2-} mass mobilograms recorded with and without ion activation. Dots: experimental data; dashed lines: individual Gaussian distributions; solid line: sum of these two Gaussian distributions.

Table 5.2.I. Set of constants characterizing the two Gaussian distributions that were obtained using the procedure outlined in the text.

	Cone Voltage = 20 V		Cone Voltage = 50 V		Cone Voltage = 70 V	
	short drift time	**long** drift time	**short** drift time	**long** drift time	**short** drift time	**long** drift time
Area under the curve (A_i)	224 ± 7	1747 ± 8	311 ± 12	1838 ± 12	307 ± 13	1802 ± 13
Center of the curve (n_i)	91.7 ± 0.2	107.54 ± 0.04	91.5 ± 0.2	107.45 ± 0.06	93.2 ± 0.2	107.85 ± 0.06
Standard deviation (σ_i)	5.1 ± 0.1	6.98 ± 0.03	5.3 ± 0.1	7.30 ± 0.05	5.8 ± 0.1	7.19 ± 0.04
Percentage of the Gaussian distribution	11.4	88.6	14.5	85.5	14.5	85.5

Discussion

In our gas phase H/D exchange study of dinucleotides, a kinetic model including simultaneous exchanges on the experimental time scale was proposed. In the framework of such a model, an observed bimodal exchange behavior can result not only from the presence of two gas-phase conformations with different exchange rates but also from the difference in accessibility of two H groups within a single structure. Indeed, by simulating H/D exchange kinetic plots (Matlab, The MathWorks, Inc., Natick, MA) and by extracting from them the relative abundances of the deuterated species [D(X)], bimodal profiles resulted from the presence of two groups of hydrogens within one structure (unpublished data). To distinguish experimentally between these two limit cases, it is necessary to combine complementary approaches:

i. the analysis of the influence of collisional activation on H/D exchange kinetics helps probing the height of the activation barriers connecting conformers and exchanged species;
ii. mobility measurements provides us with information on the presence of structures having different spatial extensions; recording how ion activation affects the mobility data makes the connection between both sets of experiments possible.

The aim of the present discussion is to present a model, described in Figure 5.2.5., which provides a consistent picture of the observed exchange and mobility data.
In the model, we have considered four stable species connected by activation barriers: two conformers and their respective perdeuterated species. It must be mentioned right away that this model simplifies the situation in at least two ways. First, each conformer is possibly representative for a group of conformers displaying close exchange rates and possibly low interconversion barriers. Second, the deuteration reaction is rather a multistep procedure with consecutive enthalpy and entropy bottlenecks. The different situations displayed in Figure 5.2.5.a-c correspond to three limiting cases with, however, a constant feature: the H/D exchange barriers can be overcome at room temperature on the experimental time-scale. In Figure 5.2.5.a, a stable conformer is separated from a less stable one by a barrier exceeding the energy deposited upon activation. In Figure 5.2.5.b, the isomerization barrier can be easily crossed at room temperature, while in Figure 5.2.5.c, such a crossing is negligible and requires heating the system up using

collisional activation. We now show that these three cases may correspond, respectively, to dC_6^{2-}, to dTG^- and to C_6^{2-}.

In the case of dC_6^{2-}, the mobility data (Figure 5.2.3.b) identify only a single conformer (in the sense defined in the previous paragraph, i.e. possibly a group of conformers with similar properties). H/D exchange data are monomodal and remain unaffected upon activation. These observations are consistent with the situation depicted in Figure 5.2.5.a but for the activation behavior where an apparent contradiction arises which will be dismissed below. The largest stability of one conformer together with the high isomerization barrier prevents any other possible conformer to show up. The exchange rate, however, should be affected by the collisional heating, a prediction at odds with the experimental data (see Results section). This behavior may result from two mechanisms. First the low H/D exchange activation barriers reduce the slope of the rate constant variation with temperature. Second and probably most important, fast collisional cooling takes place once acceleration is over. It is essential to remind here again that acceleration is limited to a short path at the entrance of the collision cell. The collisions that occur during this path are most probably only activating. Afterwards, the many collisions experienced by the ions within the collision cell lead to their being cooled down to room temperature, so that the effect of the activation process on the exchange rate is cancelled. It is hard to evaluate the duration of both processes (activation and cooling) but they are likely to be shorter that 0.01 s since no influence of the acceleration step is observed even at this shortest experimental time.

Figure 5.2.5.b accounts for the behavior of dTG^- which displays a bimodal H/D exchange but a monomodal mobilogram and no influence of the activation step. The observation of a bimodal H/D exchange and of a monomodal mobilogram can result as well from one conformer with two groups of exchangeable hydrogens as from two conformers that interconvert rapidly at room temperature. Neither H/D exchange experiments, nor ion mobility measurements at room temperature can distinguish these two situations. Only a detailed structural study by molecular modeling [14] or ion mobility measurements at lower temperatures [21] can answer the question. These latter experiments led to the conclusion that the monomodal mobilogram results from the fast interconversion between the conformers separated by a small barrier, leading to an equilibrium between both species, and that the bimodal exchange pattern results from the different rates for

both conformers, governed by their respective H/D exchange barriers. The absence of any activation signature is explained as in the previous paragraph by the desactivating collisions experienced by the trapped ions.

The third situation that we consider corresponds to an isomerization barrier that is higher than the exchange ones and that can be substantially overcome only once the ions have been activated (Figure 5.2.5.c). This case corresponds to C_6^{2-}. Let us deal first with the non activated ions, i.e. with the room temperature situation. Due to the high barrier preventing fast isomerization, both conformers are present with proportions not necessarily in equilibrium and which depend in an unknown manner on the situation in solution and on the ionization mechanism. Each conformer exchanges H and D at its own rates, leading to a bimodal mass spectrum (Figure 5.2.1.). In addition, the mobility data plead for two conformers with distinguishable spatial extensions (Figure 5.2.3.c). Collisional activation increases the interconvertion rate constants and leads to a new concentration ratio between both conformers that we assume now to be in equilibrium but that is eventually frozen when the ions are cooled down. This cooling process has the effect of reducing the isomerization rate constants to a point that the relaxation back to equilibrium is hindered on the experimental time-scale. The system is left in a non equilibrium situation where each conformer remains trapped in its own potential well. This is consistent with the observation that ion acceleration changes the ratio of the two contributions but not their positions because the exchange rates are kept unmodified. Moreover, because the population modification is frozen after the cooling process, the influence of ion acceleration is observed at each reaction time until complete exchange, where no difference should be observed. It is a signature of the activation process which takes place during a very short time at the entrance of the collision cell. In a similar way as for H/D exchange, C_6^{2-} ion acceleration through the increase of the cone voltage changed the ratio of the two mobility peaks without affecting their drift times (Table 5.2.I., Figure 5.2.4.): this is again in favor of a rapid cooling after the acceleration step.

It is observed that the concentration ratio of both conformers levels off between 50 V and 70 V. We propose the following tentative explanation. If we assume that the activation step leads to a sufficient increase of the isomerization rates for an equilibrium to obtain, this ratio is given by the equilibrium constant, i.e.,

$K = e^{-\frac{\Delta_r G^0}{RT}} = e^{\frac{\Delta_r S^0}{R}} e^{-\frac{\Delta_r H^0}{RT}}$. Overcoming the high activation barrier requires depositing an amount of energy much larger than Δ_rH^0. It has previously been shown that a temperature can usually be assigned to the activated ions and correlated to the cone voltage [28]. In other words, when the cone voltage ≥ 50 V, RT >> Δ_rH^0 and $K \rightarrow e^{\frac{\Delta_r S^0}{R}}$. From the concentration ratio at 50 and 70 V, Δ_rS^0 = – 14.8 J mol^{-1} K^{-1} can be estimated, a value consistent with a smaller entropy for the more compact structure. The fact that in both H/D exchange and ion mobility experiments, the results tend to level off when the voltage is increased is an indication that an equilibrium distribution results from the activation step.

The C_6^{2-} conformer whose proportion increases upon ion acceleration is the one that exchanges the largest number of hydrogens and that has the most compact structure (Figure 5.2.2. and Figure 5.2.4.). Other studies have reported identical observations of compact structures (small cross section) with fast H/D exchange [5,17]. Although it is intuitively surprising, it is conceivable that a compact structure possesses exchangeable hydrogens with high H/D exchange rate constants. In order to account for these high rate constants, direct accessibility of hydrogens or more probably various intramolecular "relay" mechanisms (not to be confused with the relay mechanism which is mentioned in the mononucleotides studies [7-11]) that can bring deuteriums into the compact structure, and/or H/D exchange barriers changes upon folding can be evoked. A detailed structural study of C_6^{2-} searching for different stable structures and possibly comparing the theoretical and experimental cross sections would be very relevant. Even if this study is time-consuming due to the complexity and the large number of possible relevant conformations of C_6^{2-}, it is planned and will hopefully be presented in a forthcoming publication.

The observation of a compact structure with a fast H/D exchange shows that the H/D exchange and ion mobility methods are not directly comparable but are complementary as accessibility and compactness are connected to different physical properties. In addition, both methods probe different timescales. In summary H/D exchange can resolve different families of conformers that can be not resolved using ion mobility and vice versa [5]. An ion could display a mono-modal H/D exchange and be detected as a double mobility peak, and vice versa.

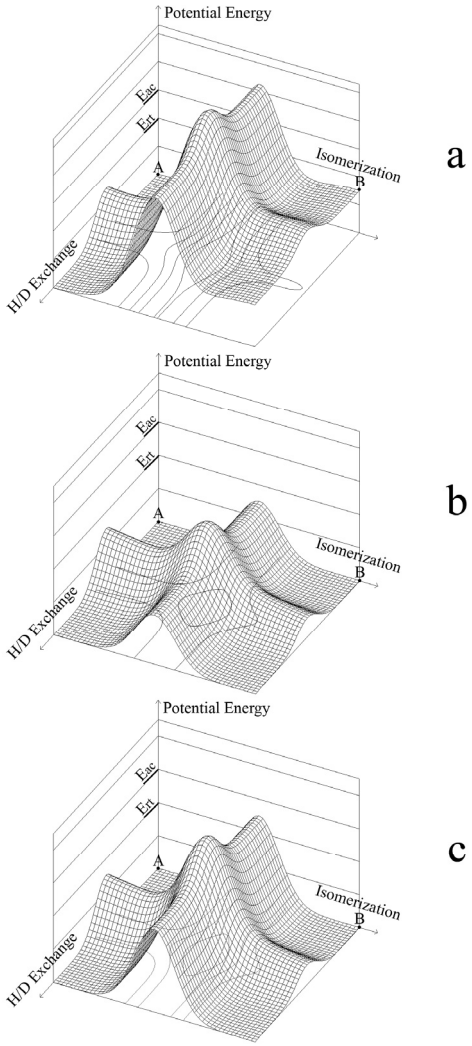

Figure 5.2.5. Proposed model. E_{ac} is the internal energy of the ion reached during the ion acceleration process. E_{rt} is the internal energy of the ion at room temperature. The H/D exchange and isomerization nuclear coordinates are assumed to be independent. The two conformers A and B, possess different H/D exchange properties. Although the relative energies have a significant impact on the conformer abundances, the two conformers are represented, in the situations (**b**) and (**c**), with identical zero-point energies to simplify the model and to make the picture more readable.

Conclusions

In this work, gas-phase H/D exchange is shown as an efficient tool for detecting the presence of one structure (or one group of structures having similar exchange rates) or the presence of several conformers (or groups of conformers) that possess different exchange properties. Moreover, if several structures are observed, increasing the internal energy of the ions at the entrance of the H/D exchange cell gives access to a qualitative estimation of the relative height of the isomerization barrier compared to the H/D exchange barriers. Ion mobility experiments can confirm the H/D exchange results on the basis of independent data. The ion mobility experiments allow us to distinguish between two groups of situations indeed: (i) on the one hand, only one structure (or one group of structures having the same compactness) is present or several conformers exist but interconvert rapidly at the experimental temperature; (ii), on the other hand, several conformers are present and do not interconvert. In the present study, the H/D exchange results for C_6^{2-} are confirmed by ion mobility experiments both for the presence of two gas-phase conformations, and for their non-interconversion at room temperature. By comparing the ion acceleration experiments for H/D exchange and for ion mobility, the C_6^{2-} conformer that possesses the fastest H/D exchange is identified as the one having the smallest measured drift time and therefore the smallest collision cross section. The hydrogen accessibility and the compactness are structural properties that are connected to different physical parameters. The compactness of the structure and its H/D exchange rates can not be analyzed with only one of the two methods. For the study of biomolecule gas-phase conformations, the combination of H/D exchange and ion mobility provides us with extra information compared to the two individual methods used alone.

Acknowledgements

This work was supported by the FRS-FNRS (Fonds de la Recherche Scientifique-FNRS, Belgium).

5.3. Identification of fragmentation channels of dinucleotides using deuterium labeling

This study has been published in the Journal of The American Society for Mass Spectrometry (*J. Am. Soc. Mass Spectrom.* **2009**, *Accepted*). To improve the reading quality, it is presented in author post-print format.

Identification of fragmentation channels of dinucleotides using deuterium labeling

Balbeur Dorothée[1], Dehareng Dominique[2], De Pauw Edwin[1]

[1] Laboratory of Mass Spectrometry, University of Liège, Liège, Belgium
[2] Center for protein Engineering, University of Liège, Liège, Belgium

The fragmentation of the totally deuterated dinucleotide dAT^- in labile positions (heteroatom-bound hydrogens) was compared for different MS/MS methods: CID, IRMPD, and EID. These experiments allowed us to affirm the coexistence of several fragmentation channels. They can be classified according to the involvement of non-labile or labile protons in the fragmentation process. Moreover, double resonance experiments were performed in IRMPD and EID. They demonstrated the existence of consecutive fragmentation processes. The probability with which each channel is taken depends on the fragmentation technique used, i.e., the energy and the time scale of the method. The fragmentation channels that involve labile protons requiring peculiar three-dimensional structures are entropically unfavorable and enthalpically favorable. They are more observed in IRMPD and EID. The involvement of labile, and therefore exchangeable protons in the fragmentation mechanism casts doubt on the use of tandem mass spectrometry to localize incorporated deuteriums in oligonucleotides.

Introduction

Oligonucleotide ions can be formed using different ionization methods, the most frequently used being those of electrospray ionization (ESI) and Matrix Assisted Laser Desorption Ionization (MALDI). A wide range of activation methods can also be applied to nucleic acid ions for MS/MS experiments including Collision Induced Dissociation (CID), InfraRed MultiPhoton Dissociation (IRMPD), Blackbody Infrared Radiative Dissociation (BIRD), Sustained Off-Resonance Irradiation (SORI) and more recently, fragmentation methods involving electron-ion interactions, such as Electron Capture Dissociation (ECD), Electron Detachment Dissociation (EDD) and Electron Induced Dissociation (EID). The knowledge of detailed dissociation channels of oligonucleotides is essential for successful fragmentation pattern recognition and fragment ion prediction. This can also help to assess the use of tandem mass spectrometry to localize the incorporated deuteriums following hydrogen/deuterium exchange experiments. The deuterium migration during ion activation and fragmentation has been actively discussed for peptides [29-33] but not for oligonucleotides. In order to contribute to the understanding of the fragmentation mechanism, we examined, in this paper, the fragmentation of a totally deuterated dinucleotide, dAT^-, in labile positions (heteroatom-bound hydrogens). The main aim of the work being to determine which hydrogens are involved in the fragmentation process.

Several fragmentation mechanisms were proposed to explain the formation of base loss, w and [a-B] ions (see McLuckey's nomenclature [34]) in collision-activated dissociation [34]. These mechanisms, which are useful for later discussion, are illustrated in Figure 5.3.1., and are briefly described in this paragraph. In 1986, Cerny et al. [35] proposed a mechanism for loss of B^- in Fast Atom Bombardment (FAB) mass spectrometry, which was later supported by Phillips and McCloskey [36]. In this mechanism (Figure 5.3.1.**1.1.**), B^- is lost by backside nucleophilic attack on C1' by negatively charged phosphate. Cerny et al. also suggested a mechanism for w ion formation (Figure 5.3.1.**1.2.**). Its process is induced by nucleophilic attack of the phosphate oxygen on the 2'-hydrogen via a six-membered ring intermediate. In 1993, McLuckey and Habibi-Goudarzi [37] suggested in ESI two 1,2-elimination processes to explain losses of neutral and negatively charged bases, and the subsequent formation of [a-B] and w ions (Figure 5.3.1.**2.**). This was followed by Rodgers and co-workers [38] who proposed, in FAB, a proton-bound intermediate as the common precursor for

losses of both neutral and charged bases (Figure 5.3.1.**3.**). In 1995, Barry et al. [39] proposed in ESI a two-step 1,2-elimination mechanism (Figure 5.3.1.**4.**) where the N-glycosyl bond cleavage is catalyzed by the phosphate group. In the same year, Nordhoff and co-workers [40] proposed a mechanism to explain fragmentation of MALDI-generated ions. This corresponds to a charge-remote, base-elimination mechanism catalyzed by intramolecular proton transfer followed by subsequent cleavage of the 3'- and 5'-phosphoester bonds (Figure 5.3.1.**5.1.**). Nordhoff et al. also explained the formation of a base-loss fragment thanks to a charge translocation mechanism (Figure 5.3.1.**5.2.**). Still in MALDI, Zhu et al. [41] opted for proton transfer from the matrix to a nucleobase instead of intramolecular proton transfer as the initial step for base loss (Figure 5.3.1.**6.**). Wan and Gross [42-45] proposed other hydrogen atoms than the ones located on the deoxyribose ring for the proton transfer to the nucleobase. Thanks to H/D exchange [43,44] and methylphosphonate substitution experiments [45] in ESI, Wan and Gross suggested a fragmentation mechanism involving proton transfer from the adjoining 5'-phosphate to the nucleobase. The zwitterionic $[M-B]^-$ intermediate, which has a third charge site, serves as the common precursor for the formation of [a-B] and the complementary w ions (Figure 5.3.1.**7.**). More recently, Liu et al. [46] proposed a novel mechanism of N-glycosidic bond cleavage in nucleoside. Instead of a new double bond generating between C1' and C2' as often previously reported, they suggested that with H/D exchange experiments the proton of 5'-hydroxyl group on ribose moiety should be removed by the departing anionic nucleobase, resulting in a novel five-member ring via bond formation between the 5'-oxygen and 1'-carbon (Figure 5.3.1.**8.**).

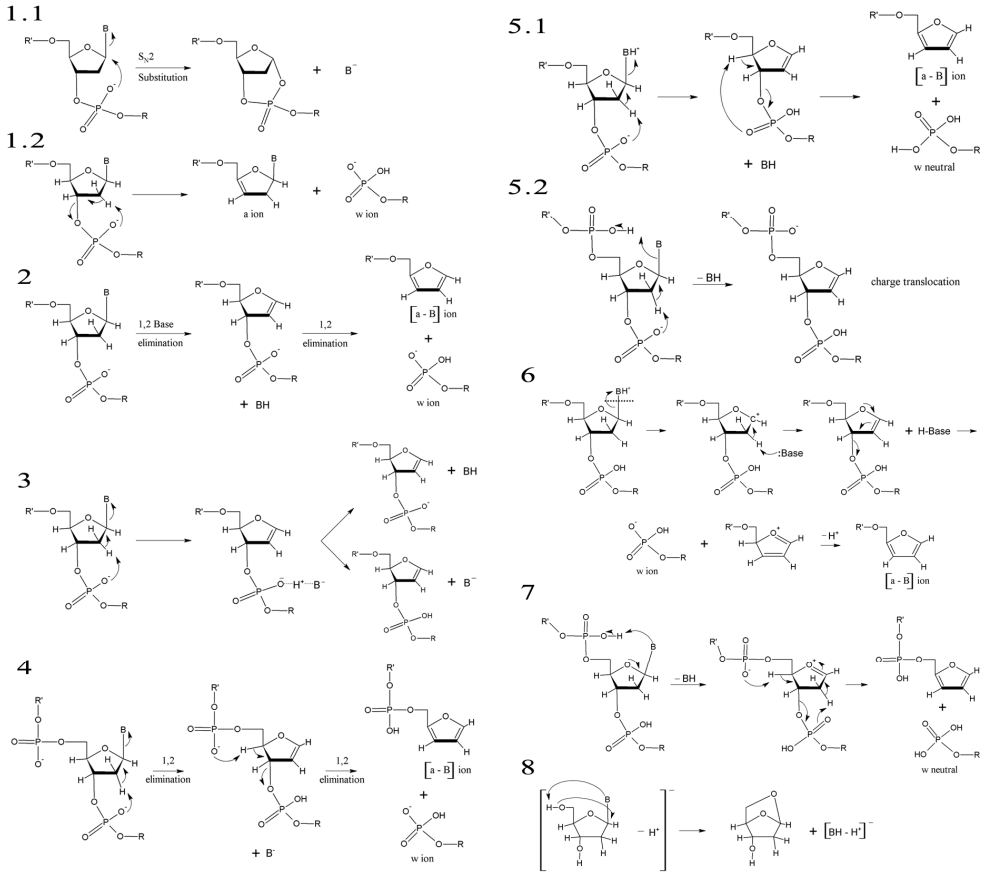

Figure 5.3.1. Summary of previously proposed fragmentation mechanisms.

The different mechanisms presented above can be classified in two categories: (i) the ones involving protons that are non-labile and are bound to the carbon atoms of the ribose ring and (ii) those involving labile protons which are bound to phosphate and 5'-hydroxyl group on ribose moiety. These fragmentation mechanisms involving the transfer of labile protons are supposed to require particular three-dimensional conformations with spatial closeness between labile proton donor and acceptor sites in order to occur. In this work, the fragmentation of the totally deuterated dinucleotide dAT^- in labile positions was compared for different MS/MS methods and discussed regarding the existence of the two categories. The different fragmentation techniques used were CID, IRMPD and EID. dAT^- was chosen following our previous study of gas-phase H/D exchange of dinucleotide ions [47]. Because it is a heterogenous dinucleotide (the w and d

fragments, and (M-Base) ions have different masses) and because it is known to show a low number of different conformations, dAT^- corresponds to a situation for which the fragmentation channels proposed to explain the data can be straightforwardly linked to conformations.

IRMPD is often described as an alternative vibrational excitation method [48,49], providing similar oligonucleotides fragmentation patterns as CID. Because IRMPD is also a "slow heating" fragmentation technique, it is usually proposed to proceed through the same mechanism as in CID. Thanks to double resonance (DR) IRMPD experiments, Kinet et al. [50] and Yang et al. [51] supported the mechanism proposed by Gross and co-workers involving neutral base loss as the first step of the fragmentation process.

In the EDD experiment, irradiation of the precursor anion with > 10 eV electrons is proposed to produce an excited intermediate that can undergo electron detachment (EDD) or direct decomposition (EID). EID originally referred to electron irradiation of singly charged anions, and has not been much applied to oligonucleotides [50]. However its application to small molecules and peptides [52-54] has shown fragmentation similar to that of CID or IRMPD. Thanks to DR-EDD experiments, Kinet et al. [50] showed that on the contrary to IRMPD neutral base loss is not the first step of the fragmentation process.

For the purpose of obtaining more information about the fragmentation channels, especially the possible consecutive fragmentation channels, DR-IRMPD and DR-EID experiments were performed.

Experimental

Sample Preparation

The DNA dinucleotide, dAT, was obtained from Eurogentec (Seraing, Belgium). D_2O and CD_3OD were purchased from Euriso-Top (Gif sur Yvette, France). All these compounds were used without further purification. Totally deuterated dAT in labile positions was obtained by dissolving in D_2O. The injection solution was prepared by adding the appropriate amount of CD_3OD to obtain a CD_3OD/ D_2O ratio of 15/85 (vol/vol) and a dinucleotide concentration of 10^{-5} M. The

protonated dAT solution was obtained by following the same procedure with protonated solvents.

Collision Induced Dissociation experiments

CID experiments were performed on a Q-Tof Ultima Global (Micromass UK Limited, Manchester, UK) electrospray mass spectrometer. The z-spray was operated in the negative ion mode at a capillary voltage of 2.5 kV and the solutions were infused at a flow rate of 240 µL/h. The source block temperature was 80°C and the desolvation gas (N_2) temperature was 120°C. The RF Lens 1 voltage was set to 50 V. As dAT^- can exchange five hydrogens, totally deuterated dAT^- in labile positions presents an isotopic distribution with a major peak at M_0 + 5 m/z (the zero subscript refers to a full H and full C_{12} molecule, and the added number indicates the number of extra nucleons (D or C_{13})) which is noted M_0+5 (see point B in Figure 5.3.2.). This isotopic peak was selected in the quadrupole before activation by collision with argon in the hexapole. To perform this activation, the acceleration voltage at the entrance of the hexapole was increased from 6 V (MS) to 25 V (MS/MS). All mass spectra were acquired and processed with MassLynx 4.0 (Service Pack 1). All the peaks were centroided with suitable parameters in order to obtain a vertical line passing through the center of gravity of each isotopic peak. The resulting centered spectrum gave the centers of the isotopic peaks and their "areas". These latter correspond to the sum of the intensities of the points across the peak in the continuum trace.

InfraRed MultiPhoton Dissociation experiments

These experiments were performed with a 9.4 tesla Apex-Qe FTICR mass spectrometer (Bruker Daltonics, Billerica, MA) in negative ion mode. The dinucleotide solutions were infused via an external Apollo electrospray source at a flow rate of 180 µL/h with the assistance of N_2 nebulizing gas. The off axis sprayer was grounded, the end-plate was set to 3 kV and the inlet capillary was set to 3.5 kV. A N_2 heated drying gas (250°C) flow assisted desolvation of ESI droplets. Ions were accumulated in the first hexapole for 1 s, transferred through the mass-selective quadrupole (15 Da isolation window) and mass selectively accumulated in the second hexapole for 0.01 s. The ions were transferred through high-voltage ion optics and captured by static trapping in the ICR cell. Before the IRMPD irradiation, the M_0+5 isotopic peak of dAT^- full D was isolated in the ICR

cell by cleanup resonant ejections (cleanup shots) of undesired peaks. IRMPD was performed using a 25 W laser (Synrad, Mukilteo, WA) with a wavelength of 10.6 μm. The laser beam passes through the center of the hollow dispenser cathode. Ions were irradiated for 100 ms at 15 and 20 % laser power. All spectra were acquired with XMASS (version 7.0.8, Bruker Daltonics) in broadband mode with 512 k data points and summed over 80 scans. A mass list, in which m/z values and peak heights are recorded, was created using DataAnalysis^{TM} (version 3.4, Bruker Daltonics).

Electron Induced Dissociation experiments

These experiments were performed with a 9.4 tesla Apex-Qe FTICR mass spectrometer (Bruker Daltonics, Billerica, MA) in negative ion mode as previously described for IRMPD with the exception that ions were accumulated in the first hexapole for 2.5 s. The M_0+5 isotopic peak was also isolated in the ICR cell by cleanup shots before electron irradiation. The electrons were emitted by a cylindrical indirectly heated hollow dispenser cathode. A heating current of 1.9 A was applied to the heater element located behind the cathode. A lens of 6 mm diameter located in front of the cathode ensures the focalization of the electron beam. The lens voltage was equal to -18.8 V and the electrons were accelerated using a bias voltage of -18.4 V. The ions trapped in the ICR cell were subjected to 1 s irradiation by the electron beam. The spectra were summed over 500 scans.

Data processing

Step 1: determination of the deuterated species that constitute the isotopic peak at M_0+5

The procedure is illustrated in Figure 5.3.2. First, the composition of deuterated species D(X) (X exchanged hydrogen atoms) was determined for the isotopic distribution of the non-isolated dAT^- full D (point B in Figure 5.3.2.). To do that an in-house software was used. This software utilizes the known isotopic distribution (percentage of each peak obtained via the peak "areas" in CID and the peak heights in IRMPD and EID) of the non-deuterated ion (point A in Figure 5.3.2.). Moreover, it is considered that the ion with a fixed number X, of exchanged hydrogens has the same isotopic distribution but shifted by X/z unit. The software determines the composition of each deuterated species (point C in

Figure 5.3.2.) that best fits the experimental isotopic distribution (point B in Figure 5.3.2.). Then as the isotopic peak at M_0+5 m/z corresponds to D(5) with zero C_{13} atom, D(4) with one C_{13} atom, … the isotopic distribution (percentage of each peak) of the non-deuterated dinucleotide ion and the composition of each deuterated species determined for the full deuterated ion were used to calculate the ratio of the deuterated species that constituted the isotopic peak at M_0+5 (point D in Figure 5.3.2.).

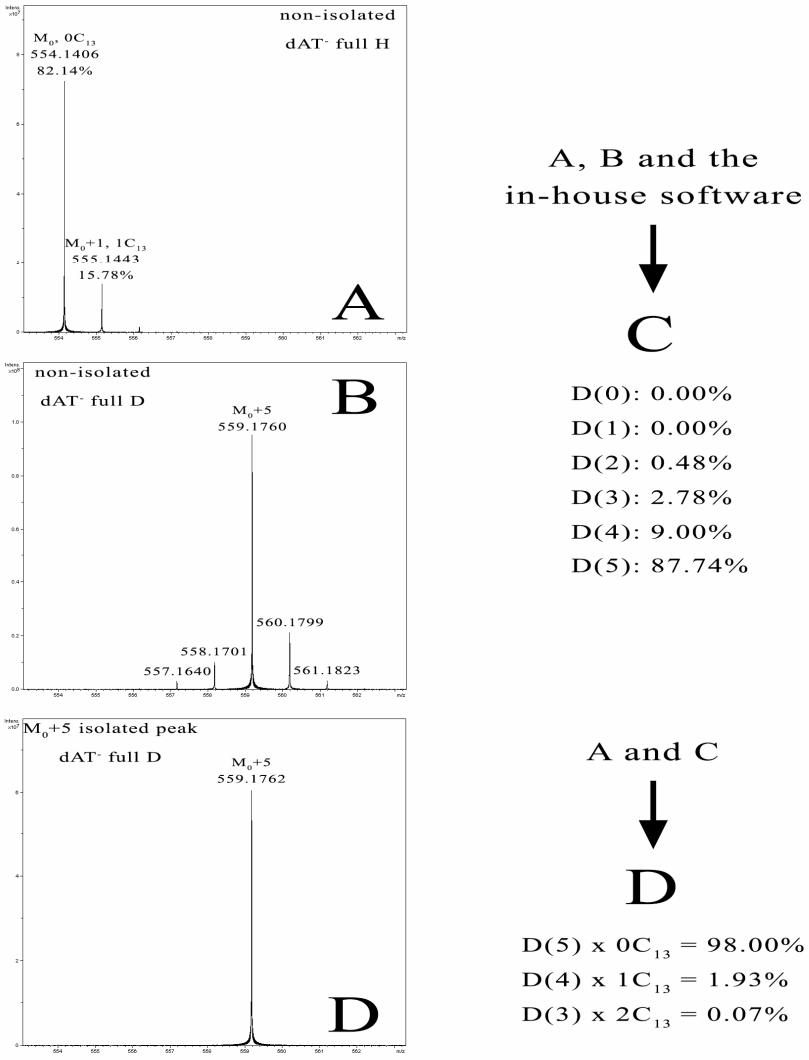

Figure 5.3.2. Illustration of the first step of the data processing.

Step 2: experimental and theoretical patterns of deuteration

As mentioned in the Introduction, the proposed mechanisms of fragmentation can be classified in two categories. Two models of fragmentation were considered according to these two categories. In the first model, the non-labile protons that are bound to the carbon atoms of the ribose ring are proposed to be involved in the fragmentation. The second model involves the labile protons of the hydroxyl groups in 5' (nucleoside A) and 3' (nucleoside T) on ribose moieties. According to both these models and knowing the ratio of the deuterated species that constitute the isotopic peak at M_0+5, the theoretical deuteration patterns of the fragments were determined. Only the D(5) with zero C_{13} atom and the D(4) with one C_{13} atom species were considered, the D(3) with two C_{13} atoms species being always lower than 0.1% and so negligible. As dAT^- has five exchangeable hydrogens, five different structures correspond to the D(4) with one C_{13} atom species (five positions for the non-exchanged hydrogen). Each of these structures can be divided into two cases according to the position of the C_{13} atom in the nucleoside A or in the nucleoside T (same number of carbon atoms in each nucleoside). In total ten structures correspond to the D(4) with one C_{13} atom species, each one existing with a probability of 1/10 of the previously calculated ratio. The procedure followed in order to determine the theoretical deuteration patterns is illustrated in Figure 5.3.3. for the D(5) with zero C_{13} atom and two complementary D(4) with one C_{13} atom species. It should be noticed that for the neutral base loss fragments, the fact that the C_{13} atom can be in the base or in the ribose ring (same number of carbon atoms) is taken into account. These theoretical patterns were compared to those obtained using CID, IRMPD and EID.

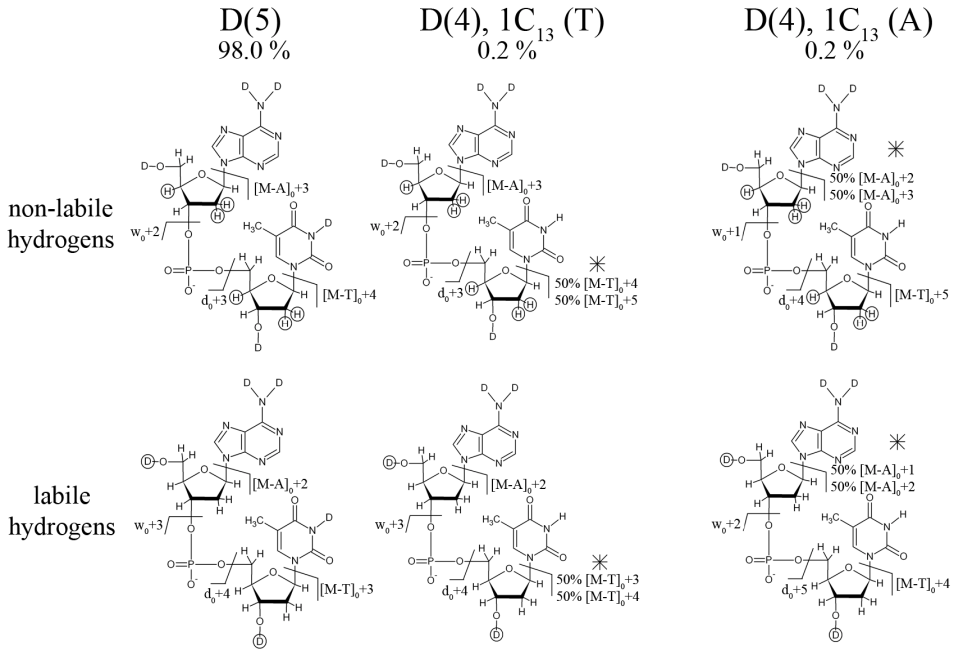

Figure 5.3.3. Illustration of the second step of the data processing: the hydrogen or deuterium atoms involved in the mechanisms are circled and for each fragment, the added number indicates the number of extra nucleons (D or C_{13}) in comparison to the obtained fragment for the non-deuterated and full C_{12} dinucleotide. The asterisk is placed at the level of the nucleoside that possesses the C_{13} atom.

Double resonance experiments

Double resonance experiments consisted in continuous ejection of a specific fragment ion during the whole IRMPD or EID irradiation time. A modified experimental pulse program was used to perform these experiments. The pulse sequence for DR was the following: (1) start of ion ejection, (2) start of the IR or electron irradiation 10 µs after (1), and (3) simultaneous stop of the irradiation and the ion ejection. The m/z ratio of the ion to be ejected from the ICR cell was converted in its cyclotron frequency by the software, and the excitation voltage (200 $V_{P\text{-}P}$) was attenuated by 10 dB in IRMPD and 20 dB in EID. For these experiments, the parent ion was the non-deuterated dinucleotide and the M_0 isotopic peak at M_0 m/z was selected in the ICR cell thanks to cleanup shots before the IRMPD or EID irradiation.

Results and discussion

Fragmentation of the totally deuterated dinucleotide dAT⁻ in labile positions in CID, IRMPD and EID

As suspected in the Introduction, the same fragments are observed in CID, IRMPD and EID. These fragments are the neutral base T loss [M−T], the neutral base A loss [M−A], the w ion, the d ion, the neutral base T and A losses [M−T−A], the [w−$T_{neutral}$] and/or the [d−$A_{neutral}$] ions (same mass) and the base A ion. They are observed with different ratios in the different fragmentation methods. Despite the fact that the fragments are the same, their deuteration patterns change according to the used fragmentation technique. This is reported fragment by fragment in the following paragraphs.

The neutral base A loss

As illustrated in Figure 5.3.4.a, the experimental CID deuteration pattern is similar to the theoretical one obtained considering that the non-labile protons are involved in the fragmentation process. The CID pattern shows a major peak at $[M-A]_0$ + 3 m/z which corresponds to A-H loss from the fully deuterated dinucleotide ion in labile positions (the zero subscript refers to a full H and full C_{12} molecule, and the added number indicates the number of extra nucleons (D or C_{13})). Quite the reverse, the experimental IRMPD and EID deuteration patterns show a major peak at $[M-A]_0$ + 2 m/z in agreement with the involvement of labile protons in the fragmentation process. The A base takes a deuterium to be lost as a neutral group. It is important to notice that the loss of A-D can also be explained with a process involving non-labile protons if an intramolecular migration (scrambling) of labile and non-labile protons takes place. The ribose moiety fixed to the A base possesses eight hydrogens including one labile, exchangeable. If there is scrambling, the deuterium has a probability of 1/8 to be at each position. Considering the 1,2-elimination mechanism where one of the two protons at the 2' position on the ribose is lost with the base, the peak at $[M-A]_0$ + 2 m/z should have at the most an intensity of 25% which is much lower than observed. It is assumed that no scrambling of labile and non-labile protons takes place. The experimental deuteration patterns cannot be explained with only one mechanism. The two proposed categories of mechanisms can be considered as different fragmentation channels and must coexist to form the neutral base A loss fragment.

Moreover as the deuteration pattern varies from one fragmentation technique to another, the different fragmentation channels coexist but are taken with different ratios for each MS/MS method.

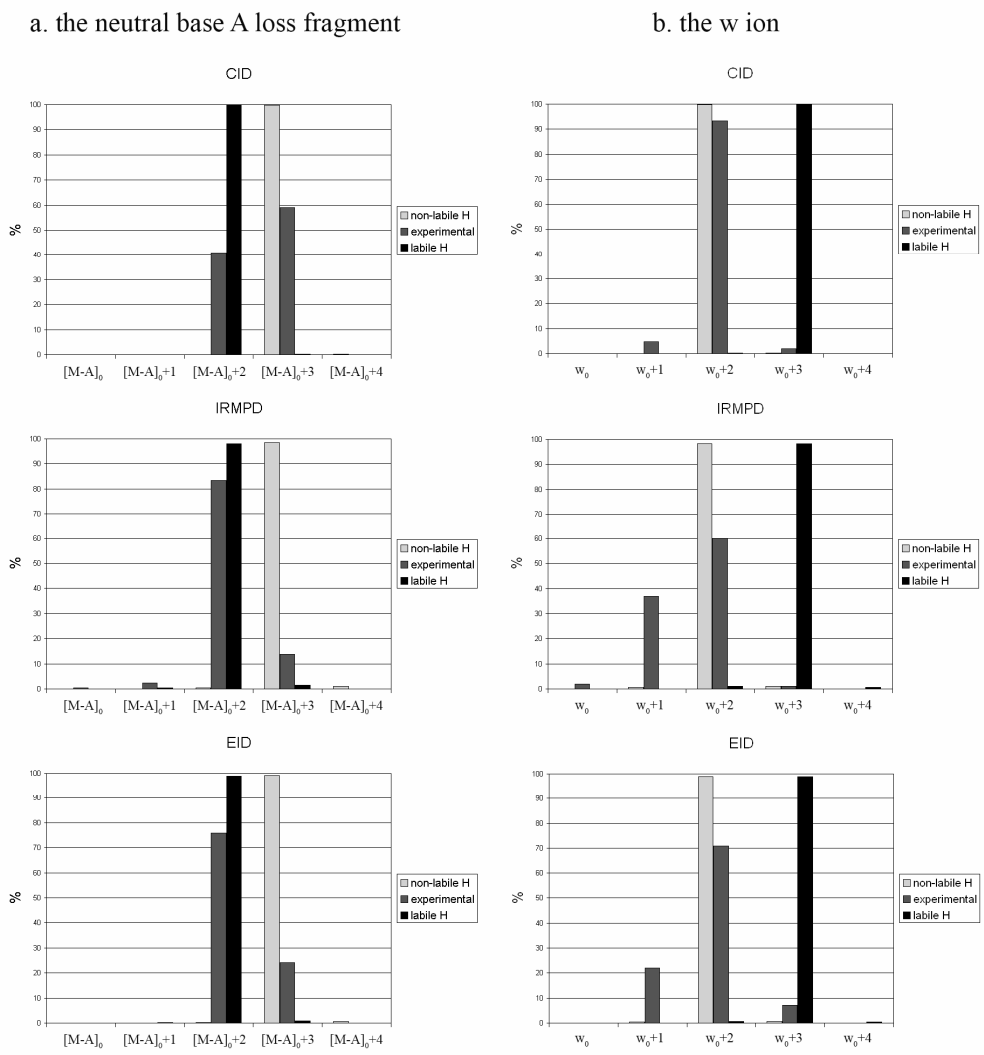

Figure 5.3.4. The deuteration patterns of the neutral base A loss fragment (a) and the w ion (b).

The neutral base T loss

Unlike the loss of neutral A base, the experimental deuteration patterns are the same for all the fragmentation methods. They correspond to the theoretical pattern that involves non-labile protons in the fragmentation process. The fragmentation channel where the T base takes a proton to be lost as a neutral group is the only accessible channel and is therefore the one used in all the chosen MS/MS techniques.

The w ion

For all the fragmentation methods (Figure 5.3.4.b), the experimental deuteration pattern is more similar to the theoretical one obtained considering that the non-labile protons are involved in the fragmentation process. As mentioned in the Introduction, the neutral base loss is proposed to be the first step of the fragmentation process for CID and IRMPD. In this case and if the A base takes the deuterium of the 5'-hydroxyl group to be lost as a neutral species, the w ion has no other choice than to take a proton of the ribose ring (with subsequent double bond generation) to be formed. As the A base significantly leaves with a deuterium, this could explain the low intensity of the peak at $w_0 + 3$ m/z. To check the possibility of neutral A loss as the first step of the fragmentation, double resonance experiments have been performed in IRMPD and EID. Their results are presented and discussed later in this section.

Another important result is the observation of a significant amount of ions at $w_0 + 1$ m/z mostly in IRMPD and EID (Figure 5.3.4.b). This $w_0 + 1$ ion corresponds to a w fragment with only one deuterium. It is one less deuterium compared to the theoretical w ion obtained considering that non-labile protons are involved in the fragmentation process. One scenario can explain this observation: if the w ion is formed from the neutral base A loss, if the A base takes the deuterium at the 3'-hydroxyl position on the ribose of the T nucleoside, and if the w ion takes a proton to be formed, the w ion will present a peak at $w_0 + 1$ m/z. The second condition is checked thanks to the analysis of the different conformations adopted by the dinucleotide. These conformations were investigated by dynamic simulations that were carried out with Yasara (YASARA Biosciences & CMBI Outstation Austria, http://www.yasara.org). Amber99 was used as the force field. The distances (Figure 5.3.5.) between the hydrogen atom of the 3'-hydroxyl group

(ribose of the T nucleoside) and the different nitrogen atoms of the A base rings were monitored during the dynamic simulations (100 ns at 295 K). The distances d1, and especially d3 were often between 1.8 Å and 2 Å, which is characteristic for a hydrogen bond. A hydrogen transfer from the 3'-hydroxyl group to the A base is probable via either d3 or d1. The nitrogen of the N-glycosidic bond does not seem to be included in this transfer as the distance noted d4 was always higher than 3 Å which is not small enough for a direct interaction. From these dynamic simulations, it can be concluded that the A base is allowed to take the deuterium of the 3'-hydroxyl group to be lost as a neutral fragment. These calculations also support the idea that the fragmentation mechanisms involving labile protons require peculiar three-dimensional structures that locate the labile proton donor and acceptor sites close to each other. As just previously mentioned, the first condition is checked thanks to DR experiments that are discussed later in this section.

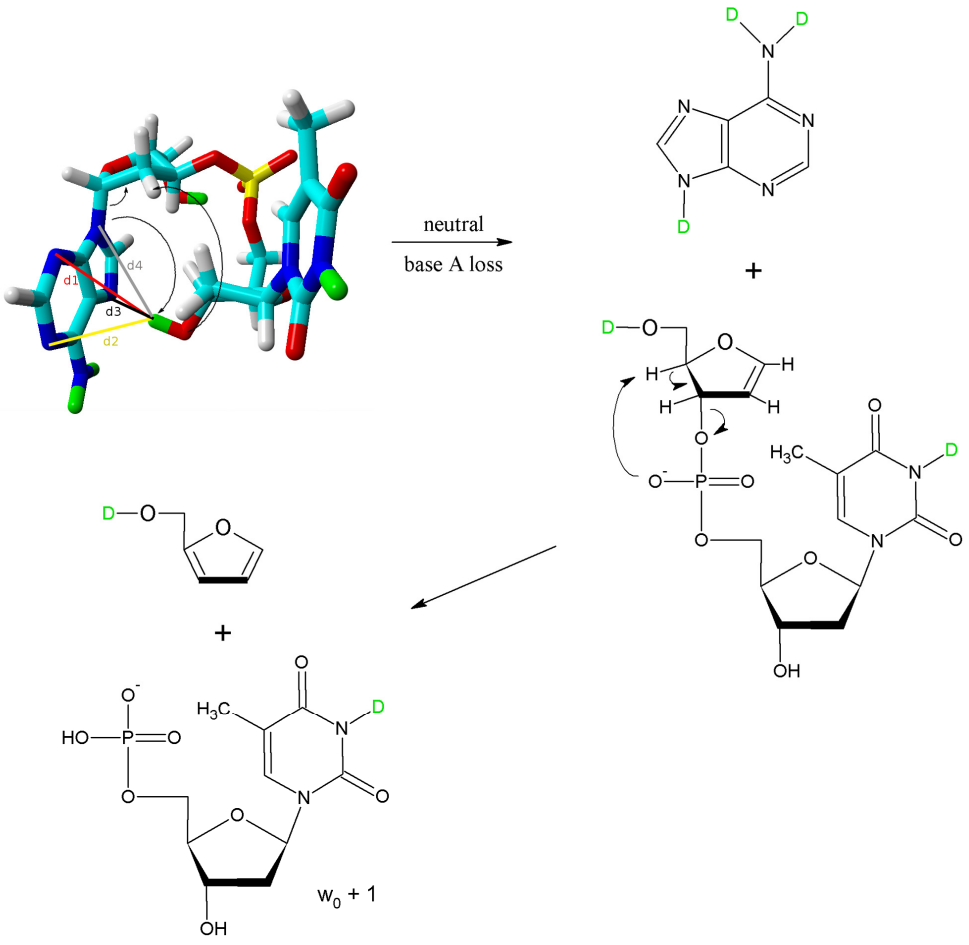

Figure 5.3.5. A relevant structure of dAT^- obtained during dynamic simulations followed by the mechanism (in two dimensions) leading to the w_0 +1 ion formation. The distances (d1, d2, d3 and d4) between the hydrogen atom of the 3'-hydroxyl group on the ribose of the T nucleoside and the different nitrogen atoms of the A base rings are shown, and the deuterium atoms are highlighted in green. Even if an arrow goes from the nitrogen of the N-glycosidic bond to the 3'-hydroxyl group, this nitrogen atom does not seem to be involved in the initial transfer of the proton (see the results and discussion section).

The d ion

In IRMPD, the d ion was not intense enough to be exploited. Experimental deuteration patterns were only obtained in CID and EID. These patterns are more similar to the theoretical one obtained considering that the labile protons are involved in the fragmentation process. The d ion mostly takes the deuterium of the 3'-hydroxyl group to be formed. The observation of a peak at d_0 + 3 m/z can be justified by the fact that the fragmentation channel involving non-labile protons also exists.

The fragment that corresponds to the losses of both the neutral bases A and T presents deuteration patterns that are in agreement with the sum of the neutral base A loss and the neutral base T loss patterns. This was expected as the [M−A−T] fragment most probably comes from the neutral base T loss from the [M−A] fragment and the neutral base A loss from the [M−T] fragment with the same fragmentation channels followed as previously proposed.

The fragment ion corresponding to the $[w-T_{neutral}]$ and/or the $[d-A_{neutral}]$ ions was not analyzed, these theoretical deuteration patterns being too complicated to generate (too many possibilities).

As expected, the A^- ion was only observed with two deuteriums.

All the fragmentation experiments of the totally deuterated dinucleotide in labile positions show clearly the coexistence of several fragmentation channels. These can be classified according to the involvement of non-labile (on ribose ring) or labile (hydroxyl groups) protons in the fragmentation process. For the proton transfer to take place, a spatial closeness between donor and acceptor sites is needed. For the fragmentation mechanisms that imply the transfer of non-labile protons, this closeness pre-exists. But for those involving the transfer of labile protons, a conformational rearrangement of the molecule has to happen to place the donor site near that of the acceptor. Such particular three-dimensional structures are observed for a dynamic simulation of 100 ns: 0.3% of the time for the A base and the 5'-hydroxyl group (ribose of the A nucleoside), and 9% of the time for the A base and the 3'-hydroxyl group (ribose of the T nucleoside). Moreover, when considering the bonds involved in the proton transfers, the transfers involving non-labile protons are suspected to need more energy than

those involving labile protons. The transfer of labile protons could therefore be encountered when the internal energy is increased in small steps. The fragmentation channels that involve non-labile protons are entropically favorable and enthalpically less favorable. Conversely, the fragmentation channels that involve labile protons are enthalpically favorable and entropically less favorable. As the deuteration pattern varies from a MS/MS technique to another, the different fragmentation channels coexist but are taken with different ratios according to the fragmentation method used. This can be discussed regarding the transferred energy under activation and the accessible experimental time scale of each MS/MS technique. For CID in a Q-Tof instrument, the transferred energy under activation is higher than in IRMPD and EID and the time scale is relatively short going from 10^{-5} s to 10^{-3} s. In IRMPD and EID, the ions are activated during respectively 10^{-1} s and 1 s, and the transferred energy under activation is relatively low. According to the RRKM theory, it can be deduced that in CID fragmentation, the channels which are entropically favorable and enthalpically less favorable are characterized by higher rate constants than those which are enthalpically favorable and entropically less favorable. The opposite is found in IRMPD and EID (low energy activation methods); the channels which are enthalpically favorable and entropically less favorable are characterized by higher rate constants. This agrees with the findings of the experiments as the fragments coming from the labile proton fragmentation channels are observed more in IRMPD and EID (see [M−A] ion, observation of $w_0 + 1$ m/z…).

Double resonance experiments

Double resonance experiments were performed in IRMPD and EID with the aim of checking the existence of fragmentation channels where the neutral base loss would be the first step. The selected C_{12} isotope of the non-deuterated dinucleotide anion was activated in IRMPD or EID and the mono-isotopic $(M-AH-H^+)^-$ fragment ion was continuously ejected during the irradiation.

DR-IRMPD

Firstly, it was not possible to completely eject the [M−A] fragment despite the length and the intensity of the resonant shot. The [M−A] fragment intensity (stated in percent regarding the parent ion intensity) was decreased 8.8 and 4.1 times respectively at 15% and 20% laser power, which was expected as the [M−A]

fragment is more produced at 20% laser power. The fragment intensities without and with double resonance at 15% and 20% laser power are shown in Figure 5.3.6.a and b.

The [M−T] fragment intensity decreases during DR experiments even though its formation does not depend on the [M−A] fragment one. The [M−T] fragment (428.1 m/z) having a mass near to the [M−A] fragment one (419.1 m/z) and considering the low attenuation (10 dB) of the resonant shot, the [M−T] fragment is probably a bit resonantly activated by side activation bands.

The d fragment is observed at 20% laser power, not at 15%. Its intensity is decreased 3 times even though its formation does not depend on the [M−A] fragment one. This decrease can be explained not by side activation bands because the d fragment mass (330.1 m/z) is quite different from the [M−A] fragment one, but by the fact that the d fragment could be formed from the [M−T] fragment.

The w fragment intensity is decreased 14.6 and 8.2 times at respectively 15% and 20% laser power. These decreases are quite important which prove that at least some w ions originate from the decomposition of the $(M-AH-H^+)^-$ ion. In double resonance experiments, the observation that a fragment is reduced but does not totally disappear when its suspected parent ion is ejected can be interpreted in different ways. In this case, an explanation is easily found as the [M−A] ion is not totally ejected but other justifications exist: (i) several ion formation channels coexist, and (ii) the fragment is formed and detected before the ejection is complete. This second justification corresponds to a limitation of double resonance experiments. To be freed from this limitation, the time it takes to eject an ion by resonant ejection must be much faster than the time required for the consecutive products to be formed from the ejected ion.

As expected, the [M−A−T] fragment decreases and even disappears. This disappearance can be explained by the fact that the [M−A] and also the [M−T] ions are ejected by the resonant shot and by the low intensity of the [M−A−T] fragment.

The $(w-TH)^-$ and/or the $(d-AH)^-$ (same mass) fragment totally disappears at 15% laser power and is decreased 19.9 times at 20% laser power. This is explained in the same way as for the [M−A−T] fragment.

The A^- fragment is decreased 6 and 2.2 times at respectively 15% and 20% laser power. Some A^- ions are linked to the $(M–AH–H^+)^-$ ion formation.

DR-EID

Unlike DR-IRMPD experiments the $(M–AH–H^+)^-$ ion was completely ejected, which was expected as the [M–A] fragment is less intense in EID that in IRMPD. As illustrated in Figure 5.3.6.c, no influence of double resonance is observed for the $(M–TH–H^+)^-$, the d and the A^- ions.

The w ion intensity is decreased 2.5 times which means that at least some of the w ions originate from the decomposition of the $(M–AH–H^+)^-$ fragment. As previously mentioned the observation that the w fragment is reduced but does not totally disappear is interpreted in two ways: (i) several fragmentation channels coexist for the formation of the w ion, and/or (ii) the w ion is formed and detected before the ejection of $(M–AH–H^+)^-$ is complete.

This was expected because by being linked to the [M–A] or w ion, the $(M–AH–TH–H^+)^-$ and the $(w–TH)^-$ ion intensities are decreased 3 and 1.7 times in double resonance experiments.

All these double resonance experiments show that there are fragmentation channels which correspond to consecutive fragmentation processes. In particular, some w ions originate from the decomposition of the $(M–AH–H^+)^-$ fragment ion. The DR influence seems to be more important in IRMPD than in EID. This is similar to that shown by Kinet et al. [50] and Yang et al. [51]. However, the non-complete ejection of the $(M–AH–H^+)^-$ ion in IRMPD and the fact that the ejection and ion formation times are unknown prevent this from being affirmed.

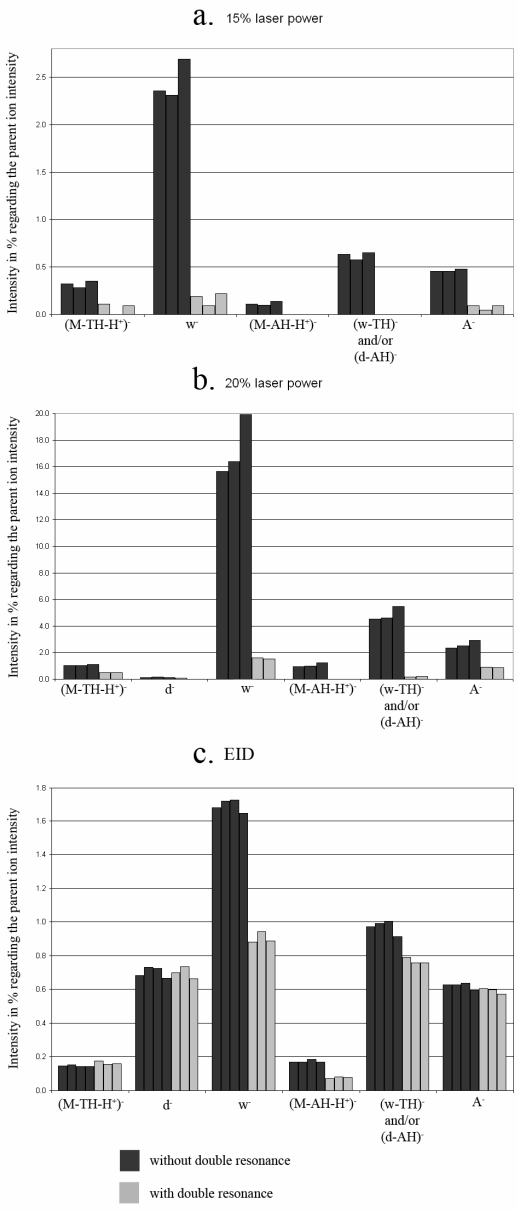

Figure 5.3.6. The fragment intensities without and with double resonance (a) at 15% laser power in IRMPD, (b) at 20% laser power in IRMPD and (c) in EID.

Conclusions

The fragmentation of a totally deuterated dinucleotide in labile positions demonstrates the coexistence of several fragmentation channels that can be classified in relation to the involvement of the non-labile or labile protons in the fragmentation process. These channels are taken with different ratios according to the used MS/MS technique, which means according to the transferred energy under activation and the accessible time scale associated with this method. Fragmentation channels involving labile protons are enthalpically favorable and entropically less favorable as they require particular three-dimensional conformations of the dinucleotide. The involvement of labile protons in the fragmentation mechanisms are more observed in IRMPD and EID.

Double resonance experiments demonstrate the existence of consecutive fragmentation processes. The probability that such processes happen depends also on the MS/MS technique used.

The coexistence of so many fragmentation channels does not make obvious the localization by MS/MS of the incorporated deuteriums in oligonucleotides. Further to particular conformations that are adopted by the oligonucleotide, exchangeable protons can be involved in the fragmentation process. In this case, labile protons are no longer at their initial positions and the localization results obtained by tandem mass spectrometry are distorted.

Acknowledgments

This work was supported by the FRS-FNRS (Fonds de la Recherche Scientifique-FNRS), Belgium.

Supplementary material

The deuteration patterns of the neutral base T loss fragment

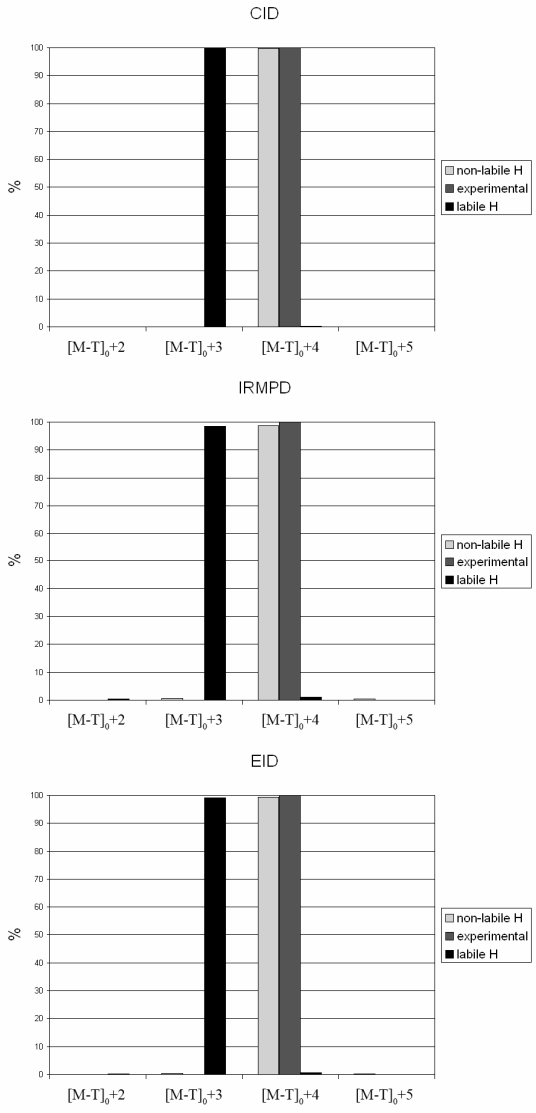

The deuteration patterns of the d ion

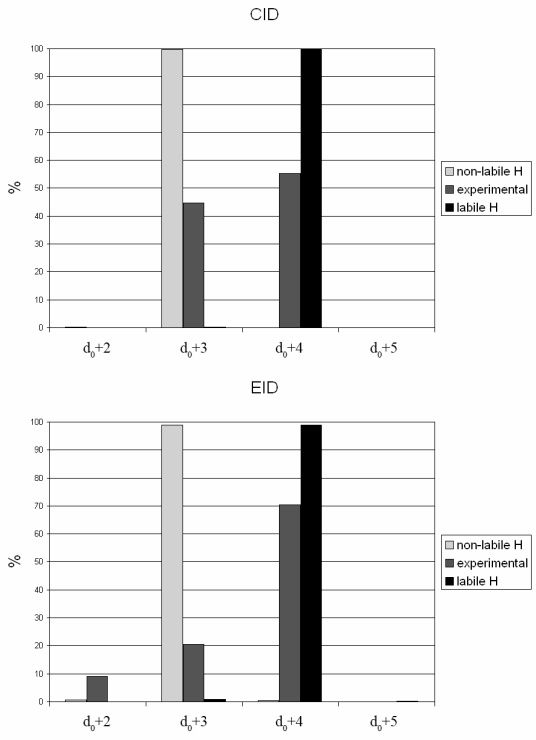

The full CID, IRMPD and EID mass spectra

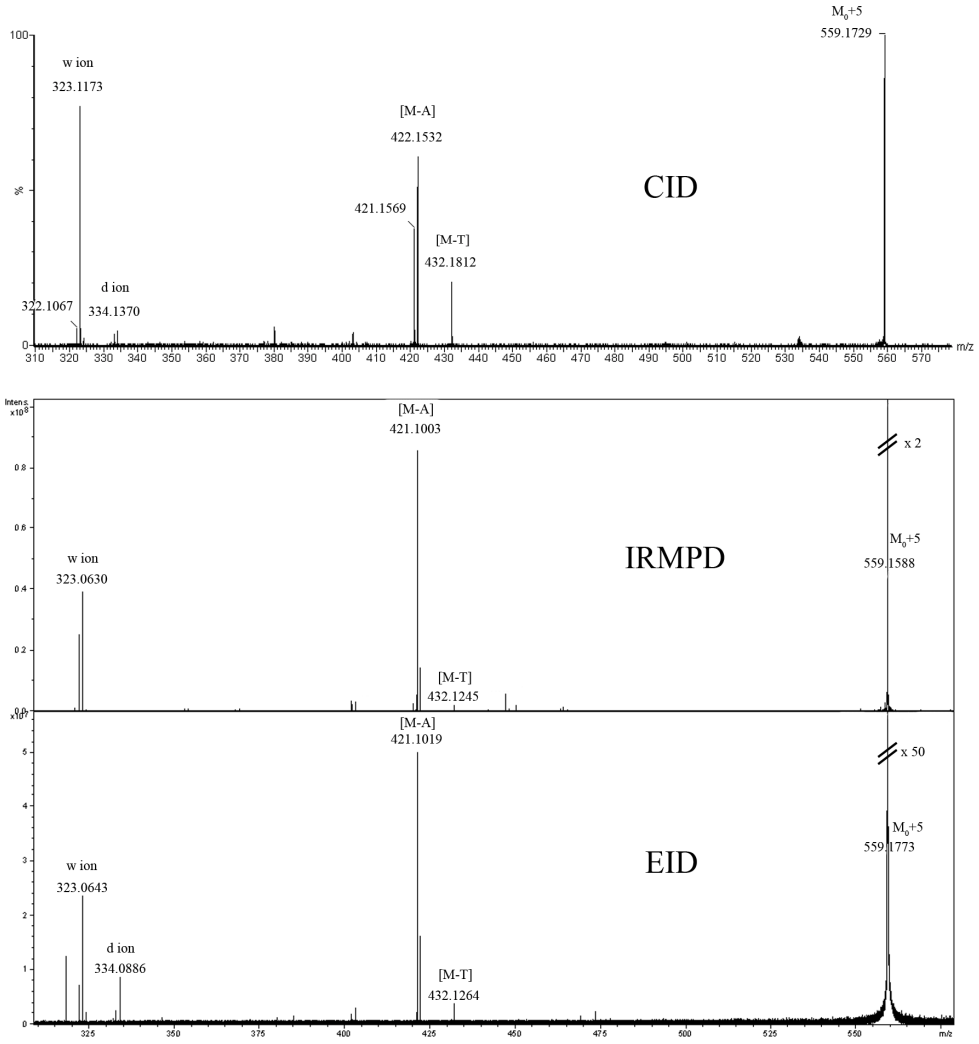

References

1. Gard, E.; Green, M. K.; Bregar, J.; Lebrilla, C. B. Gas-Phase Hydrogen/Deuterium Exchange as a Molecular Probe for the Interaction of Methanol and Protonated Peptides. *J. Am. Soc. Mass Spectrom.* **1994,** *5*, 623-631.

2. Campbell, S. C.; Rodgers, M. T.; Marzluff, E. M.; Beauchamp, J. L. Deuterium Exchange Reactions as a Probe of Biomolecule Structure. Fundamental Studies of Gas Phase H/D Exchange Reactions of Protonated Glycine Oligomers with D_2O, CD_3OD, CD_3CO_2D, and ND_3. *J. Am. Chem. Soc.* **1995,** *117*, 12840-12854.

3. Wang, F.; Freitas, M. A.; Marshall, A. G.; Skyes, B. D. Gas-Phase memory of Solution-Phase Protein Conformation: H/D Exchange and Fourier Transform Ion Cyclotron Resonance Mass Spectrometry of the N-terminal Domain of Cardiac Troponin C. *Int. J. Mass Spectrom.* **1999,** *192*, 319-325.

4. Herrmann, K. A.; Kuppannan, K.; Wysocki, V. H. Fragmentation of Doubly-Protonated Peptide Ion Populations labeled by H/D Exchange with CD_3OD. *Int. J. Mass Spectrom.* **2006,** *249-250*, 93-105.

5. Robinson, E. W.; Williams, E. R. Multidimensional Separations of Ubiquitin Conformers in the Gas Phase: Relating Ion Cross Sections to H/D Exchange Measurements. *J. Am. Soc. Mass Spectrom.* **2005,** *16*, 1427-1437.

6. Sawyer, H. A.; Marini, J. T.; Stone, E. G.; Ruoloto, B. T.; Gillig, K. J.; Russell, D. H. The Structure of Gas-Phase Bradykinin Fragment 1-5 (RPPGF) Ions: An Ion Mobility Spectrometry and H/D Exchange Ion-Molecule reaction Chemistry Study. *J. Am. Soc. Mass Spectrom.* **2005,** *16*, 893-9.

7. Freitas, M. A.; Shi, S. D. H.; Hendrickson, C. L.; Marshall, A. G. Gas-Phase RNA and DNA Ions. 1. H/D Exchange of the $[M-H]^-$ Anions of Nucleoside 5'-Monophosphates (GMP, dGMP, AMP, dAMP, CMP, dCMP, UMP, dTMP), Ribose 5-Monophosphate, and 2-Deoxyribose 5-Monophosphate with D_2O and D_2S. *J. Am. Chem. Soc.* **1998,** *120*, 10187-10193.

8. Robinson, J. M.; Greig, M. J.; Griffey, R. H.; Venkantraman, M.; Laude, D. A. Hydrogen/Deuterium Exchange of Nucleotides in the Gas Phase. *Anal. Chem.* **1998,** *70*, 3566-3571.

9. Freitas, M. A.; Marshall, A. G. Gas-Phase RNA and DNA Ions. 2. Conformational Dependence of the Gas-Phase H/D Exchange of

Nucleotide-5'-Monophosphates. *J. Am. Soc. Mass Spectrom.* **2001,** *12*, 780-785.

10. Crestoni, M. E.; Fornarini, S. Gas-Phase Hydrogen/Deuterium Exchange of Adenine Nucleotides. *J. Mass Spectrom.* **2003,** *38*, 854-861.

11. Chipuk, J. E.; Brodbelt, J. S. Gas-Phase Hydrogen/Deuterium Exchange of 5'- and 3'-Mononucleotides in a Quadrupole ion Trap: Exploring the Role of Conformation and System Energy. *J. Am. Soc. Mass Spectrom.* **2007,** *18*, 724-736.

12. Felix, T.; Reyzer, M.; Brodbelt, J. Hydrogen/Deuterium Exchange of Nucleoside Analogs in a Quadrupole ion Trap Mass Spectrometer. *Int. J. Mass Spectrom.* **1999,** *191*, 161-170.

13. Gree-Church, K. B.; Limbach, P. A.; Freitas, M. A.; Marshall, A. G. Gas-Phase Hydrogen/Deuterium Exchange of Positively Charged Mononucleotides by Use of Fourier-Transform Ion Cyclotron resonance Mass Spectrometry. *J. Am. Soc. Mass Spectrom.* **2001,** *12*, 268-277.

14. Balbeur, D.; Dehareng, D.; De Pauw, E. Conformationally Driven Gas-Phase H/D Exchange of Dinucleotide Negative Ions. *J. Am. Soc. Mass Spectrom.* **2007,** *18*, 1827-1834.

15. Hofstadler, S. A.; Griffey, R. H. Analysis of noncovalent complexes of DNA and RNA by mass spectrometry. *Chem. Rev.* **2001,** *101*, 377-390.

16. Mo, J.; Hakansson, K. Oligonucleotide Gas-Phase Hydrogen/Deuterium Exchange with D_2S in the Collision Cell of a Quadrupole-Fourier Transform Ion Cyclotron Resonance Mass Spectrometer. *Anal. Chem.* **2007,** *79*, 7893-7898.

17. Gabelica, V.; Rosu, F.; Witt, M.; Baykut, G.; De Pauw, E. Fast gas-phase hydrogen/deuterium exchange observed for a DNA G-quadruplex. *Rapid Commun. Mass Spectrom.* **2005,** *19*, 201-208.

18. Griffey, R. H.; Greig, M. J.; Robinson, J. M.; Laude, D. A. Gas-phase Hydrogen-Deuterium Exchange in Phosphorothioate d(GTCAG) and d(TCGAT). *Rapid Commun. Mass Spectrom.* **1999,** *13*, 113-117.

19. Gidden, J.; Bowers, M. T. Gas-Phase Conformation of Deprotonated and Protonated Mononucleotides Determined by Ion Mobility and Theoretical Modeling. *J. Phys. Chem.* **2003,** *107*, 12829-12837.

20. Liu, D.; Wyttenbach, T.; Bowers, M. T. Hydration of Mononucleotides. *J. Am. Chem. Soc.* **2006,** *128*, 15155-15163.

21. Gidden, J.; Bowers, M. T. Gas-phase conformational and energetic properties of deprotonated dinucleotides. *Eur. Phys. J. D* **2002,** *20*, 409-419.

22. Gidden, J.; Bowers, M. T. Gas-Phase Conformations of Deprotonated Trinucleotides (dGTT$^-$, dTGT$^-$, and dTTG$^-$): The Question of Zwitterion Formation. *J. Am. Soc. Mass Spectrom.* **2003,** *14*, 161-170.

23. Hoaglund, C. S.; Liu, Y.; Ellington, A. D.; Pagel, M.; Clemmer, D. E. Gas-Phase DNA: Oligothymidine Ion Conformers. *J. Am. Chem. Soc.* **1997,** *119*, 9051-9052.

24. Gidden, J.; Baker, E. S.; Ferzoco, A.; Bowers, M. T. Structural motifs of DNA complexes in the gas phase. *Int. J. Mass Spectrom.* **2005,** *240*, 183-193.

25. Baker, E. S.; Bernstein, S. L.; Gabelica, V.; De Pauw, E.; Bowers, M. T. G-quadruplexes in telomeric repeats are conserved in a solvent-free environment. *Int. J. Mass Spectrom.* **2006,** *253*, 225-237.

26. Gabelica, V.; Baker, E. S.; Teulade-Fichou, M.-P.; De Pauw, E.; Bowers, M. T. Stabilization and Structure of Telomeric and c-myc Region Intramolecular G-Quadruplexes: The Role of Central Cations and Small Planar Ligands. *J. Am. Chem. Soc.* **2007,** *129*, 895-904.

27. Pringle S.D.; Giles K.; Wildgoose J.L.; Williams J.P.; Slade S.E.; Thalassinos K.; Bateman R.H.; Bowers M.T.; Scrivens J.H. An investigation of the mobility separation of some peptide and protein ions using a new hybrid quadrupole/travelling wave IMS/oa-ToF instrument. *Int. J. Mass Spectrom.* **2007,** *261*, 1-12.

28. Hoxha, A.; Collette, C.; De Pauw, E.; Leyh, B. Mechanism of collisional Heating in Electrospray Mass Spectrometry: Ion Trajectory Calculations. *J. Phys. Chem. A* **2001,** *105*, 7326-7333.

29. Jorgensen, T. J. D.; Gardsvoll, H.; Ploug, M.; Roepstorff, P. Intramolecular Migration of Amide Hydrogens in Protonated Peptides upon Collisional Activation. *J. Am. Chem. Soc.* **2005,** *127*, 2785-2793.

30. Rand, K. D.; Jorgensen, T. J. D. Development of a Peptide Probe for the Occurrence of Hydrogen (^{1}H/^{2}H) Scrambling upon Gas-Phase Fragmentation. *Anal. Chem.* **2007,** *79*, 8686-8693.

31. Rand, K. D.; Adams, C. M.; Zubarev, R. A.; Jorgensen, T. J. D. Electron Capture Dissociation Proceeds with a Low Degree of Intramolecular Migration of Peptide Amide Hydrogens. *J. Am. Chem. Soc.* **2008,** *130*, 1341-1349.

32. Bache, N.; Rand, K. D.; Roepstorff, P.; Jorgensen, T. J. D. Gas-Phase Fragmentation of Peptides by MALDI in-Source Decay with Limited Amide Hydrogen (^{1}H/^{2}H) Scrambling. *Anal. Chem.* **2008,** *80*, 6431-6435.

33. Zehl, M.; Rand, K. D.; Jensen, O. N.; Jorgensen, T. J. D. Electron Transfer Dissociation Facilitates the Measurement of Deuterium Incorporation into Selectively Labeled Peptides with Single Residue Resolution. *J. Am. Chem. Soc.* **2008,** *130*, 17453-17459.

34. Wu, J.; McLuckey, S. A. Gas-phase fragmentation of oligonucleotide ions. *International Journal of Mass Spectrometry* **2004,** *237* (2-3), 197-241.

35. Cerny, R. L.; Gross, M. L.; Grotjahn, L. Fast atom bombardment combined with tandem mass spectrometry for the study of dinucleotides. *Analytical Biochemistry* **1986,** *156* (2), 424-435.

36. Phillips, D. R.; McCloskey, J. A. A comprehensive study of the low energy collision-induced dissociation of dinucleoside monophosphates. *International Journal of Mass Spectrometry and Ion Processes* **1993,** *128* (1-2), 61-82.

37. McLuckey, S. A.; Habibigoudarzi, S. Decompositions of Multiply-Charged Oligonucleotide Anions. *Journal of the American Chemical Society* **1993,** *115* (25), 12085-12095.

38. Rodgers, M. T.; Campbell, S.; Marzluff, E. M.; Beauchamp, J. L. Low-Energy Collision-Induced Dissociation of Deprotonated Dinucleotides - Determination of the Energetically Favored Dissociation Pathways and the Relative Acidities of the Nucleic-Acid Bases. *International Journal of Mass Spectrometry and Ion Processes* **1994,** *137*, 121-149.

39. Barry, J. P.; Vouros, P.; Vanschepdael, A.; Law, S. J. Mass and Sequence Verification of Modified Oligonucleotides Using Electrospray Tandem Mass-Spectrometry. *Journal of Mass Spectrometry* **1995,** *30* (7), 993-1006.

40. Nordhoff, E.; Karas, M.; Cramer, R.; Hahner, S.; Hillenkamp, F.; Kirpekar, F.; Lezius, A.; Muth, J.; Meier, C.; Engels, J. W. Direct Mass-Spectrometric Sequencing of Low-Picomole Amounts of Oligodeoxynucleotides with Up to 21 Bases by Matrix-Assisted Laser-Desorption Ionization Mass-Spectrometry. *Journal of Mass Spectrometry* **1995,** *30* (1), 99-112.

41. Zhu, L.; Parr, G. R.; Fitzgerald, M. C.; Nelson, C. M.; Smith, L. M. Oligodeoxynucleotide Fragmentation in Maldi/Tof Mass-Spectrometry Using 355-Nm Radiation. *Journal of the American Chemical Society* **1995,** *117* (22), 6048-6056.

42. Wang, Z.; Wan, K. X.; Ramanathan, R.; Taylor, J. S.; Gross, M. L. Structure and fragmentation mechanisms of isomeric T-rich oligodeoxynucleotides: A comparison of four tandem mass spectrometric methods. *Journal of the American Society for Mass Spectrometry* **1998,** *9* (7), 683-691.

43. Gross, J.; Hillenkamp, F.; Wan, K. X.; Gross, M. L. Metastable decay of negatively charged oligodeoxynucleotides analyzed with ultraviolet matrix-assisted laser desorption/ionization post-source decay and deuterium exchange. *Journal of the American Society for Mass Spectrometry* **2001,** *12* (2), 180-192.

44. Wan, K. X.; Gross, J.; Hillenkamp, F.; Gross, M. L. Fragmentation mechanisms of oligodeoxynucleotides studied by H/D exchange and electrospray ionization tandem mass spectrometry. *Journal of the American Society for Mass Spectrometry* **2001,** *12* (2), 193-205.

45. Wan, K. X.; Gross, M. L. Fragmentation mechanisms of oligodeoxynucleotides: Effects of replacing phosphates with methylphosphonates and thymines with other bases in T-rich sequences. *Journal of the American Society for Mass Spectrometry* **2001,** *12* (5), 580-589.

46. Liu, J.; Cao, S.; Jia, B.; Wei, D.; Liao, X.; Lu, J.; Zhao, Y. A theoretical and mass spectrometry study of the novel mechanism of N-glycosidic bond cleavage in nucleoside. *International Journal of Mass Spectrometry* **2009,** *282* (1-2), 1-5.

47. Balbeur, D.; Dehareng, D.; De Pauw, E. Conformationally Driven Gas-Phase H/D Exchange of Dinucleotide Negative Ions. *J. Am. Soc. Mass Spectrom.* **2007,** *18*, 1827-1834.

48. Sannes-Lowery, K. A.; Hofstadler, S. A. Sequence confirmation of modified oligonucleotides using IRMPD in the external ion reservoir of an electrospray ionization fourier transform ion cyclotron mass spectrometer. *Journal of the American Society for Mass Spectrometry* **2003,** *14* (8), 825-833.

49. Keller, K. M.; Brodbelt, J. S. Collisionally activated dissociation and infrared multiphoton dissociation of oligonucleotides in a quadrupole ion trap. *Analytical Biochemistry* **2004,** *326* (2), 200-210.

50. Kinet, C.; Gabelica, V.; Balbeur, D.; De Pauw, E. Electron detachment dissociation (EDD) pathways in oligonucleotides. *International Journal of Mass Spectrometry In Press, Accepted Manuscript*.

51. Yang, J.; Hakansson, K. Characterization of oligodeoxynucleotide fragmentation pathways in infrared multiphoton dissociation and electron detachment dissociation by Fourier transform ion cyclotron double resonance. *Eur. J. Mass Spectrom.* **2009,** *15* (2), 293-304.

52. Wang, B. H.; Mclafferty, F. W. Electron-Impact Excitation of Ions from Larger Organic-Molecules. *Organic Mass Spectrometry* **1990,** *25* (10), 554-556.

53. Lioe, H.; O'Hair, R. A. J. Comparison of collision-induced dissociation and electron-induced dissociation of singly protonated aromatic amino acids, cystine and related simple peptides using a hybrid linear ion trap-FT-ICR mass spectrometer. *Analytical and Bioanalytical Chemistry* **2007,** *389*, 1429-1437.

54. Wolff, J. J.; Laremore, T. N.; Aslam, H.; Linhardt, R. J.; Amster, I. J. Electron-Induced Dissociation of Glycosaminoglycan Tetrasaccharides. *Journal of the American Society for Mass Spectrometry* **2008,** *19* (10), 1449-1458.

Chapter 6: Gas-phase H/D exchange of non-covalent complexes

In Chapter 4, under experimental conditions (the type and pressure of the exchange gas) such that the H/D exchange reaction is not the limiting step, H/D exchange has been shown to be controlled by hydrogen accessibility. Since this hydrogen accessibility is in direct relationship with the biomolecular conformation, the study of the gas-phase conformation of larger biomolecules including non-covalent complexes may be considered. In this chapter, several non-covalent complexes were studied with the aim of assessing the ability of the gas-phase H/D exchange method for locating the bond site of a ligand and detecting structural modifications following ligand binding.

6.1. DNA duplexes

Duplex or double-stranded DNA consists of two strands of DNA held in a double helix by complementary base pairing between A and T and between G and C, and by base stacking in the inner part of the helix. The two strands are oriented in an antiparallel way to each other. The [(dGGGGGG)•(dCCCCCC)] noted $(GC)_6$ and the [(dGGGGAATTGGGG)•(dCCCCAATTCCCC)] noted $(GC)_{12}$ duplexes were studied. Since DNA duplexes with high GC content are more stable than DNA duplexes with low GC content, these two duplexes are suspected to be quite stable in solution. The predicted melting temperature (Tm) is equal to 26.6°C for $(GC)_6$ and to 54°C for $(GC)_{12}$ [1]. Unfortunately, no thermal denaturation was performed). The mass spectra of the two duplexes are illustrated in Figure 6.1.1.

Although the $(GC)_6$ duplex is observed in mass spectrometry, the fact that all six nucleobases of the single strands are involved in the pairing has not been established. The single strands are perhaps paired only on a part of their length. Moreover, even though a hexameric duplex is formed, it is known to be not long enough to form a helix turn because the latter requires at least 10 base pairs. However the hexameric duplex contains important elements of a helix such as backbone torsions, sugar conformations and glycosidic bonds for pyrimidines [2].

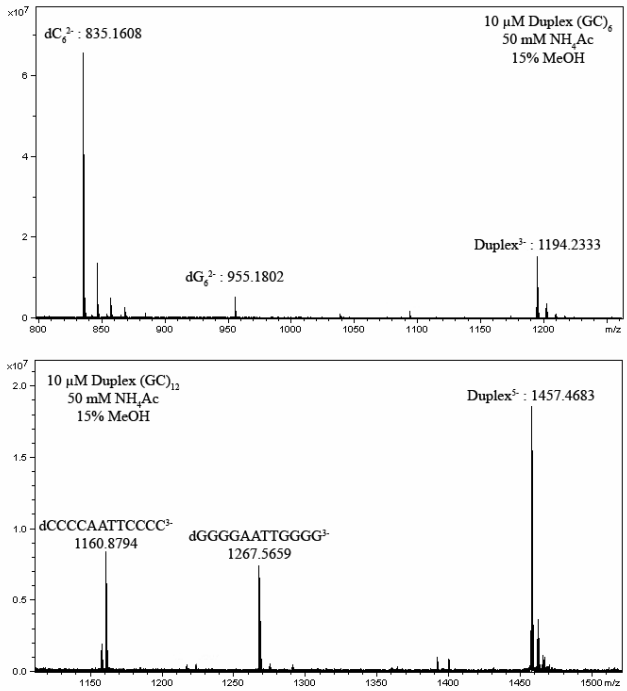

Figure 6.1.1. The mass spectra of the $(GC)_6$ and $(GC)_{12}$ duplexes. The duplex solutions, at a concentration of single strands equal to 10 µM in a 50 mM solution of ammonium acetate buffer, were annealed by heating to 80°C for 3 min and slowly cooling down to room temperature.

Gas-phase H/D exchange experiments were performed on the two duplexes with the main aim of determining whether their exchangeable nucleobase hydrogens involved in base pairing would be protected from exchange and thereby display slower exchange rates. The gas-phase H/D exchange of the duplex was compared to the theoretical exchange obtained by adding the H/D exchange of the respective single strands. Because the sum of the charge states of the single strands is not equal to the charge state of the duplex, the exchange mass spectra were not added. The comparison was made using the deuterated species abundances. These abundances were obtained through the use of our in-house software or of the Hasselt lab software (see point 2.3.3.1. in Chapter 2). The relative abundances of the deuterated species are presented as bar charts in Figure 6.1.2. for dC_6, dG_6 and the respective duplex $(GC)_6$ after 120 s of H/D exchange reaction.

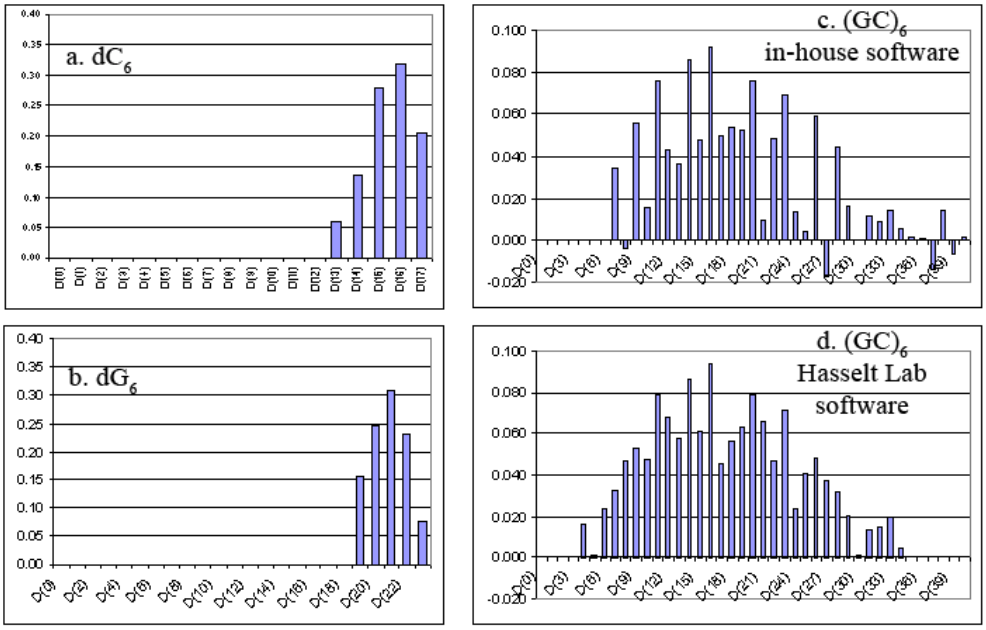

Figure 6.1.2. The relative abundances of the deuterated species after 120 s of gas-phase H/D exchange reaction: **a**. dC_6, **b**. dG_6, **c**. $(GC)_6$ analyzed with the in-house software and **d**. $(GC)_6$ analyzed with the Hasselt lab software. All gas-phase H/D exchange experiments were performed in the second hexapole of the 9.4 T Apex-Qe FT-ICR mass spectrometer.

Because no constraint with respect to sign is included in the in-house software, and because the H/D exchange mass spectrum of the duplex is very broad (32 isotopic peaks), a few negative values appear in the abundance data of Figure 6.1.2.c. It can be reminded that for least-squares methods, if a large number of peaks are observed in the mass spectrum with a low signal-to-noise ratio, the matrix is not well conditioned and its inverse becomes unstable (see point 2.3.3.1. in Chapter 2). The comparison of the two distributions of the relative abundances, i.e. the deconvoluted mass spectra, obtained respectively with the in-house software and the Hasselt lab software shows that they are globally similar and that, in particular, the maxima are at the same locations ($\overline{D_{in-house}}$=17.7 and $\overline{D_{Hasselt}}$=17.4, where $\overline{D}$ is the average position of the distribution, and $\Delta D_{in-house}$=6.14 and $\Delta D_{Hasselt}$=6.75, where ΔD is the standard deviation of the

deuterated species distribution). The deconvoluted mass spectrum obtained with the Hasselt lab software will be compared to the theoretical one.

For adding the H/D exchange of the respective single strands, we based our reasoning on the formula of the isotope distribution (binomial law):

$$(a+b)^n = a^n + na^{n-1}b + \frac{n(n-1)a^{n-2}b^2}{2!} + \frac{n(n-1)(n-2)a^{n-3}b^3}{3!} + \ldots \quad (1)$$

where a and b are the abundances of the isotopes. In the present case, the combination of two distributions can be written:

$$(a+b+c+d+\ldots+n)^1 \times (f+g+h+i+\ldots+m)^1 \quad (2)$$

where a, b… are the relative abundances of the deuterated species calculated for the single strands. The theoretical relative abundances for the duplex are given by:

$$I(M) = \sum_{m=m_{\min}}^{m=m_{\max}} I_{st1}(M-m) \cdot I_{st2}(m) \ , \ M = (m_{\min,st1} + m_{\min,st2}),\ldots,(m_{\max,st1} + m_{\max,st2}) \quad (3)$$

where I and $I_{st1,st2}$ are the relative abundances of the deuterated species calculated for the duplex and the respective single strands, and M and m are the number of incorporated deuteriums in the deuterated species.

The theoretical H/D exchange of the $(GC)_6$ duplex obtained with Eq(3) is illustrated in Figure 6.1.3. The comparison of this theoretical exchange with the experimental one (Figure 6.1.2. d) shows clearly that the duplex displays slower exchange rates than its corresponding single strands. Hydrogen bonding involved in base pairing protects nucleobase hydrogens from H/D exchange. Since 3 hydrogens are involved in each GC Watson-Crick base pair, 18 hydrogens should be protected from H/D exchange by hydrogen bonding in the $(CG)_6$ duplex. As the average of the theoretical distribution is located at 36 exchanged hydrogens ($\overline{D}_{theory}$=36.3), if 18 hydrogens are subtracted, the average of the experimental distribution should be located at 18 exchanged hydrogens. This average position corresponds, by one deuterium, to the average of the experimental deconvoluted mass spectrum.

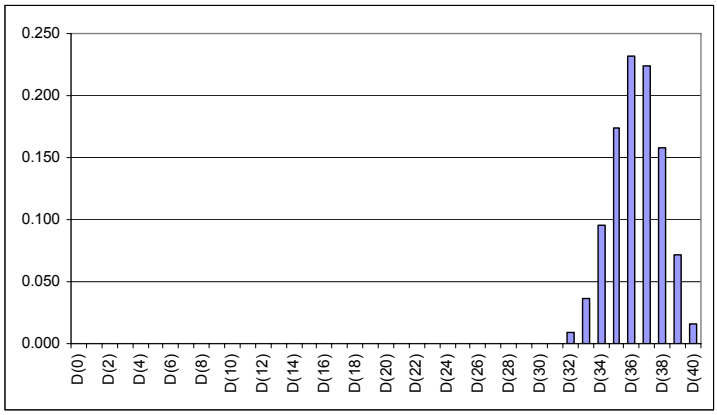

Figure 6.1.3. The theoretical H/D exchange of the $(GC)_6$ duplex.

Because the experimental deconvoluted mass spectrum displays a large number of deuterated species (broad distribution), it is suspected to correspond to several conformations. In order to check this assumption, more detailed analyzes of the H/D exchange and comparison with theoretical predicted conformations (molecular modeling…) should be performed. Regarding the H/D exchange analyses, the study of the exchange kinetics could allow groups of protons associated with different structures to be identified. For such studies, high-performance softwares for deconvoluting H/D exchange mass spectra and extracting the H/D exchange rate constants from the deuterium level evolution must be used. However, these softwares have not been developed yet. A collaboration with the Hasselt lab for designing such softwares is under way. The software presented in point 2.3.3.1 (Chapter 2) (least-squares method with a constraint for respecting the positive sign) corresponds to a first adjustment and the result presented in Figure 6.1.2. d corresponds to one of its first applications. Finalizing the Hasselt lab software and maybe developing a maximum entropy method (currently, no software is commercially available for deconvoluting H/D exchange mass spectra) could allow the H/D exchange data to be investigated more in-depth.

The H/D exchange of the $(GC)_{12}$ duplex being even more complex than the $(GC)_6$ one, it has not been analyzed yet.

6.2. Small oligonucleotide-peptide complexes

Interactions between nucleic acids and proteins play an important role in numerous biochemical processes including DNA replication, recombination and repair. Juhasz and Biemann were the first to reveal that attachment could be observed between highly acidic DNA and basic peptides [3]. They detected large complexes between histone H_4 and dT_{10} in MALDI. Tang et al. explored non-specific interactions between peptides and oligonucleotides [4]. They studied the complexation of dT_n with small basic dipeptides in positive ion mode MALDI-MS. They showed that the complex formation is correlated with the type of oligonucleotide bases and with the amino acid composition of the peptides. Among the four DNA homooligomers, dT_n was observed to form abundant peptide-nucleic acid complexes whereas negligible attachment was detected for dA_n, dC_n and dG_n.

The complexes studied in this chapter are summarized below. Since the formation of the complex is promoted when the peptide contains basic residues, peptides with one or two basic amino acids (Arginine or Lysine) were chosen. These peptides were also composed of either one acid residue (Glutamic acid) or two Prolines. All the MS experiments were performed in the negative ion mode with the 9.4 T Apex-Qe FT-ICR mass spectrometer.

dT_5 – Arg-Gly-Glu-Ser	=	dT_5 – RGES	●
dT_5 – Gly-Pro-Arg-Pro	=	dT_5 – GPRP	●
dT_5 – Arg-Lys-Glu-Val-Tyr	=	dT_5 – RKEVY	● - ■
dAATCG – Arg-Lys-Glu-Val-Tyr	=	dAATCG – RKEVY	▲
dAATCT – Arg-Lys-Glu-Val-Tyr	=	dAATCT – RKEVY	▲
dT_6 – Arg-Lys-Glu-Val-Tyr	=	dT_6 – RKEVY	▲ - ■
dT_7 – Arg-Lys-Glu-Val-Tyr	=	dT_7 – RKEVY	■
dTCCGTTAA – Arg-Lys-Glu-Val-Tyr	=	dTCCGTTAA – RKEVY	
dA_6 – Arg-Lys-Glu-Val-Tyr	=	dA_6 – RKEVY	▲
dC_6 – Arg-Lys-Glu-Val-Tyr	=	dC_6 – RKEVY	▲
dG_6 – Arg-Lys-Glu-Val-Tyr	=	dG_6 – RKEVY	▲

These complexes were organized in several groups with the aim of studying the following points:

- The influence of the amino acid content of the peptide (●)
- The influence of the nucleobase content of the oligonucleotide (▲)
- The influence of the oligonucleotide size (■)

First of all, considerable amounts of complex were observed for all considered oligonucleotides and peptides. Several fragmentation experiments were performed on the full H complexes. The different MS/MS methods used were CID, IRMPD and EDD. The CID experiments were preformed in the collision hexapole (h2). Figures 6.2.1., 6.2.2. and 6.2.3. illustrate the MS/MS spectra of the complexes dT_5 – RGES, dT_5 – GPRP and dT_5 – RKEVY.

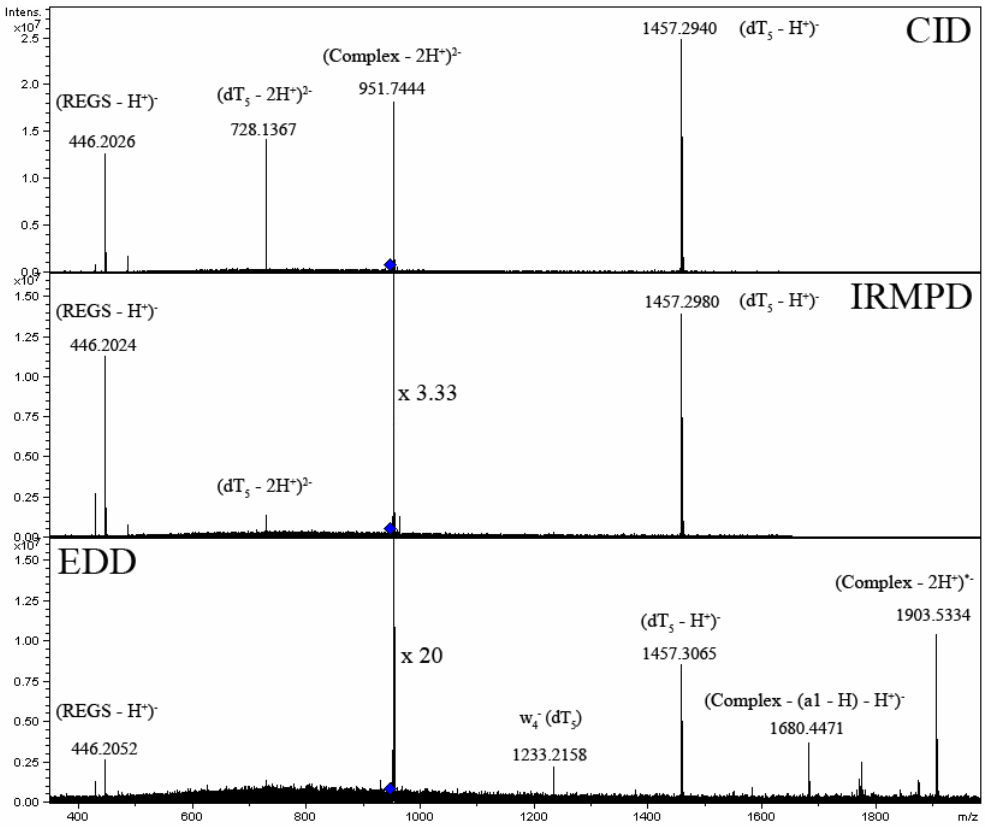

Figure 6.2.1. MS/MS spectra of the dT_5 – RGES complex.

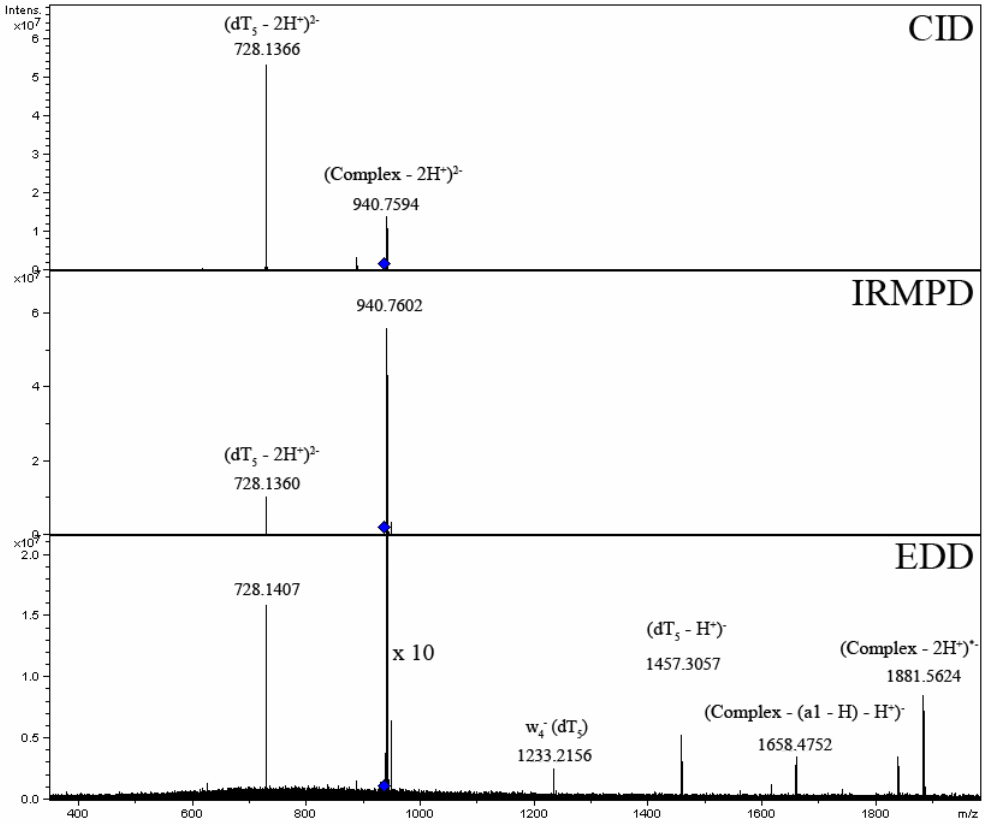

Figure 6.2.2. MS/MS spectra of the dT_5 – GPRP complex.

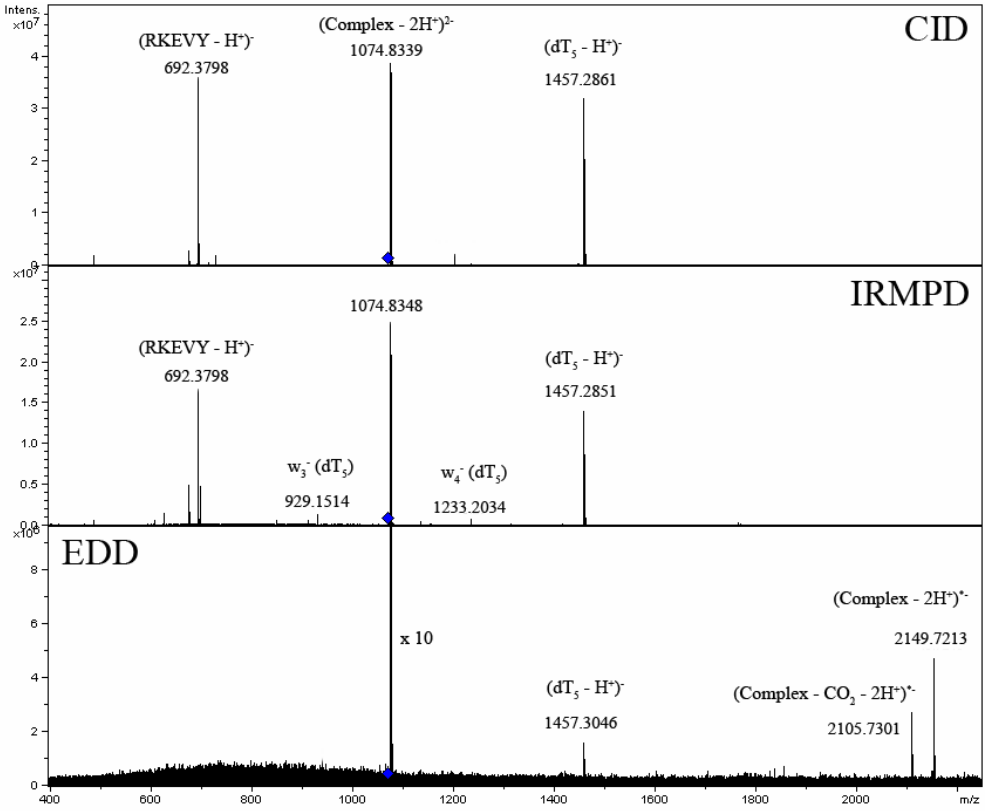

Figure 6.2.3. MS/MS spectra of the dT_5 – RKEVY complex.

Although the observed fragments showed some differences from one complex to the other, no general rule or trend could be inferred with respect to the different points mentioned above.

However, in view of the EDD mass spectra, some interesting future experiments are suggested. EDD fragmentation could be performed on the complex, the oligonucleotide and the peptide in order to obtain the radical species $M^{(x-1)*-}$ with M^{x-} as the precursor ion. These radical species could then be fragmented in IRMPD. These experiments could allow to probe which partner is the more suitable for bearing the radical.

Gas-phase H/D exchange experiments were also performed on these oligonucleotide-peptide complexes. It is important to notice that the ideal H/D exchange experiment should consist in carrying out:

- The gas-phase H/D exchange of the oligonucleotide
- The gas-phase H/D exchange of the peptide
- The gas-phase H/D exchange of the complex from which the contribution of the two partners could be separated.

The H/D exchange of the two partners alone and in the complex should then be compared with the aim of locating the bond site and detecting structural modifications induced by the binding of the two partners.

A mean of separating the partners of the deuterated complex is to fragment the latter after H/D exchange. The CID, IRMPD and EDD methods have been observed to produce the peptide and the oligonucleotide isolated (Figure 6.2.1.). However, as previously discussed in Chapter 2 (section 2.3.) and in Chapter 5 (section 5.3.), intramolecular migration of exchangeable protons can occur upon activation (scrambling). Even if proton scrambling during fragmentation of a non-covalent complex into its components has not been demonstrated, the involvement of exchangeable protons in the fragmentation mechanism of peptides and oligonucleotides makes the use of tandem mass spectrometry questionable to determine the deuterium content of the two partners of the complex. Since it is not guaranteed that labile protons remain at their initial positions after fragmentation of the complex, these experiments have not yet been performed.

Another possibility may be considered to separate the exchange contributions of the two partners from the exchange of the complex: the analysis of the H/D exchange kinetics. However, this procedure comes up against several difficulties. First, as discussed in point 6.1., if a broad H/D exchange distribution (mass spectrum with a large number of peaks) is observed, our in-house software yields negative-magnitude abundances. Secondly, if modifications of H/D exchange rate constants are observed, their interpretation is not necessarily unambiguous. Not only protections of the hydrogens due to the binding of the oligonucleotide and the peptide, but also structural modifications of the two partners following the formation of the complex can affect the exchange rate constants. Obtaining and analyzing the H/D exchange kinetics are not at all obvious. Because we are waiting for high-performance softwares for deconvoluting the H/D exchange mass spectra and for extracting the exchange rate constants from the time evolution of

the deuterium levels, the present data focusing on the H/D exchange of oligonucleotide-peptide complexes have not yet been analyzed. With such softwares and through analyses of proton groups, we hope to be able to separate the H/D exchange contributions of the two partners.

6.3. Duplex - II metal cation complexes

Metal ions play a central role in cellular processes. Besides their function as cofactors of proteins, especially in replication, transcription and translation, they induce folding and cross-linking of nucleic acids and result in a stabilization of these structures. One of the most notable cationic effects is the stabilization of the oligonucleotides resulting from nonspecific electrostatic attraction between the negatively charged phosphate groups and the metal cations. Moreover, metal binding may occur through a specific coordination of the metal ion, either directly to the phosphate as well as to the sugar oxygen atoms and to the base oxygen and nitrogen sites or through bridging water molecules [5]. While the metal ion-phosphate interactions seem dominant in biological oligonucleotides, the inner-sphere coordination involving nucleobases matters in several genetic processes.

Anichina and Bohme [6] investigated the interaction of a hexameric duplex with first row transition metal dications. The short, self-complementary hexadeoxynucleotide dGCATGC was chosen as the nucleic acid of interest because of its high GC content. As dGCATGC is a self-complementary Watson-Crick sequence, the number of species that are formed in solution should be reduced. Addition of different excesses of the salts of the first row transition metal dications (Mn^{2+}, Fe^{2+}, Co^{2+}, Ni^{2+}, Cu^{2+} and Zn^{2+}) to the annealed solution of dGCATGC resulted in the formation of multiply-metallated species; addition of up to four metal dications was observed for the duplex in charge state 3-. CID MS/MS experiments were performed on the singly, doubly and triply metallated species. They were found to dissociate non-covalently to form two single strands with metal ions still attached to one of them or to both depending on the extent of metallation. MS/MS experiments were not performed with quadruply-metalleted trianions due to the very low yields of these ions. Relative gas-phase stabilities of the duplex-metal dication complexes were found to follow the order Mn(II) > Fe(II) > Co(II) > Ni(II) > Zn(II) > Cu(II). Overall, the presence of the metal dications was found to increase the gas-phase stability of the duplex against dissociation with the exception of singly- and triply-metallated copper.

The overall number of the phosphates in a double-stranded hexadeoxynucleotide is 10. In order to achieve a charge state 3- upon addition of four metal dications, 11 protons must be lost from the duplex. If a complete deprotonation of all the phosphate groups is supposed, an extra proton should be lost to achieve the observed charge state. Through H/D exchange experiments on the duplex without and with from 1 to 4 metal dications, we would like to identify the origin of this additional proton (phosphate groups, nucleobases or hydroxyl groups). In analyzing the exchange kinetics of all the duplex species, we hope to identify groups of protons and to follow their evolution from one duplex species to another. The full H and gas-phase H/D exchange (60 s of reaction) mass spectra are illustrated for the duplex species with Mn^{2+} in Figure 6.3.1. and with Zn^{2+} in Figure 6.3.2.

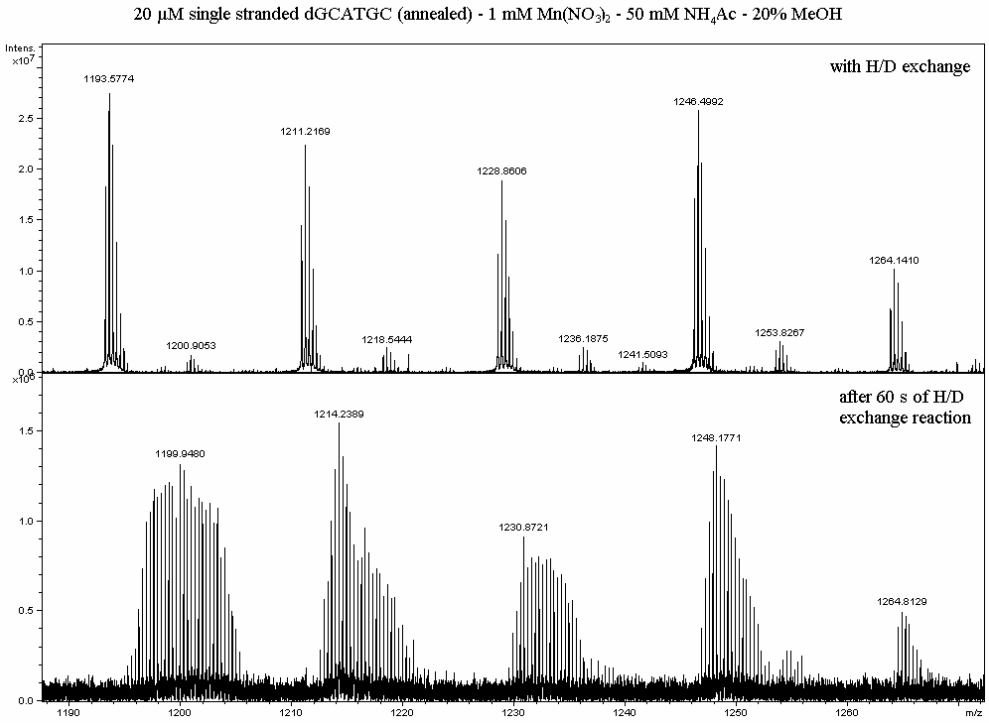

Figure 6.3.1. The full H and gas-phase H/D exchange mass spectra of the duplex – Mn(II) metal dication complexes.

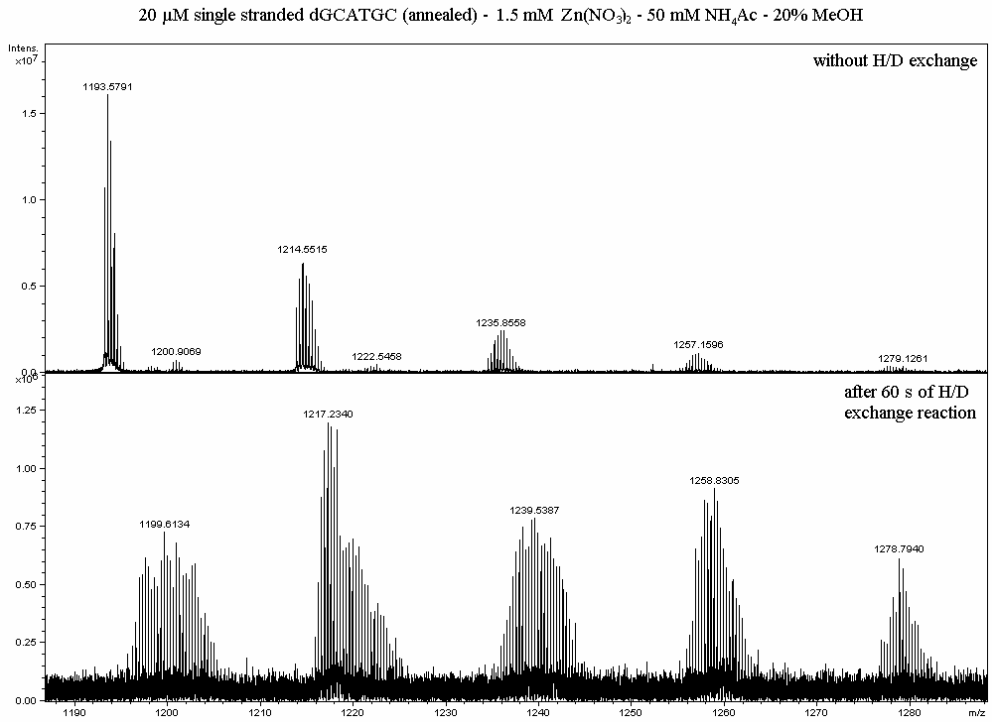

Figure 6.3.2. The full H and gas-phase H/D exchange mass spectra of the duplex – Zn(II) metal dication complexes.

As previously explained, we are waiting for high-performance softwares for deconvoluting the H/D exchange mass spectra and extracting the exchange rate constants from the deuteration level evolution. The H/D exchange experiments of the different duplex – II metal cation complexes have therefore not yet been analyzed.

References

1. http://www.bioinfo.rpi.edu/applications/hybrid/ 2009.

2. Zimmer, C.; Wahnert, U. *Prog. Biophys. Mol. Biol.* **1986,** *47*, 31.

3. Juhasz, P.; Biemann, K. Mass spectrometric molecular-weight determination of highly acidic compounds of biological significance via their complexes with basic polypeptides. *Proc. Natl. Acad. Sci. U. S. A.* **1994,** *91*, 4333-4337.

4. Tang, X.; Callahan, J. H.; Zhou, P.; Vertes, A. Noncovalent Protein-Oligonucleotide Interactions Monitored by Matrix-Assisted Laser Desorption Ionization Mass Spectrometry. *Anal. Chem.* **1995,** *67*, 4542-4548.

5. Cowan, J. A. *Inorganic Biochemistry. An Introduction;* VCH Publishers ed.; New York, 1993.

6. Anichina, J.; Bohme, D. K. Mass-Spectrometric Studies of the Interactions of Selected Metalloantibiotics and Drugs with Deprotonated Hexadeoxynucleotide GCATGC. *J. Phys. Chem. B* **2009,** *113*, 328-335.

Chapter 7: General conclusion

Mass spectrometry, through all its variants (H/D exchange, ion mobility, fragmentation, cross-linking…), has shown its remarkable potential for studying the structure of proteins. It is an essential and routine tool for primary structure analysis and it provides a lot of information about high order structures (localization of contact sites in complexes, kinetic studies of structural interconversion, identifications of flexible regions, folding/unfolding studies…). However, these methods have not been much transposed for analyzing nucleic acid structures. The present work assesses the capabilities of these emerging mass spectrometry methods, and especially the gas-phase H/D exchange technique, for the structural analyzes of oligonucleotides. With the final aim of having a routine method which allows structural information to be obtained straightforwardly, gas-phase H/D exchange was preferentially chosen to solution H/D exchange. Performing the H/D exchange experiments in solution indeed requires several meticulous manipulations of the sample before analysis in mass spectrometry. As only monophosphate nucleotides had already been studied in detail by gas-phase H/D exchange experiments, we first studied dinucleotides in order to design our experiments and to identify the major parameters governing the extent and rates of exchange. Then, larger nucleic acids such as duplexes and non-covalent complexes having higher order structures that are observed in biologically relevant systems were studied. Other analytical methods were also used to validate the gas-phase H/D exchange technique and to obtain supplementary structural information.

We first used gas-phase H/D exchange to study single stranded oligonucleotides. Previous monophosphate nucleotide studies had shown that gas-phase H/D exchange depends on the nucleobase (identity, orientation and gas-phase acidity of the exchangeable hydrogens) and the position and flexibility of the phosphate group. Unlike these experiments that had been performed at low exchange gas pressure (10^{-8} – 10^{-7} mbar) in IRC cells, our H/D exchange experiments were conducted at higher pressure (10^{-3} mbar) in the collision cell of our FT-ICR MS. In these experimental conditions and by integrating the experimental and theoretical results from molecular dynamic calculations, the H/D exchange was shown to be controlled by hydrogen accessibility. The data analysis was performed without taking into account the chemical nature of the heteroatom bearing the hydrogen. In our experimental conditions, the interpretation of the

gas-phase H/D exchange experiments was shown to be more straightforward since the dominant factor is hydrogen accessibility which is in direct relationship with the biomolecular conformation.

Gas-phase H/D exchange was shown to be an efficient tool for detecting the presence of one structure or several conformers that possess different exchange properties. Moreover, when several structures were observed, ion activation was performed by accelerating the ions at the entrance of the H/D exchange cell under conditions promoting exclusively collisional isomerization: this led us to qualitatively estimate the relative height of the isomerization barrier compared to the H/D exchange ones. Ion mobility, a technique which probes different physical properties of an ion than H/D exchange, independently confirmed the H/D exchange results. In particular, for C_6^{2-}, both the presence of two gas-phase conformations, and their non-interconversion at room temperature have been confirmed. The comparison of these two parallel experiments showed that the C_6^{2-} conformer that possesses the fastest H/D exchange is the one having the smallest collision cross section. As compactness and hydrogen accessibility are connected to different physical parameters, they cannot be probed with only one of the two methods. The combination of H/D exchange and ion mobility provided extra structural information compared to the two individual methods used alone.

Two other methods having independent principles of operations were sequentially combined: solution H/D exchange and fragmentation. The aim of this work was to determine which hydrogens are involved in the fragmentation process for assessing the capabilities of tandem mass spectrometry to localize incorporated deuteriums in nucleic acids. By fragmenting a totally deuterated dinucleotide in labile positions, the coexistence of several fragmentation channels was demonstrated. The latter were classified according to the involvement of non-labile or labile protons in the fragmentation process. The branching ratios between the available channels depended on the fragmentation method used (CID, IRMPD or EID). For the fragmentation mechanism implying the transfer of labile protons, a conformational rearrangement of the molecule has to happen to place the donor site near the acceptor one. Moreover, considering the bonds involved in the proton transfers, those involving non-labile protons are suspected to need more energy than those involving labile protons. Fragmentation channels involving labile protons are therefore enthalpically favored and entropically less favored, an interpretation which was in agreement with their larger observation in IRMPD

and EID. Double resonance experiments were also performed and demonstrated the existence of consecutive fragmentation mechanisms. The coexistence of a large number of fragmentation channels does not make the localization of the incorporated deuteriums in oligonucleotides by MS/MS obvious. Moreover, the involvement of labile, i.e. exchangeable, protons casts doubts on the use of tandem mass spectrometry for localizing exchanged protons.

Several non-covalent complexes were studied to explore whether the gas-phase H/D exchange method can display structural changes and locate the binding site of a ligand. For example, a duplex displayed slower exchange rates than its corresponding single strands. This means that the exchangeable nucleobase hydrogens involved in base pairing are protected from H/D exchange. This reveals interesting possibilities for characterizing higher order structure of folded nucleic acids. Small oligonucleotide-peptide complexes and duplex – metal cations (II) complexes were also studied. With the aim of locating the binding site and detecting structural modifications following the ligand binding, the H/D exchange of the two partners alone and in the complex must be compared. For that purpose, the contributions of the two partners in the complex need to be separated. A mean of separating the partner contributions is to fragment the complex after H/D exchange. However, exchangeable protons are known to be involved in the fragmentations processes of proteins and oligonucleotides in some MS/MS methods. Even if proton scrambling during fragmentation of a non-covalent complex into its two components has not yet been demonstrated, it casts doubts about the use of tandem mass spectrometry to identify the H/D exchange contributions of two partners of a complex.

Another possibility that may be considered to obtain information about structural modifications during ligand binding and about the location of the binding site is a detailed analysis of the H/D exchange kinetics. Since in our experimental conditions hydrogen accessibility is the main factor for the exchange rates, identifying proton groups of the partners alone and of the complex could provide us with this kind of information. Such detailed analyses have not yet been performed for large oligonucleotides and complexes. These compounds usually display broad H/D exchange distributions which require a high-performance software to be deconvoluted. Such a software is not currently commercially available. In-house softwares based on the least-squares method have been used

but their results are not always reliable for wide exchange distributions with low signal-to-noise ratio.

Overall, gas-phase H/D exchange has demonstrated its usefulness for distinguishing between isomeric species, for deducing information about reaction mechanism, and for inferring structural features of relatively small nucleic acids. Gas-phase H/D exchange of larger nucleic acids like non-covalent complexes has not yet shown all its potential because of difficulties for deconvoluting broad H/D exchange distributions. While a detailed analysis of H/D exchange kinetics could help to localize the incorporated deuteriums, tandem mass spectrometry was shown to involve exchangeable protons. In this case, labile protons are no longer at their initial positions and the localization results are distorted.

As alluded to previously in this general final conclusion, theoretical studies (quantum chemical calculations, molecular dynamics) were performed in parallel to all our experiments. The comparison of information derived from experiment and from theory data is an essential aspect of the analysis of our results.

It can be reminded that H/D exchange studies of proteins and their complexes have been widely performed in solution. Solution H/D exchange – MS experiments localizing the incorporated deuteriums requires quench and digestion conditions with limited back-exchange. Such experiments have not yet been reported for nucleic acids. It would be interesting to develop solution H/D exchange – digestion – MS experiments for nucleic acids as it could correspond to a quite automatic and straightforward way for localizing the exchanged protons and obtaining information about the location of the binding site and about structural modifications during ligand binding.

Another promising method should be the coupling of H/D exchange with gas-phase spectroscopy. Since for an identical structure, N-H and N-D, and O-H and O-D do not vibrate at the same frequencies, the exchanged protons might be localized. This emphasizes, once again, the idea that any structural technique is more valuable when combined with another one.